

**HETEROGENEITY IN THE PETROPHYSICAL
PROPERTIES OF CARBONATE
RESERVOIRS**

Thesis submitted for the degree of

Doctor of Philosophy

At the University of Leicester

By

Peter James Rowland Fitch MGeol. (Leicester)

Department of Geology

University of Leicester

July 2010

Heterogeneity in the Petrophysical Properties of Carbonate Reservoirs.

Dedicated to Susan Fitch
(January 1945 – September 2000)

Abstract

Heterogeneity in the Petrophysical Properties of Carbonate Reservoirs.

Peter James Rowland Fitch

In comparison to sandstone reservoirs, carbonate exploration is commonly more challenging because of intrinsic heterogeneities, occurring at all scales of observation and measurement. Heterogeneity in carbonates can be attributed to variable lithology, chemistry/mineralogy, pore types, pore connectivity, and sedimentary facies. These intrinsic complexities can be related to geological processes controlling carbonate production and deposition, and to changes during their subsequent diagenesis. The term ‘heterogeneity’ is rarely defined and almost never numerically quantified in petrophysical analysis although it is widely stated that carbonate heterogeneities are poorly understood.

This work has investigated how heterogeneity can be defined and how we can quantify this term by describing a range of statistical heterogeneity measures (e.g. Lorenz and Dykstra-Parsons coefficients). These measures can be used to interpret variation in wireline log data, allowing for comparison of their heterogeneities within individual and multiple reservoir units. Through this investigation, the Heterogeneity Log has been developed by applying these techniques to wireline log data, over set intervals of 10, 5, 2 and 1m, through a carbonate reservoir. Application to petrophysical rock characterisation shows a strong relationship to underlying geological heterogeneities in carbonate facies, mud content and porosity. Zones of heterogeneity identified through the successions show strong correlation to fluid flow zones. By applying the same statistical measures of heterogeneity to established flow zones it is possible to rank these units in terms of their internal heterogeneity. Both increased and decreased heterogeneity is documented with high reservoir quality in different wireline measurements, this can be related to underlying geological heterogeneities. Heterogeneity Logs can be used as a visual indicator of where to focus sampling strategies to ensure intrinsic variabilities are captured.

Acknowledgements

First of all many thanks go to Dr. Sarah Davies and Prof. Mike Lovell for setting up the initial project outline and for their continued support, encouragement and guidance as things needed re-developing and “tweaking” along the way – I could not have asked for two better supervisors, thank you both for allowing me to take the reins and control this most heterogeneous voyage!

This project was a NERC funded studentship (NER/S/A/2005/13367) with BG-Group plc. as CASE support. I would like to acknowledge, with thanks, all who have supported me and my project at BG-Group, special thanks go to Tim Pritchard, Kambeez Sobhani, Clive Sirju and Adam Moss for petrophysical and industrial guidance. Special thanks to Paul Wright (BG-Group) for additional reservoir specific information and ideas. Additional thanks go to the academic, clerical and technical staff (and associates) in the Geology Department of the University of Leicester for a fantastic 10 years with the most amazing group of people; particular thanks to Kip Jeffrey, Pete Harvey and Tim Brewer. Thanks to the London Petrophysical Society (LPS), especially to Mike Millar and Dick Woodhouse, for providing a warm and welcoming group that supports and nurtures young petrophysical specialists.

Through the course of my PhD studies I had two additional experience which further developed my research skills, petrophysical understandings, and general life skills; Thanks to Jeremy “Jez” Lofts, Terry Quinn and Stephen Morris for a fantastic internship at Baker Hughes INTEQ, Houston – a great opportunity to see a different side of industry, play with new data, tools and experience how everything’s bigger in Texas! To the shipboard and scientific participants of IODP Expedition 320 – thank you all for a fantastic experience, for your support and encouragement during and post expedition; notable thanks to Howie Scher, Peggy Delaney, Adam Klaus, and the various “Night-Shifters”.

There have been so many postgraduates that have passed through the department and imparted knowledge and experiences over my time in Leicester, thanks and happy memories to Becky Williams, Alex Lemon, Simon Jowitt, Dan Smith, and Ben Ellis – particular acknowledgement must go to my office mate Nick Roberts for tolerating my musical delights and the string of visitors at times! Special thanks to Andy Shore and Joanne Tudge (my fellow musketeers/5th years) for support, laughs, mini-golf and many enlightening discussions over the years. My house has been home to many writing up “waif and strays” over the years; to Rowan Whittle and Helen Crowther – thanks for showing me that writing up doesn’t have to be stressful, and to Steve Rippington for imparting your nut-belay based scientific reasoning! To “Sarah’s Angels”

Heterogeneity in the Petrophysical Properties of Carbonate Reservoirs.

(Louise Anderson, Jenny Inwood, and Sally Morgan) thank you ladies for all the encouragement, laughs and allowing me to pop-down and vent! To “House Awesome and friends”, particularly Mike Williams, Heather “Fev” Carson, and Camille Burgess; thank you guys for keeping me grounded during the last few years and reminding me of undergrad fun times.

To my Dad, John Fitch, I can never fully express my thanks and gratitude – it’s been a long and “interesting” road to this point; all your support, guidance, encouragement, nagging and faffing has helped keep me going. Ann, thank you so much for supporting me since you joined the Fitch clan – your encouragement, cooking and northern tongue will always be appreciated! To my Mum, Susan Fitch, I know you would not have understood a word of this thesis, but the depths of your love and pride are still felt. Finally I would like to thank Chris McDonald, you will never know how your unconditional support and encouragement have helped in the completion of this thesis – I hope one day that I can reciprocate if/when you join the crazy PhD wagon!

Table of Contents

	<u>Page</u>
Chapter 1: Introduction	1-1
Chapter 2: Background: Carbonate Petrophysics, a review of the key issues	2-1
Chapter 3: Overview of Reservoir Geology and Petrophysical Analysis	3-1
Chapter 4: Heterogeneity; definition, quantification and basic application to carbonate petrophysical data	4-1
Chapter 5: How To Make a Heterogeneity Log	5-1
Chapter 6: Reservoir Characterisation Using Numerical Heterogeneity	6-1
Chapter 7: Conclusions	7-1
Appendices	
References	

Chapter Contents

	<u>Page</u>
Abstract	iii
Acknowledgements	iv
Contents	vi
Chapter 1: Introduction	
1.1 Preamble	1-1
1.2 Aims and Objectives of this Study	1-3
1.3 Structure of this Thesis	1-4
Chapter 2: Background; Carbonate petrophysics, a review of the key issues	
2.1 Introduction	2-1
2.2 Carbonate Sedimentology	2-2
2.2.1 <i>Diagenetic Processes in Carbonates</i>	2-8
2.3 Key Physical Properties in Carbonate Reservoirs	2-11
2.3.1 <i>Porosity</i>	2-12
2.3.2 <i>Saturation</i>	2-13
2.3.3 <i>Permeability</i>	2-16
2.3.4 <i>Capillary Pressures</i>	2-17
2.3.5 <i>Porosity-Permeability relationships</i>	2-20
2.4 Carbonate Petrophysical Properties – the issues	2-21
2.4.1 <i>Complex Lithologies</i>	2-23
2.4.2 <i>Porosity Systems</i>	2-29
2.4.3 <i>Archie Parameters</i>	2-43
2.4.4 <i>Diagenesis and other complexities</i>	2-48
2.5 Summary	2-55
2.6 Concluding Remark	2-57
Chapter 3: Overview of Reservoir Geology and Petrophysical Analysis	
3.1 Introduction	3-1
3.2 Panna-Mukta	3-1
3.2.1 <i>Geological Overview</i>	3-1
3.2.2 <i>The Panna-Mukta Dataset</i>	3-8
3.2.3 <i>Petrophysical Analysis of the Panna Dataset</i>	3-9
3.2.4 <i>Petrophysical Analysis of the Mukta Dataset</i>	3-14

3.2.5 <i>Comparison of Panna and Mukta Petrophysical Properties</i>	3-20
3.3 Abiod, Miskar	3-21
3.3.1 <i>Geological Overview</i>	3-21
3.3.2 <i>The Miskar Dataset</i>	3-23
3.3.3 <i>Petrophysical Analysis of the Abiod Dataset</i>	3-24
3.4 Summary	3-29
Chapter 4: Heterogeneity; definition, quantification and basic application to carbonate petrophysical data	
4.1 Introduction	4-1
4.2 Defining Heterogeneity	4-2
4.2.1 <i>Carbonate Heterogeneity</i>	4-7
4.2.2 <i>Petrophysical Heterogeneity</i>	4-9
4.2.3 <i>Geological Scales and Tool Resolution</i>	4-11
4.3 Quantification of Heterogeneity	4-14
4.3.1 <i>Characterising Heterogeneity</i>	4-17
4.3.1(a) <i>Semi-variogram Analysis</i>	4-20
4.3.2 <i>Heterogeneity Measures</i>	4-22
4.3.2(a) <i>Lorenz Coefficient</i>	4-22
4.3.2(b) <i>Coefficient of Variation</i>	4-24
4.3.2(c) <i>Dykstra-Parsons Coefficient</i>	4-26
4.3.2(d) <i>Dual Lorenz Coefficient</i>	4-27
4.3.2(e) <i>t-Tests</i>	4-29
4.4 Use of Heterogeneity Measures	4-31
4.5 Summary of Heterogeneity Measures from the Whole Reservoir Datasets	4-34
4.5 Conclusions	4-36
Chapter 5: How To Make a Heterogeneity Log	
5.1 Introduction	5-1
5.2 Heterogeneity Measures – a summary	5-1
5.2.1 <i>Lorenz Coefficient</i>	5-1
5.2.2 <i>Coefficient of Variation</i>	5-2
5.2.3 <i>Dual Lorenz Coefficient</i>	5-2
5.2.4 <i>t-Tests</i>	5-3
5.3 The Heterogeneity Log – basic principles	5-4
5.4 Offsetting the Data Windows	5-11

5.5 Normalisation	5-16
5.6 Summary of the Heterogeneity Logs for the Studies Reservoir Units	5-20
5.7 Conclusions	5-28

Chapter 6: Reservoir Characterisation Using Numerical Heterogeneity

6.1 Introduction	6-1
6.2 Carbonate Petrophysical Properties Relationships to the Heterogeneity Logs	6-1
6.2.1 <i>Shale Volume and Heterogeneity</i>	6-2
6.2.2 <i>Porosity and Heterogeneity</i>	6-3
6.2.3 <i>Permeability and Heterogeneity</i>	6-6
6.2.4 <i>Heterogeneity Logs and Petrophysical Properties: discussion</i>	6-8
6.3 Heterogeneity Zones	6-10
6.3.1 <i>D² – Generalised Distance Boundary Method</i>	6-11
6.3.2 <i>Stratigraphic Modified Lorenz (SML) Method</i>	6-15
6.3.3 <i>Comparison of D² and SML zoning methods</i>	6-18
6.3.4 <i>Heterogeneity Zones; aiding the identification of flow barriers and flow zones</i>	6-20
6.4 Reservoir Quality and Heterogeneity	6-31
6.4.1 <i>Summary</i>	6-37
6.5 Can optimal sampling strategies be identified using the Heterogeneity Log?	6-39
6.6 Summary and Conclusions	6-42
6.6.1 <i>The Heterogeneity Log and Petrophysical Properties</i>	6-42
6.6.2 <i>Heterogeneity Zones</i>	6-43
6.6.3 <i>Heterogeneity and Reservoir Quality</i>	6-44
6.6.4 <i>Optimal Sampling and Heterogeneity</i>	6-45
6.6.5 <i>Concluding Remarks</i>	6-45

Chapter 7: Conclusions

7.1 Discussion of the Hypotheses	7-1
7.2 Suggested Further Work	7-6

Appendices

A – Glossary

B – Petrophysical Analysis Methodology

 B.1 Shale Volume B-1

 B.2 Porosity B-4

Heterogeneity in the Petrophysical Properties of Carbonate Reservoirs.

B.3 Saturation	B-8
B.4 Permeability	B-14
B.5 Fluid Flow Zones	B-16
C – Supplementary Data	
C.1 Chapter 5: Offset Data Tables (Table 5.1)	C-1
C.2 Chapter 6: Reservoir Quality – Heterogeneity Plots (Figure 6.26)	C-4

Bibliography

Chapter 1. Introduction

1.1. Preamble

Exploring for a wide range of hydrocarbon reservoirs, including carbonate systems, is increasingly important in times of higher resource demand and progressively dwindling reserves. Exploration for carbonate systems is generally more difficult than siliciclastic reservoir exploration because of intrinsic heterogeneities, occurring at all scales of observation and measurement. Heterogeneity in carbonates can be associated with variable lithology, mineralogy, pore types, connectivity, facies and textures. Each of these can be related to geological processes controlling their original deposition and/or subsequent diagenesis. Many authors have provided reviews of what they perceive as the dominant problems in carbonate petrophysical evaluation which result from these highly variable rock properties (Akbar *et al.* 2001; Cerepi *et al.* 2003; Kennedy 2002; Lucia 1999).

Carbonate lithology and mineralogy can be highly variable, both vertically and horizontally through a succession. Carbonate depositional environments produce a diverse range of sedimentary facies which contain different porosity types with varying degrees of connectivity, producing complex and irregular pore networks. Minerals such as calcite, aragonite, and dolomite may co-exist within a single rock unit in varying proportions. Carbonate minerals have different stabilities and are susceptible to the many post-depositional processes of diagenesis.

Diagenesis can act to enhance or diminish reservoir properties, such as porosity and permeability, within a carbonate unit. For example, dissolution may initially increase pore volume, while subsequent cementation can either decrease pore size or result in occlusion and therefore decreased connectivity. Post-depositional processes may concentrate uncommon or “exotic” elements, such as uranium, within the mineral structure of carbonate rocks. This can drastically affect the measurement and interpretation of rock properties by traditional petrophysical analysis leading to under- or over-estimation of reservoir potential.

Carbonate porosity is generally more complex than siliciclastic porosity because of the numerous different pore types. Schemes by authors such as Archie (1952), Choquette and Pray (1970), and Lucia (1995; 1999) attempt to impose a workable classification. More recent studies reveal how the existence of dual- and tri-porosity systems can produce misleading wireline log responses that in turn introduce errors into permeability, or hydrocarbon volume calculations.

When applying standard industrial techniques developed for “simple homogeneous sandstones”, such as Archie’s Law, to calculations of saturation in carbonate reservoirs, the estimated hydrocarbon in place volumes are commonly misleading. Archie’s saturation equation uses two exponents, porosity/cementation (m) and saturation (n), which for clastic rocks can often be assumed equal to 2. Detailed core analysis suggests the cementation exponent (m) can be highly variable with different porosity types (Ragland 2002), ranging from <1 to >7 . Indeed, these exponents may be equally variable within individual pore-type classes, depending on the size and shape of pores.

Porosity-permeability relationships in carbonate reservoirs are notoriously poorly defined, although work by authors such as Lucia (1995; 2000) suggest correlations can be derived from pore type and grain size relationships. The ability to predict porosity and permeability relationships in carbonates continues to be an area of industry research interest. Reservoir zonations are often established using poro-perm features through complex statistical analysis, although traditional placement of flow zone boundaries comes down to visual assessment and an analyst’s experience and expectations.

Published literature clearly shows that detailed and specific understanding of carbonate heterogeneities will greatly advance this field of research and carbonate reservoir exploration (Akbar *et al.* 1995; Elkateb *et al.* 2003; Kennedy 2002; Nurmi *et al.* 1990), while rarely defining the term heterogeneity or trying to numerically quantify this heterogeneity throughout a reservoir. If, however, we look toward other scientific disciplines, from geographical and environmental to mathematical and computer sciences, there is a wealth of literature discussing

the definition and numerical quantification of heterogeneity. Pulling these definitions together, heterogeneity can be viewed as the spatial and/or temporal variability of a specific and individual property within a defined space and scale.

Consequently many statistical techniques have been developed and applied across the sciences to characterise and define heterogeneity in a dataset. Simple statistics and semi-variogram analysis can be used to characterise variability but do not provide a single value for cross-comparison. Heterogeneity measures, such as the Lorenz and Dykstra-Parsons coefficients (Lake and Jensen 1991), can be used to numerically quantify the variability with a data population (where zero generally shows homogeneity through to extreme heterogeneity at one). These techniques have had basic applications within the hydrocarbon industry as part of modelling protocols; however detailed application and interpretation are rarely achieved.

This research project demonstrates that developing these techniques and applying them to carbonate petrophysical data in novel ways can have further application to characterising poro-perm relationships, fluid flow zone identification and sampling strategies.

1.2. Aims and Objectives of this Study

The overarching aim of this study is to investigate numerical heterogeneity in terms of petrophysical properties measured by wireline logs in carbonate reservoirs. A selection of heterogeneity measures and other statistical techniques are studied, and these are developed and modified toward achieving this aim.

Initially this research provides a comparative study of the different heterogeneity measures by applying them to a variety of reservoir units. The benefits and weaknesses of each technique, and their application to different petrophysical data types, exploration requirements and underlying controls are discussed. This study seeks to ascertain whether a most appropriate “fit for purpose” heterogeneity measure can be identified.

Once a best technique, or selection of techniques, is identified these are developed into a best practice for applying the technique(s) to carbonate petrophysical well-log datasets through reservoir units. Key issues for discussion focus on the scalar aspect of geological and physical property heterogeneities; at what scale should wireline heterogeneity studies be focused?; what scale of geological heterogeneity is being sampled with different wireline heterogeneity indicators?; is there an optimal scale for the investigation and quantification of numerical heterogeneity in wireline log responses?

This project tests the following hypotheses, connecting the quantification of numerical heterogeneity to reservoir characterisation:

- H1 Scale-dependent geological and physical property heterogeneities within carbonate reservoirs can be clearly defined through the integration of wireline, core and electrical borehole image data;
- H2 Numerical techniques from a range of disciplines (e.g. geology, soil mechanics, environmental science and ecology) can be used to investigate and quantify numerical heterogeneities in carbonate reservoirs;
- H3 Carbonate reservoir heterogeneity can be used to constrain poro-perm relationships, and to identify key fluid flow zones;
- H4 Numerical heterogeneity can be linked to reservoir quality in carbonates;
- H5 An improved understanding of numerical heterogeneity can be used to inform optimal sampling strategies through a reservoir succession.

1.3. Structure of this Thesis

This thesis begins by outlining important concepts in carbonate sedimentology and associated physical properties in Chapter 2 before discussing the current key issues in carbonate reservoir petrophysical exploration.

Chapter 2 investigates issues such as the impact of carbonate lithologies, porosity systems, and geochemical abnormalities on petrophysical analysis. In particular it discusses their representation in wireline and logging while drilling (LWD) responses along with more detailed discussion of application of hydrocarbon saturation estimates such as Archie's equation and situations of low / extremely high resistivity pay. In summary, chapter 2 suggests that geological and physical property heterogeneities provide an underlying cause for key problems in carbonate exploration.

Chapter 3 provides an introduction to the datasets available for this study and a summary of the reservoir geology for each example, synthesising published and industry information. A detailed petrophysical analysis is then presented, with comparisons to the established reservoir model where relevant. Some of the novel techniques identified in chapter 2 are applied here to further constrain the model.

The concept of "*heterogeneity*" is discussed in Chapter 4, utilising a comprehensive literature review across a broad range of scientific disciplines. Techniques for the characterisation and quantification of heterogeneity are described, before applying the techniques to wireline data for reservoir units identified in Chapter 3. This illustrates the basic application of these techniques and allows for comparison of the strengths and weaknesses of each technique.

A novel technique developed for this study, *the Heterogeneity Log*, is described in Chapter 5. The multi-scale insights of wireline log heterogeneity are investigated, while alternative approaches and modifications to the basic technique are discussed.

The applications of numerical heterogeneity quantification and the Heterogeneity Log to carbonate reservoir characterisation are investigated in Chapter 6. Relationships between physical properties and wireline heterogeneity are presented, and then methods for establishing heterogeneity zones are reviewed and applied to the reservoir units of this study. Connections between reservoir quality and heterogeneity are also investigated. Underlying geological features and processes are related to these findings to aid interpretations and application to the

current reservoir models. The final section of Chapter 6 determines whether numerical heterogeneity in wireline measurements can be used to ascertain optimal sampling strategies.

Chapter 7 brings together the conclusions of the previous chapters, addressing the hypotheses posed in section 1.2, before providing final conclusions and suggestions for additional work to further this study.

Chapter 2. Background: Carbonate Petrophysics, a review of the key issues

2.1. Introduction

The oil and gas industry is regularly in the world's press with comments, statements and figures stating that our hydrocarbon resources are running low with limited life expectancies (Duey 2008; Kennedy 2002; Montaron 2008b, a). Much of our current exploration efforts and techniques are focussed on relatively "simple" clastic examples where rock properties, such as sand grains, pore space and flow paths and the arrangement of reservoir / barrier systems have been well studied and documented over decades of detailed research and exploration.

Carbonates have typically had low recoveries in the past, typically much below the 35% average for all global reservoirs, and below 10% in some fractured carbonates (Montaron 2008b).

Developments are therefore key in improving oil & gas recovery.

Carbonate reservoirs contain around 60% of the world's oil and 40% of the world's gas resources (Duey 2008; Montaron 2008b, a). The largest gas reservoir in the world is found in the Middle East; the South Pars and North Field. This carbonate is thought to hold ~30% of all known gas reserves in the world (Montaron 2008b). Although the majority of hydrocarbon reserves occur in carbonate reservoirs, yet of the 32 billion barrels produced worldwide, 22 billion barrels come from clastic reservoirs (Montaron 2008a). At current exploration and consumption rates Montaron (2008a) suggests that clastic reservoirs have around 20 years of production remaining, while proven and probable carbonate reservoirs have ~80 years left.

Carbonate reservoirs will therefore become increasingly important. In 2007 the huge carbonate field, Tupi, was discovered offshore Brazil. Figures have yet to be fully published on the volume of hydrocarbon present, current estimates suggest 30,000 barrels of oil per day from an appraisal well (Burrows & Thethi 2010). This is one of the first discoveries of an "ultra deep, sub-salt carbonate territories"; it is expected that exploration of these non-traditional geological

environments will lead to the next boom with carbonate reservoir exploitation far surpassing traditional clastic examples.

This literature review provides an overview of carbonate sedimentology and related physical properties, including lithology and pore systems in particular, as a means of introducing some of the specific terms, ideas and concepts used throughout this thesis. Then the key issues and problems in the exploration of carbonate reservoirs will be reviewed, with examples from published case studies.

2.2. Carbonate Sedimentology

There are two overriding controls on carbonate sedimentation, tectonics and climate, both of which can have a drastic effect on sea level (Tucker & Wright 1990). Tectonics controls hinterland topography and river drainage which in turn controls the supply of siliciclastic material, along with regional water depths and stabilities. The presence of siliciclastic material in the environment can also have a direct effect on carbonate precipitation by biological organisms. Climate may also affect siliciclastic supply by altering drainage patterns (rainfall) and affecting water conditions, for example temperature and salinity. Changes in temperature may affect rates of carbonate precipitation from sea water, the conditions available for organisms, and other environmental factors that are important for carbonate precipitation and the growth of carbonate secreting organisms; including salinity, substrate, energy levels of the system and the presence of siliciclastic material (Moore 2001a; Nichols 2001; Tucker & Wright 1990). Carbonate rocks commonly form in warm, low energy, shallow marine environments with little or no siliciclastic supply. It is thought that over 90% of carbonate sediments found in modern environments are of biological origins under marine conditions (Moore 2001b).

The depositional settings of carbonate deposition can be divided into five broad groups recognised on the basis of their morphology; shelf (rimmed), ramp, epeiric platform, isolated platform and drowned platform (Figure 2.1).

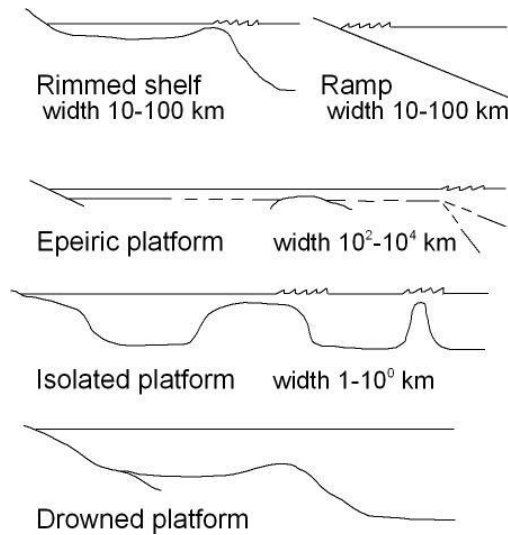


Figure 2.1. Sketches illustrating the 5 main categories of carbonate depositional settings, or platforms (adapted from Tucker & Wright, 1990).

Carbonate rocks may consist of four main minerals; low magnesium calcite and high magnesium calcite (< 4 and >4 mole% MgCO₃ respectively), aragonite and dolomite. A carbonate rock can consist completely of a single mineral type or a mixture of two or more depending upon depositional and diagenetic settings.

Constituent	Description	Origins
Non-Skeletal Grains		
Ooids	Spherical coated grain of concentric calcareous laminae (cortex) and a nucleus of variable origin.	Polygenetic origins. Chemical precipitation out of agitated warm, carbonate saturated waters. Uncertain biological origins.
Oncoids	Coated grain with calcareous cortex or irregular, partially overlapping laminae, and nucleus of variable origin.	As above.
Peloids	Round, sand-sized grain of microcrystalline carbonate. No internal structure.	Commonly biological origins, as faecal pellets of marine organisms. Chemical origins as micritised grains.

Grain Aggregates	Several carbonate grains/particles bound or cemented together. Often strongly micritised.	Bound by filamentous micro-organisms, then cementation of the filaments creates a solid. Further encrustation and recrystallisation may occur.
Intraclasts	Fragments of calcareous material, clearly different to the surrounding rock.	Reworked fragments of at least partially lithified carbonate sediment. Commonly drying out of lime mud during subaerial exposure or broken reef framework.
Skeletal Grains	Whole or broken pieces of the hard body parts of organisms with a calcareous mineral structure. Varying mineralogy and microstructure.	Biological examples commonly include; Mollusc, Brachiopods, Echinoderm, Crinoids, Corals, Foraminifera, Algae, Bryzoa, and Stromatolites.
Micrite , Carbonate Mud or Lime Mud	Fine-grained calcium carbonate particles (<4µm). May appear homogeneous but generally poorly sorted grain size and shape.	Purely chemical precipitation from calcium carbonate saturated water. Breakdown of skeletal fragments. Algal / bacterial origins. Cementation (?).
Sparite	Medium- to coarse-grained calcium carbonate crystals (>4µm), often found infilling pores between grains.	Chemical precipitation from calcium carbonate-rich fluids, commonly during early stages of diagenesis.

Table 2.1. Detailing the most common components of carbonate rocks and their likely origins (Moore 2001b; Nichols 2001; Tucker & Wright 1990).

The composition of carbonate rocks can also be separated into three main components; grains, matrix and cement (Table 2.1). Carbonate grains can be subdivided into skeletal and non-skeletal groups. Non-skeletal grains include coated grains (ooids, oncoids), peloids, grain aggregates and clasts. There are a wide variety of organisms capable of producing calcareous skeletons, spines and shells, and so there is a huge variety of skeletal grain types which can be identified by their shape, size and microstructure (Table 2.1). Generally they will be named after

the organism that produced them, unless the grain is unidentifiable in this way. Transport regime and compaction are the main depositional factors controlling the orientation of grains within carbonate rocks (Tucker & Wright 1990).

The grains of a carbonate rock are commonly found within a matrix or cement, unless the rock is grain-rich (grain/clast supported). A carbonate matrix is generally composed of micrite, cement is considered sparite. Micrite is another name for carbonate mud (grains less than 4µm in size). Micrite can form by chemical precipitation or by the breakdown of larger grains/fragments (Table 2.1). A micrite matrix is commonly deposited with the grains, however it is possible to find that microbial micritisation of bioclasts and other grains occurred during burial (Tucker & Wright 1990). Sparite is commonly observed as calcite or aragonite crystals that are coarser than micrite. Sparite is generally precipitated within the sediment or rock, either during deposition or is introduced later during diagenesis (Tucker & Wright 1990).

										>10% Allochems Allochemical Rocks (I and II)		<10% Allochems Microcrystalline Rock (III)		Undisturbed Bioherm Rocks (IV)
										Sparry Calcite Cement > Microcrystalline Ooze Matrix	Microcrystalline Ooze Matrix > Sparry Calcite Cement	1-10% Allochems	<1% Allo- chems	
Volume Allochem Composition		<25% Intraclasts		>25% Intra- clasts		Intrasparrudite Intrasparite		Intramicrudite Intramicrite		Intraclasts: Intraclast- bearing Micrite		Most Abundant Allochem		Micrite: if distributed, Dismicrite; if primary dolomite, Dolomicrite
Volume ratio of fossils to pellets		>3:1		Biosparrudite Biosparite		Biomicrudite Biomicrite		Fossils: Fossiliferous Micrite		Pellets: Pelletiferous Micrite		Biolithite		
													<1:3	
<1:3		3:1-1:3		Pelsparite		Pelmicrite		Pellets: Pelletiferous Micrite						

Figure 2.2. The Folk (1959) classification for limestones (adapted from Nichols, 2001).

Carbonate rocks are classified in numerous ways depending upon their mineralogical and/or component content and distribution. Two of the most commonly used limestone classifications are provided by Folk (1959) and Dunham (1962). Folk (1959) classified limestones in terms of the nature of the main framework grains (the allochems), matrix and cement. The four main

groups of the Folk (1959) classification are sparry allochemical limestone, micritic allochemical limestone, micritic limestone and biolithite, Figure 2.2. Nichols (2001) suggests that a name from this classification scheme provides more information about the diagenetic history of the rock than the depositional processes.

Percent Allochems	Over 2/3 lime mud matrix				Subequal spar and lime mud	Over 2/3 spar cement		
	0-1%	1-10%	10-50%	Over 50%		Sorting Poor	Sorting Good	Rounded & abraded
Representative rock terms	Micrite and dismicrite	Fossiliferous micrite	Sparse biomicrite	Packed biomicrite	Poorly washed biosparite	Unsorted biosparite	Sorted biosparite	Rounded biosparite

Figure 2.3. The Folk (1962) textural maturity classification of limestones (Tucker & Wright 1990).

Depositional texture recognizable										Depositional texture not recognizable
Original components not bound together during deposition					Original components organically bound during deposition					
Contains mud (clay and fine silt-size carbonate)		Grain-supported	Lacks mud and is grain-supported	>10% grains >2mm		Boundstone	Bafflestone	Bindstone	Framestone	
Mud-supported	Less than 10% grains			More than 10% grains	Matrix-supported					
Mudstone	Wackestone	Packstone	Grainstone	Floatstone	Rudstone	Boundstone	Bafflestone	Bindstone	Framestone	Crystalline

Figure 2.4. The Dunham (1962) classification of carbonate sedimentary rocks, note that subdivision of boundstones were added to Dunham’s original scheme by Embry and Klovan (1971) (Nichols 2001).

The Folk (1962) classification builds on his previous classification by dividing limestone further into groups within a spectrum of textural maturity, Figure 2.3. Tucker and Wright (1990) suggest that this is a genetic classification system, and that its use provides an idea of the energy levels of the depositional environment as well as classification of the rock. The Folk classifications are fairly complex and so are thought more useful in a laboratory-based petrographic study (Moore 2001b).

The Dunham (1962) classification uses the fabric and nature of the matrix, grains and rock framework to categorise carbonate rocks in terms of being matrix- or grain-supported, crystalline, and/or biologically bound (Nichols 2001; Tucker & Wright 1990). This is the most commonly used and simplest classification for carbonate description (Figure 2.4). Tucker and Wright (1990) note that the significance of each carbonate class in terms of energy level is relatively clear, for example the mud-supported classes (mudstone and wackestone) clearly represent low-energy environments.

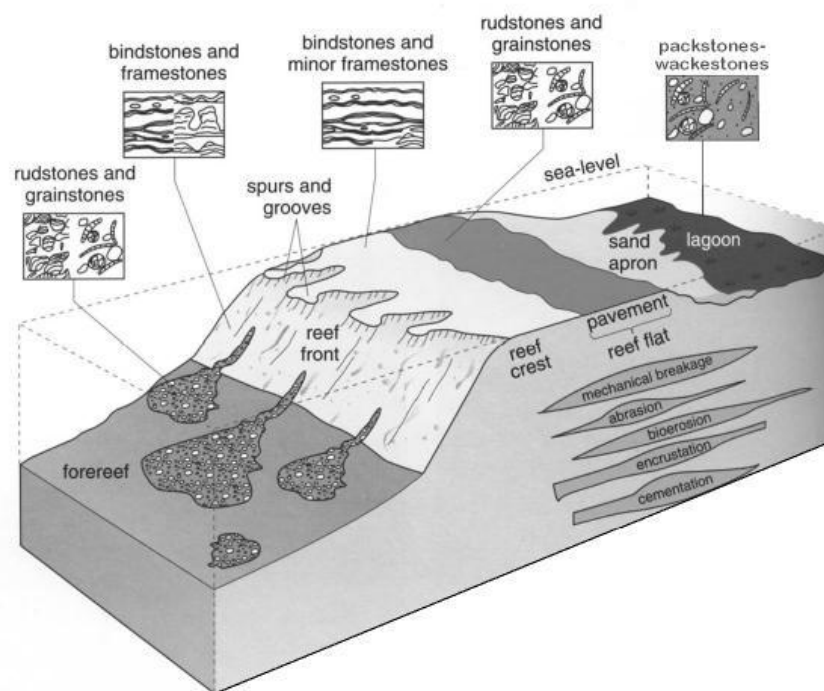


Figure 2.5. An idealised 3D block diagram of a modern coral reef (Coe 2003).

An example of how Dunham's classification can be applied to an environment of deposition, in this case a coral reef, is shown in figure 2.5. The mud-supported classes (wackestone and packstones) occur in sheltered, low energy lagoonal settings while more grain-dominated classes (packstone–rudstones) occur in higher energy environments such as the shallow reef flat and in debris flows/fans in the deeper basin. The boundstone and framestones of coral and encrusting algae are not obviously representative of a particular energy environment. Spatial variation in lithofacies architecture often reflects changes in carbonate production, which depends on changes in accommodation and/or basin-floor morphology (Pomar & Ward 1999).

In siliciclastic systems the highest rates of sediment supply occur during falling relative sea-level due to an increase in fluvial processes of erosion and transport (at this time reduced accommodation space and increased siliciclastic supply means that carbonate production is limited / shut off), whereas carbonate systems have their highest rates of sediment supply/production during rising to highstand relative sea-level (when siliciclastic input is reduced due to flooding of sources).

A facies is a body of rock with specified/distinct characteristics that formed under certain conditions of sedimentation, which indicate a particular process, set of conditions or environment (Reading 1996). Sedimentary facies can be defined in terms of grain characteristics, fossil content, and structures. In carbonate rocks grain characteristics can generally be classified by textural classifications, such as Dunham. More detailed facies can be determined using thin sections and acetate peels, these are referred to as microfacies. Facies variation can be considered to be a larger-scale variation than that of mineralogy alone. Tucker and Wright (1990) state that an individual facies will commonly be found to recur several times within a sequence and one facies may pass vertically or laterally into another facies by a change in one or several of its characteristics. The way in which one facies may pass laterally into another can be gradual (graded), sudden or be seen as inter-stratified mixing of the two. Laterally within a succession facies may be randomly arranged or repeated in regular cycles. Tucker and Wright (1990) suggest that carbonate facies should be studied at several scales during a sedimentological study to obtain maximum information

2.2.1 Diagenetic Processes in Carbonates

Diagenesis is the processes of physical and chemical changes that alter the characteristics of deposited material (Nichols 2001). The final fabric of a carbonate rock is governed by both original deposition and subsequent diagenetic processes, therefore it is suggested that any description should not focus on one classification scheme in particular. Instead Tucker and Wright (1990) suggest that we should use, for example, Dunham's classification of texture and the nature of grains and matrix with an added note about diagenesis (including bioturbation).

Diagenetic Process	Controlling Factor(s) / Environment	Effects
Calcite Carbonate Cementation	Initial Depositional Texture. Shallow marine, shallow meteoric and simple burial in water.	Decreased porosity.
Mechanical and Chemical Compaction		Grain interpenetration, breaking and deformation. Stylolites. Decreased porosity.
Selective Dissolution		Vugs (separate). Karst. Increased porosity (decreased porosity elsewhere due to precipitation).
Dolomitization	Fluid Flow (precursor permeability). Refluxing hypersaline evaporated sea water.	Dolomite overprinting. Increased particle size. Modified pore-size distribution. Replaces calcite and microporosity. Possible Vugs (separate & touching). Effects CO ₂ mud fabric more than grain fabrics.
Evaporite Mineralisation		Anhydrite and Gypsum. Pseudomorphs. Evaporite textures (poikilotopic, nodular, pore filling and bedding).
Massive Dissolution, Cavern Collapse and Fracturing	Exploitation of precursor diagenetic fabrics and Fluid Flow.	Various porosity and permeability changes. Fracture enlargement. Cavern formation. Karsts. Touching vug porosity. Collapse breccia.

Table 2.2. Carbonate diagenetic processes, controlling factors and key effects (Akbar *et al.* 2001; F.J. Lucia 1999, 2000a; Moore 2001a; Nichols 2001; Tucker & Wright 1990).

Carbonate rocks are well known for their limited chemical stabilities. This means that they are often more susceptible to the chemical effects of various fluids migrating through them during their syn- and post-depositional life times. Key diagenetic processes are summarised in table 2.2, along with the known effects on the carbonate rock fabric. It is obvious from table 2.2 that diagenesis can lead to significant changes in reservoir properties throughout the life of a carbonate body.

Ulu and Karahanoğlu (1998) found that various types of porosity measurement decrease with depth, and suggest that this indicates that pores are compressed at depth due to overburden, accompanied by a decrease in the effects of dissolution. As a rock is taken deeper into the crust burial diagenesis occurs as progressive gradual occlusion of pore space by coarse cements (Ehrenberg 2004). These effects appear difficult to quantify as they are dependent on a number

of factors, from fluid changes to local environmental variations in temperature and pressure. Early hydrocarbon migration into a carbonate reservoir can inhibit later porosity loss by cementation (Alam *et al.* 1999). It is noted that this does not affect the overall decrease in porosity with depth that is seen globally in carbonate reservoirs (Ehrenberg & Nadeau 2005).

The Walker Creek field, Southern Arkansas, is characterised by stacked oolitic grainstones isolated by lagoonal carbonate muds. Here the primary porosity was preserved because of the vadose diagenetic environment during and shortly after deposition (Moore & Becker 1977). Diagenetic patterns are highly influenced by primary porosity as it controls the flow of these diagenetic fluids through the formation (Pomar & Ward 1999). In turn this interaction between primary and secondary porosity can lead to heterogeneous and compartmentalised reservoirs as seen here.

Multiple phase diagenesis has been found to greatly alter the primary porosity of coarse-grained bioclastic grainstones of the Liuhua 11-1 Field (Zampetti *et al.* 2005). Four phases of diagenesis, including marine, meteoric, burial and the formation of saddle dolomites have led to a significant increase in the porosity of these carbonate. Wilson and Evans (2002) provide examples of how porosity and permeability can be affected by the heterogeneous nature of multi-phase carbonate diagenesis (early marine, followed meteoric to burial diagenesis with localised karstification). Early marine diagenetic processes occluded porosity and permeability. These carbonates show examples of diagenesis preferentially affecting particular facies; with micritisation being most common to bioclastic and wackestone facies and marine cements dominating the marginal facies. Truncation of cements indicates that different lithologies were affected at different times. Particularly, platform top lithologies such as those seen in the buildups of onshore Kalimantan show primary intergranular porosity enhanced by secondary leeching (Wilson & Evans 2002).

Clearly diagenesis does not always lead to the enhancement of a reservoir. In an example from the Kutai Basin, Indonesia, diagenesis is clearly documented to have increased the

heterogeneous nature of this reservoir which in turn has decreased the reservoir quality by occluding primary and secondary porosities (Alam *et al.* 1999). Any porosities formed during early diagenesis, or preserved through it, are often subsequently completely filled with calcite cements.

Dolomitization is the process of replacing calcium with magnesium in a carbonate mineral (Tucker & Wright 1990). Dolomite has a higher density than calcite, sedimentological studies have suggested that this density change is associated with a change in volume that creates voids in the rock (Nichols 2001; Tucker & Wright 1990). This observation indicates that dolomitization will increase the porosity in a sample. However, Lucia (2000) suggests that dolomitization does not make porosity but mimics the porosity of the precursor lithology, and that dissolution to form vuggy porosity does not increase the overall porosity as the dissolved carbonate is precipitated locally. In fact during dolomitization only a small amount of this carbonate precipitate will actually come from the dolomitizing fluid (Lucia *et al.* 2004). Here we see that fluid flow through the sediment is a key control on the effects of dolomitization, in terms of whether dolomitizing fluids originate locally or externally.

A poor overall correlation between porosity and dolomitization is seen in facies from the southern Barents Sea carbonates (Ehrenberg 2004). Here, low porosity in some grainstones and packstones results from heavy cementation by coarse calcite spar, whereas the low porosity in wackestones and mudstones is thought to be a result of compaction and cementation of the mud matrix.

2.3. Key Physical Properties in Carbonate Reservoirs

Many of the commonly used petrophysical concepts and parameters, such as porosity, permeability and Archie's equations, were originally established for use with clastic reservoirs. Even although carbonate reservoirs differ greatly to clastic reservoirs in a variety of ways (section 2.2 and 2.4) the basic and most common petrophysical principles are still applicable and outlined below, more detail and techniques are provided in Chapter 3 and Appendix B.

$$HCIP = GRV \times \emptyset \times (N/G) \times (1 - S_w) \times FVF \quad (\text{Equation 2.1})$$

where: *HCIP* - hydrocarbons initially in place, *GRV* - gross rock volume, \emptyset – porosity, *N/G* - net to gross ratio, *S_w* - water saturation, *FVF* - Formation Volume Factor

The common equation used for estimating the amount of hydrocarbon initially in place (Tiab & Donaldson 1996) is shown above (equation 2.1). It illustrates the point that if one mistake is made in the calculation of parameters such as porosity or water saturation then it can have a major effect on calculated reserve volumes.

2.3.1 Porosity

Porosity is a measure of the potential storage volume for hydrocarbons in the reservoir. In carbonates porosity varies from 1% to 35% with dolomite typically at 10% and limestone typically at 12% (Lucia 1999). The general definition of porosity is the fraction of the bulk reservoir volume that is not occupied by solid rock, this can be expressed as equation 2.2 (Hook 2003).

$$\emptyset = \frac{V_p}{V_b} = \frac{V_p}{V_p + V_{gr}} \quad (\text{Equation 2.2})$$

Where: \emptyset = porosity, *V_b* = bulk volume of the reservoir rock, *V_{gr}* = grain volume (volume of matrix material), *V_p* = pore volume.

Porosity is controlled by the original grain shape and size distribution, but can also be affected by secondary processes involving compaction, cementation and the introduction of clay particles. There are three generic porosity types; (1) Total porosity, all the pore volume including clay bound water (CBW); (2) Connected porosity, interconnected pores including CBW; and (3) Effective porosity, connected porosity excluding CBW (Hook 2003). It is the effective porosity which has the potential to store accessible hydrocarbons, and this is particularly important when evaluating siliciclastic reservoirs.

Porosity can be determined through either visual or laboratory-based measurements.

Laboratory-based methods use a variety of techniques (such as volumetric displacement, summation of fluids and gas expansion/Boyles Law) to calculate the bulk volume of the rock and either the pore volume or the grain volume.

A number of wireline log-based interpretation methods have been developed to calculate or estimate porosity; these are detailed in appendix B. These in-situ porosity measurements can then be calibrated to core-based measurements. It is noted that core measurements may be misrepresentative of in-situ measured porosity, because of pressure/temperature differences and retardation of clays during drying processes (Hook 2003). Care should be taken, and attention drawn to suspicious values and the core analysis techniques used.

2.3.2 Saturation

Saturation refers to the fraction of pore space occupied by water (S_w) and/or hydrocarbons (S_{hc}). It can be calculated using equations 2.3 and 2.4 respectively (Serra 1986), and is expressed as a percentage or fraction.

$$S_w = \frac{V_w}{V_p} \quad \text{(Equation 2.3)}$$

$$S_{hc} = \frac{V_{hc}}{V_p} = 1 - S_w \quad \text{(Equation 2.4)}$$

Where: S_w = water saturation, S_{hc} = hydrocarbon saturation, V_{water} = volume of water, V_p = volume of pore space, V_{hc} = volume of hydrocarbons.

In most reservoirs you would expect to move from gas to oil and then into water as you travelled deeper due to their increasing density (or decreasing buoyancy). The irreducible water saturation (S_{irr}) is the percentage of water which cannot be removed from a rock without applying undue pressure and temperature (Ellis & Singer 2007), this water may be absorbed onto grain surfaces or held in small pores and pore throats by capillary pressures (covered in more detail later in this section). As detailed above we can define a total and effective porosity value. Depending on which is used we can also calculate a total and effective saturation. Care must be taken to be consistent as if effective water saturation is quoted with total porosity then the volume of hydrocarbons will be greatly overestimated (Lovell & Kennedy 2005).

In a rock that is 100% water saturated, the rock resistivity is related to the amount of water present (the porosity), the resistivity of the water, and the pore geometry (Lucia 1999). The

Formation Resistivity Factor (F) is a fundamental concept in the interpretation and analysis of resistivity wireline logs. It is the ratio of the resistivity of a completely saturated rock (100%) to the resistivity of the saturating fluid, shown below (Sundberg 1932).

$$F = \frac{R_o}{R_w} \quad \text{(Equation 2.5)}$$

Where: F = Formation Resistivity Factor, R_o = resistivity of water saturated rock,

R_w = resistivity of the saturating fluid.

The Formation Factor can be plotted against porosity (both on a logarithmic scale), and generally shows a linear correlation (figure 2.7). The gradient of the slope (m) can be related to the cementation factor used in later equations, combined with the intercept on the porosity axis (a). It can be seen that as grain shape changes from spherical to irregular m , the porosity exponent, increases from 1 to 2.

$$F = \frac{a}{\phi^m} \quad \text{(Equation 2.6)}$$

Where: a = intercept with porosity fraction axis, m = porosity exponent, F = Formation Resistivity Factor.

Equation 2.6 (Tiab & Donaldson 1996) shows the relationship of a and m to porosity. These values can therefore be used with resistivity data to calculate porosity and/or saturation using the following additional Archie equations (2.7 and 2.8 (Archie 1942)). Note that equation 2.7 is a special case in fully saturated rocks ($S_w=1$).

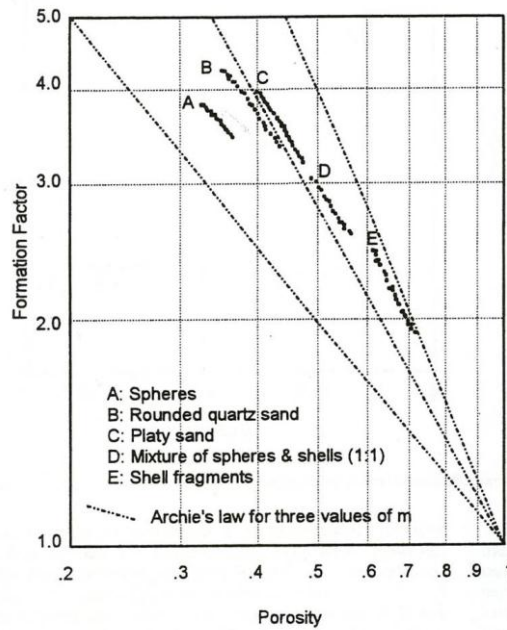


Figure 2.7. Formation factor plotted against porosity, showing the effect of particle shape on the Archie m exponents (Jackson *et al.* 1995).

Archie's equation (1).

$$R_o = R_w \times \phi^{-m} \tag{Equation 2.7}$$

Archie's equation (2).

$$R_o = R_w \times \phi^{-m} \times S_w^{-n} \tag{Equation 2.8}$$

Where: R_o = resistivity of fully water saturated rock, R_w = resistivity of saturating fluid, ϕ = porosity, S_w = water saturation, m = porosity exponent, n = saturation exponent.

Archie's Law (equation 2.9 and 2.10) is a fundamental petrophysical concept that shows the relationship between resistivity, porosity and saturation. It is an empirical equation which fits the data for many clean rocks (reservoir rocks with no shale content). The exponents a , m and n are generally considered to be constant and so can be looked up in textbooks, or preferably measured on core during special core analysis (SCAL). However in reality m and n vary greatly within carbonate reservoirs and this will be dealt with in more detail in 2.4.1. Archie assumed the tortuosity factor, a , equalled 1 however later work has shown that this can be highly variable (Winsauer *et al.* 1952).

Archie's Law.

$$R_t = a \times R_w \times \phi^m \times S_w^n \quad (\text{Equation 2.9})$$

which can be rearranged to show;

$$S_w = \sqrt[n]{\frac{a \times \phi^m \times R_w}{R_t}} \quad (\text{Equation 2.10})$$

Where: R_o = resistivity of fully water saturated rock, R_t = resistivity of partially water saturated rock ("true resistivity"), R_w = resistivity of saturating fluid, ϕ = porosity, S_w = water saturation, m = porosity exponent, n = saturation exponent.

2.3.3 Permeability

Permeability refers to how easy it is for a fluid to flow through a material (Tiab & Donaldson 1996). Permeability can be shown to be dependent on the cross-sectional area, as well as pressure changes and the viscosity of the fluid(s) involved. Permeability is a dynamic parameter (Babadagli & Al-Salmi 2004). Darcy's Law (equation 2.11) shows the relationships between these parameters. Permeability is measured in Darcies and, more commonly in the hydrocarbon industry referred to in millidarcies (mD).

$$Q = \frac{k \times A \times \Delta P}{\mu L} \quad (\text{Equation 2.11})$$

where: Q = volumetric flow rate, A = cross-sectional area, $\Delta P/L$ = pressure change over pore length (decrease), μ = viscosity of the fluid, k = permeability (constant of proportionality).

If a rock is 100% saturated with a single fluid type then it is considered to have an absolute or intrinsic permeability. Where a mixture of two or more immiscible fluids (e.g. water, gas or oil) is present in a rock, the permeability of the rock to one of the fluids is known as the effective permeability with respect to that fluid. Generally when two or more fluids are present they will interfere with each other during movement, and the sum of the effective permeabilities will be less than the absolute permeability (Tiab & Donaldson 1996). The ratio of effective permeability for one fluid to the absolute permeability is the relative permeability of the rock to that phase. As with porosity, permeability can be seen to be primary (originating from deposition) or secondary (for example from fractures). These factors can result in isotropic or

anisotropic flow paths. Darcy's Law does not work for turbulent / high velocity flow zones (for example close to the borehole) or in the presence of the Klinkenberg effect. The Klinkenberg effect refers to the slippage of gases, at low pressures, along the pore walls which causes an apparent dependence of permeability on pressure (this is especially important in low permeability rocks). A Klinkenberg correction can be applied to convert the gas permeability to a pseudo-liquid permeability.

The estimation of permeability from core analysis and in-situ permeability measurements using wellbore devices generally relies on pressure/rate relationships (Babadagli & Al-Salmi 2004). The prediction of permeability in this way is generally considered to use static information, Babadagli and Al-Salmi (2004) group these predictions into two categories of pore-scale (micro) and field-scale (macro) data or properties. Pore-scale models are based on porosity, specific surface area and tortuosity. They also consider irreducible water saturation, shale content, grain size and grain-size distribution. Permeability is primarily measured using cylindrical core plugs, oriented relative to the borehole being recorded so that any heterogeneity or anisotropy within the formation is reflected in the laboratory. Field-scale models commonly apply techniques such as Multivariable Regression Analysis (MRA) and Artificial Neural Network (ANN) to well-log data.

Permeability can be measured from wells while the reservoir pressure reduces as fluid is produced in proportion to the rate of production (Lucia 1999). This fluid transmissibility can be expressed as permeability-feet (Kh) and uses the rate of pressure change and production volumes from test intervals. Lucia (1999) suggests that pressure build ups can be used to test reservoir pressure, effective permeability and well-bore damage.

2.3.4 Capillary Pressures

The difference in pressure between two immiscible fluids (for example water and air or hydrocarbon), across a curved interface at equilibrium, is referred to as a capillary pressure (Tiab & Donaldson 1996). Capillary pressures result from the interaction of adhesive and

cohesive forces. The magnitude of these forces affects the wettability of a rock. Wettability is a measure of the preference of a rock surface to be wetted by a particular fluid phase (wetting refers to the ability of a fluid to migrate along a surface), it defines the shape and form of relative permeabilities and capillary pressure curves; and controls the distribution of fluids in the reservoir (Lovell & Kennedy 2005).

The wettability angle is the angle between a solid and a liquid meniscus. Theoretically, if the angle is greater than 90° then it is referred to as non-wetting, when the angle is less than 90° it is considered wetting. This is shown in figure 2.8, in the water wet system the adhesive forces are greater than the cohesive forces and so water moves along the pore walls trapping the oil in the centre, while in an oil wet system the opposite occurs. In reality contact angles of less than 70° indicate the fluid will preferentially wet surfaces (Tiab & Donaldson 1996).

If we think of a capillary as being a pore throat (or a simple straw) the wetting phase moves along the capillary wall because the adhesion forces between the wetting phase and the wall is greater than those of the non-wetting phase and wall (Lucia 1999). As stated above the wetting angle of the wetting fluid is less than 90° . This gives the interface between the fluids a characteristic convex shape, where the interface is seen to be convex into the wetting fluid (figure 2.9). Capillary pressure is inversely proportional to the pore throat radius (Lovell & Kennedy 2005), i.e. the smaller the pore throat radius the further the wetting phase moves into the pore throat.

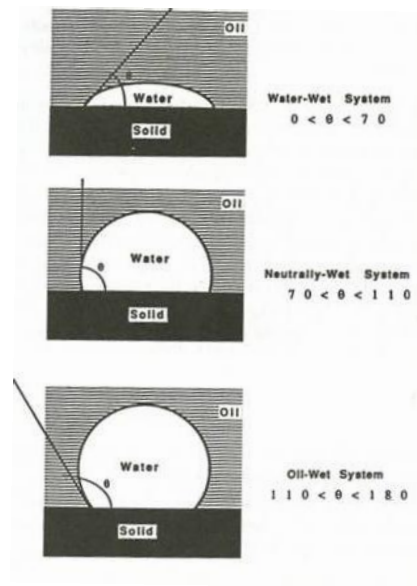


Figure 2.8. Schematic diagram of wettability in water wet and oil wet systems (Tiab & Donaldson, 1996).

Various laboratory studies (commonly mercury injection pressure, centrifuge and porous plate experiments) have been used to investigate the effect of capillary pressures on fluid movement through pores. If oil is introduced into a water-wet reservoir at first it is the larger pores which hold the oil. As buoyancy pressure increases, progressively smaller pores are penetrated by the oil as the pressure of the oil phase becomes greater than the pressure of the water phase; note that the pressure difference between oil and water is due to buoyancy/density. The radius of curvature of the oil phase therefore decreases so that it can move past the water (Lucia 1999). This continues until a point is reached when no more water (the wetting fluid) can be flushed from the system. This 'un-removable' water is referred to as the irreducible water saturation (S_{irr}). It is thought that the best reservoirs have low irreducible water saturations, along with a very short transition zone from depth where a reservoir is totally water-saturated to the depth where irreducible water saturation is first observed (Lovell & Kennedy 2005).

Capillary pressure curves can also be used to investigate pore-size distribution. These measurements of pore throats can then be related to porosity and permeability, once the data is normalised (Lucia 1999). The gradient of slopes in figure 2.10 suggests that pore throat size has a greater effect on permeability than porosity.

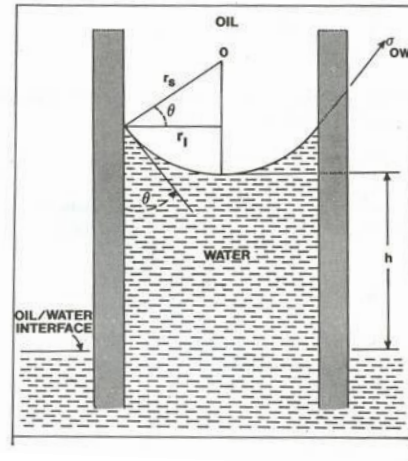


Figure 2.9. The relationship between tube radius and height of wetting fluid column for a range of capillary tubes (Tiab & Donaldson, 1996).

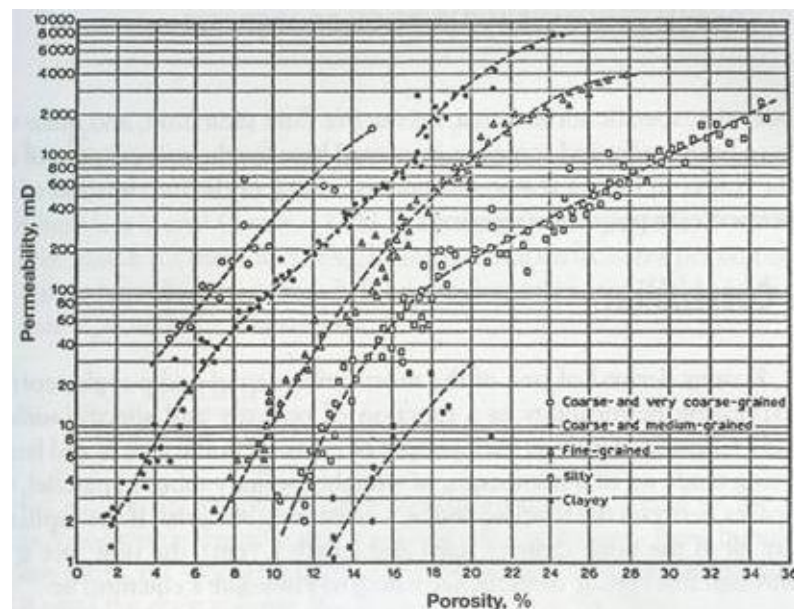


Figure 2.10. Permeability-positivity plot with pore throat size information. This example is for a siliciclastic system therefore porosity is intergranular, not total porosity (Tiab & Donaldson, 1996).

2.3.5 Porosity-Permeability Relationships

It is possible to get high porosity rocks with low or no permeability, for example pumice, shale and chalk, on the other hand it is also possible to get rocks with very little porosity and yet high permeabilities such as micro-fractured carbonates. It is generally found however that these parameters do have a correlation, for example porosity increasing with permeability (Tiab & Donaldson 1996; Lovell & Kennedy 2005). Consequently porosity-permeability relationships can be expressed as a crossplot with permeability as a logarithmic y-axis and porosity as a linear

x-axis. Typically good correlations are seen within individual formations. An example of typical porosity-permeability relationships can be seen in figure 2.11. The log-scale of permeability illustrates the large variability in permeability; it is worth noting that a small change in porosity is generally accompanied by a large change in permeability. Tiab and Donaldson (1996) comment that these porosity-permeability relationships are useful in the understanding of fluid flow through porous materials. Figure 2.11 is an example of porosity-permeability relationships in carbonate rocks. Although strong relationships are implied in this figure, in reality these trendlines are defined from a highly scattered dataset where interpretations will be highly biased on the log analyst's experience and expectations. Numerous authors urge caution in using such correlations to define porosity-permeability relationships (Akbar *et al.* 1995; Kennedy 2002).

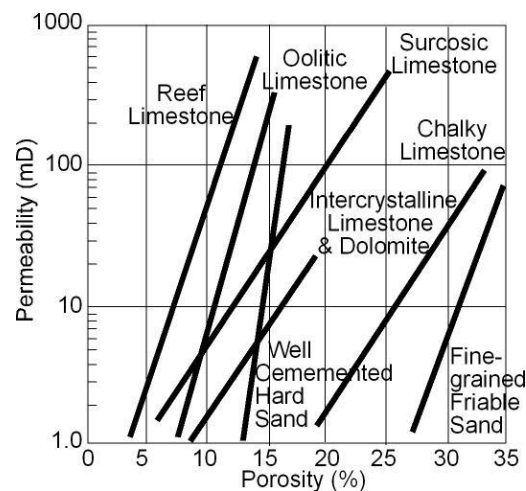


Figure 2.11. Typical porosity-permeability relationships for various rock types (adapted from Tiab & Donaldson, 1996).

2.4. Carbonate Petrophysical Properties – The Issues

*“In carbonates chaos rules at all scales.”(Akbar *et al.* 1995)*

Carbonate reservoirs are well documented for their complex internal structure, variability and spatial distribution of petrophysical properties, such as porosity and saturation. There is a large volume of literature published on carbonate reservoirs from across the world, spanning numerous geological settings and ages.

Effective exploitation of carbonate reservoirs requires knowledge of the distribution of petrophysical properties, porosity, capillarity and permeability (Lucia 2000b). The challenge in carbonate reservoirs is that a wide range of reservoir controls need to be identified and characterised before well-test results and performance histories are understood, matched and modelled (Cerepi *et al.* 2003). Akbar *et al.* (2001) add that the two classic carbonate problems are (a) matrix permeability values being immeasurably low, while fluids flow like rivers through fractures, and (b) pre-existing petrophysical models often fail on carbonate reservoirs.

The main problems with the analysis of carbonate reservoirs, outlined by authors such as Kennedy (2002), are as follows;

- Intermingled carbonate lithologies
- Different porosity systems make up the total porosity in various combinations and distributions
- Water saturation parameters (m & n) are commonly different from the established sandstone values, and these often vary throughout the reservoir
- Dry oil can be produced from rocks with high water saturation estimates (a form of low resistivity pay)
- Porosity distributions commonly encompass a wide range of values
- Miscellaneous geochemical effects can cause large errors in log analysis
- Carbonate rocks tend to be very “heterogeneous”

The majority of these problems are related to the numerous ways in which carbonate grains and matrix coexist, controlled by deposition and diagenetic processes and fabric described above. The susceptibility of carbonate minerals to chemical change once removed from, or even within, the environment of deposition means that diagenetic processes are more significant (Ahr *et al.* 2005). Carbonate reservoirs have lower median and maximum porosity values for a given depth than clastic reservoirs because of the greater chemical reactivity of carbonate minerals relative to quartz (Ehrenberg & Nadeau 2005). The prediction of permeability in heterogeneous

carbonates, from well-log data, presents a difficult and complex problem (Babadagli & Al-Salmi 2004). Porosity, permeabilities, flow zone indicators and pore-throat radii are all highly variable and are difficult to predict spatially in most carbonate reservoirs, some authors state that understanding internal architecture and geometries is key for future carbonate exploration efforts (Jennings & Lucia 2003; Moore *et al.* 1999). Key to this is integration of data, techniques and interpretations; integrating lithology, diagenesis, petrophysical and fracture modelling to describe and quantify reservoir variations at scales from seismic to pore-networks (Moore *et al.* 1999).

The following sections of this literature review bring together the various published works that detail exploration and exploitation of carbonate reservoirs, and the problems encountered, allowing an exploration of the key problems within the field of carbonate petrophysical analysis. This is a review of the key problems in carbonate petrophysical analysis, relevant to this study, rather than a discussion of new techniques and methodologies presented in the various papers cited.

2.4.1 Complex Lithologies

The basic sedimentological and petrophysical concepts outlined above provide a first look at the differences between carbonate and siliciclastic lithologies. Table 2.3 illustrates the differences in the physical properties of calcite and dolomite to quartz, and how they can be recognized in log responses.

The two end-member minerals which commonly make up carbonate reservoirs are calcite and dolomite (table 2.3). Log analysts commonly believe that carbonates are solely one or the other mineral (Kennedy 2002), however in reality carbonate reservoirs are rarely mono-mineralic, this clearly complicates well log analysis.

	Calcite	Dolomite	Quartz
Chemical Formula	CaCO ₃	CaMg(CO ₃) ₂	SiO ₂
Crystal System	Trigonal	Trigonal	Trigonal
Density (g/cm³)	2.71	2.87	2.65
Sonic Transit Time (μs/ft) [compressional slowness]	47	44	55.5
Shear Slowness (μs/ft)	88	74 (±2)	88
Thermal Neutron Capture xc	84 mb	47mb	
Thermal Neutron Scatter xc	145mb	135mb	
Uma (barn/cm³)	13.8	9	4.79
PEF	5.1	3.1	1.81

Table 2.3. The physical properties of calcite, dolomite and quartz. Note that aragonite (CaCO₃) is orthorhombic variation of calcite with a density of 2.94g/cm³. (Gribble & Hall 1999; Lovell & Kennedy 2005; Lucia 1999; Nichols 2001; Tucker & Wright 1990).

When the rock matrix is a mixture of different minerals, perhaps varying composition with depth, the identification of lithology and petrophysical modelling becomes an even more complex task (Bhattacharya *et al.* 2005). There is a 5% difference in the density of calcite and dolomite (Table 2.3). If a density of 2.6g/cm³ is recorded then the computed porosity value can be either 5% for limestone or 10% for dolomite (Kennedy 2002). This illustrates the importance of correctly identifying lithology (and hence grain density) prior to log interpretation otherwise large errors in the log-derived petrophysical parameters may occur. In terms of well-log analysis, carbonate lithology is commonly taken to be either limestone or dolomite, therefore the porosity value is most likely to be close to one of these extremes (Lovell & Kennedy 2005). It is clear that if lithology is incorrectly identified then it can have drastic effects and may produce misleading reservoir characterisation models. An added mineralogical complexity in carbonates may be present in the form an anhydrite. Underestimating the presence of this high density mineral (2.96 g/cm³) can result in an under-estimation of rock quality as anhydrite has extremely low to no porosity (Gomaa *et al.* 2006).

The photoelectric effect is related to the average atomic number of the formation. It reflects replacement of calcium by magnesium and so can be used as a measure of the degree of dolomitization (Kennedy 2002). The photoelectric factor (PEF) for pure calcite reads 5.1 barns/electron, and pure dolomite is 3.1 barns/electron (Lovell & Kennedy 2005). Cerepi *et al.* (2003) note that a PEF cut-off around 4 can be used to differentiate between limestone (>4) and dolomite (<4). PEF has a power law dependence on average atomic number and so small quantities of heavy elements, such as uranium, iron and barites, can have significant effects on this value, along with porosity and fluid type. Bhattacharya *et al.* (2005) suggest that cross plots of PEF against apparent bulk density (from wireline log measurements) can be used to analyse lithologic composition of the reservoir, figure 2.12 shows an example from a cherty carbonate.

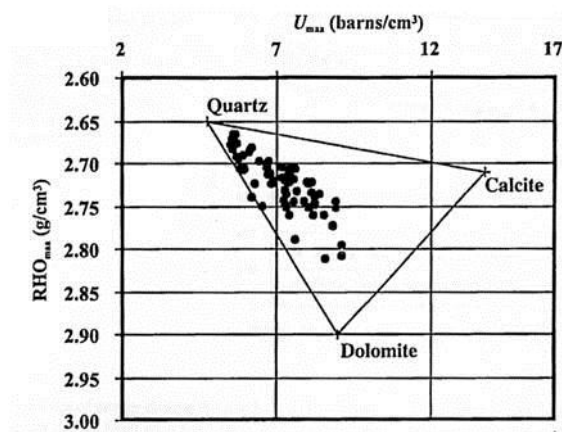


Figure 2.12. Crossplot of apparent density (RHO_{maa}) vs. volumetric photoelectric absorption of the matrix (U_{maa}) constructed using petrophysical log data, from the Mississippian interval of the Schaben field, Kansas (Bhattacharya *et al.* 2005).

Lovell and Kennedy (2005) comment that the PEF curve is typically only accurate to ± 0.3 , and that the physics of measuring PEF means it is inherently imprecise, so that a value in between the two extreme values does not relate proportionally to the volume of calcite and dolomite present. Therefore, although the PEF curve is a useful quick visual estimate of lithology it should always be used with care and the analyst should be aware of all of its pit falls.

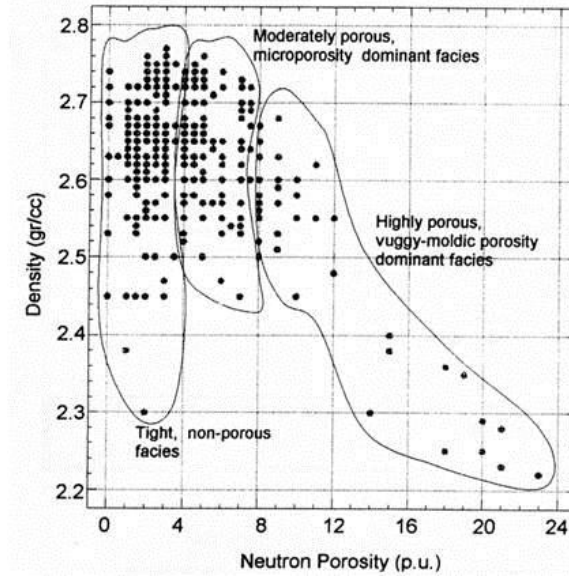


Figure 2.13. Crossplot of density and neutron porosity values obtained from well logs. Karababa-C member, Karababa Formation, Karakuş Oil Field, Turkey (Ulu & Karahanoglu 1998).

Density and neutron logs are the most useful logs for distinguishing between limestone and dolomite. The curves are often chosen so that they overlap for pure limestone (density of 2.71g/cm^3 , porosity of zero), meaning that dolomite can be easily recognised as a positive separation. Figures 2.13 and 2.14 show examples of the use of neutron-density logs as lithological indicators, following calibration to petrographic studies on core. The separation between the density and neutron logs will vary depending upon the tools used, the natural variation in dolomites around the world, environmental conditions (e.g. temperature and pressure) and the presence of light hydrocarbons masking or even reversing the separation (Kennedy 2002). As with PEF, if this separation is to be used as a quantitative measure then care should be taken.

Another problem with the use of density-neutron separation in identifying and quantifying lithology is that the density and neutron tools both have different volumes and depths of investigation. The density tool measures the scattering of gamma-rays emitted from the tool itself, and therefore has a focussed volume of investigation into the formation. Also by its nature the density tool has a shallow depth of investigation ($\sim 13\text{cm}$). The neutron tool has a larger depth of investigation ($\sim 20\text{-}15\text{cm}$), and a broad elliptical volume of investigation around the

tool. The difference in depths and volume of investigation between the density and neutron tool is not a problem in a homogeneous formation. However, carbonates are commonly highly variable and so the log analysts should be aware of this when attempting to estimate carbonate lithology in this way. Other logs that respond to lithology include gamma-ray, resistivity and acoustic measurements.

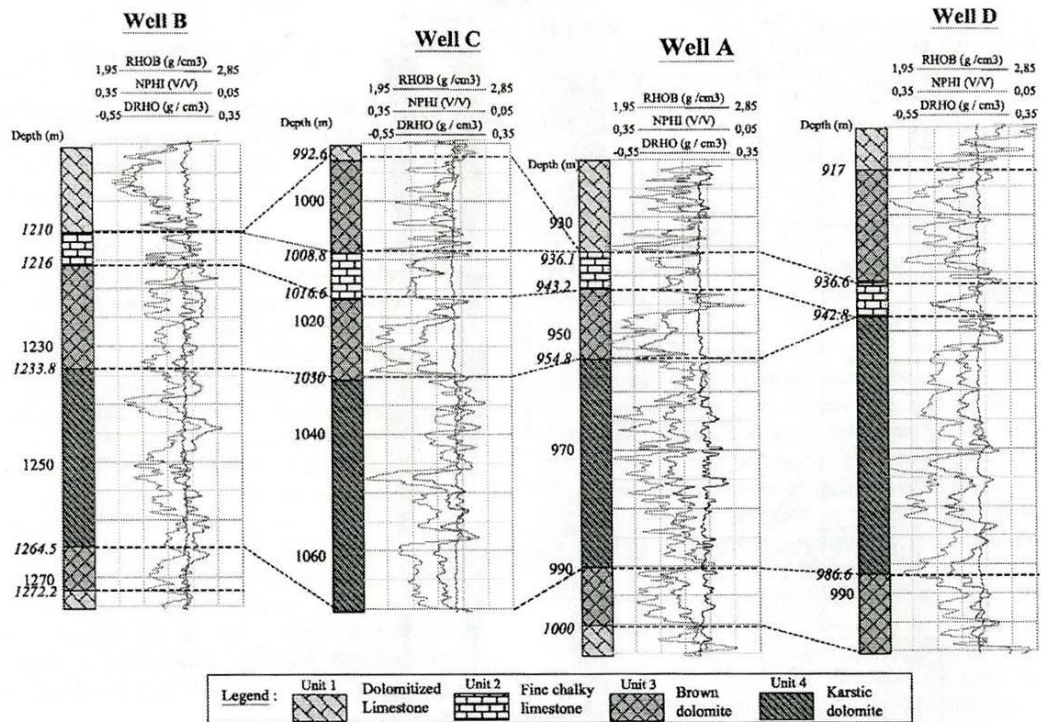


Figure 2.14. Correlation of Neutron-Density (NPHI-RHOB) log data between four wells: A, B, C and D in the Danian Lower R2 carbonate reservoir of the Aquitaine Basin, France (Cerepi *et al.* 2003).

There is a strong perception that mineralogical evaluation in carbonates is not difficult and can be accomplished with basic logs (Ramamoorthy *et al.* 2008). This can be seen to be true in some major carbonate reservoirs where lithological changes occur over significant scales (figure 2.14). However carbonate lithology can be further complicated by the presence of organic matter and anhydrite (as described for PEF measurements previously). In cases where the presence of anhydrite provides additional complication Ramamoorthy *et al.* (2008) suggest using neutron capture spectroscopy to measure sulphur concentration, providing an accurate volume of anhydrite, whilst also capturing magnesium content which can in turn be used to discriminate dolomite from calcite. A high content of organic matter and/or amorphous

cryptocrystalline silica can drastically lower the grain density of a carbonate rock from 2.71g.cm³ to around 2.48g.cm³ which would result in an overestimation of porosity, therefore care must be taken (Boya-Ferrero *et al.* 2004).

The concept of sedimentary facies in carbonate rocks is discussed in section 2.2 above. The principle that carbonate facies should be studied and compared over several scales should also be applied to the petrophysical study of carbonate rocks, especially when bearing in mind the averaging effect of a number of the downhole tool measurements at relatively low resolutions. In terms of petrophysical properties, sedimentological facies may be associated with changes in porosity, pore size distributions, densities and shale content; all of which may be identified with common log responses. However, care must be taken as in some cases (for example the presence of anhydrite or pyrite discussed previously) may result in different facies having similar log responses despite differences in pore size and connectivity (Rose *et al.* 2003).

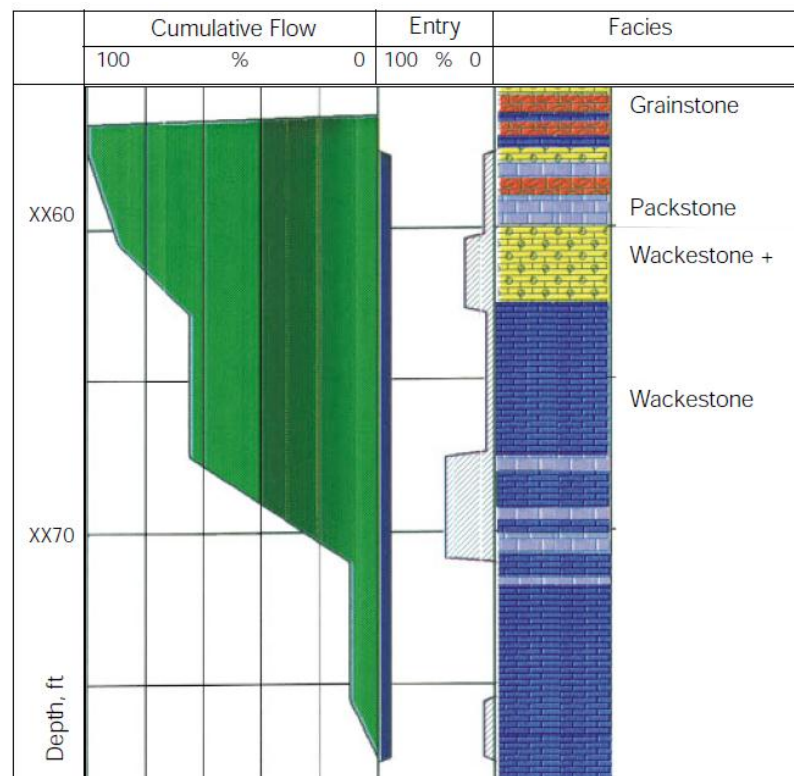


Figure 2.15. Matching well tests with Dunham style evaluation in an Indian offshore carbonate field to provide permeability values for main facies types (Akbar *et al.* 1995).

Akbar *et al.* (1995) determined a permeability value for each of the common carbonate sedimentary facies found within the studied reservoir. Figure 2.15 shows well test data and the related facies. Sections of increased cumulative flow indicate increased permeability. This data was used to provide a range of permeability values for each of the facies, indicating that grainstone and wackestone were the most permeable.

Westphal *et al.* (2004) describe how facies variation contributed to reservoir properties in a strongly diagenetically overprinted carbonate reservoir. Cyclic stacking of carbonate facies was found to be one of the main factors resulting in variations in reservoir quality. Dolostone facies with intercrystalline porosity was found to produce a good reservoir porosity and permeability. Ulu and Karahanoğlu (1998) found micritic matrix-rich facies had low primary porosities, although burial diagenesis has enhanced the porosity in places. Additionally, facies with vuggy-moldic dominated facies were found to have the best economic storage potentials, although sections containing diagenetic calcite spar cementation had decreased effective porosities.

It seems imperative that mineralogical and/or sedimentary facies are determined prior to any other petrophysical analysis; calibration to core in other boreholes within a reservoir may suffice for a well with no core recovery itself. Different lithologies and facies clearly have different properties which may require different methods and constants to be used in the derivation of further interpretations from wireline log and core analyses. The analyst must be aware of the limitations of the various tools/methods and their application to different lithologies. Clearly all available data types should be used to ensure the lithology is determined correctly.

2.4.2 Porosity Systems

Most problems in carbonate reservoir exploration are concerned with the large variation in porosity systems encountered. This is complicated further by the fact that a carbonate initially has a high porosity which it will lose gradually over a long period of time (Lucia 2000b). In carbonates porosity may increase as sorting decreases (Lucia 1999). When comparing

carbonates and sandstones Ehrenberg and Nadeau (2005) state that although both show trends of decreasing maximum porosity with depth, carbonates have lower average and maximum porosity for a given depth than sandstones, abundant low-porosity zones (<8%) can occur in carbonates but not sandstones, and that reservoirs have a greater relative proportion of high permeabilities at low porosities.

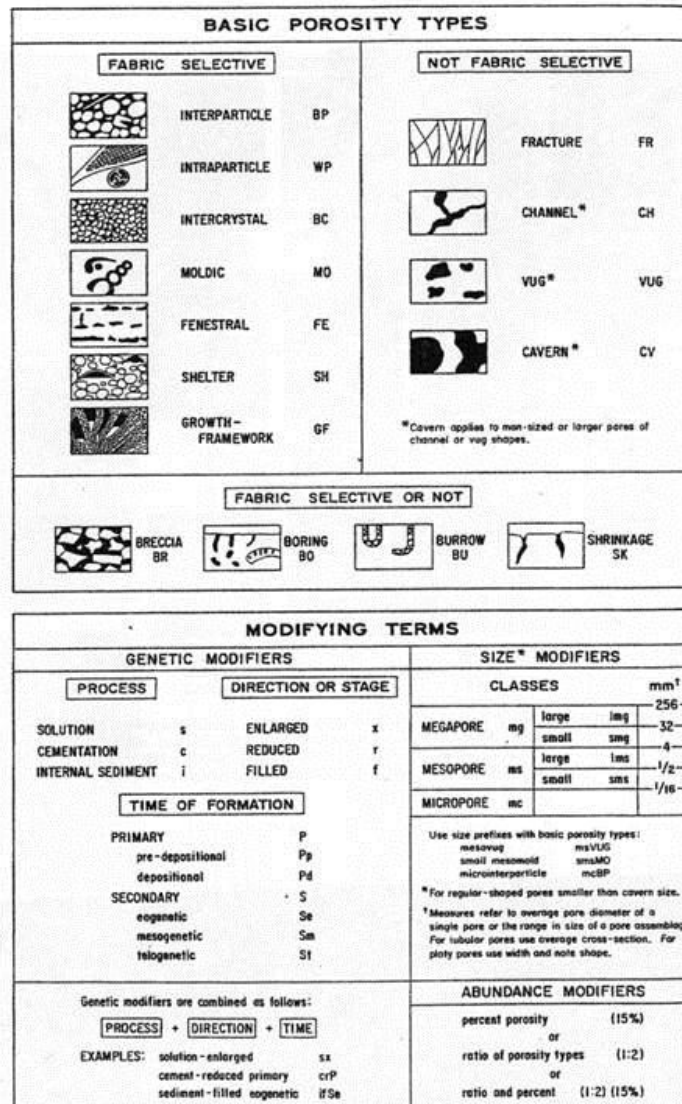


Figure 2.16. The Choquette and Pray classification of carbonate porosity (Choquette & Pray 1970).

Akbar *et al.* (2001) suggest that porosity and permeability cannot be determined properly for carbonates without understanding pore-typing and pore-size distribution. Therefore before discussing carbonate porosity it is important to detail the carbonate pore space classification

schemes that have been provided by previous research studies. The initial classification by Archie (1952) simply subdivided porosity in hand specimen into matrix and 4 classes of visible porosity (*A* – less than 0.01mm diameter, *B* – 0.01-0.1mm, *C* – 0.1-2mm, and *D* – greater than 2mm (Archie 1952)). This classification can be successfully used to estimate porosity, permeability and capillary properties but by its nature is difficult to relate to depositional and diagenetic facies/fabrics (Lucia 1995).

Choquette and Pray (1970) identify 15 basic types of porosity, figure 2.16, and emphasise the importance of pore-space formation, using a fabric and non-fabric selective class. In this classification fabric selective is where porosity and fabric elements have a dependent relationship. Lucia has demonstrated in various papers (Lucia 1999, 1995, 1983) that these porosity systems have different effects on petrophysical properties and so should be grouped separately. The Lucia classification (Lucia 1983, 1995, 1999), shown in figures 2.17 and 2.18, is composed of interparticle (grain and crystal), separate vug (e.g. moldic and intraparticle) and touching vug (e.g. fracture and solution enlarged). Separate vugs are defined as vugs that are only interconnected through interparticle network, while touching vugs form a pore system which is interconnected.

In non-vuggy carbonates the particle size, sorting and interparticle porosity can be used to describe the pore-size distribution. The relationship between mercury/air displacement pressure and average particle size for non-vuggy carbonates rocks is independent of porosity and results in a hyperbolic curve. It suggests that there is an important particle-size boundary at 100 μ m and 20 μ m (Lucia 1995; 1999; Moore 2001b; Tiab & Donaldson 1996). Lucia (1995) has shown that this can be used to produce three porosity/permeability fields around the 100 μ m and 20 μ m boundaries on a porosity-air permeability crossplot of a variety of non-vuggy limestone rocks (figure 2.19). Table 2.4 illustrates which carbonate rock/facies types can be found in each of the permeability fields, or petrophysical classes. Moore (2001b) notes that dolomite crystal size, grain size, and sorting define similar permeability fields.

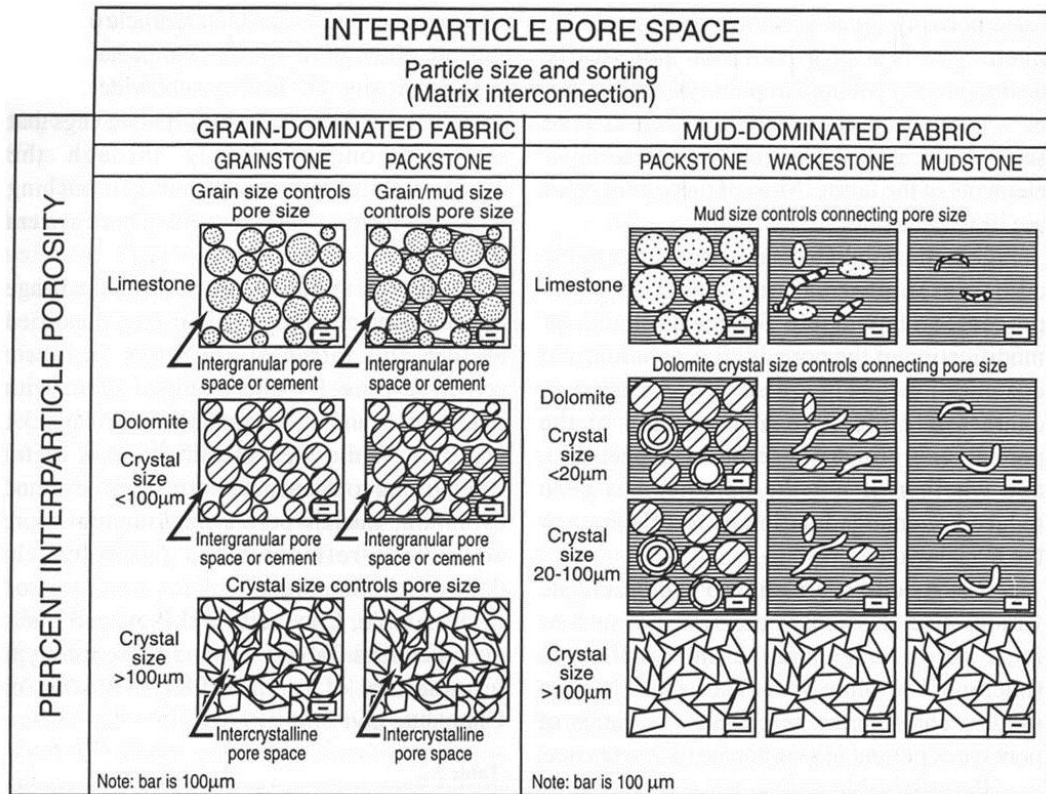


Figure 2.17. The Lucia (1995) geological and petrophysical classification of carbonate interparticle pore space (Moore 2001b).

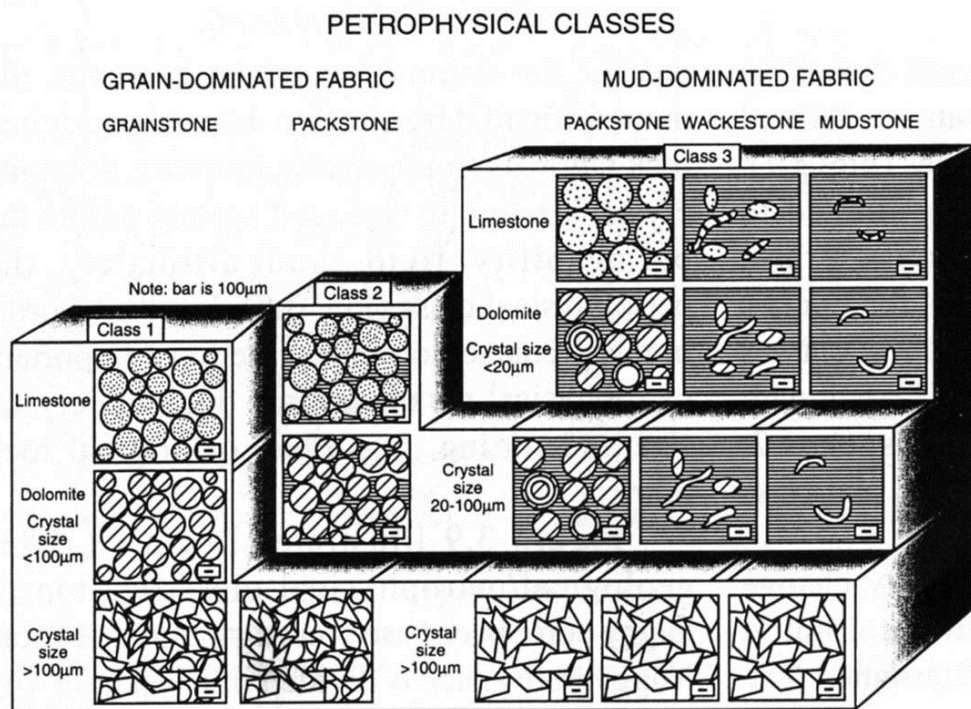


Figure 2.18. The Lucia (1995) geological and petrophysical classification of vuggy pore space, based on vug interconnection (Moore 2001b).

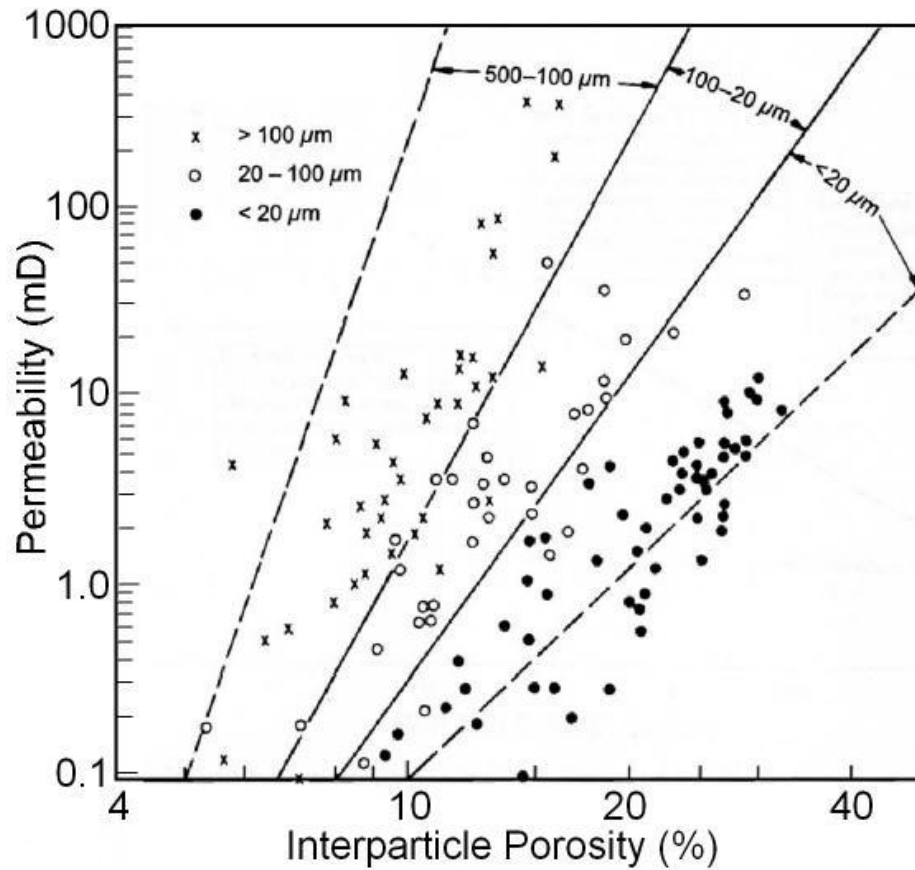


Figure 2.19. Porosity-air permeability crossplots for non-vuggy limestone rock fabrics compared with the three permeability fields; A) 400μm ooid grainstone, Ste. Genevieve, Illinois, B) Grain-dominated packstone data, Wolfcamp, west Texas, C) Wackestones with microporosity between 5μm crystals, Shuaiba, United Arab Emirates, D) Coccolith chalk, Cretaceous (adapted from Lucia, 1995).

Porosity/permeability field (petrophysical class).	Limestone	Dolomite
500-100 μm (Class 1)	Grainstones	Grainstone, large crystalline grain-dominated dolopackstone and mud-dominate dolostones
100-20 μm (Class 2)	Grain-dominated packstones	Fine- to medium-grained crystalline grain-dominated dolopackstones, and medium-crystalline mud-dominated dolostones
<20 μm (Class 3)	Mud-dominated fabrics (e.g. packstone, wackestone and mudstone)	Fine crystalline mud-dominated dolostones

Table 2.4. Illustrating the types of limestone and dolomite documented to occur in each of the permeability fields detailed by Lucia (1995; 1999).

Aguilera (2004) comments that the intersect for all lines on an expanded version of the porosity-air permeability crossplot (porosity 3.5%, permeability 0.0015md; figure 2.20) is also found in Pickett plots which he developed, for his “rock-fabric number” methodology. He also shows that if particle size is plotted against the rock-fabric number then a straight line semi-log correlation is observed (i.e. increased particle size gives a decrease in the rock-fabric number). A log-log crossplot of porosity versus true resistivity should result in a straight line for intervals with a constant rock-fabric number (Aguilera 2004).

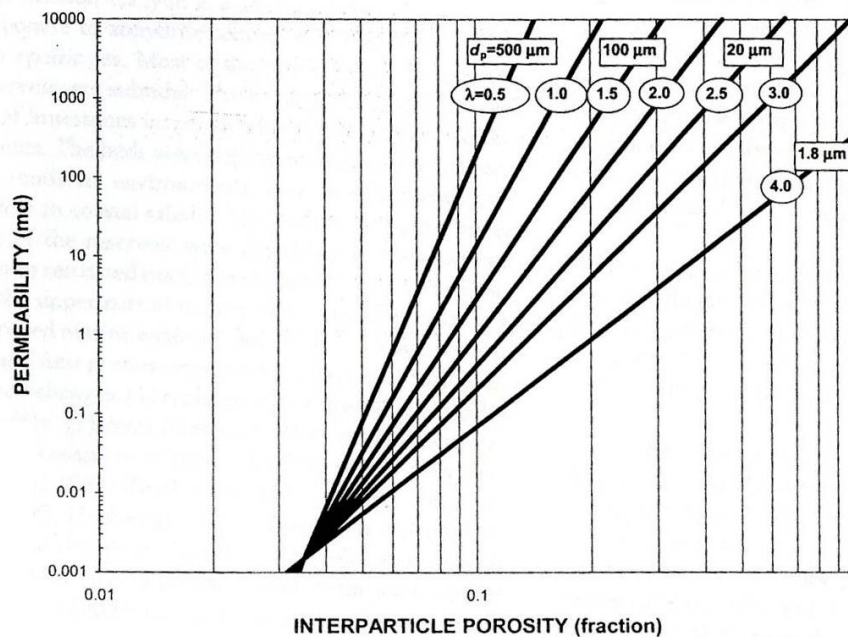


Figure 2.20. Permeability vs. porosity graph showing particle size (d_p) and rock-fabric number (λ). All lines intersect at porosity of 3.5% and permeability of 0.0015md (Aguilera 2004).

Lonoy (2006) comments that porosity cut-offs used for defining net to gross estimates for carbonate reservoir are strongly dependent upon pore-type definitions, which he feels can still be considered quite general. He has therefore developed the Choquette and Pray (1970) classification of carbonate pore types to include porosity distributions, mudstone microporosity, dividing inter- and intraparticle porosity into twelve subgroups based on pore and grain size, and finally dividing moldic pores into a micro- and macro- subgroup. Figure 2.21 illustrates Lonoy’s sub-divisions of the Lucia interparticle classes 1-3, showing improved correlation between porosity and permeability. Cut-offs derived from this new scheme provide estimated

reserves 370% higher for this Devonian field in Russia compared to a previous estimate using uniform pore size distribution pore classifications.

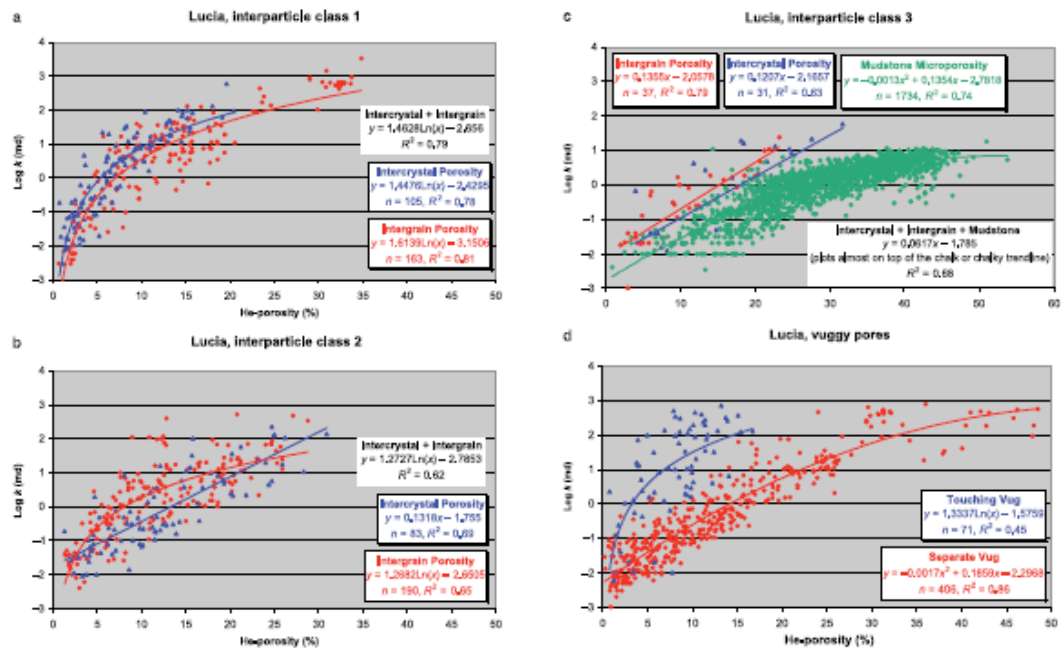


Figure 2.21. (a-c) Data from pore systems of the study plotted as Lucia interparticle classes 1-3. In these plots, the complete spread of data corresponds to the coefficient of determination shown in the black text boxes. The blue and red data points demonstrate the effects of differentiating the data into intercrystalline and intergrain pore types. The effect on the coefficients of determination is shown – indicating this distinction is based on grain size and porosity. We can also clearly see the need for including a mudstone microporosity pore type. (d) plots touching- and separate vug pore types of Lucia, these correspond to interprticle, moldic (micro- and macro-) and vuggy pores in the new scheme. For all plots the trendline yielding the highest R2 value was chosen (Lonoy 2006).

When commenting on the fact that a large proportion of carbonate reservoirs can be expected to have abundant vugs, Ehrenberg and Nadeau (2005) suggest that you would expect to see lower permeability values for a given porosity in carbonates compared to sandstones. However this has not actually been observed. It is believed that this characteristic reflects a greater incidence of fracture permeability in carbonates (Ehrenberg & Nadeau 2005). Lucia (1999) notes that carbonates have small fractures and stylolites that become flow channels in unconfined conditions which result in considerably overestimated permeability values; fractures are dealt with further in section 2.4. This suggests that carbonates (and perhaps all rock types) should always be measured at confining pressures equivalent to in situ conditions. It is also important

to remember that permeability, and indeed all petrophysical (and sedimentological) parameters, are highly variable on all scales within carbonate reservoirs.

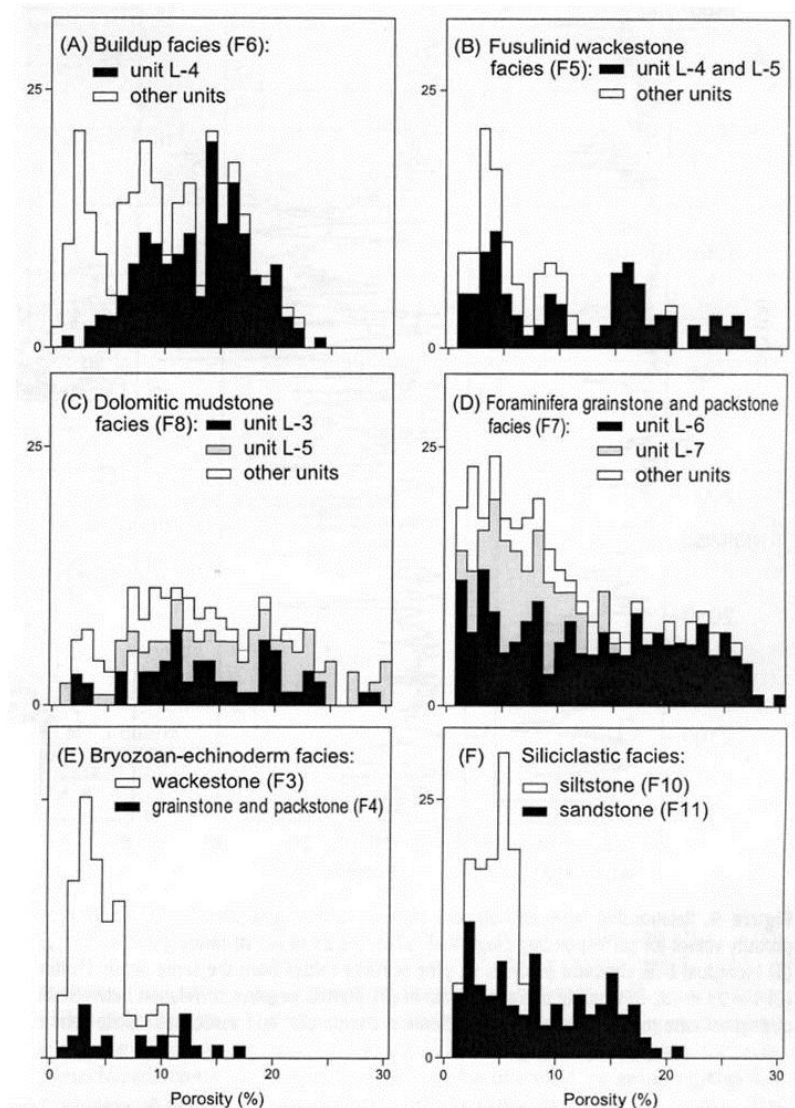


Figure 2.22. Frequency distributions of porosity in different facies categories, from core samples, comprising the Gipsdalen Group, south Barents Sea, offshore north Norway. Plugs were assigned to facies based on core descriptions and thin sections (Ehrenberg 2004).

We often find two or more porosity systems in a single carbonate reservoir. Different porosity systems often have different petrophysical properties, such as porosity-permeability relations, water saturation and Archie parameters (section 2.3). Several of the porosity types typical of carbonate reservoirs are characterised by a large range of pore sizes and shapes, which may exist as single units or link to form long conduits (Lovell & Kennedy 2005). As with lithology, porosity systems in carbonates are highly heterogeneous. Kennedy (2002) comments that

different porosity systems do not form distinct clusters on porosity-permeability cross plots and so cannot be easily recognised. This may also be true for different pore systems within the same reservoir or formation. There is potential for obtaining carbonate pore types from the NMR well log T_2 -distribution, however published results and methods are limited and not discussed in this review.

Considerable porosity and permeability variability, strongly related to facies variation, is recorded in the carbonates of the Mangkalihat Peninsula, Borneo (Wilson & Evans 2002). Here packstones and grainstones commonly have moderate to good porosity and permeability, composed primarily of intergranular and biomouldic pores, whereas the more muddy facies often have moderate biomouldic porosity with low permeabilities. Ehrenberg (2004) shows that the relative proportions of different pore types vary widely between different facies and between individual core plugs from the same facies category in studied carbonate successions from the southern Barents Sea (figure 2.22). Here, certain facies, such as the bryzoan-echinoderm facies (E), are more porosity prone in particular stratigraphic intervals. Porosity variations are easily related to lithological and facies variation within a reservoir.

Decimetre-scale porosity heterogeneities can be separated into four basic geometrical types; Layered, Interwoven, Porous Isolate, and Non-porous Isolate (figure 2.23). Nurmi *et al.* (1990) classified these, primarily, from fabrics seen in electrical borehole images. A layered geometry can be a function of depositional history (especially large-scale porosity), stratified cementation and/or selective compaction. It is usual to find that within a reservoir there are alternating layers of more and less/non-porous material. The Khuff reservoir of the Arabian platform has thin porous layers, which provide significant flow, however these are frequently not recognised because of the averaging effect of standard wireline logs (Nurmi *et al.* 1990). Layered porosity can also be seen in carbonates, such as that associated with cross-bedding in a grainstone, where the foresets will have a great effect on porosity.

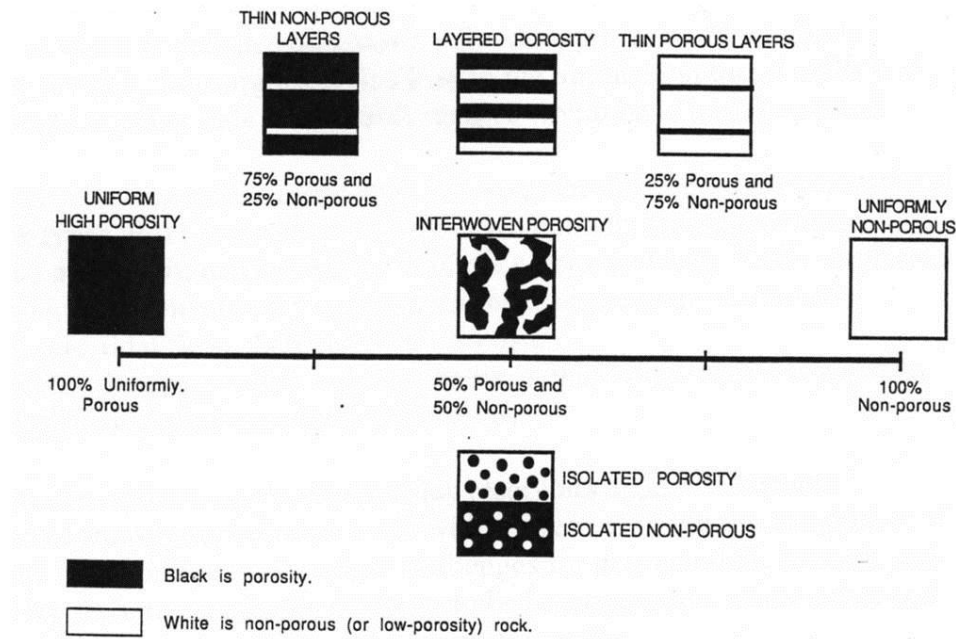


Figure 2.23. Geometric classification of decimetre-scale porosity/resistivity fabrics present in carbonate rocks (Nurmi *et al.* 1990)

Interwoven porosity is a mixture of porous and non-porous rock which occurs because of selective preservation or destruction of original porosity systems, related to diagenetic processes such as cementation and burrowing (Nurmi *et al.* 1990). Low porosity patches, such as anhydrite nodules or patchy cement distribution, may form unexpected blockages to fluid pathways. Patches of increased porosity can be remnants of intergranular/moldic porosity that have been cemented or unleached calcite patches following dolomitization. Nurmi *et al.* (1990) suggest that if such patches are connected then the reservoir capacity can be greatly improved, while if they are isolated then the reservoir potential may be lower than expected from traditional log analysis.

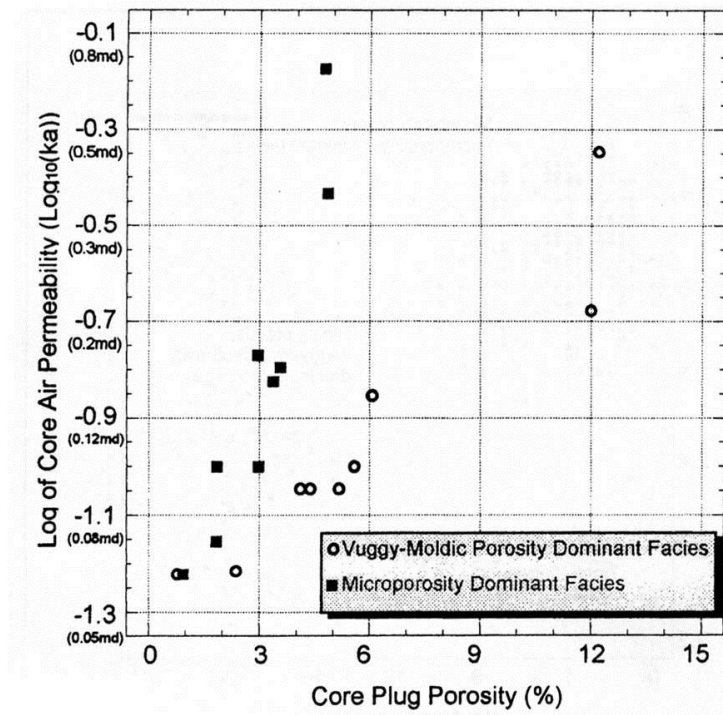


Figure 2.24. Crossplot of core plug porosity and logarithm of core plug air permeability (Ulu & Karahanoglu 1998).

The effects of isolated pore geometries are illustrated in a study by Ulu and Karahanoglu (1998), where a poro-perm crossplot of core measured values reveals two distinct trends that correspond to vuggy-moldic porosity dependent and micro-porosity dependent facies with high and low permeability respectively (figure 2.24). It can be seen that the slope of the vuggy-moldic trend is smaller than the micro-porosity trend, suggesting that even if porosity increases with vugs and moulds the permeability does not increase as much as would be expected. This may suggest that the extra vugs and moulds are isolated from the rest of the pore network.

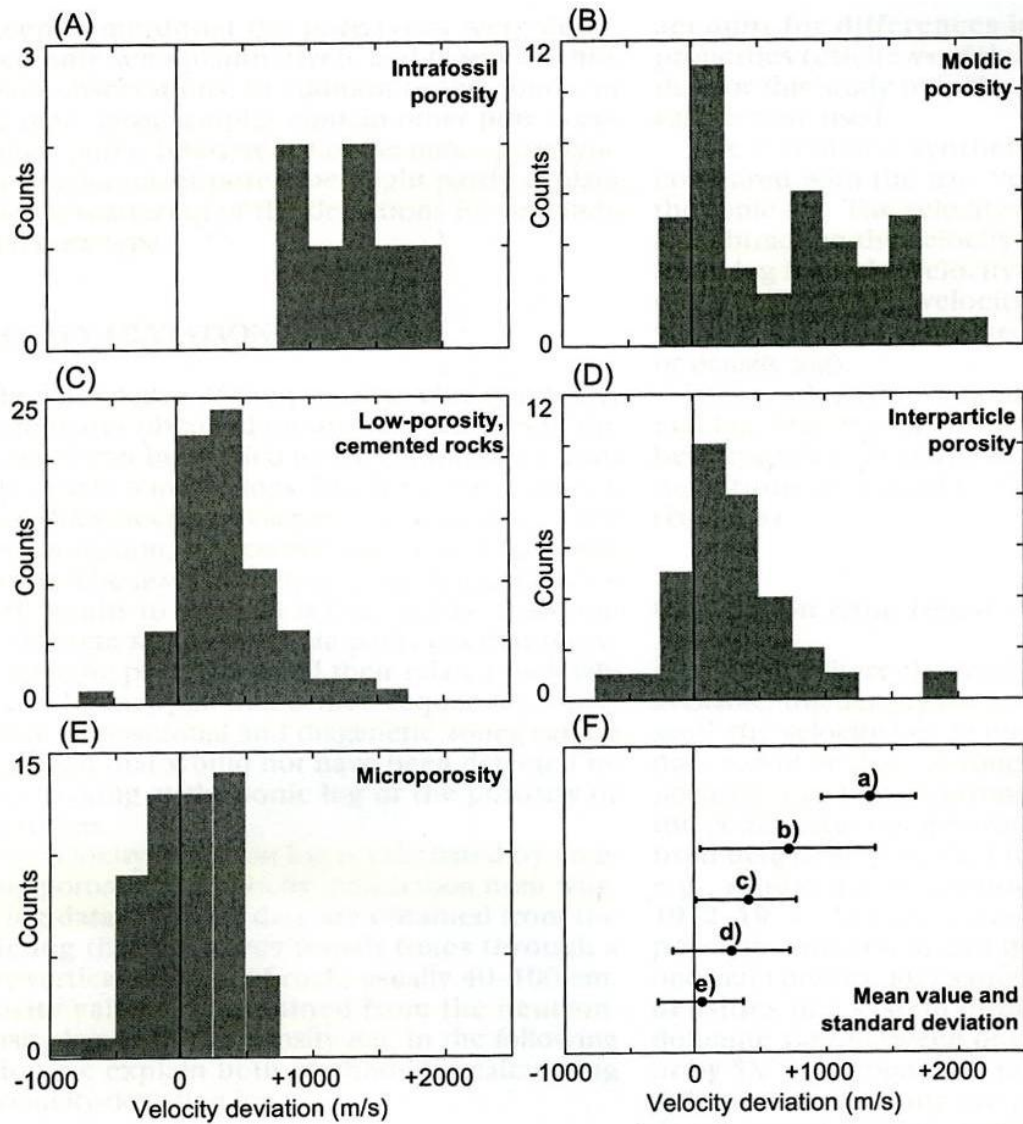


Figure 2.25. Velocity deviations of pore type categories. Porosity-velocity values of samples with zero deviation (vertical line) are exactly described by empirical time-average equation for calcite. (F) shows mean values and standard deviations of the five pore types (Anselmetti & Eberli 1999).

The porosity difference between density and sonic logs is often termed secondary porosity, and is commonly attributed to the presence of vugs and fractures which are not detected in the traditional sonic signal (Anselmetti & Eberli 1999). Nurmi *et al.* (1990) and Anselmetti and Eberli (1999) suggest that the presence of interwoven and patchy porosity fabrics, with different pore geometries can add to erroneous secondary porosity values. These effects of secondary porosity in sonic-derived porosity values can exceed 40%. Figure 2.25 illustrates that the scatter seen on most Wyllie sonic transform plots is controlled primarily by pore system and geometry. Larger scale porosity types, intrafossil and moldic, can be seen to generate larger

differences than the smaller-scale micro- and interparticle porosity types. In fact Anselmetti and Eberli (1999) comment that micro- and interparticle porosities may have negative deviation, indicating that in this case the sonic log is underestimating porosity. They believe that this positive versus negative deviation can be used to identify these two porosity subgroups downhole.

Ghafoori *et al.* (2008) state that secondary porosity is one of the main controls on flow units in carbonate reservoirs. Secondary porosity is referred to as that which is created post deposition, such as fractures, fissures and vugs. They go on to outline three subgroups of secondary porosity based on controlling processes; solution, dolomitization, and tectonic fracture porosity.

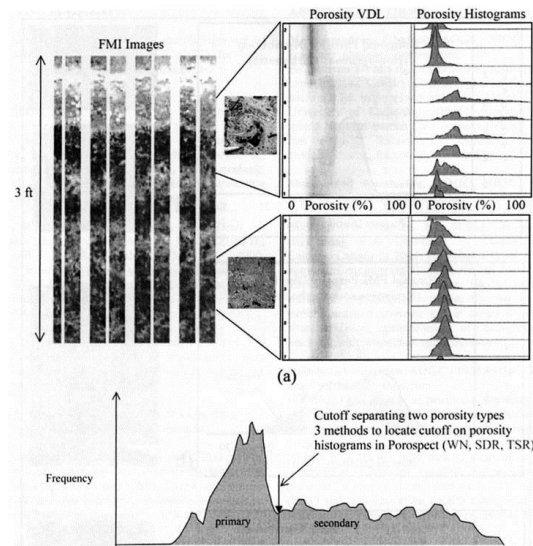


Figure. 2.26. (a) Two small intervals of FMI which are transformed into porosity domain as shown by porosity histograms and variable density display (VDL), (b) the cut-off indicates the boundary between matrix and macro secondary pores (leached pores of different origin), here the area under the high porosity tail beyond the cut-off gives the amount of macro secondary pores (Ghafoori *et al.* 2008).

The generation of secondary porosity may result in homogeneous matrix and intergranular primary porosity becoming patchy and irregular with over-printed pore networks, because of this Ghafoori *et al.* (2008) suggest the best way to choose intervals for perforation is to find zones with high secondary porosity and possible permeability, identified from combined FMI and NMR analysis (figure 2.26). The term dual-porosity should be applied to this coexistence of primary and secondary porosity (Kazatchenko *et al.* 2005). It is common that primary porosity

consists of small-scale pore type (matrix, intergranular) from original deposition, whilst secondary porosity includes larger-scale features such as vugs, channels and cracks.

Knackstedt *et al.* (2008) show that many carbonates have multi-modal pore size distributions across several decades of length scale, exhibiting pore sizes ranging from sub-micron to centimetres. Ghafoori *et al.* (2008) state that having multiple pore types with complex pore size distributions result in wide permeability variations for a single total porosity value, adding further complexities to completion strategies (figure 2.27). This highlights the existence of dual porosity systems; i.e. more than one porosity type coexisting and intermingling within one rock unit.

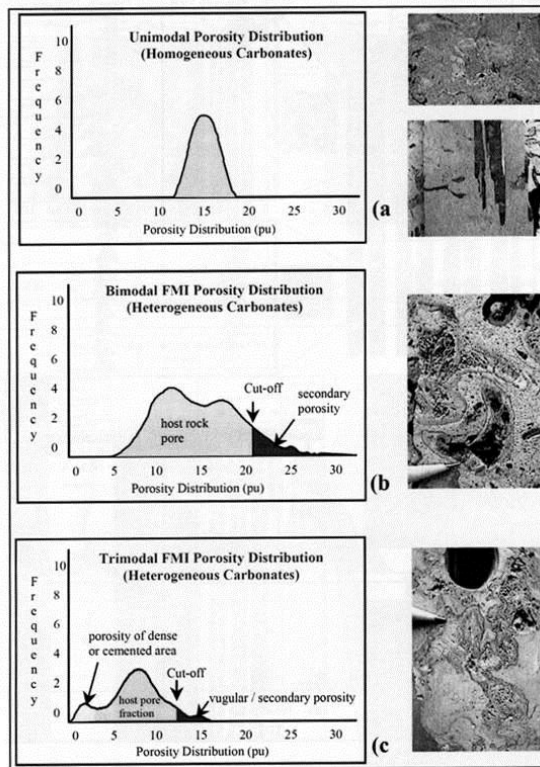


Figure. 2.27. Typical FMI porosity histogram over homogeneous (a) and heterogeneous (b & c) carbonates. Note that the secondary porosity cut-off for fractures and vugs is obtained by applying an empirical cut-off to the porosity histogram (Ghafoori *et al.* 2008).

2.4.3 Archie Parameters

The standard approach for investigating saturation and its relationship to porosity and pore geometries in the hydrocarbon industry is Archie’s law (equations 2.9 & 2.10, for more detail see section 2.2).

$$R_t = a \times R_w \times \phi^{-m} \times S_w^{-n} \tag{Equation 2.9}$$

$$S_w = \sqrt[n]{\frac{a \times \phi^m \times R_w}{R_t}} \tag{Equation 2.10}$$

Where: R_o = resistivity of fully water saturated rock, R_t = resistivity of partially water saturated rock (“true resistivity”), R_w = resistivity of saturating fluid, ϕ = porosity, S_w = water saturation, m = porosity exponent, n = saturation exponent, a = tortuosity.

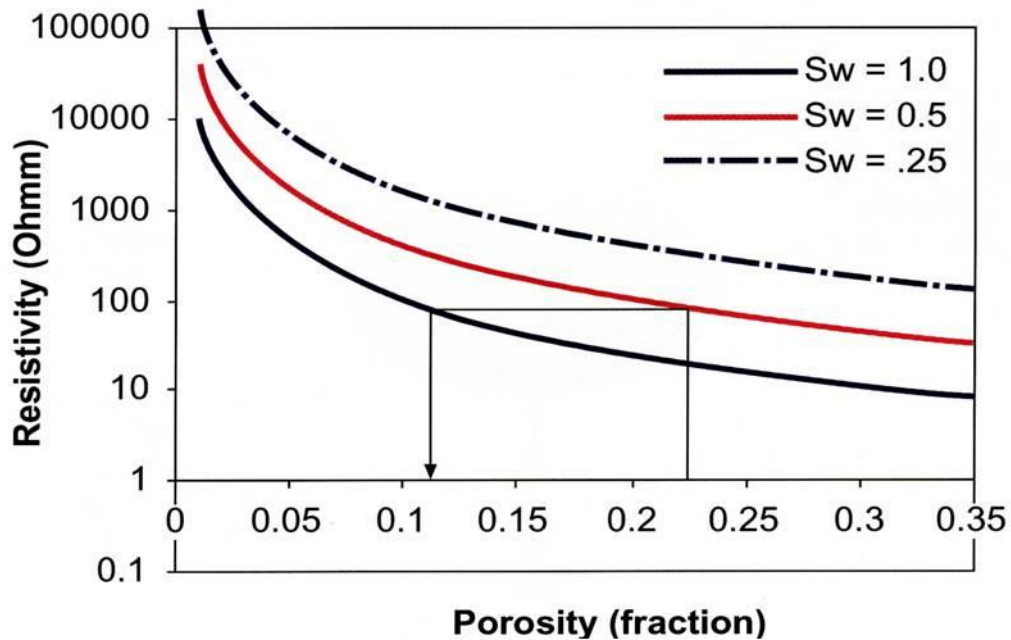


Figure 2.28. Resistivity vs Porosity plot, showing the effect of reducing water saturation from 100%, to 50% and 25% on resistivity. Archie’s equation: $a=1$, $m=2$, $n=2$ and $R_w=1$ assumed (Lovell & Kennedy 2005).

Figure 2.28 illustrates that a single resistivity value can indicate a range of porosity values depending upon the water saturation. It is clearly important to apply the correct a , m and n values. The importance of correctly interpreting lithology and, in turn, calculating porosity (and in measuring R_w from a representative pore fluid sample) is also highlighted.

Published work for many carbonate reservoirs suggests that the parameters m (the cementation or porosity exponent) and n (the saturation exponent) tend to be significantly different to the

established value of 2, used for most clastic sandstone and oolitic carbonate reservoirs. If we use a value of 2 when in fact the value is lower then the water saturation values will be calculated to be much lower than they actually are (Akbar *et al.* 1995; Akbar *et al.* 2001; Kennedy 2002). Figure 2.29 shows that as the m value increases from 2, when true water saturation is 100%, much lower saturation values are produced if the m value used is too low; it is noted that the water saturation appears to fall unexpectedly with decreasing porosity. Lovell and Kennedy (2005) suggest that this feature can be observed directly on log data, providing the analyst with a suggestion that m is lower than the true value. Watfa *et al.* (1997) suggest that the cementation exponent can vary with porosity and facies because conductive paths are influenced by different types of pores. While the saturation exponent in mixed porosity carbonate systems is a function of wettability and the saturation found in each porosity type, variations in n will occur across the oil-water transition zone in carbonate sequences (Watfa *et al.* 1997). This is thought to be due to the presence of very small micro-pores within the micritic matrix that keep the matrix water-wet, allowing an oil producing reservoir to have low resistivities similar to water-bearing formations (Akbar *et al.* 1995).

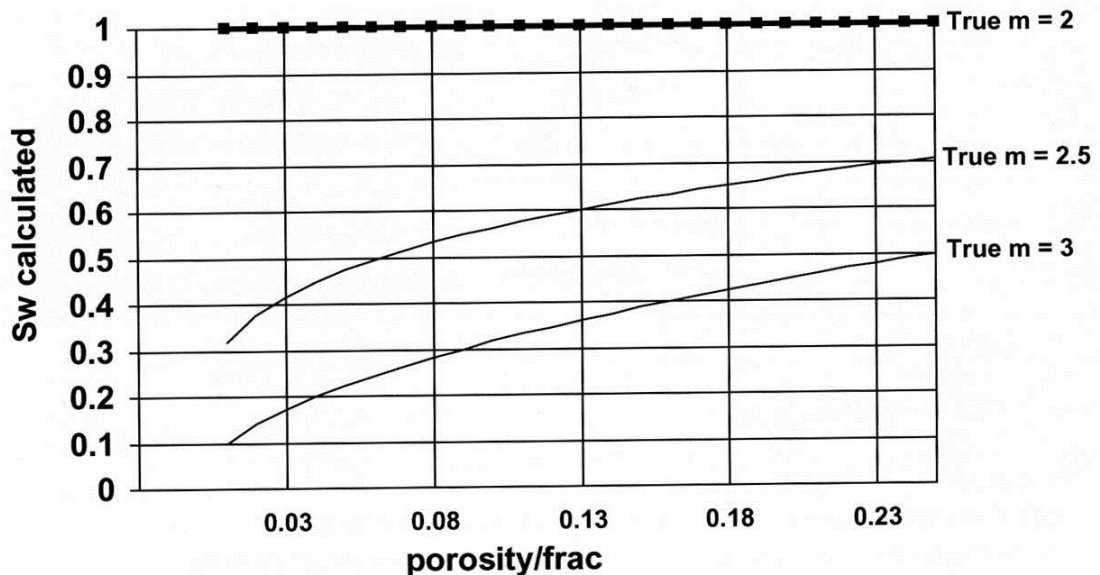


Figure 2.29. Water saturation (S_w) as a function of porosity, calculated using $m=n=2$. Actually a water-bearing reservoir, $R_w = 0.5$ Ohms (Lovell & Kennedy 2005).

Akbar *et al.* (1995) suggest that a typical m value for a fractured carbonate is found to be around 1, and that in carbonates with non-connecting vugs this can be higher than 3. Asquith (1985) provides an interesting case study from the Pennsylvanian carbonate where one log analyst used an m value of 2 and found a zone of 22% water saturation with a porosity of 24%. However a second analyst was called in to double check this and found the same zone to be wet (water-bearing). Production testing recorded only water being recovered. It was found that vuggy porosity was present within the zone, and so a cementation factor of greater than two was clearly required. Figure 2.7 shows that for unconsolidated formations (i.e. loose grains) the Archie m exponent is controlled by the shape of grains, where a perfect sphere has an m less than 1.5. Jackson *et al.* (1995) state that m is constant and approximately 2 when interparticle porosity dominates, and that it is more variable and substantially higher when porosity is moldic or vuggy. Aguilera (2004) comments that when a rock has non-touching vugs then the value of m is larger than the porosity exponent for the interparticle porosity, while m is smaller when connected vugs or fractures are present.

Ragland (2002) provides a review of m values obtained for different carbonate pore systems using laboratory-measured resistivity and porosity data, compared to thin section analysis of the pore systems. She comments that earlier attempts to derive standardised equations for the determination of m not only required some prior knowledge of rock and pore types, but the equations were often tied to well log data and were usually field- or well-specific. An average m value of 2.16 was found for moldic pore systems, ranging from 1.29 to 3.77 with an overall increasing trend with porosity volume (figure 2.30). Ragland (2002) notes that estimations of m is problematic depending upon the connectivity of moldic pores. The m values for interparticle pore systems show a similar wide range from 1.29 to 3.23, as samples may be dominated by another pore type (figure 2.31). However, Ragland (2002) comments that 1.7 to 1.9 are reasonable m values for interparticle porosity dominated systems. The m value was found to decrease from 2.21 to 1.93 with increasing intercrystalline pore volumes. Ragland (2002)

suggests that in a carbonate with abundant connected non-fabric selective dissolution pores a value of 2.0 may be appropriate, although the overall trend is unclear (figure 2.32).

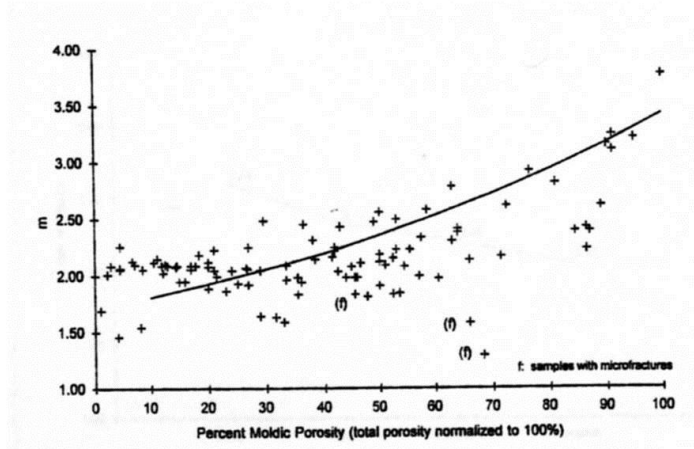


Figure 2.30. General upward trend in m values with increasing moldic porosity, 102 samples studied (Ragland 2002).

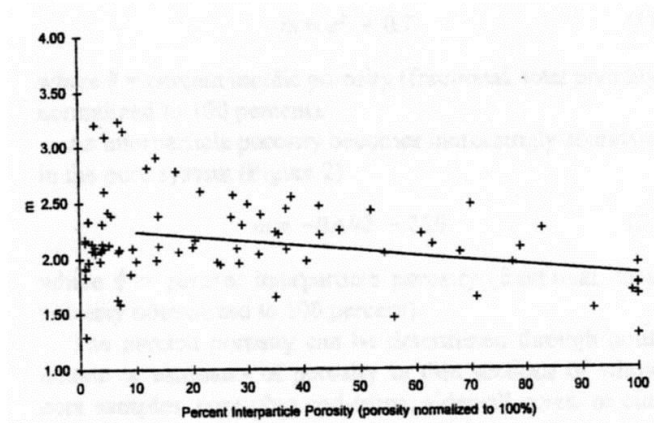


Figure 2.31. General downward trend in m values with increasing interparticle porosity, 81 samples studied (Ragland 2002).

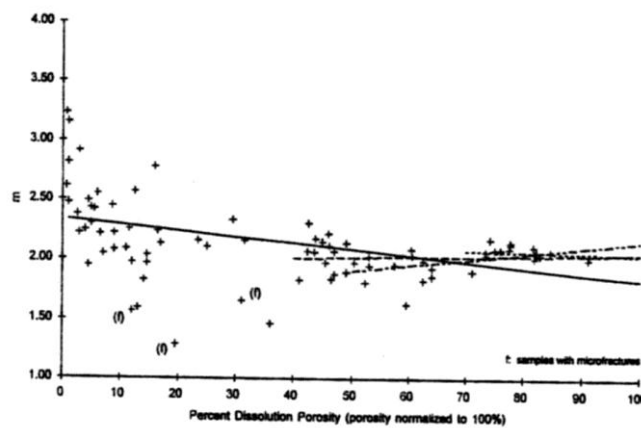


Figure 2.32. Variation in m values with increasingly connected dissolution porosity, 70 samples studied (Ragland 2002).

Figure 2.33 shows a slight downward trend in m with increasing microporosity, with an average value of 2.08 to 2.02 for systems with abundant microporosity. Ragland (2002) concludes that as pore systems become more complex, m values either decrease or increase depending upon the number of auxiliary pore types and their relative abundance.

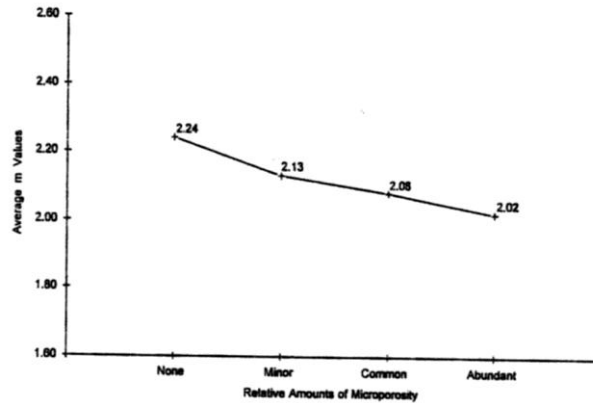


Figure 2.33. Apparent trend in average m values as microporosity increases, estimated from 4 thin sections (Ragland 2002).

As well as varying with individual pore type, several authors suggest that dual porosity systems (section 2.4.2) will influence the m and n values in carbonates. Combined experimental and theoretical studies demonstrate that many of the methods used to estimate fluid saturation in carbonate reservoirs contain great errors, which can be traced back to a poor understanding of such dual-porosity systems (Aguilera & Aguilera 2003; Kazatchenko *et al.* 2005). Kazatchenko *et al.* (2006) take this further by stating that ignoring the influence of dual porosity systems can lead to an underestimation of water saturation in vuggy formations, or overestimation in formations with cracks and channels (figure 2.35). These researchers are currently working to improve this understanding and develop more suitable techniques for saturation estimation.

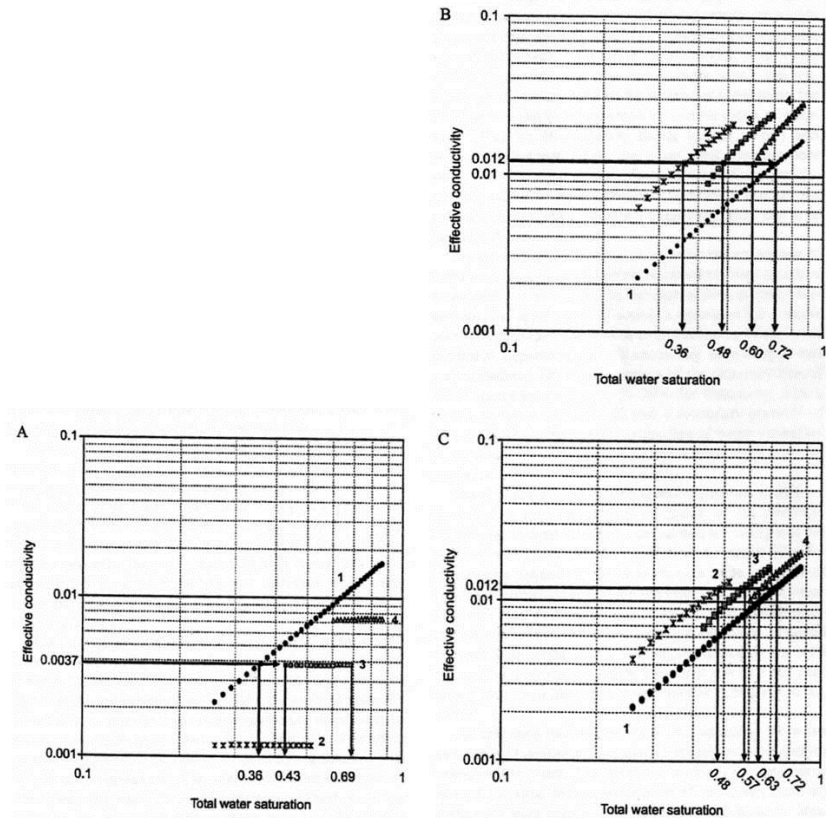


Figure 2.35. Effective electrical conductivity of media with (A) vugs, (B) cracks, and (C) channels, with different saturations of primary and secondary pores ($S_{ws} = 0.25-1$). Numbers correspond to: (1) Archie saturation exponent 1.68, with water saturation of matrix pores ($S_{wm} = 0.25$) (2), 0.50 (3), and 0.75 (4). Modelled with matrix porosity of 10%, secondary porosity of 5% and water conductivity of 1.0 Sm^{-1} . (Kazatchenko *et al.*, 2006).

The Pickett plot is commonly used to refine the parameters of the Archie equation (Bhattacharya *et al.* 2005; Asquith 1985), however it is noted that a variety of new log-based techniques are in development to further refine this understanding based on porosity-resistivity relationships (Akbar *et al.* 1995; Watfa *et al.* 1997).

2.4.4 Diagenesis and other Complexities

The processes of carbonate diagenesis were discussed in section 2.2.1. Here we review how other anomalous characteristics associated with diagenesis may impact upon traditional log analysis in carbonate reservoirs.

2.4.4(i) Key Geochemical Anomalies

Carbonates are precipitated from ionic fluids, and to be a true limestone must contain more than 50% carbonate minerals (Tucker & Wright 1990). Carbonates are documented to be highly chemically unstable, in comparison to siliciclastic examples (Nichols 2001). This precipitated nature and chemical instability, allows for the existence of co-precipitated minerals and ionic substitution in the carbonate matrix (Kennedy 2002; Nichols 2001; Reading 1996; Tucker & Wright 1990). The most common example is the replacement of calcium ions by uranium. This uranium will result in an increase in the gamma-rays emitted and so may mask the presence of a limestone if shale content is estimated only from the gamma-ray curve. 10ppm uranium in a carbonate rock can produce a gamma-ray signal similar to argillaceous or shale-rich facies (Kennedy 2002). It is important to realise that the thickness of the uranium containing interval is as important as the actual concentration of uranium in terms of the intensity of the associated gamma-ray spike (Raddadi *et al.* 2005).

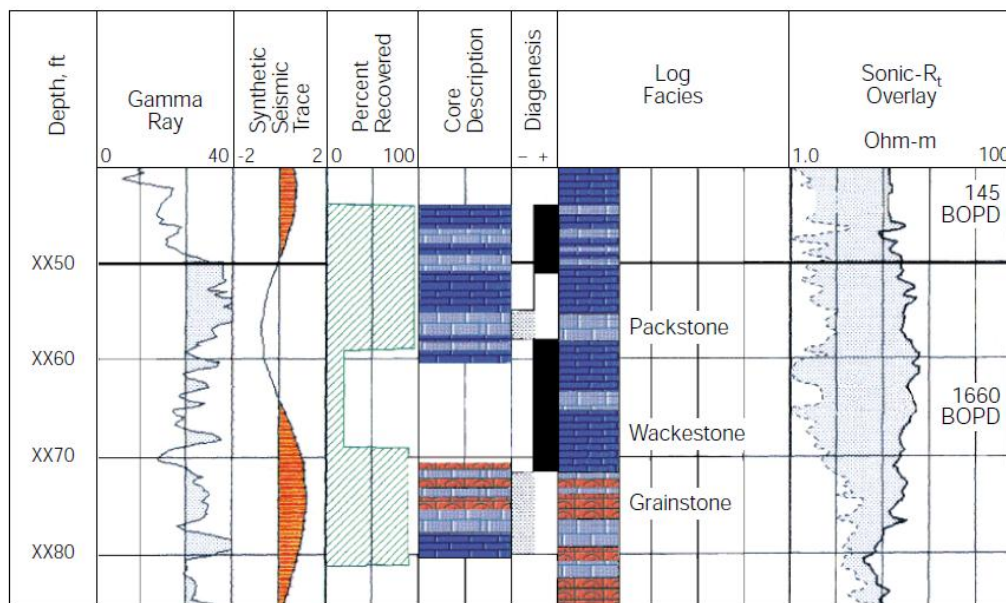


Figure 2.36 An example facies interpretation using statistical calibration between log data and petrologic analysis from cores in an offshore carbonate field, India. This calibration was used to allow facies to be mapped across the field using other logged wells without cores (Akbar *et al.* 1995).

On a slight side note, Akbar *et al.* (1995) comment that without electrical borehole images the mapping of carbonate facies between boreholes using gamma ray signatures often proves

unreliable, again highlighting the importance of calibrating interpretation results with core data (figure 2.36). The use of electrical borehole images will also aid in the confirmation of whether high gamma ray signatures are due to the presence of shale.

Raddadi *et al.* (2005) suggest that care should be taken when interpreting clay-rich horizons from high uranium concentrations in carbonate rocks. Exposures in the Western Alps shows gamma-ray measurements decreasing with an increased abundance of clay, in this case uranium is concentrated at calcrete-rich sequence boundaries and within enriched echinoderm fragments representing maximum flooding zones (Raddadi *et al.* 2005).

2.4.4(ii) Fractures and Stylolites

An additional post-deposition feature of importance in carbonate exploration and production are fractures and stylolites. They may act to enhance or decrease reservoir potential depending upon their size, orientation and fill material (Akbar *et al.* 1995).

A fracture is defined as a discontinuity across which there has been displacement (Kearey 2001). Fractures are particularly common in carbonate rocks because of their brittle nature, relative to, interbedded, more ductile fine-grained siliciclastics (Moore 2001b). Stylolites will act as either permeability barriers or pathways, depending on whether the infill material is more or less porous than the surrounding material.

Moore (2001b) comments that while the actual amount of porosity gained from fracturing is not always clear, because of difficulty in its measurement, the benefits of fractures to ultimate reservoir production are well known. Fractures are generally considered to be permeability enhancers, indeed many carbonates rely almost exclusively on fractures to achieve production (Akbar *et al.* 1995). Pöppelreiter *et al.* (2008) provide an example where a conductive fracture network acted initially as conduit for porosity enhancing corrosive fluid, which now act as fluid pathways for production (figure 3.37).

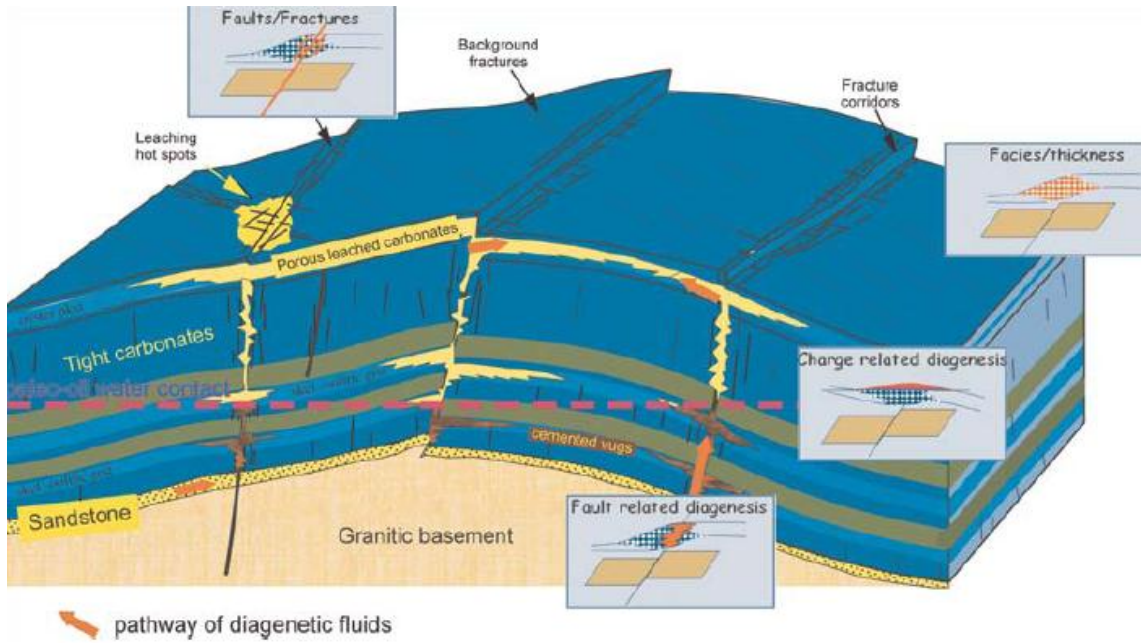


Figure 3.37. Conceptual model showing the distribution of vuggy pores and fractures in the Cogollo reservoir. The tectonic evolution plays a major role in the development of porosity (Poppelreiter *et al.* 2008).

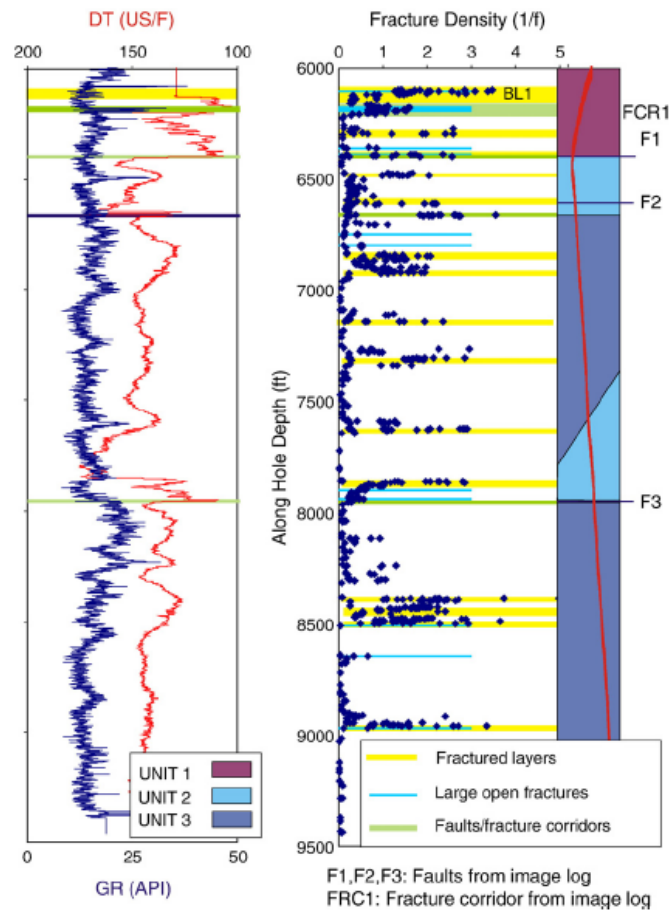


Figure 3.38. Three major faults are clearly evidenced by sharp changes in acoustic log. Fractured layers correspond to low porosity intervals. Mishref Formation, Kuwait (Ozkaya *et al.* 2007)

A fracture corridor is defined as a tabular region of intense fracturing, within which there is a dominant fracture orientation sub-parallel to the zone, these commonly occur in carbonate reservoirs rather than siliciclastic examples (Questiaux *et al.* 2010). Fracture corridors may act as major flow conduits.

It is possible to find mineralised fractures within an otherwise porous rock, here the fractures will act as significant barriers to fluid flow (Nurmi *et al.* 1990). Ulu and Karahanoğlu (1998) suggest that high deep resistivity values combined with low micro-resistivity zones correspond to tight non-fractured intervals. Ozkaya *et al.* (2007) show that faults and fractures can be identified in downhole acoustic slowness measurements, and note that fractured intervals are associated with low porosity (figure 3.38). The impact of this is that in well log analysis the high flow potential from fractures can go un-noticed, again highlighting the importance of core analysis and geological modelling.

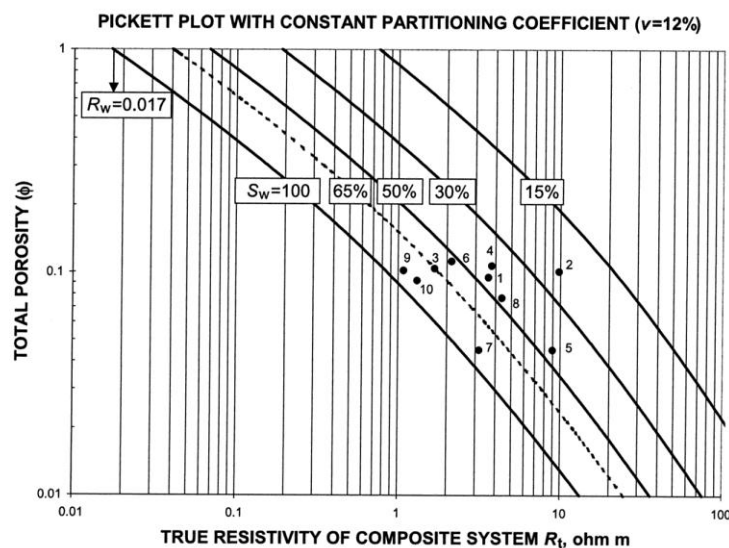


Figure 2.39. Pickett plot of total porosity vs. true resistivity of the composite system for a reservoir made up of matrix and fractures shows curved lines instead of the customary straight lines for constant values of water saturation (Aguilera 2004).

Aguilera (2004) states that fracture intensity has a major, misleading, influence on the estimation of water saturation in carbonate reservoirs using a standard porosity-resistivity Pickett plot. In weakly fractured units data points can be easily identified as fractured and

removed, however formations which are more strongly fractured show a strong downward curvature of the established porosity-water saturation relationship (away from the standard straight line) in intervals of constant water saturation (figure 2.39).

Aguilera (2006) shows high oil recovery, with decreased water saturation, in prolific low porosity reef reservoirs of Alberta. He states that natural fractures are responsible for this recovery in low porosity dolomitized carbonates, reversing the usual trend of water saturation increasing with porosity. This highlights the importance of comprehensive fracture analysis prior to petrophysical analysis leading to an improved understanding of cut-offs so that fractured, low porosity, reservoirs are not left untested (Aguilera 2006).

Stylolites form by pressure solution during compaction of the carbonate sediment, fine-grained insoluble residues become concentrated along what appear to be irregular planes of discontinuity (Nichols 2001; Akbar *et al.* 1995; Tucker & Wright 1990). Wilson and Evans (2002) have found that the distribution and spacing of stylolites varies from a few centimetres to metres. In their study of secondary porosity in FMS images, Ghafoori *et al.* (2008) identify stylolitic planes in a porous reservoir which have conductive traces, while the area around them appears resistively dense. This is thought to indicate reduction of porosity and permeability in the matrix around the stylolites, resulting in the stylolite acting as a permeability barrier. It is often possible to identify stylolites downhole based on uranium gamma spikes, resulting from concentration of uranium (leached from organic matter) by dissolving fluids (Ehrenberg 2004). Zampetti *et al.* (2005) provide a more typical example where stylolitisation during burial has lead to an increase in the porosity of the effected interval (unit E of figure 2.40), it is noted that this is part of a much more complicated diagenetic history.

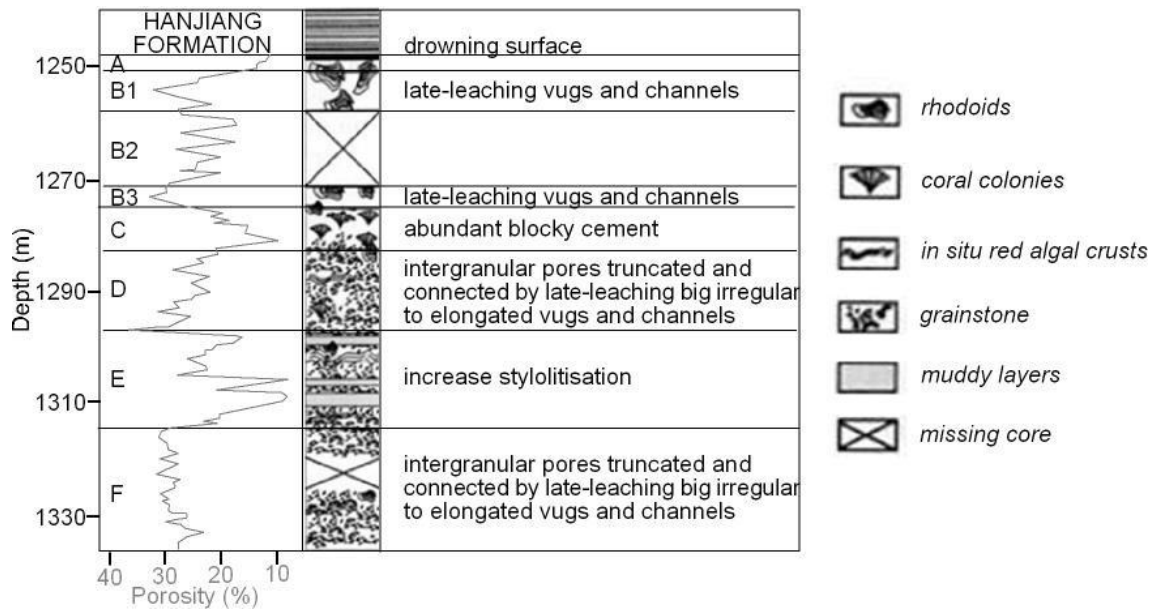


Figure 2.40. Porosity and sedimentology logs and main diagenetic events for LH11-1-4 (adapted from Zampetti *et al.*, 2005).

2.4.4(ii) Formation Fluids

Formation fluids with uncommon compositions (e.g. calcium chloride-rich) are often associated with carbonate units. These fluids will have different properties which may drastically affect the log response if the fluid type is not recognised. For example CaCl-rich fluids are significantly denser than NaCl-rich fluids and can result in a 30% underestimation of porosity (Kennedy 2002). The mixing of formation brines with an external fluid at high temperatures causes major corrosion in reservoirs, which forms volumes of porosity prior to hydrocarbon emplacement (Esteban & Taberner 2003). Many carbonate reservoirs of the Middle East are known to contain varying volumes of tar or bitumen which may also have a significant effect on reservoir performance (Ramamoorthy *et al.* 2008). Tars and associated hydrocarbons will have a much lower viscosity (10-100cP) and so can seriously decrease production potential unless correctly identified and modelled, however Ramamoorthy *et al.* (2008) suggest that new NMR interpretation techniques show potential for identifying low viscosity hydrocarbons based on their hydrocarbon index. Kennedy (2002) cites an example from Western Canada where formation waters are known to be fresh water. Using neutron decay logging in these gas reservoirs was deemed unsuitable, meaning that the exploration company would lose this

valuable data type; however chemical analysis of the formation fluids showed high concentrations of boron ions which gave the waters similar properties to sodium chloride-rich fluids enabling use of neutron-decay and other standard logging tools.

2.5. Summary

- Carbonate reservoir rocks are highly variable in terms of geological components; for example grain type, mineralogy, sedimentary facies. A variety of classification schemes have been developed for carbonate rocks, application of these is dependent upon the geologist's experience and understandings although the Dunham (1962) classification is most frequently used
- Carbonate rock textures are controlled by a wide variety of depositional and diagenetic processes. These processes can be diagnosed from detailed sedimentological analysis, and will have effects on reservoir properties
- Most standard techniques used by the hydrocarbon industry in petrophysical analysis were developed on "simple" siliciclastic models, where grains are assumed to be perfect spheres with limited variability. Application to carbonate reservoirs is possible, but assumptions must be noted and correction parameters are often required
- The problems associated with the petrophysical analysis of carbonate reservoirs can be grouped into 4 groups; a) Lithological variation, b) pore types & pore distribution, c) poor constraint on water saturation parameters, and d) miscellaneous geochemical effects
- Carbonate lithologies can vary in terms of rock type (limestone, dolomite and shale content), sedimentary facies, and mineralogy (calcite, dolomite, aragonite, and associated minerals such as pyrite). While all these features can be constrained using petrophysical analysis, some signals are misleading without core calibration
 - Incorrect identification of calcite-dolomite content can lead to a 5% difference in porosity values

- Density-neutron separation lithological identification can be misleading in the presence of accessory minerals (anhydrite & pyrite) and organic matter
- Gamma ray index-based shale indicators can be incorrect in the presence of diagenetic uranium enrichment
- Different sedimentological facies may have different reservoir qualities, but have similar well log characteristics
- At least 15 basic porosity types are classified in carbonate rocks, these can co-exist at a variety of scales. These can impact on permeability and reservoir quality in different ways, and the multi-scalar aspect can be problematic for well log interpretation. Published work suggests a generic model is not feasible, quantification and calibration for individual reservoirs (and formations) is key;
 - Pore typing can be used to aid interpretation of poro-perm relationships in carbonates
 - Dual-porosity systems increase scatter in log responses
 - Secondary porosity, associated with fractures, can be hard to estimate from traditional well logs
- Water saturation parameters m and n (Archie) are shown to be highly variable with pore type and lithology. Ragland (2002) shows variability in m from 1.29 to 3.23, depending on pore type. These should be individually constrained in laboratory analysis for individual reservoirs, and formations.
- The low chemical stability of carbonate rocks means that misleading signatures can be generated in wireline log measurements, for example uranium enrichment generating shale-like gamma ray values
- Fractures and stylolites may occur as reservoir quality enhancers or limiters, depending upon their infill and orientation/prevalence. Some carbonate reservoirs rely on fracture and stylolite networks for production from otherwise isolated pore types. Combined core, well log and seismic studies aid understandings of such systems

- For example, low porosity carbonate is commonly well fractured. This results in improved reservoir potential not seen in traditional well log analysis
- Formation fluids are susceptible to alteration in carbonate reservoirs, resulting in misleading reservoir property estimation
 - Dense CaCl-rich fluids may decrease porosity estimation
 - Tar and bitumen can significantly decrease reservoir producibility

2.6. Concluding Remarks

A broad range of the key problems associated with carbonate reservoir analysis is presented. It is noted that most of the published work referenced here addresses tools and techniques developed, and in development, for dealing with the issues and problems discussed. As with siliciclastic reservoir exploration and production efforts, core calibration, outcrop analogues and full data integration are of upmost importance in ensuring improved and enhanced hydrocarbon recovery is not a myth that is never realised.

One key thread through this review has been variability, or rather heterogeneity, in physical components, chemical nature, porosity, and geological features on all scales of observation and at different intensities. However although features are regularly described as “*heterogeneous*” rarely is the term actually defined or numerically quantified. An exception to this statement is however made in terms of modelling, where variation in derived porosity and permeability values may be investigated, however techniques used here are predominantly simple and over large scales. A detailed understanding of the intrinsic scales of carbonate heterogeneity is currently missing but has the potential to aid exploration greatly.

Chapter 3. Overview of Reservoir Geology & Petrophysical Analysis

3.1. Introduction

This study uses wireline well log, electrical borehole images and core data from 3 reservoirs as its basic dataset. Petrophysical analysis will provide additional, derived, parameters such as porosity, permeability, and water-hydrocarbon saturation. To ensure a fully comprehensive study we also need an understanding of the underlying geological environment and features. This was gained from industry reports, published work and discussions with asset specific geologists.

This chapter provides an overview of the geology of each reservoir, before outlining the available data and summarising the results of detailed petrophysical analysis. The reservoirs investigated here are (1) Panna-Mukta; a heterogeneous Eocene-Oligocene carbonate reservoir located offshore India, hosting oil and gas reserves, and (2) the Abiod member of Miskar, offshore Tunisia, which is described as a homogenous chalk unit.

3.2. Panna - Mukta

3.2.1. Geological Overview – Panna-Mukta

The Panna-Mukta fields are located on the Heera-Bassein Block of the offshore Bombay Basin in central west India (figure 3.1). It is composed of Eocene-Oligocene limestones, and has a broad, low relief anticlinal trap structure. The hydrocarbon reserves comprise a 20m thick oil rim and 50m thick gas column (Khanna *et al.* 2007).

The Bombay offshore basin is a passive margin basin, split into longitudinal horst and graben stripes by a series of basement controlled NW-SE to N-S trending faults. Basin development was controlled predominantly by Early- to Mid-Cretaceous rifting, associated with the

subsequent opening of the Arabian Sea (Naik *et al.* 2006). Associated with this was the extrusion of the Decan Trap lavas from Late Cretaceous, into the Palaeocene, covering the basin with basaltic lavas (Goswami *et al.* 2007). This rifting was followed by moderate subsidence during the Late Cretaceous, leading to the development of widely spread carbonate platforms. The sediments of the Panna region are shown in the generalised vertical section of figure 3.2.

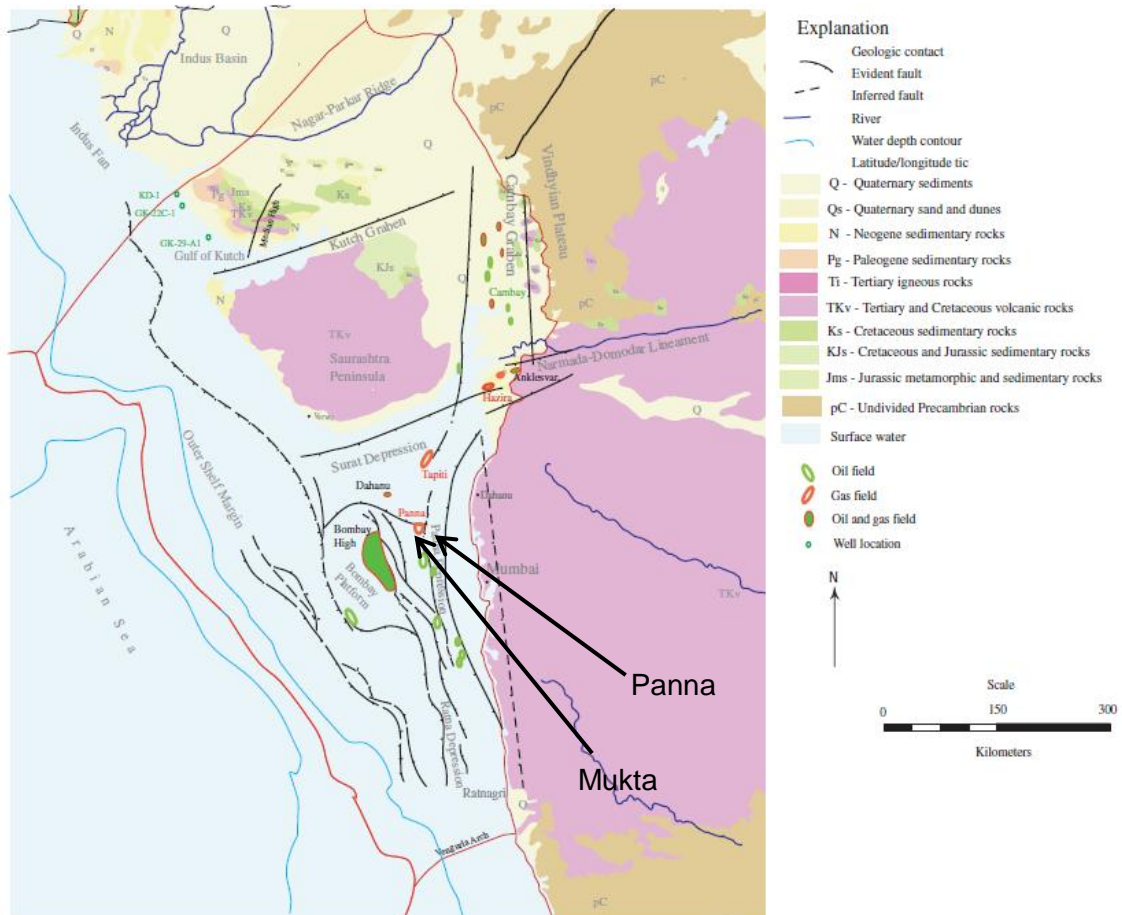


Figure 3.1. Location of the Panna and Mukta Field within the regional structure of the offshore India basin and the Bombay High (Wandrey 2004).

Naik *et al.* (2007) suggest that the Panna area was part of a megahigh land mass, the Greater Bombay High, during the Palaeocene. This high initially acted as the major supply for sediments to the half grabens; these siliciclastic sediments are referred to as the Panna units. The widespread Panna Shale (also known as the Cambay Shale) has acted as the main hydrocarbon source rocks for this region (Naik *et al.*, 2007).

From the early Eocene retrogradation is observed, leading to a decrease in the volume of clastic material brought into the system. Carbonate deposition occurred as a series of shallowly dipping clinoforms representing transgressively stacked facies belts, prograding into the basin (Estebaan 1998). Figure 3.3 illustrates the depositional environments of Panna carbonate facies, outlined in table 3.1. A general cyclic depositional cycle is seen, where limestones are deposited in shallowing water depth followed by abrupt transgressions, allowing deposition of a tight shale-rich limestone before re-commencing deposition of reservoir limestone units. Wright (2007) notes the presence of an unconformity between Formation-A and -B, represented by a rubbly clay, which is most likely the basal part of a much thicker weathering profile truncated during the transgression preceding Formation-A deposition.

Following carbonate deposition, an extensive shale was deposited post-Miocene which has acted as the regional cap rock for the reservoir, although it is noted that localised shale beds within the limestone act as local cap rocks for different pay zones (Goswami *et al.* 2007).

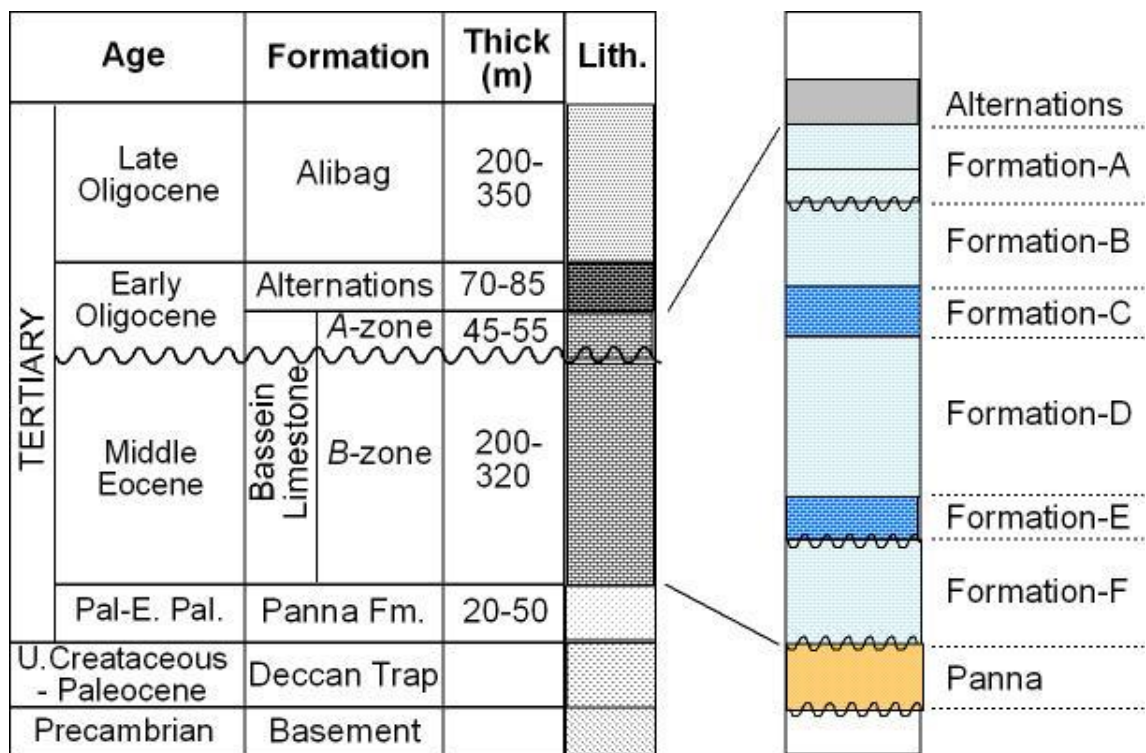


Figure 3.2. Generalised vertical section through the Panna-Mukta sediments. (modified from Khanna *et al.*, 2007).

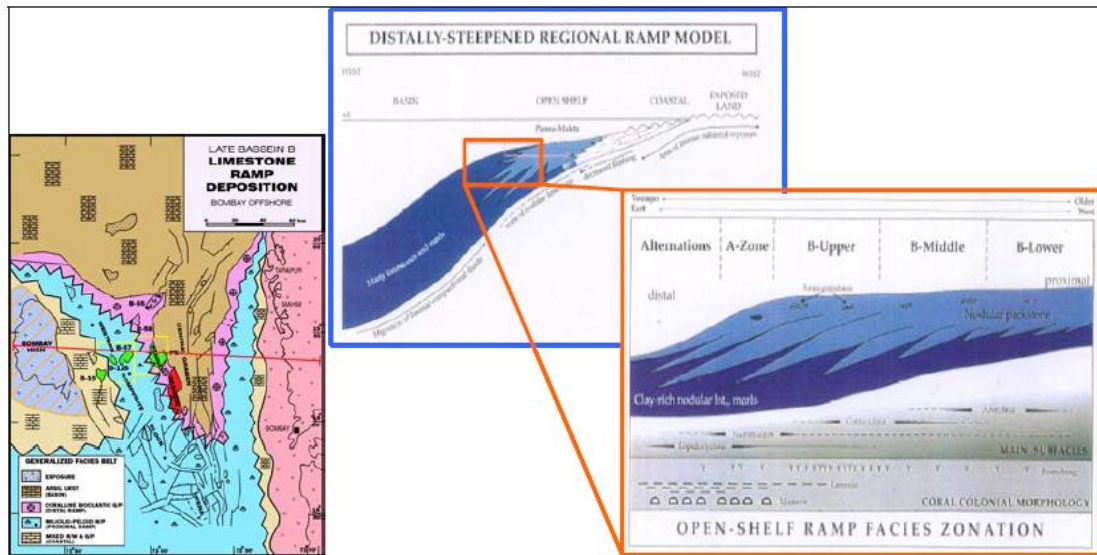


Figure 3.3. Depositional model for Panna-Mukta Field showing a ramp model (Estebaan 1998).

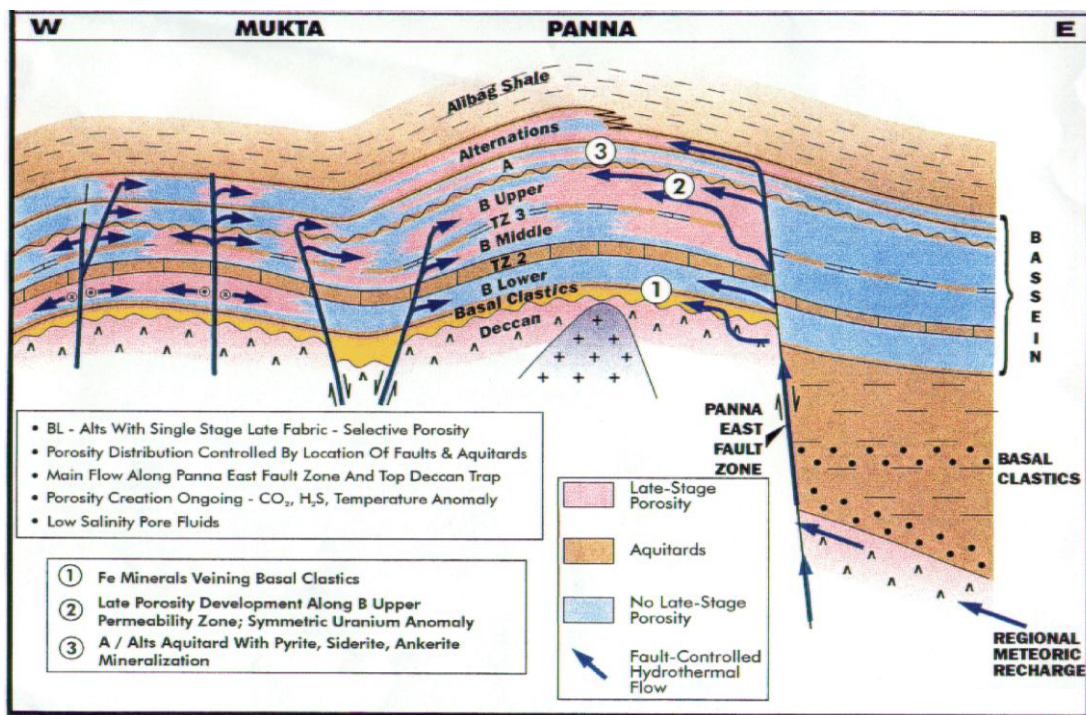


Figure 3.4. Sketch section illustrating the anticlinal structure of Panna-Mukta Eocene-early Oligocene sediments, deposited upon the Heera-Bassien block. Diagenetic porosity enhancement mechanisms are indicated, originating from basement faults controlling the horst-graben basin structure (Wright 2007).

Wright (2007) provides a synthesis of the sedimentological work completed for Panna-Mukta cores, suggesting a complex diagenetic history which controlled porosity and permeability development. The main processes forming porosity are of late stage dissolution (Khanna *et al.* 2007). The best porosity is generally seen in non-nodular, clean, limestone facies with stylolites and associated fractures. Burial corrosion, late stage dissolution and hypogenic karstification are

apparent throughout the reservoir units, often occurring to such a strong intensity that the whole rock is affected.

Following deposition and extensive cementation of early diagenesis the limestone units of Panna-Mukta were effectively tight. It is noted that Formation-A and Formation-B to -F show different diagenetic styles and ferroan cements, related to the unconformity and palaeokarst which separates them and would have acted as a flow barrier for marine and meteoric-derived fluids (Wright 2007). Extensive compaction and pressure solution, with later burial, lead to the development of stylolites and micro-stylolites, which in turn developed perpendicular fractures within the tight limestone (figure 3.5). Wright (2007) then suggests a phase of “mechanical inversion” opened up the stylolites to allow fluids to flow through them and into the host limestone, this fluid would have originated deeper in the Panna sediments and travelled up basement controlled faults (figure 3.4). This allowed for a major phase of dissolution that began by selectively removing micrite before spar cements were destroyed by late corrosion. Calcite cementation and the precipitation of saddle dolomite completed this process. A second phase of corrosion, affected all previous features, and is associated with minor pyrite and major dickite precipitation.

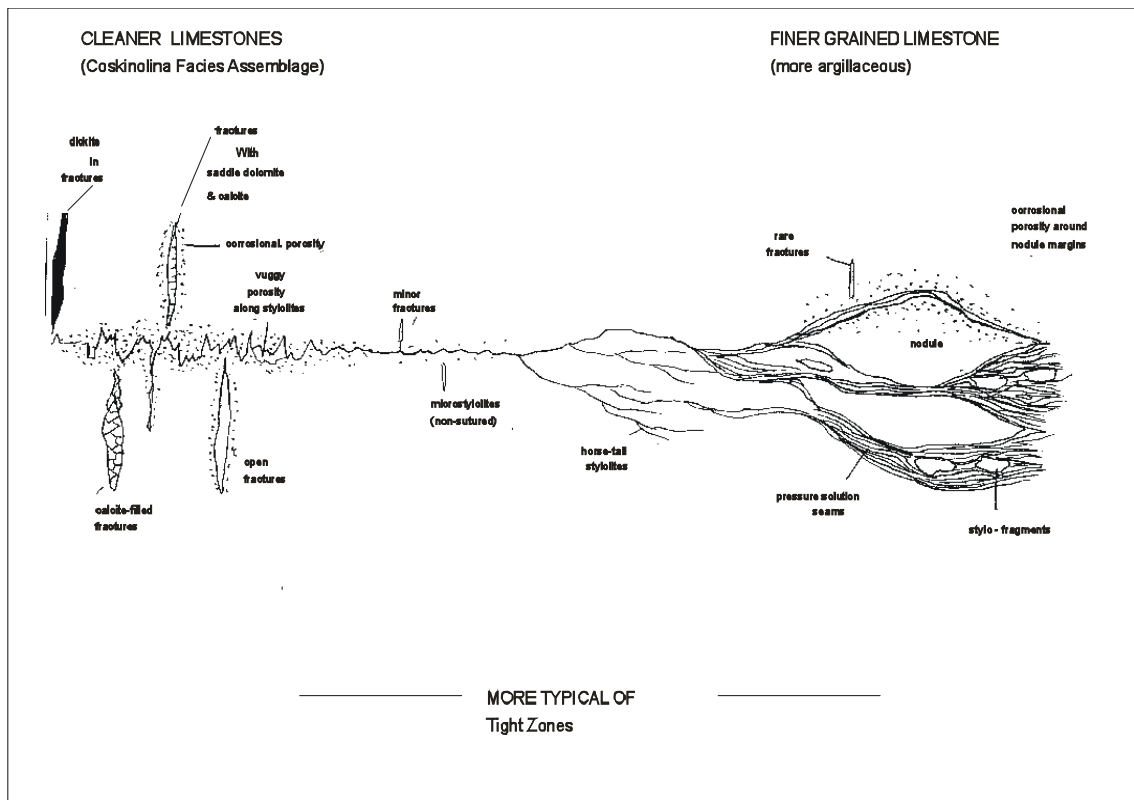


Figure 3.5. Sketch illustrating major diagenetic features in the Bassein Limestone units. Cleaner (less clay-rich) grainstones and packstones developed high amplitude stylolites associated with fractures. Microstylolites with fewer, shorted fractures developed in finer lithologies. It is noted that nodular fabrics and clay seams are found in most matrix-rich lithologies (Wright 2007).

Wright (2007) states that the presence of dickite associated with leaching of a clastic source rock by organic-rich acids and high temperature fluids are indicative of a hydrothermal dolomite reservoir. The presence of bitumen along some stylolites supports the idea that hydrocarbon maturation and migration was related to the movement of corrosive fluids through source and reservoir rocks. The en-echelon like fractures suggest limited effects of a strike-slip structural setting, supportive of conditions seen with other hydrothermal dolomite reservoirs (Wright 2007).

Khanna *et al.* (2007) and Wright (2007) both comment that porosity formed by corrosion is more prevalent on Panna than Mukta, citing that this suggests Panna was closer to the fluid source (figure 3.4). For example mouldic porosity in corals is common in Panna but rare in Mukta, indicating calcite cements were more heavily leached in the former.

Age	Formation	Thickness (m)	Key Lithology	Description	Key Porosity Types	
Early Oligocene	A	72	Limestone	Wackestone-Packstone (minor mudstone & grainstones). Variable argillaceous micritic matrix, with finely disseminated pyrite. Limited dickite. Limited dolomitization and fractured..	Micro- and matrix-porosity. Minor vugs, inter & intra granular porosity.	
			Minor Shale	Massive shale. Slightly calcareous & dolomitic, trace disseminated pyrite.	N/A	
Middle Eocene	B	57	Limestone	Grainstone, Clean, good bio-moldic porosity.	Less porous packstone and wackestones, poor-moderate local intergranular porosity.	Mouldic, matrix- and micro porosity. Patchy stylolite and fracture porosity.
	C	13	Limestone	Carbonate mudstone, Nodular and fragmented. Micritic, clean and no visible porosity.		Limited micro-porosity.
	D	68	Limestone	Grainstone-Packstone, Micritic, clean.	Minor carbonate mudstone, Fine-micro crystalline, tight.	Mouldic, matrix- and micro porosity. Stylolites dominate.
	E	58	Limestone	Carbonate mudstone, Clean and tight.		N/A
			Minor Shale	Argillaceous siltstone, Silty shale, disseminated pyrite.		N/A
	F	25	Limestone	Grainstone & Wackestone-Packstone, Limited dolomitization, Massive, with limited tight baffles (high frequency stylolites).		Intercrystalline (dolomite zones), intragranular & micro-porosity.
V Minor Shale			Siltstone (argillaceous), Carbonaceous, contains loose pyrite.		N/A	

Table 3.1. Outline of lithology and carbonate facies comprising the main reservoir unit of Panna-Mukta Field, thickness are from well P. Note unconformity between Formation-A and -B is represented by a rubbly clay horizon. (Estebaan 1998; Khanna *et al.* 2007; Naik *et al.* 2006; Reddy *et al.* 2004; Thakre *et al.* 1997; Wright 2007).

3.2.2. The Panna & Mukta Datasets

Work on the Panna reservoir has focussed on a detailed investigation of an individual well (well P), before investigating differences with the less diagenetically altered Mukta field (well M).

The available wireline log and core data from these wells is summarised in table 3.2 and 3.3 respectively. This work has assumed that depth matching of multiple logging runs is complete and correct. Comparison of gamma ray logs from subsequent runs, as part of log QC/QA, shows strong correlation.

Wireline Log	P	M
Caliper	X	X
Natural Gamma Ray	X	X
Bulk Density	X	X
Neutron Porosity	X	X
Photoelectric Factor	X	X
Compressional Sonic Velocity	X	X
Deep Resistivity	X	X
Fullbore Microresistivity Imager	X	
Service Company	SLB	SLB

Table 3.2. Wireline log data used in this study from the wells P and M. Service company; *SLB* – Schlumberger.

Core Measurement	Well P	Well M
Depth	X	X
Length	X	X
Porosity (%)	X	X
Permeability (mD)	X	X
Grain Density (g.cm ⁻³)	X	X
Lithology/facies	X	X

Table 3.3. Core data acquired for 115 samples from well P, and 264 samples from well M.

3.2.3. Petrophysical Analysis of Panna Dataset

Here the results of the detailed petrophysical analysis completed on well P are presented. A detailed account of the petrophysical workflow and techniques used is provided in Appendix B. This analysis includes estimation of the standard parameters; shale volume, porosity, permeability and water/hydrocarbon saturation, and fluid flow zonations. Petrophysical analysis has been completed using the Recall Log Interpretation software module (Petris 3), and Microsoft Excel.

The basic well log dataset for Formation-A to -D is shown in figure 3.7. The caliper measurements shown in track 1 indicate a consistent borehole throughout the section at 8.5-9 inches, this is supported by information from the well-site completion report showing no problems occurred during either drilling or logging runs. Unfortunately no DRHO measurements (density correction applied by service company) are available for the study section of this well, DRHO can act as an additional check for bad hole data. It is noted that as the bulk density curve follows that of compressional slowness, then the data is suggested to be of good quality (Ellis & Singer 2007). Natural gamma ray is shown with the potassium-thorium ratio (obtained from spectral gamma ray analysis, Appendix B), in the Panna field it is well documented that gamma ray alone is not a suitable measure of shale content because of the prevalence of diagenetic uranium enrichment (Khanna *et al.* 2007). Bulk density and neutron porosity measurements are plotted with a limestone overlay at 2.71g/cm^3 and 0.0pu, shifts to the left indicating an increase in porosity. Compressional P-wave transit-time is presented increasing from right to left. Deep and shallow resistivity measurements are plotted on standard logarithmic scale (LLD and LLS respectively). Formation-A is highly variable in all measurement types, compared to the lower frequency and amplitude variations Formation-B to -D.

Results of detailed petrophysical analysis (detailed in appendix B) are presented in figure 3.8. Shale volume is highly variable in Formation-A from 0-93%, it is noted again that shale volume is determined from spectral gamma potassium-thorium ratio and density-neutron separation.

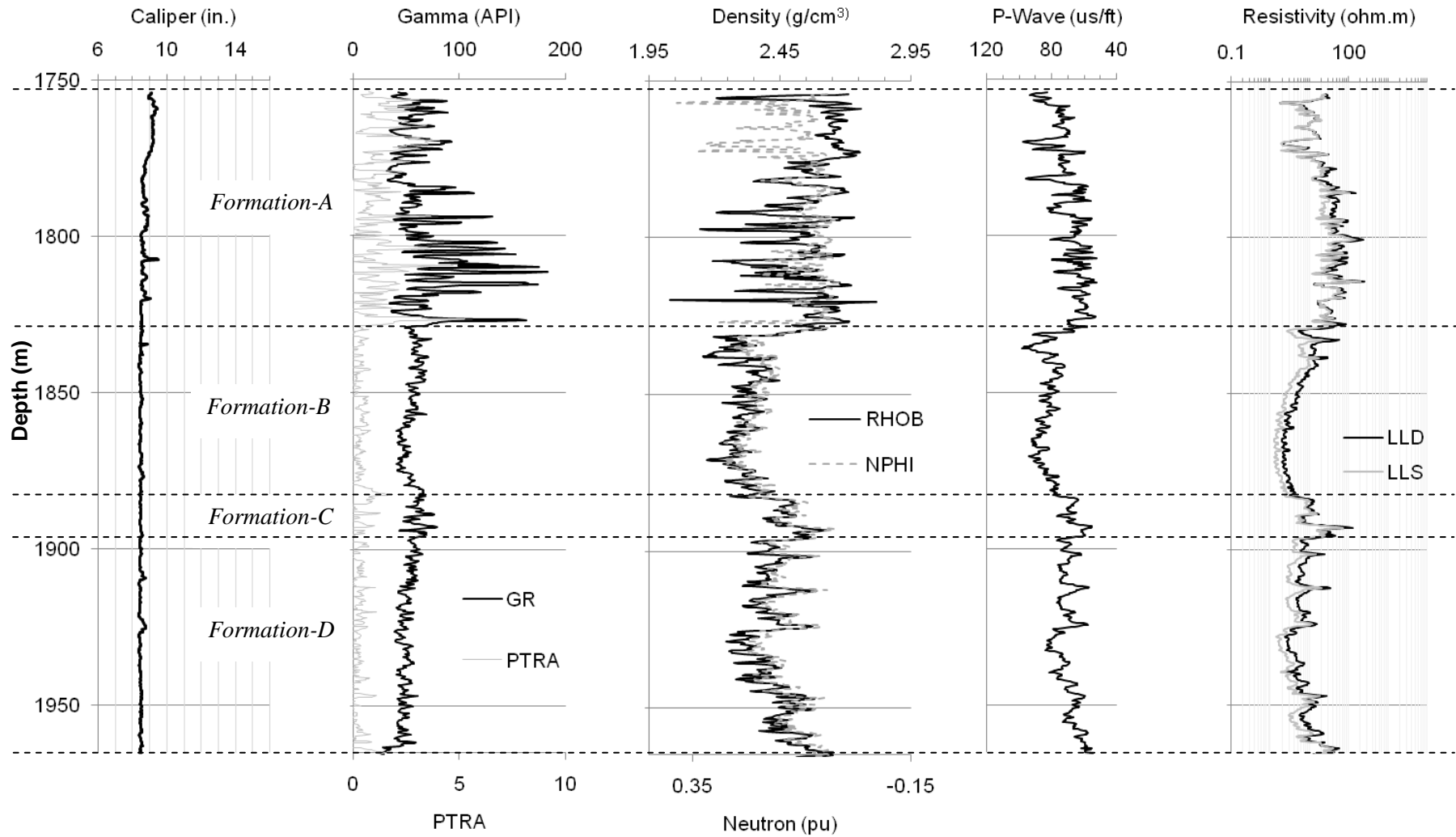


Figure 3.7. Depth plots of raw wireline dataset for well P, with annotation showing geological zonations. PTRA – potassium-thorium ratio from spectral gamma ray data.

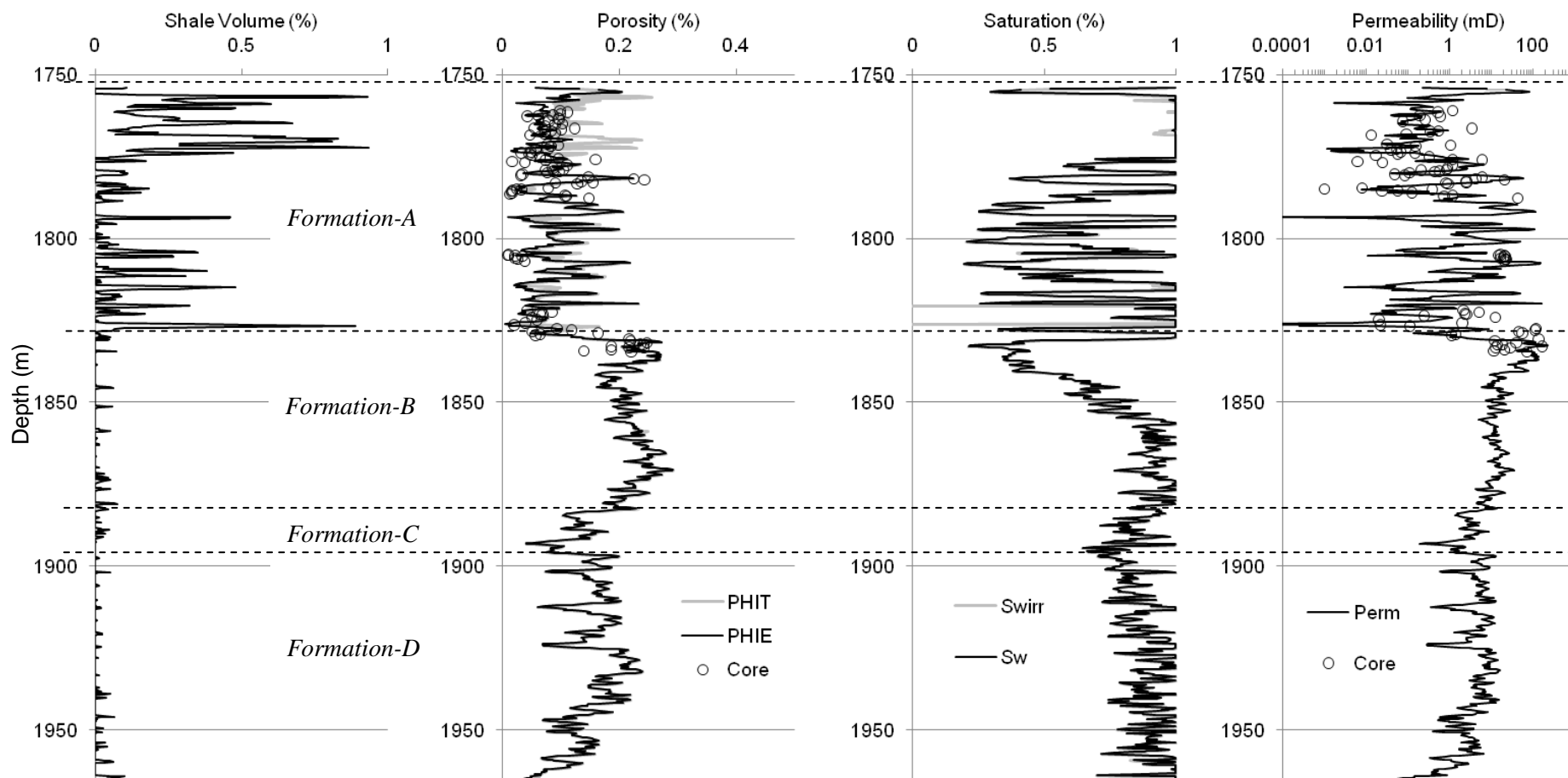


Figure 3.8. Depth plots of wireline log-derived petrophysical parameters for well P, with annotation showing geological zonations. Note that routine core measured porosity and permeability measurements are shown for comparison, full dataset calibrated for the complete dataset of core data available for the Panna field (Appendix A).

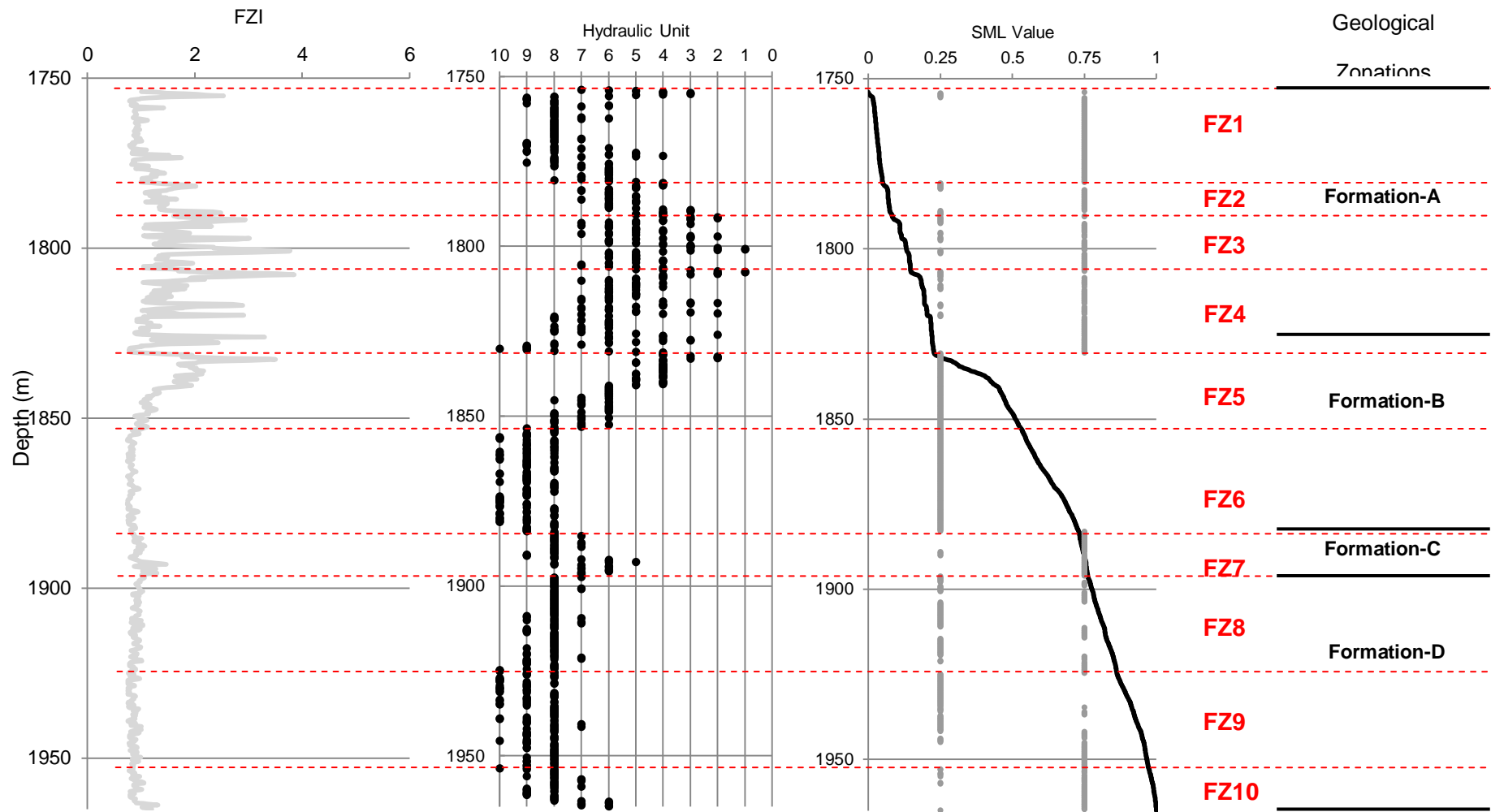


Figure 3.9. Interpreted Fluid Flow Zones from log-derived porosity and permeability data, with geological zonations for well P. Left to right; flow zone indicator (FZI) plot, hydraulic units depth plot, stratigraphic modified Lorenz (SML) depth plot.

This is supported by basic interpretation of the electrical borehole image log (FMS) where we see shale beds ranging in thickness from centimetres to metres. Shale volume is found to be much lower in Formation-B to -D as predicted from limited core and neighbouring well studies, varying from 0-10%. The FMS image confirms this analysis with only limited shale horizons of a few centimetres being recorded. Log derived porosity measurements show good correlation with core measurements (R^2 value 0.78). It is noted that in the upper Formation-A, core measurements show a stronger correlation to the total porosity (PHIT) than effective porosity (PHIE) which is considered to be a result of core plug processing with variable background shale contents. In Formation-A porosity shows high frequency variation from 0-23%, decreasing with increased shale. The transition into Formation-B is marked by a sharp rise in porosity to 29%, followed by lower frequency variation between 18-28%. Tight Zone 3 corresponds to an abrupt decrease in porosity ~10% followed by a sharp increase in porosity into Formation-D, where porosity shows lower frequency variation from 10-24%.

Log-derived water saturation is seen to be highly variable through Formation-A (20-100%), with a sharp decrease to ~20% at the top of Formation-B. Water saturation gradually increases to 90% through the upper section of this zone, where it shows low frequency variation into Formation-C. This tight zone shows a decrease in water saturation (65-80%), before returning to 80-100% values in the Formation-D. Well log-derived permeability shows strong correlation with core measured values (R^2 value of 0.8), observed differences are considered to relate to the presence of fractures and stylolites in core samples. Well log-derived permeability is seen to be highly variable in Formation-A, showing a mix of high and low frequency and amplitude variations from 0.0001-157mD (note is made that standard industry permeability cut-off for “non-permeable” rocks is 0.1mD for gas reservoirs (Worthington & Cosentino 2005)). The top of Formation-B is marked by an increased permeability to ~220mD, just below the palaeokarstic unconformity with Formation-A. Permeability falls gradually to ~10mD at the top of Formation-C, with a low frequency variation superimposed on this longer term trend. Formation-C shows a sharp decrease in permeabilities to 0.2-10mD. Through Formation-D a

high frequency/ low amplitude variation around 10-20mD is punctuated by higher frequency variations to 0.2mD at horizons of significantly lower porosity. A general decrease in permeability to 0.1mD is seen to the bottom of this section.

The complete succession has been broken down into fluid flow zones based on flow zone indicators (FZI), hydraulic units (Amaefule *et al.* 1993), and the stratigraphic modified Lorenz plot (Buckles 1965); methodologies are explained in Appendix B. Fluid flow zonations are assigned based on sharp contrasts downhole (figure 3.9). The succession is broken down into 10 fluid flow zones which show good correlation to the pre-existing geological zonations, it is noted that some smaller-scale zones within Formation-A have been grouped together for discussion here but will be expanded upon in chapter 6. A fluid flow zone is shown to consist of a transmissive upper section with a storage or barrier type lower part.

Formation-A is divided into 4 main fluid flow zones, which correspond to pre-existing geological subzones (chapter 6). The lower geological boundary of Formation-A shows 5m offset with the FZ4-5 boundary. Formation-B consists of fluid flow zones 5 and 6, it can be seen that these two zones would be expected to act as one, however their division is based on the significant contrast in hydraulic unit and FZI around 1855m indicating a high quality top section. Formation-C is represented by FZ7, a lower quality unit indicated by previously discussed porosity and permeability data. Formation-D consists of the remaining three flow zones, corresponding to the moderate quality of FZ6.

3.2.4. Petrophysical Analysis of Mukta Dataset

Here the results of the detailed petrophysical analysis completed on well M are presented. A detailed account of the petrophysical workflow and techniques used is provided in Appendix B (with examples from well P). This analysis includes estimation of the standard parameters; shale volume, porosity, permeability and water/hydrocarbon saturation, and fluid flow zonations. Again, petrophysical analysis has been completed using the Recall Log Interpretation software module (Petris 3), and Microsoft Excel.

The wireline well log measurements are presented in figure 3.10. The caliper indicates very good hole conditions through the succession at around 9 inches, except for the 4 inch increase between 2118-2121m. The origins of this feature are unclear, and it clearly has an effect on the density, neutron, P-wave and resistivity measurements (suggesting increased porosity at this horizon). These data will be processed alongside the rest of the succession, but care will be taken in interpretations. The DRHO curve (density correction applied by service company based on difference short- and long-spaced detectors) is presented with the caliper. The majority of data is near zero, indicating good contact between tool and formation. One exception occurs at 2151m with a large positive spike, indicating poorer quality data in the presence of borehole rugosity, seen slightly in the caliper. This coincides with the location of the basal karst unconformity of Formation-A. However, as the bulk density curve follows that of compressional slowness, then the data itself is suggested to be of corrected to good quality (Ellis & Singer 2007). As above, natural gamma ray is shown with the potassium-thorium ratio; it is documented that gamma ray alone is not a suitable indicator of shale content because of the prevalence of diagenetic uranium enrichment in the Panna field and so the same is assumed true for Mukta. Bulk density and neutron porosity measurements are plotted with a limestone overlay at 2.71g/cm^3 and 0.0 pu, shifts to the left indicate an increase in porosity. Compressional P-wave slowness values are presented increasing from right to left. Deep resistivity (R_t) measurements are plotted on standard logarithmic scale. Formation-A can be seen to be variable in all measurement types, compared to the lower frequency and amplitude variations in Formation-B to -D. It is noted that Formation-B variability is not as extreme as seen in well P above.

Figure 3.11 shows the results of detailed petrophysical analysis on well M. Formation-A has significantly higher shale content which is variable through the succession from 0 to 70%. Higher shale content is indicated toward the base of Formation-A, above the basal unconformity.

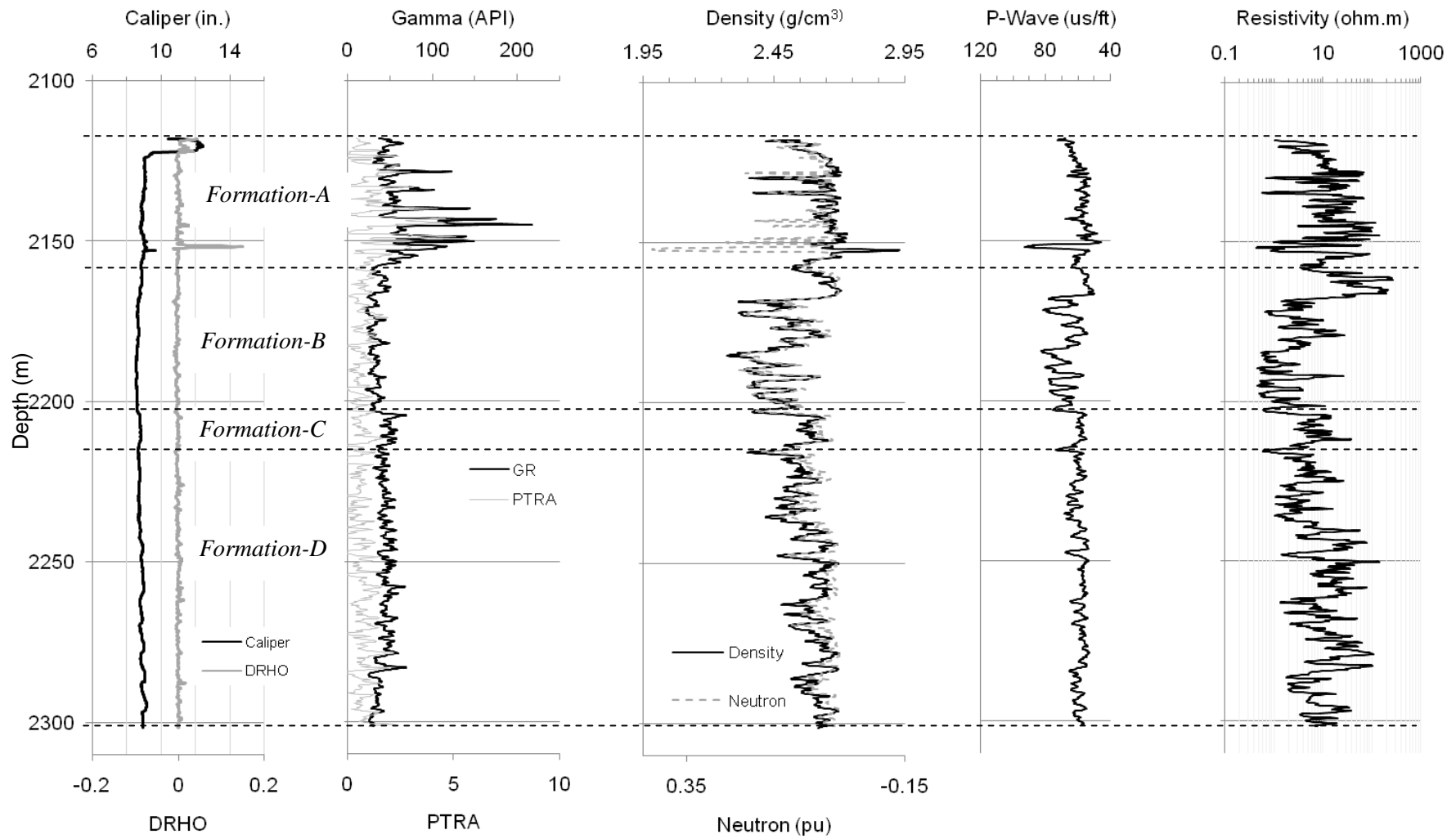


Figure 3.10. Depth plots of raw wireline dataset for well M, with annotation showing geological zonations. PTRA – potassium-thorium ration from spectral gamma ray log.

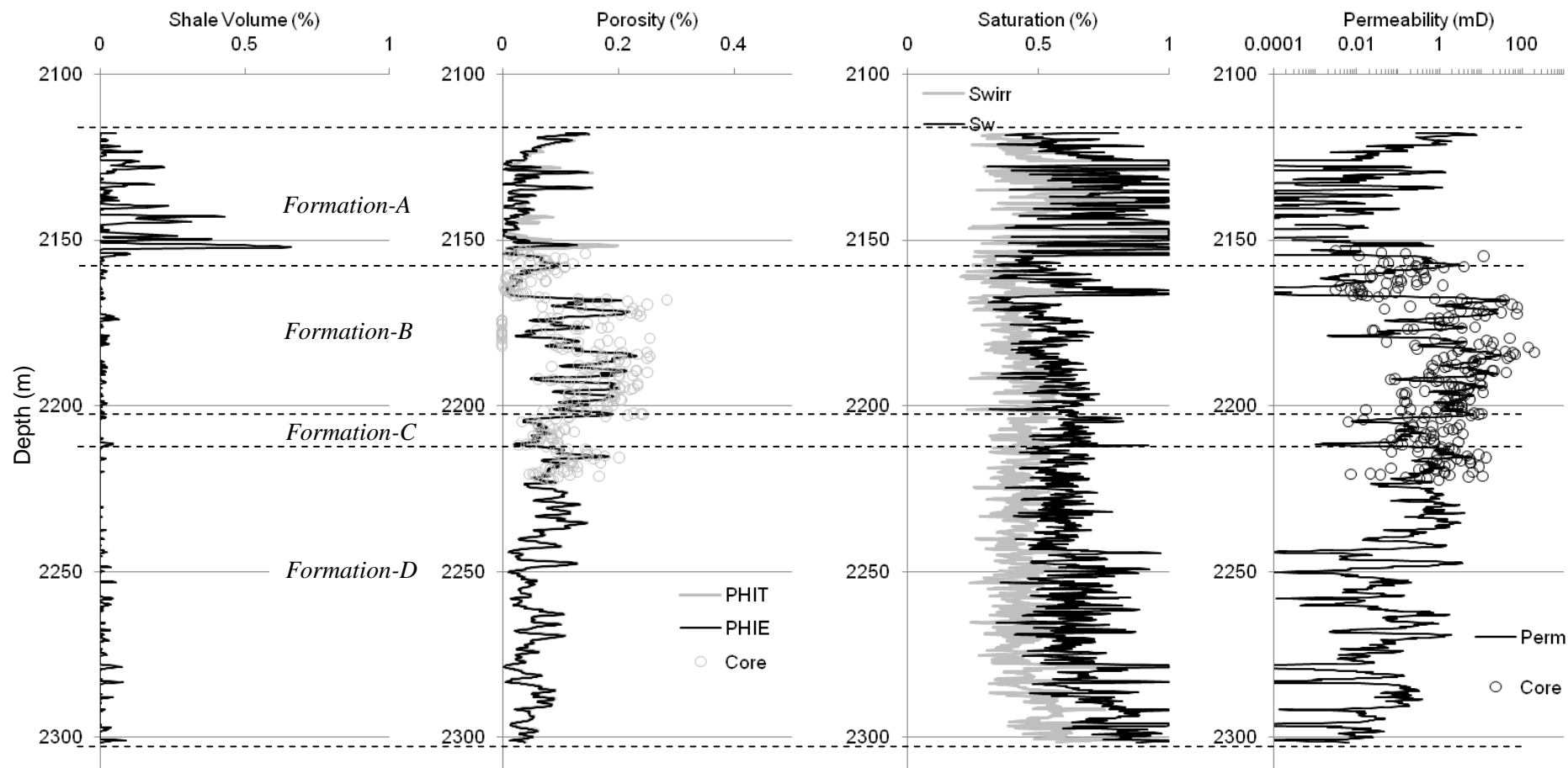


Figure 3.11. Depth plots of wireline log-derived petrophysical parameters for well M, with annotation showing geological zonations. Note that routine core measured porosity and permeability measurements are shown for comparison.

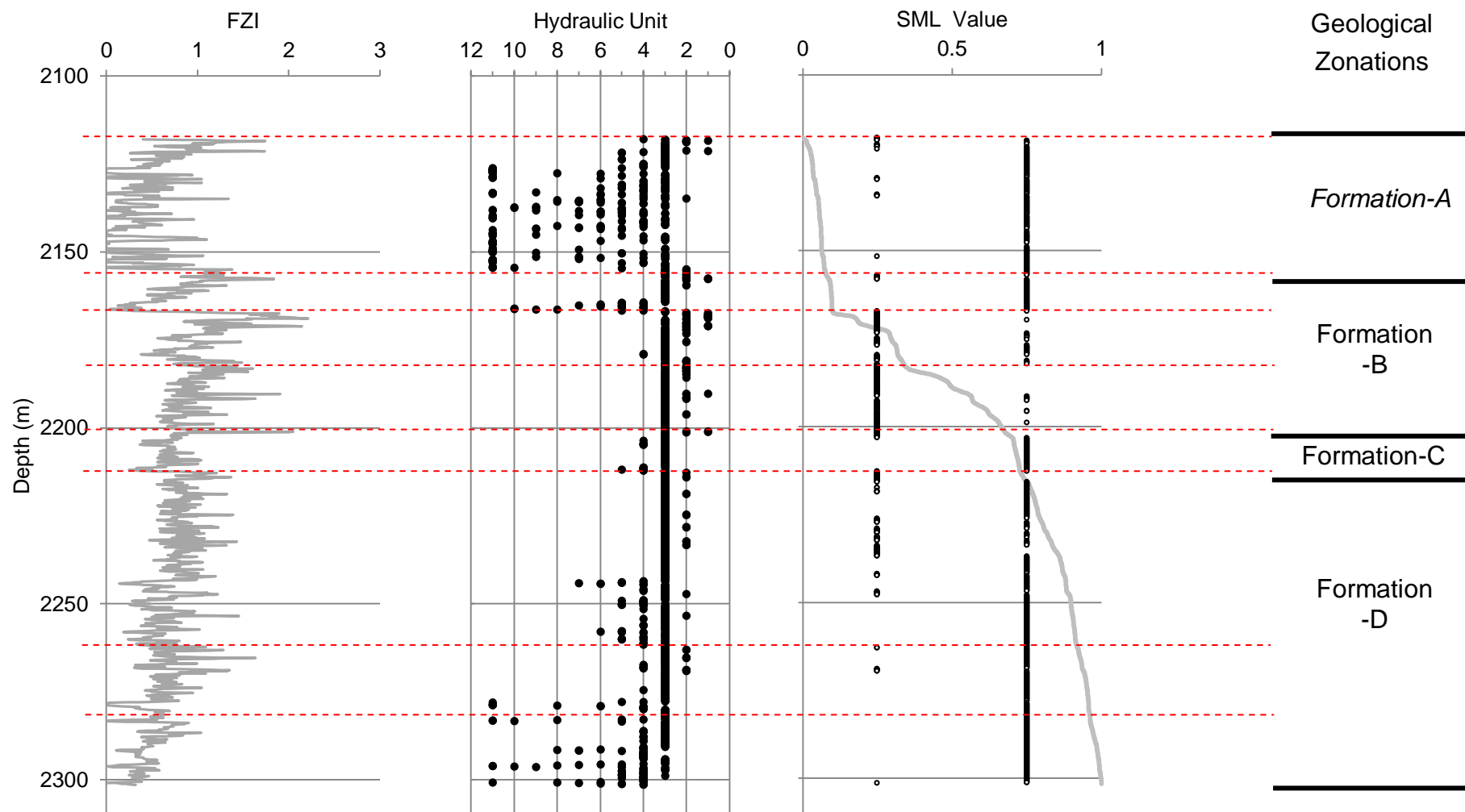


Figure 3.12. Interpreted Fluid Flow Zones from log-derived porosity and permeability data, with geological zonations for well M. Left to right; flow zone indicator (FZI) plot, hydraulic units depth plot, stratigraphic modified Lorenz (SML) depth plot.

Throughout Formation-B and -C limited shale content is indicated, with low frequency variation from 0 to 10%, averaging 0.1%. Well log-derived properties show good correlation to core measured values, although there is significant scatter in the core data. Log-derived values capture an average trend, whilst also capturing the maximum and minimum values (figure 3.11). Porosity is found to be predominantly lower in Formation-A of well M, averaging 5%, with high frequency variation to a maximum of 18%. The first 5m of Formation-B show low porosity ~1%, rising sharply to ~24% where values show low frequency/high magnitude variation through the remainder of the zone. Formation-C sees a sharp decrease in porosity to ~10%, before returning to low frequency variation in porosity in the Formation-D (5-20%).

Water saturation is highly variable through Formation-A, with a long term rising trend through the zone. The Formation-A /-B boundary records a sharp decrease in water saturation to ~50%, which increases to 100% through the tight upper 5m of Formation-B. Water saturation then drops suddenly to ~40% before gradually increasing to 65% at Formation-C. From Formation-C to the bottom of the Formation-D we see a gradual rise in water saturation ~100%, with a higher frequency variation of $\pm 5\%$ superimposed throughout. Well log-derived permeability is highly variable throughout Formation-A (0.0001-10mD), showing a decreasing trend toward the basal unconformity. The top of Formation-B is marked by a sharp rise in permeability to 10mD, followed by a decline through the tight section of this zone. Permeability then rises to ~50mD, maintaining a low frequency variation through the rest of the zone. Formation-C sees a sudden decrease in permeability to <0.1mD before rising back to ~5mD at the top of Formation-D. Permeability has a long term decreasing trend through Formation-D to 0.01mD, with a low frequency variability of $\pm 10\%$ superimposed.

Again, the complete succession is divided into fluid flow zones based on flow zone indicators (FZI), hydraulic units (Amaefule *et al.* 1993), and the stratigraphic modified Lorenz plot (Buckles 1965), methodologies detailed in Appendix B. Fluid flow zonations are assigned based on sharp contrasts downhole (figure 3.12). A fluid flow zone is shown to consist of a transmissive upper section with a storage or barrier type lower part. The succession is broken

down into 8 fluid flow zones which show good correlation to the pre-existing geological zonations.

Formation-A consists of a single fluid flow zone (FZ1). It is noted that this zone can be further divided at a finer-scale of investigation based on the FZI and Hydraulic Units (see chapter 6). The SML values indicate that FZ2 could be grouped with FZ1, however the sharp contrasts in the other flow zone indicators indicated FZ2 to be a significant unit by itself. Formation-B relates to flow zones 2-4, all of which are shown to be high quality by the FZI values. Formation-C is again represented by a single flow zone (FZ5). The FZI and Hydraulic unit values indicate a slight decrease in the quality of FZ5, although raw permeability and porosity data support the tight geological nature of this unit. Formation-D is composed of FZ6-8, which could be grouped as a single flow zone based on the SML response, but have been further divided by the Hydraulic Unit properties.

3.2.5. Comparison of Panna and Mukta Petrophysical Properties

As described previously in the geological overview, the Panna and Mukta fields contain the same rock types and fluids but have undergone different degrees of alteration by diagenesis, Panna being more heavily corroded by multiple phases of diagenetic fluids (figure 3.4). This is clearly observed in the petrophysical property data derived from the well logs, in that although broad trends are the same in each of the geological zonations for wells P and M, porosity is 5-10% less in the Mukta well, and permeability is indicated to be a decade smaller.

The fluid flow units for wells P and M show similar correlation and patterns through the succession, although it is noted that the FZI quality indicator is smaller for the Mukta formations because of the decreased porosity and permeability. The overall features of the SML plots are remarkably similar, with relation to the geological zonations.

3.3. Abiod, Miskar

3.2.1. Geological Overview – Abiod chalk

The Miskar Field is located on the Pelagian Platform of the Gulf of Gabes, Offshore Tunisia (Figure 3.13). It is composed of Cretaceous to Eocene aged sediments, deposited on a carbonate platform within a rift system of horst and tilted fault blocks (Taylor 2003). Dominant geological units here are the Bireno, Aleg (R1 Superior and Inferior), and Abiod formations. Hydrocarbon is present as gas condensate in these reservoirs (Pritchard 2002). Gas condensate is a low density mixture of hydrocarbon liquids, condensed from raw gas as temperatures decrease below the hydrocarbon dew point of natural gas (Selly 1998). As only well log data from the Abiod chalk are used in this study, a basic overview of the other geological formations is provided here before detailing the geology of the Abiod.

Activation of N-S trending basement faults in the Upper Triassic-Jurassic formed the east-west bounding faults of the Miskar platform block. Jurassic through early Cretaceous deposition of black, organic-rich mudstone with limited carbonate content (sometime seen as thin argillaceous limestone interbeds) occurred. These mudstone units are on average 100m thick, with total organic carbon (TOC) content of 0.2-3%, and so have acted as the major source rocks in this area (Klett 2001). Subsequent Late Albian-Cenomanian extension formed an en-echelon fault bound horst-graben geometry of the platform, allowing for deposition of the Bireno, Aleg and Abiod sediments which form the main reservoir units (Taylor 2003). The Turonian aged Bireno member comprises carbonate calcispheres, peloidal wackestones and packstone of a mid- to outer ramp depositional setting. Overlaying this is the upper section of the Aleg formation (R1 inferior), a homogeneous shallowing upward succession of marine carbonates which grade into a highly heterogeneous backshoal, lagoonal-peritidal assemblage. The upper section of the Aleg formation (R1 superior) is a thinly bedded package of deep water carbonates, deposited in mid ramp settings, with increasing carbonate mudstone content upwards. This carbonate mudstone nature become a tight barrier, sealing the top of the Aleg formation (Klett 2001; Taylor 2003).

A period of uplift and erosion from Campanian to Late Maastrichtian was followed by substantial extension, allowing the deposition of a thick sequence of Abiod chalks which were subsequently faulted by Eocene extension (Taylor 2003). The Upper Cretaceous-Palaeocene El Haria mudstone lay unconformably above the Abiod chalks, acting as a major seal.

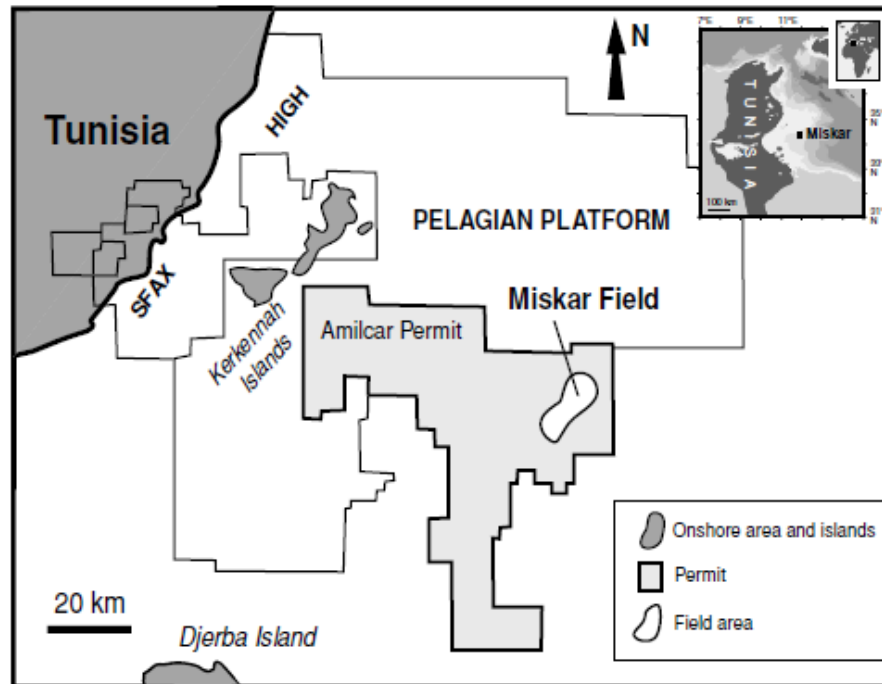


Figure 3.13. Location of the Miskar Field within the Gulf of Gabes, Offshore Tunisia (Mabrouk *et al.* 2006).

The Abiod chalks range in thickness from 60m in the centre of the structure to <10m at its rim, where they have undergone significant erosion and diagenetic alteration. The Abiod sediments (figure 3.14) were deposited in deep water (200-2500m) of the basin/outer ramp setting, and are composed of autochthonous foraminiferal nannofossil chalks, with wackestone to packstone textures (Klett 2001; Mabrouk *et al.* 2006; Taylor 2003). Centimetre thick horizons with increased clay and calcite cement occur throughout the succession, representing times of decreased chalk deposition (Taylor 2003). Porosity is predominantly present as microporosity in the packstone dominated chalk texture, although interparticle/crystalline porosity is found in areas of wackestone texture. Main fluid pathways are attributed to extensive lateral open stylolites (10-100m) and fractures (+10m in length) (Klett 2001; Taylor 2003).

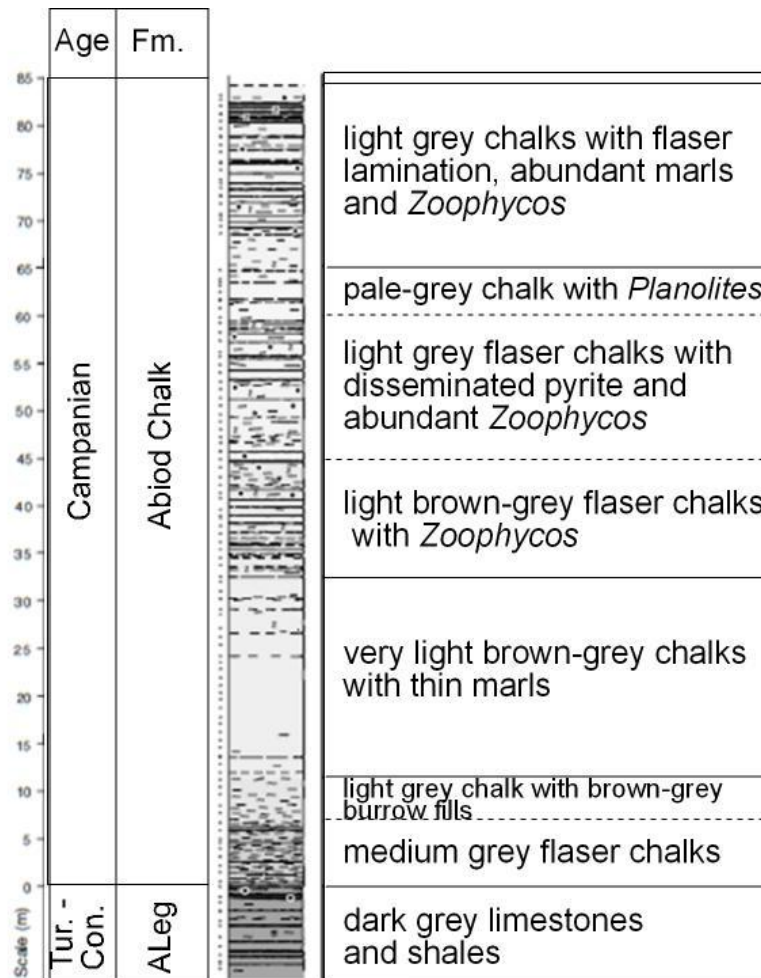


Figure 3.14. Lithostratigraphic summary and biostratigraphy zonation of Miskar (modified from Mabrouk *et al.*, 2006).

3.3.2. The Miskar Dataset

Work on the Miskar reservoir has focussed on a detailed investigation of the Miskar well-A. This well is located in the centre of the field, and documented to have limited alteration by diagenesis and erosion.

Core Measurement	Well A
Depth	X
Length	X
Porosity (%)	X
Permeability (mD)	X
Grain Density (g.cm ⁻³)	X

Table 3.4. Core data acquired for 257 samples from well A.

The available wireline log and core data from these wells is summarised in table 3.4 and 3.5 respectively. This work has assumed that depth matching of multiple logging runs is complete and correct. Comparison of gamma ray logs from subsequent runs, as part of log QC/QA, shows strong correlation.

Wireline Log	Well A
Caliper	X
Natural Gamma Ray	X
Bulk Density	X
Neutron Porosity	X
Compressional Sonic Velocity	X
Deep Resistivity	X
Service Company	SLB

Table 3.5. Wireline log data used in this study from well A. Service company; *SLB* – Schlumberger.

3.3.3. Petrophysical Analysis of the Abiod Dataset

The results of the detailed petrophysical analysis completed on the well-A dataset are presented here. A detailed account of the petrophysical workflow and techniques used is provided in Appendix B (with examples from well P). This analysis includes estimation of the standard parameters; shale volume, porosity, permeability and water/hydrocarbon saturation, along with subdivision of the derived poro-perm data into fluid flow zones. Petrophysical Analysis has been completed using the Recall Log Interpretation software module (Petris 3), and Microsoft Excel.

Figure 3.15 presents the raw well log curves used for petrophysical analysis of the Abiod chinks in well A. The caliper is seen to be constant down hole at around 8.5 inches, indicating a good borehole. Slight rugosity of the borehole (~0.5 inch) is seen at 2898m; it is suggested this may be related to the presence of a highly stylolitic horizon.

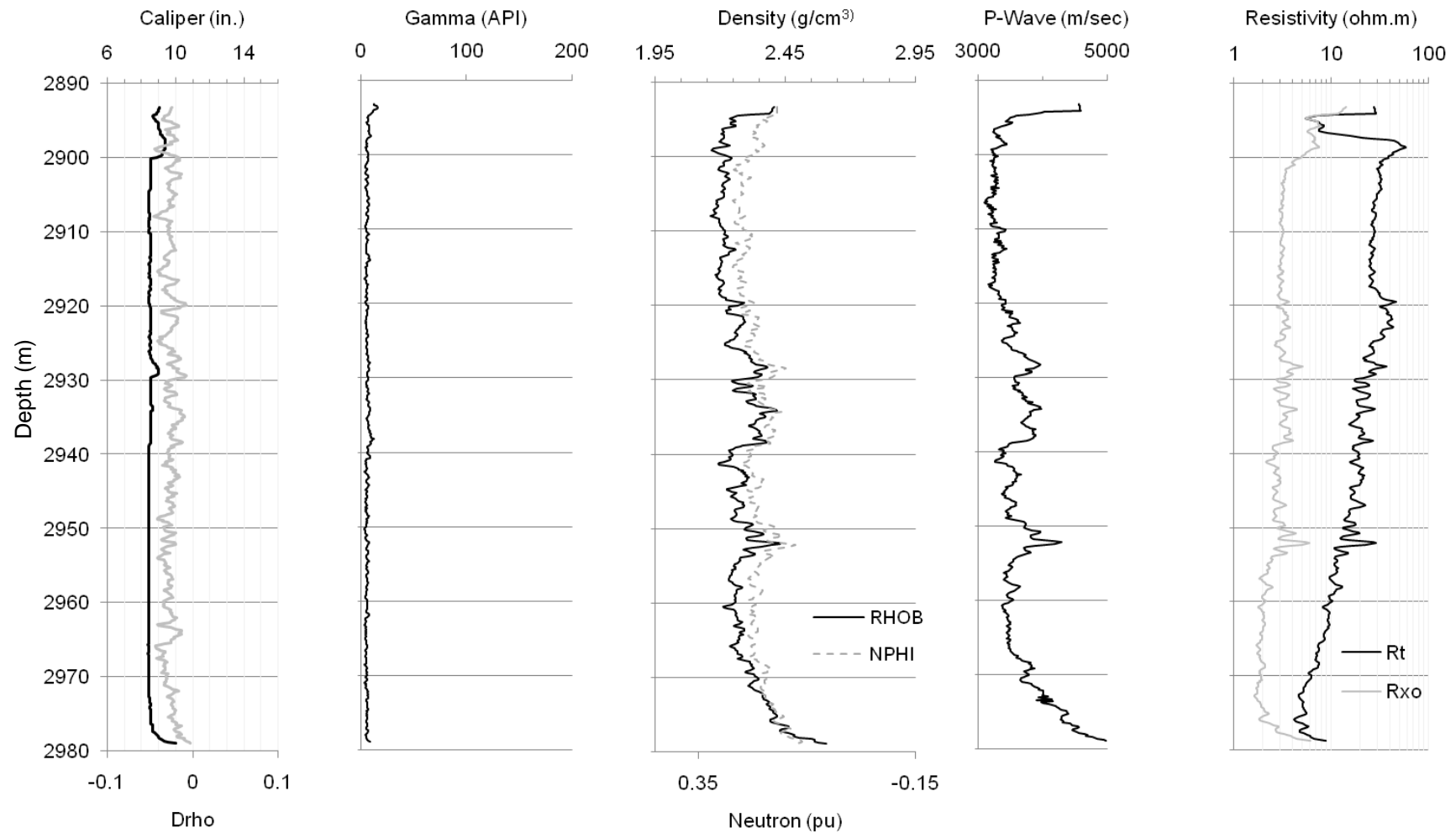


Figure 3.15. Depth plots of raw wireline dataset for the Abiod chalk of well A. Note Drho is the correction applied to bulk density measurements, displayed with the caliper track for QC reference in text.

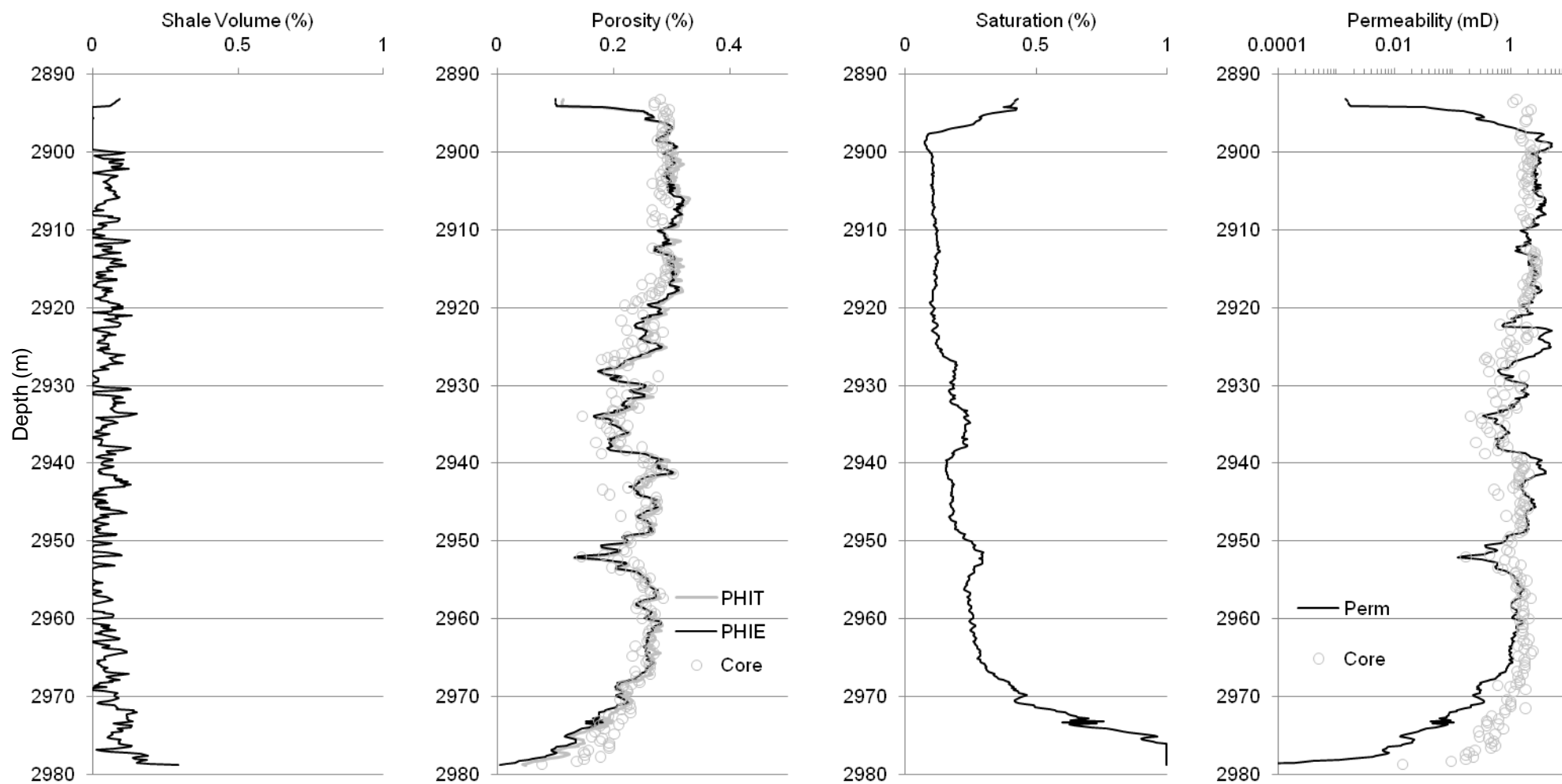


Figure 3.16. Depth plots of wireline log-derived petrophysical parameters for the Abiod chalk of well A. Note that routine core measured porosity and permeability measurements are shown for comparison.

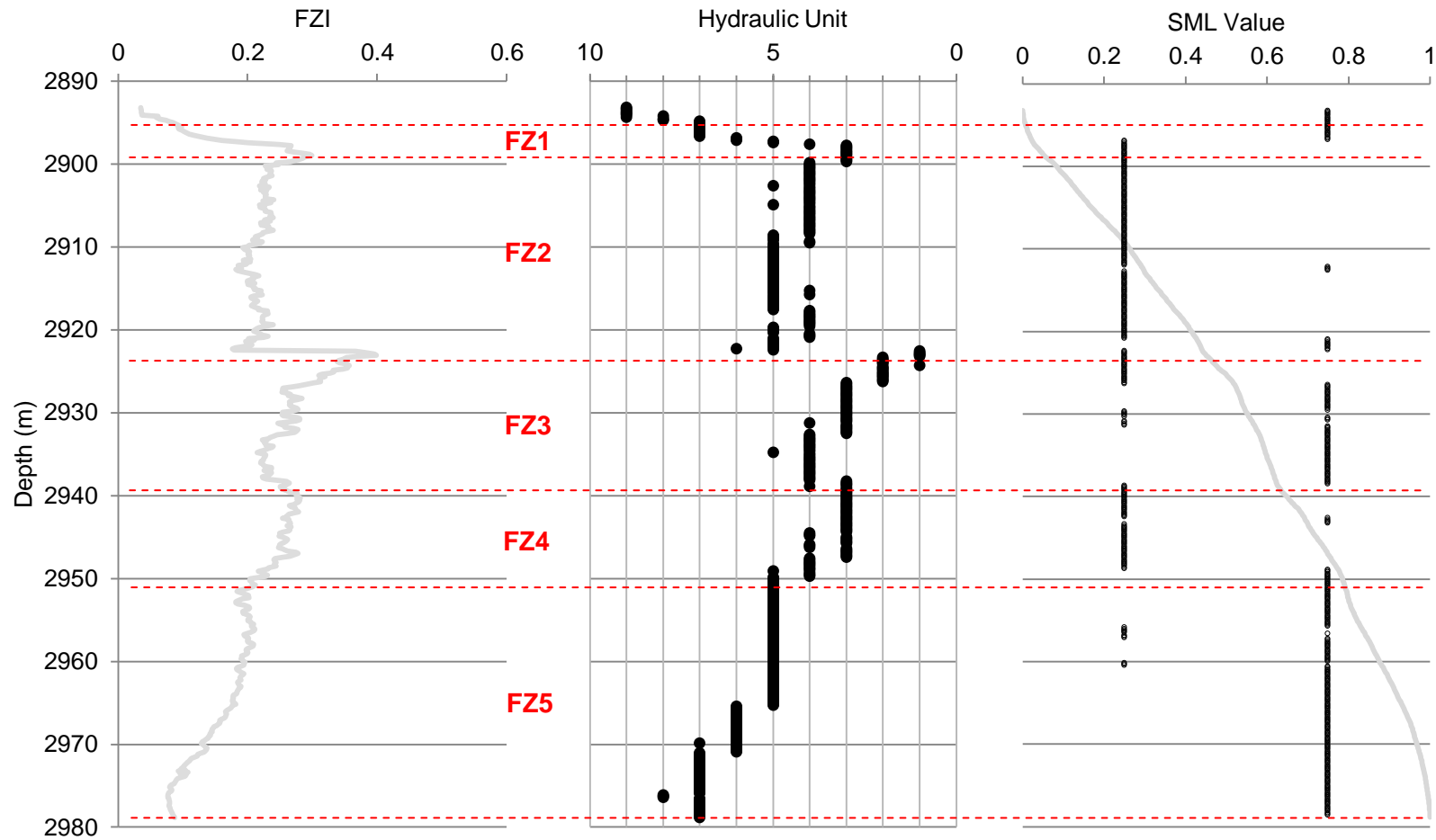


Figure 3.17. Interpreted Fluid Flow Zones from log-derived porosity and permeability data for the Abiod chalk of well A. Left to right; flow zone indicator (FZI) plot, hydraulic units depth plot, stratigraphic modified Lorenz (SML) depth plot.

Caliper also shows an increase in hole size toward the very bottom of the succession, corresponding to underlying shale-rich sediments. The DRHO values are presented with caliper measurement, identifying correction made to the bulk density well log measurement by the service provider (Ellis & Singer 2007). These are noted to be minimal and have no impact on further analysis.

Natural gamma ray measurements are very low throughout the formation, at ~10API. Little evidence of internal variation is suggested. Bulk density and neutron porosity measurements show significant variation within the formation, and are consistent with limestone matrix of variable porosities, four unit within the chalk are indicated by their combined variability downhole (at 2893-2928m, 2928-2937m, 2937-2952m, and 2952-2978m). The P-wave velocity data shows similar features to the density-neutron data. Deep resistivity (R_t) is seen to increase gradually upwards through the formation, this increase is much less noticeable in the shallow resistivity measure (R_{xo}).

The results of the petrophysical analysis are displayed in figure 3.16. Shale volume is low throughout the succession, with high frequency variation from 0-11% (average 0.04%). Well log-derived porosity shows good correlation with core measured values. Differences between core and well log porosity are thought to relate to the presence of open, and closed stylolites in core samples. Porosity is indicated to rise sharply into the Abiod chalk to ~30%, with generally low frequency/amplitude variation downhole, before falling toward the bottom of the succession. This trend is punctuated by three depths where porosity decreases to ~20%; at 2928m, 2935-2938m, and 2953m. Water saturation increases gradually down through the succession from 10-30%, with notable increase in zones of decreased porosity. Well log-derived permeability shows good correlation with both core measurements and the well log-derived porosity profile through the majority of the succession. It is noted that well-log derived values decrease sharply toward the top and bottom of the formation, not seen in core measurements. No permeability model was found to improve this, it is considered to relate to shoulder effects of over- and underlying thick shale sequences on the wireline logs.

The succession is divided into 5 fluid flow zones based on flow zone indicators (FZI), hydraulic units, and the stratigraphic modified Lorenz plot, as detailed in Appendix B. Again, fluid flow zonations are assigned based on sharp contrasts downhole (figure 3.17). As seen in the previous examples a fluid flow zone is shown to consist of a transmissive upper section with a storage or barrier type lower part. FZI is suggested to be barrier at the top of the formation, however this is expected to be more an artefact of the poor permeability model in this upper section. Flow zones 2 and 3 are high quality and well constrained units in all three methods. Flow zones 4 and 5 could be grouped as a single zone, however variation in the FZI, and comparison to the log-derived porosity and permeability data, indicate that these are separate, lower quality units.

3.4. Summary

- The data for this research comes from 3 carbonate-dominated reservoirs – Panna, Mukta and Miskar. In the Panna and Mukta reservoirs this research focuses on the heterogeneous Formation-A, and high quality – less heterogeneous Formation-B. Both of which have supporting core information. The Abiod chalk of Miskar is used as a “homogeneous” end member.
- The Panna and Mukta reservoirs are neighbouring fields. Although both contain similar rocks types and geological zonations, Panna is noted to have been more heavily affected by processes of diagenesis. This is reflected in the porosity and permeability data being significantly higher in the Panna formations than Mukta.
- Well log-derived petrophysical properties of porosity and permeability show strong correlation to the directly measured core data for each of the reservoirs.
- Geological features have strong controls on the petrophysical properties estimated from well log data in Panna and Mukta examples;
 - The heterogeneous nature of Formation-A in terms of carbonate facies and shale content is clearly seen in the high amplitude and frequency of variability

in Vsh, porosity and permeability curves. The dominant wackestone facies is seen as a notably smaller porosity in this zone.

- The basal karstic unconformity of Formation-A is seen as a decrease in porosity, with an abrupt fall in permeability. This will act as a major barrier to flow, and is identified as such by flow zone analysis.
- Formation-B shows much negligible shale content, supporting the clean limestone description. Porosity and permeability are high in this zone (averaging 22% and 20mD respectively) and show limited low frequency variation downhole. This is expected to relate to the grainstone dominated facies, combined with increase dissolution of varying grain component by the diagenetic fluids.
- Formation-C shows a marked decrease in porosity and permeability, supporting the sedimentological analysis. However Vsh estimates suggest minimal shale content.
- Formation-D shows similar variability to Formation-B. Porosity and permeability are ~10% less in this zone, this is suggested to relate to the limestone being more packstone facies-dominated, having smaller original pore types. Two horizons of tight carbonate mudstone are identified by significant decreases in both porosity and permeability in the upper part of this zone.
- Well log-derived fluid flow zonations show good correlation with geological zonations in both Panna and Mukta.
 - Formation-A is shown to comprise a number of small-scale flow zones, grouped together here (but discussed further in later chapters). The flow zones of Formation-A are clearly bound by the basal unconformity, as discussed above.
 - Formation-B is composed of two flow zones, the upper one being suggested to have higher reservoir quality.

- Formation-C correlates to an individual flow zone, of lower quality than the surrounding *B*-zone flow zones.
- Formation-D comprises 3 flow zones, of similar quality to that of the bottom section of Formation-B.
- The well log data indicates that the Miskar Abiod chalk is not as homogeneous downhole as the sedimentological descriptions of core suggest. Small scale changes in porosity and permeability through the section (for example 20-30% variation in porosity) reflects this internal variability in physical properties, although lithology is suggested to be more homogeneous (reflected in the *V_{sh}* estimate).
- This small-scale variability in physical properties, allows the Abiod to be subdivided into 5 flow zones.

Chapter 4. Heterogeneity; definition, quantification and basic application to carbonate petrophysical data

4.1. Introduction

It is important to fully understand the variability and spatial distribution of petrophysical properties, such as porosity and saturation, throughout a reservoir. This is especially true in the case of carbonate reservoirs, which often have considerable variability, as shown in Chapter 2. Common reservoir heterogeneities include grain/rock component and distribution (mineralogy, fossils and lithology), grain size distribution, cementation, fluid distribution, and pore system types, sizes and connectivity. These heterogeneities clearly affect petrophysical log responses (e.g. nuclear, resistivity and sonic) and derived petrophysical parameters such as porosity, saturation and permeability.

Reservoirs can be investigated and their properties measured at a variety of scales, from large-scale seismic surveys (kilometres) to wireline borehole logs (metres), visual core analysis and borehole image analysis (centimetres). Finer-scale detail (small than centimetre scale) can be obtained from the analysis of thin sections and SEM images, and special core analysis (SCAL) at a core-plug and chip scale. At each scale of measurement various heterogeneities may exist. A unit which appears homogeneous at one scale may be shown to be heterogeneous at a finer-scale, and vice versa. Clearly as more detailed information is obtained reservoir characterisation, and the integration of the various data types, becomes increasingly complicated.

Most, if not all, of the literature on reservoir characterisation and petrophysics refers to reservoirs as being heterogeneous in nature. However the term “heterogeneity” is rarely defined by the author, and no single definition has been produced and applied consistently across the board. Heterogeneity appears to be a term which is readily used to suggest the complex nature

of the reservoir, and the author often assumes the reader has a pre-existing knowledge and understanding of such variability. Reservoir characterisation researchers are now beginning to investigate the quantification of various heterogeneities, and the concept of heterogeneity as a scale-dependent descriptor (Frykman 2001; Jennings & Lucia 2003; Pranter *et al.* 2005; Westphal *et al.* 2004).

This chapter reviews published work on reservoir characterisation and heterogeneity, with particular reference to carbonate reservoirs. It will also look to other scientific disciplines (primarily the environmental sciences and ecology) for further definitions and methods which may be applicable to the petroleum industry. Statistical techniques will then be applied to reservoir sub-units to investigate their effectiveness for quantifying heterogeneity in petrophysical well log data.

4.2. Defining Heterogeneity

As mentioned above, the petroleum geoscience or petrophysical literature rarely provides a definition of the term heterogeneity. The Oxford English Dictionary defines heterogeneity as being diverse in character or content. This broad definition is quite simple and does not comment on the spatial and temporal component of variation. Other words/terms which may be used with, or instead of, heterogeneity include;

- Complexity
- Variability
- Deviation from a norm
- Randomness
- Discontinuity
- Dissimilarity
- Changes
- Differences
- Intricacy
- Composites
- Uncertainties

Nurmi *et al.* (1990) suggest that the distinction between homogeneous and heterogeneous is often relative, and is based on economic considerations. This highlights how heterogeneity is a somewhat fluid concept which can be changed/re-defined to describe various situations that arise during production from a reservoir, and is heavily biased by the analyst's experience and expectations. Li and Reynolds (1995) and Zhengquan *et al.* (1997) state that heterogeneity is defined as the complexity and/or variability of the system property of interest in space, in terms of the ecological sciences. Frazer *et al.* (2005) define heterogeneity, within an ecological model, as variability in density of discrete objects or entities in space. These definitions highlight that heterogeneity does not simply refer to the overall system, or rock/reservoir (or even formation), but instead should be dealt with separately for individual units, properties/parameters and measurement types.

In studies of forest canopy structure, Frazer *et al.* (2005) comment that heterogeneity is an inherent, ubiquitous and critical property that is strongly dependent on scales of observation and the methods of measurement used. They also state that heterogeneity is the degree of departure from complete spatial randomness towards regularity and uniformity. This is counterintuitive at first sight because heterogeneity is commonly regarded as being complete spatial randomness, with the introduction of regular features, such as bedding, adding to the heterogeneous (or anisotropic) nature of the formation. Nurmi *et al.* (1990) suggest that heterogeneity, in electrical borehole images, refers to elements which are distributed in a non-uniform manner or composed of dissimilar elements/constituents within a specific volume. Here, as well as looking at a specific element or property, it is also suggested that the volume of investigation influences heterogeneity, again alluding to the scale-dependence of heterogeneities. When designing ecological field experiments, Dutilleul (1993) comments that a shift of scale may create homogeneity out of heterogeneity, and vice-versa. Lake and Jensen (1991) provide a flow-based definition in their review of permeability heterogeneity modelling within the oil industry. They define heterogeneity as the property of the medium that causes the flood front to distort and spread as displacement proceeds. Here, medium refers to the rock, and fluid front is the

boundary between displacing and displaced fluids. Dutilleul (1993) suggests that heterogeneity is the variation in density of measured points compared to the variation expected from randomly spread points. Here we are beginning to see that heterogeneity may be a quantifiable term.

Five basic types of heterogeneity are identified in the literature;

- Spatial (both lateral, vertical and three-dimensional)
- Temporal (one point at different times)
- Functional (taking correlations and flow-paths into account)
- Structural (a. non-correlated, b. structures – faults, folds...)
- Stratigraphic

The three extremes of homogeneity, with regard to grain packing, can be imagined in a formation that consists of (1) a single mineralogy with (2) all grains of similar shapes and sizes with (3) no structures present. Ignoring the scalar component of heterogeneity for a moment, there are two contrasting examples of heterogeneity. The first example is a formation of consistent mineralogy and grain characteristics which has various structures (for example bedding, foresets, or syn-sedimentary faulting). The second example is structureless (massive) but has variable mineralogy and grain size and shape, and is poorly sorted. Both are clearly not homogeneous but which has the stronger heterogeneity? It is best to define heterogeneity strength in terms of the purpose of the investigation; for example in a study of fluid flow sedimentological structures may be of more importance than variation in mineralogy, while investigations of gamma ray variability would reflect more mineralogical than structural variation. Formations may have regular and penetrative structural features such as bedding and cross-bedding, or alternatively less regularly distributed features, including ripples, hummocky cross-bedding, and bioturbation. The intensity, frequency and orientation of such rock structures may additionally reflect cyclicity through the succession. A heterogeneity, in terms of the grain

component, may appear cyclic (rhythmically or repeated), patchy, gradational / transitional, or again it may be controlled by depositional structures.

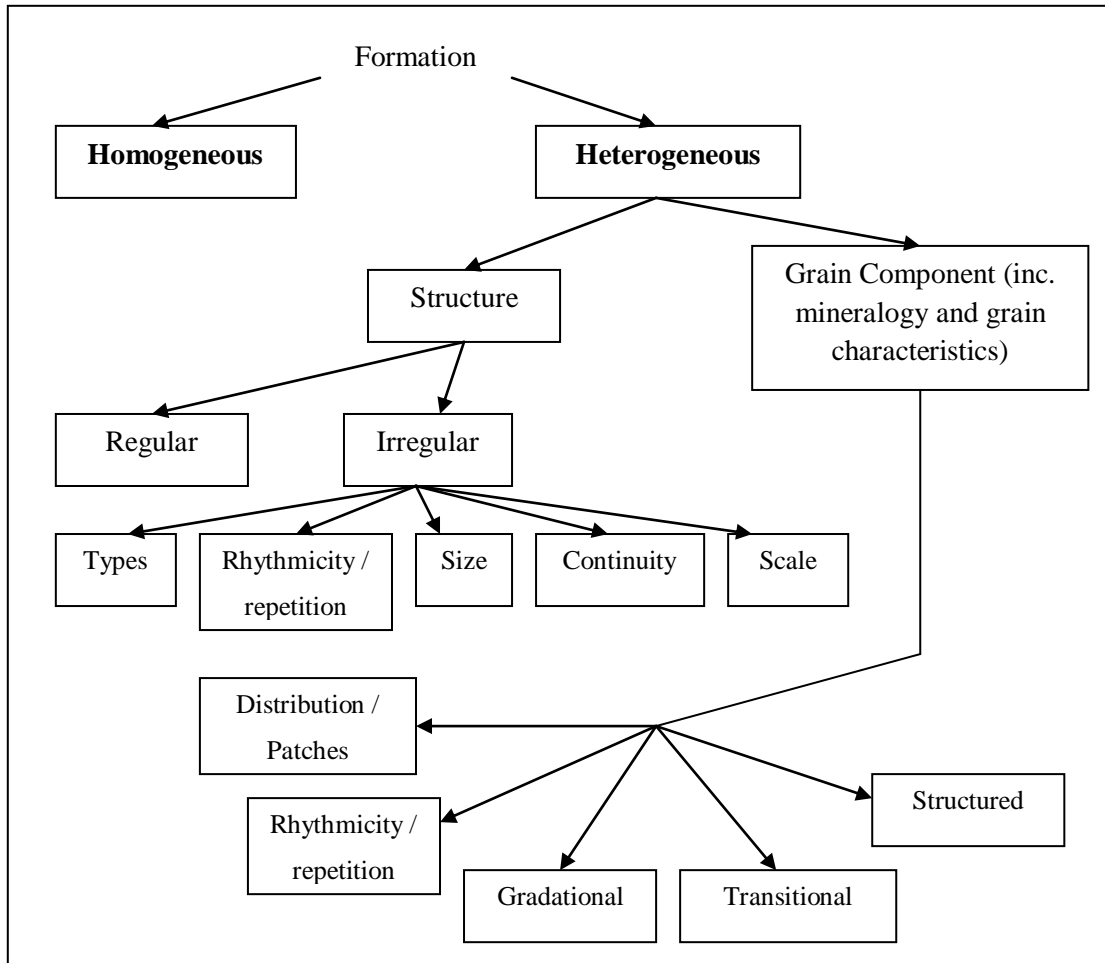


Figure 4.1. Illustrating how heterogeneity can be separated into two ‘end-members’ of structural and grain component.

Figure 4.1 illustrates how heterogeneity can be broken down into ‘end-members’. There are a number of characteristics which occur in both end-member examples provided above (for example repeated units). Neither end-member is obviously more heterogeneous than the other; there may be a relative scale between the two examples. Some researchers may perceive a regularly structured system, for example lamination/bedding, as homogeneous because these structures are spatially continuous and occur throughout the formation. The presence of structures within a formation are however more commonly interpreted as a type of heterogeneity, regardless of how regular their distribution. In this scenario, the structures are seen to represent deviation from the homogeneous mono-mineralic ‘norm’. Equally the concept

of increased heterogeneity could be viewed as simply being an increase in the random mixing of components of a formation; this does appear counterintuitive to the definitions given above.

However, in this case as the formation becomes more heterogeneous there is less structure present, so that the formation has the same properties in all directions. Here, although the rock is more heterogeneous, the actual reservoir properties (such as porosity distributions) become more homogeneous throughout the reservoir as a whole.

If grain-size alone varies, two possible extremes of heterogeneity may occur. In one example there is a complete mix of grain sizes which show no evidence of sorting. This would be classed as a heterogeneous mixture in terms of its components; however the mixture itself would appear homogeneous as, on a larger-scale, the rock properties would be the same in all directions. If this mixture of grain size was completely unsorted then it could be expected that the grains were all completely randomly distributed to the point where overall the rock appears homogeneous at a larger scale. Again this highlights the importance, and the fact that, heterogeneity is a scale-dependent descriptor. In another example, the formation contains either patches or layers (continuous or discontinuous) of a different grain size, or that are poorly sorted. This is more of a structural heterogeneity, again depending upon the scale of investigation. Looking at the individual patches of similar grain size they may appear homogeneous, however if looking at a contact between the two, or the formation as a whole then the heterogeneity will be much more obvious.

Along with defining a measure of how heterogeneous a system property is, the type of heterogeneity examined must be defined or an additional measure for the type of heterogeneity present should be included. Generally the grain or pore components and characteristics would affect fine-scale heterogeneity, while the more structural elements can occur on, and affect, a variety of scales. The presence and distribution of the various components which may describe a heterogeneity (discussed here as structures and grain/pore characteristics) will all have varying effects on the heterogeneous properties of a system. It would therefore be of interest to look into

which actual components of heterogeneity have a greater impact on petrophysical measurements and parameters, as well as on general reservoir performance.

4.2.1 Carbonate Heterogeneities

Carbonate reservoirs are well documented for their complex internal structure (Akbar *et al.* 1995; Kennedy 2002; Lucia 1999; Moore 2001; Tucker & Wright 1990). Most known carbonate reservoirs are heterogeneous by nature, even apparently simple mono-mineralic low energy shelf and basin facies are rarely homogeneous. The variation within carbonates is generally related to the numerous ways in which carbonate grains and matrix coexist. Unlike most clastic rock types, carbonates are known for being chemically unstable and undergoing substantial alteration, e.g. dissolution and dolomitization (Akbar *et al.* 1995).

Calcite and dolomite are the most common minerals in carbonate reservoirs and each has significantly different physical properties (chapter 2). In reality carbonate reservoirs are rarely mono-mineralic, this mixing and intermingling of the two minerals clearly complicates analysis even although calcite and dolomite have distinct properties. At a log-scale carbonate rocks will appear to be one mineral or the other, rather than a mixture of the two (Kennedy 2002).

Lithological variation can also be documented by changes in sedimentological facies. This facies variation generally occurs on a larger scale than that of mineralogy alone. Heterogeneities in carbonate sedimentary facies may be defined by changes in grain characteristics (e.g. size, shape, and sorting), fossil content (including trace fossils / bioturbation), and structures such as bedding, cross-bedding, grading, water-escape features, and ripples. The way in which one facies passes laterally into another can be gradual (graded), abrupt or be seen as inter-stratified mixing of the two (Nichols 2001; Tucker & Wright 1990). Within a succession facies may be randomly arranged or repeated in regular cycles.

Most problems in carbonate reservoir exploration are concerned with the large variation in porosity systems encountered. Fifteen different types of carbonate porosity systems are documented in the literature (Lucia 1999; Moore 2001), and often two or more porosity systems

exist in a single carbonate reservoir. In carbonates porosity will often increase as sorting decreases; the opposite effect is seen in clastic rocks (Lucia 1999). Carbonate porosities are complicated further by the fact that a carbonate initially has a high porosity which it will lose gradually over time (Lucia 2000).

Two other features common to carbonates which may introduce or increase heterogeneity are fractures and stylolites. Stylolites form by pressure solution during compaction of the carbonate sediment; fine-grained insoluble residues become concentrated along what appear to be irregular planes of discontinuity (Akbar *et al.* 1995; Nichols 2001; Tucker & Wright 1990). The fine-grain residue within stylolites is commonly different to the surrounding rock with a different mineralogy and/or porosity. Fractures are generally irregular and cut across pre-existing fabrics. They commonly occur in carbonates because of tectonic deformation, slumping or dissolution collapse (Tucker & Wright 1990). It is most common that fractures remain open, acting as strong porosity and permeability enhancers (Aguilera 2004).

As mentioned earlier, carbonates are known to be less chemically stable than siliciclastic rocks types and so are easily modified during diagenesis. Common diagenetic processes which affect carbonates are cementation, compaction, dissolution, and dolomitization. These processes rarely act evenly throughout a carbonate formation, generating heterogeneities which are generally considered to enhance any pre-existing variation present. It is common to find uranium substituted for calcium in calcite. This type of substitution may have occurred at deposition or may have occurred later because of the introduction of diagenetic fluids.

The various studies summarised here, and in chapters 2 and 3, have shown that heterogeneities are not chaotic or randomly distributed within carbonate reservoirs. Indeed, the detection of heterogeneities is often dependent upon the manner of examination and on the technology used (Nurmi *et al.* 1990). A more comprehensive understanding of carbonate heterogeneity and its recognition in petrophysical measurements could significantly aid exploration in these important resources.

4.2.2 Petrophysical Heterogeneities

Heterogeneities, such as those outlined in section 4.2.1, have varying impacts on log responses (both wireline and electrical images) and, in turn, on derived petrophysical properties and parameters, such as porosity and saturation. Some of this variation may be a feature of the measuring technique, for example averaging and shoulder effects, whilst other variations may relate to bedding, structures (both sedimentological and tectonic), lithological variation (including grading), and fluid content, as well as micro-scale changes in mineralogy and lithology. The heterogeneity, or rather homogeneity, of core plugs should be determined because ideally porosity, saturation and the Archie constants will be determined from analysis of an individual homogeneous core plug that is assumed to be in some way representative of the reservoir.

Different tools have different resolutions and depths of investigation, depending on tool physics and the designs of individual companies. The sonic tool investigates a circular annulus with a radius of ~5cm around the borehole whereas the neutron tool investigates an elliptical area (with ~20cm maximum width) around the tool which is off-centred within the borehole. The density tool is effectively a pad pressed against the borehole wall designed to emit and detect gamma-rays in one direction, subsequently it only responds to a 45° arc up to 10-15cm from the borehole. In a homogeneous rock the fact that the tools measure different portions of the rock surrounding the borehole would have no noticeable effect on measurements and relationships between these three tools, assuming no invasion. However as soon as a heterogeneity is present the three tools may be measuring different volumes of rock with different properties.

Lovell and Kennedy (2005) comment that the vertical resolution of the tool generally has a far smaller effect than inherent filtering. The filtering of raw logging data occurs because logging tools commonly sample every 6 inches. Therefore an individual data point actually represents an average value for the previous 6 inches of cable movement, and a lateral volume defined by the tool's volume of investigation. Any small scale heterogeneities within this 6 inch depth interval may therefore be filtered out of the data. This is of particular importance if the small-

scale heterogeneity is a porous interval within a non-porous formation (or vice-versa), or in the presence of a low porosity sealed fracture or highly cemented interval.

There are many log indicators for reservoir heterogeneity, however they do not generally reveal the type of heterogeneity present (Nurmi *et al.* 1990). Again, the different depths and volumes of investigation cause problems when investigating heterogeneous carbonate reservoirs because two different tools may not be measuring the same interval. For example neutron-density separation is used in identifying limestone- and dolomite-rich sections but if the reservoir is heterogeneous then neutron-density separation will provide an intermediate value with limited lithological relevance (Kennedy 2002). Decimeter-scale heterogeneities can cause discrepancies between the wireline log data from different runs, at different orientations, down the same hole because of shoulder or averaging effects. This lack of repeatability is often put down to technical faults, rather than being an effect of the rock itself (Nurmi *et al.* 1990).

The total cumulative hydrocarbon pore volume (HCPV) can be used to estimate the potential hydrocarbon storage of a reservoir, Equation 4.1 (Tabanou *et al.* 2004).

$$HCPV = GRV \times \emptyset \times \left(\frac{N}{G}\right) \times (1 - S_w) \times FVF \quad (\text{Equation 4.1})$$

where: *HCIIP* - hydrocarbons initially in place, *GRV* - gross rock volume, \emptyset – porosity, *N/G* - net to gross ratio, *S_w* - water saturation, *FVF* - Formation Volume Factor

Tabanou *et al.* (2004) suggest that uncertainties in HCPV are most strongly affected by uncertainties of the areal extent of the reservoir, which is poorly estimated from seismic data and areas of limited borehole drilling. Uncertainty in the estimation of HCPV can clearly be affected by heterogeneity in petrophysical properties; primarily because the net-to-gross ratio estimated from each drilled well must be propagated laterally throughout the reservoir. From the HCPV equation (4.1) it is also apparent that even a 1% error in any of the parameters will have a similar and substantial effect. Increased density drilling programmes, coupled with a better

understanding of the heterogeneous nature of a formation and its influence on petrophysical properties will further decrease the uncertainties in HCPV estimation (Tabanou *et al.* 2004).

The heterogeneities present in many carbonate reservoirs often means that a whole piece of core is commonly not representative (Akbar *et al.* 1995). In their paper outlining a new method for the evaluation of the impact of localised heterogeneity on relative permeability and capillary pressures, Egermann and Lenormand (2005) note that core heterogeneities can severely affect the determination of petrophysical parameters by special core analysis (SCAL) and their interpretations (Egermann & Lenormand 2005). Indeed petrophysical properties are rarely constant through an entire core plug, yet a single average value is commonly all that is taken for each plug.

Petrophysical characterisation of the Al Kharrata East Field of Syria, a Lower Cretaceous carbonate reservoir, revealed that the log responses were adversely affected by an extreme heterogeneity in terms of mineralogy, organic matter and the presence of crypto-crystalline silica containing water (Boya-Ferrero *et al.* 2004). In this reservoir, the standard deviation on measurements was larger than the absolute value itself (Boya-Ferrero *et al.* 2004). Even the use of core-log calibration did not aid the estimation of porosity values, as core values were thought to be underestimated while log values were also anomalously low due to the presence of organic matter. Boya-Ferrero *et al.* (2004) therefore show that integrated studies of all petrophysical and geological data will provide the key to understanding heterogeneous tightly fractured carbonate field such as this.

4.2.3 Geological Scales and Tool Resolution

In order to investigate heterogeneity at different scales and resolutions, the concept of “scale” and how it relates to different parameters should be discussed. Carbonate reservoir exploration is multi-scale in nature, as it involves dealing with geological attributes (mm – km scale), wireline log measurements (cm – dm scale) and petrophysical core measurements (mm – cm scale). This of course is simplifying the differences, as figure 4.1B illustrates with a schematic

illustration of common scales at which different geological features are documented and provides comparison to the volumes of investigation of basic wireline logging tools (table 4.1) and other reservoir data. This section introduces this topic briefly, before later sections and chapters investigate heterogeneity at different scales and resolutions; for example the remainder of this chapter will focus on a “formation-scale” investigation, in the order of tens of metres.

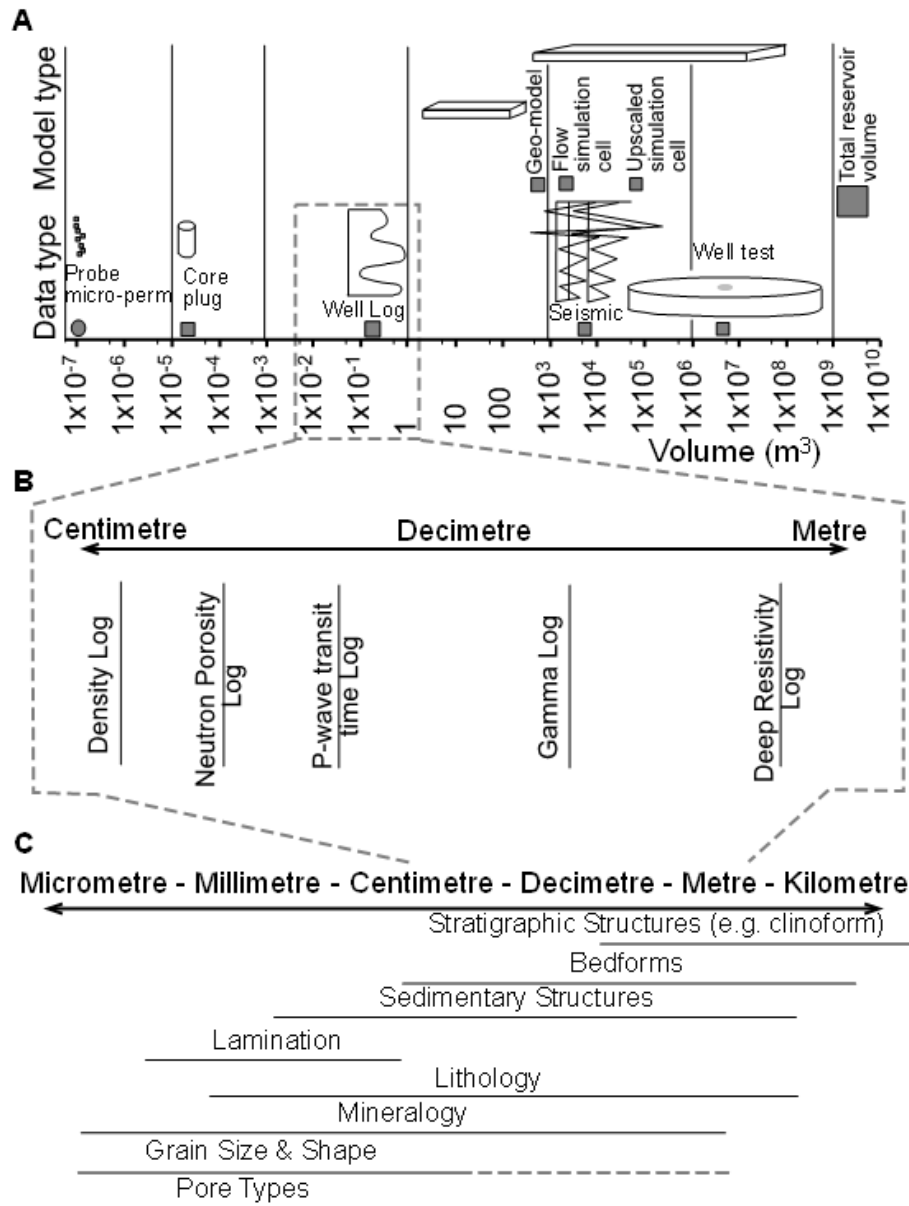


Figure 4.1B . Sketches illustrating how scales of geological features, wireline logs and different types of hydrocarbon reservoir data / model elements are related: (A) Illustration of volume measures for different types of data and model elements (after Frykman and Deutsch 2002), (B) Schematic illustration of different wireline log scales – based on tool resolution and volume of investigation (see table 1.1), and (C) Schematic illustration of key geological heterogeneities and the scales of which they exist.

Geological and petrophysical properties exist over a gradational continuum of scales (Nichols 1999; Moore 2000); figure 4.1B (c) is a schematic representation of this. An example of a geological property that can exist over multiple scales is porosity in carbonates. The variety of pore types has been previously discussed (see Chapter 2). In carbonate rocks pore size can be seen to vary from less than micrometre-size micro-porosity to millimetre-scale inter-particle and crystalline porosity. Vugs are commonly documented to vary in size from individual to tens of centimetres. Additional dissolution and erosion may create huge caves, or “mega-pores” (often being metres to kilometres in size).

Different wireline measurements will respond to, and capture, the different parts or scales of geological heterogeneity (Figure 4.1B). It would be expected that the geological features that exist under the resolution of tools shown here (Figure 4.1B b) will in effect be averaged out in the data (Ellis 2007); as such the typical types of carbonate heterogeneity suggested to be captured by these wireline logs are lithology, mineralogy, pore volume (including general mineralogy and pore volume, not indicating individual grain and pore type or size), and additionally medium-scale sedimentary structures such as cross-bedding, bedding and syn-sedimentary deformation may be sampled as discontinuities between values (Rider 2002). As with all investigations the analyst must be aware of what the measurement is sampling, along with the type and scale of underlying feature of interest. Another related topic which is not discussed further in this thesis, is that of up-scaling from detailed core measurement to petrophysical well log calibration, and eventually to subsurface and flow models of the reservoir at seismic-scale.

Following from the previous discussion defining heterogeneity; as well as detailing what type of geological heterogeneity or property is being investigated, we must also ensure awareness of the resolutions (and limitations) of the measurement device/tool in use, and how it relates to the scale of the underlying feature/heterogeneity being investigated. By doing this the analyst can be sure that appropriate assumptions are outlined and documented. Although not used in this investigation, tools such as FMI logs (table 4.0) and nuclear magnetic resonance (NMR) acquire

data at a higher resolution. These additional data may be used to extend the investigation of numerical heterogeneity into smaller-scale features.

Wireline Log (Output)	Gamma Ray	Bulk Density	Neutron Porosity	Compressional Sonic Velocity	Deep Resistivity	FMI
Tool	<i>HILT Gamma Ray Neutron Sonde (HGNS)</i>	<i>High Resolution Mechanical Sonde (HRMS)</i>	<i>HILT Gamma Ray Neutron Sonde (HGNS)</i>	<i>Dipole Sonic Logging tool (DSLTL)</i>	<i>HILT Azimuthal Laterolog Sonde (HALS)</i>	<i>Fullbore Formation MicroImage (FMI)</i>
Logging Speed (ft/hr)	3600	3600	3600	3600	3600	1800
Range of Measurement	0-1000 gAPI	1.04-3.3g.cm ³	0-60 p.u	40-200us/ft	0.2-40000 ohm-m	0.2-40000 ohm-m
Accuracy	±5%	±0.01g.cm ³	0-20pu ±1pu 30pu ±2pu 45pu ±6pu	±2us/ft	1-2000 ohm-m ±5%	Deviation ±0.2° Azimuth ±2°
Precision (Repeatability)	--	0.025g.cm ³	--	--	--	--
Vertical Resolution	12 in.	18 in.	12 in.	2 ft.	18 in. (standard)	0.2 in.
Depth of Investigation	24 in.	5 in.	~9 in.	3 in.	~32 in.	1 in.

Table 4.1. Summarising details of the logging tool specifications from Schlumberger information sheets (SLB 2004). [Note that HILT : High-resolution Integrated Logging Tool].

4.3. Quantification of Heterogeneity

This section reviews and summarises the methods of measuring and quantifying heterogeneity in petrophysical and other scientific discipline’s literature. The techniques are then applied to petrophysical well log data from Formation-A and -B of the Panna well P, detailed in Chapter 3. This chapter focuses on the bulk density, neutron porosity, and P-wave transit time well log measurements.

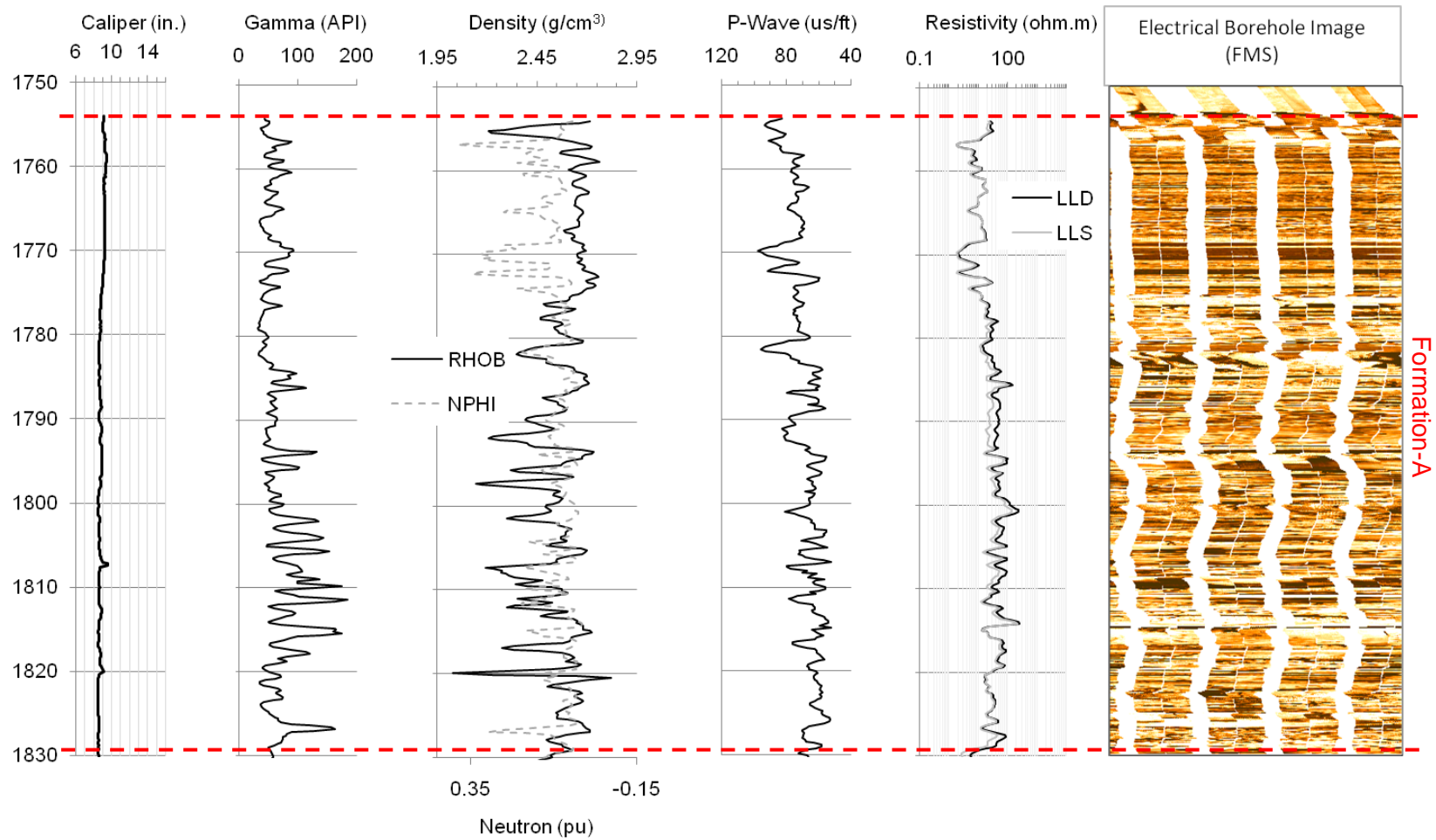


Figure 4.2. Wireline and FMS electrical image log plots for the well P Formation-A. Panels from left to right; (1) caliper, (2) gamma ray, (3) bulk density (RHOB) & neutron porosity (NPHI), (4) P-wave transit time, (5) deep and shallow resistivity (LLD and LLS respectively), and (6) FMS Electrical borehole image.

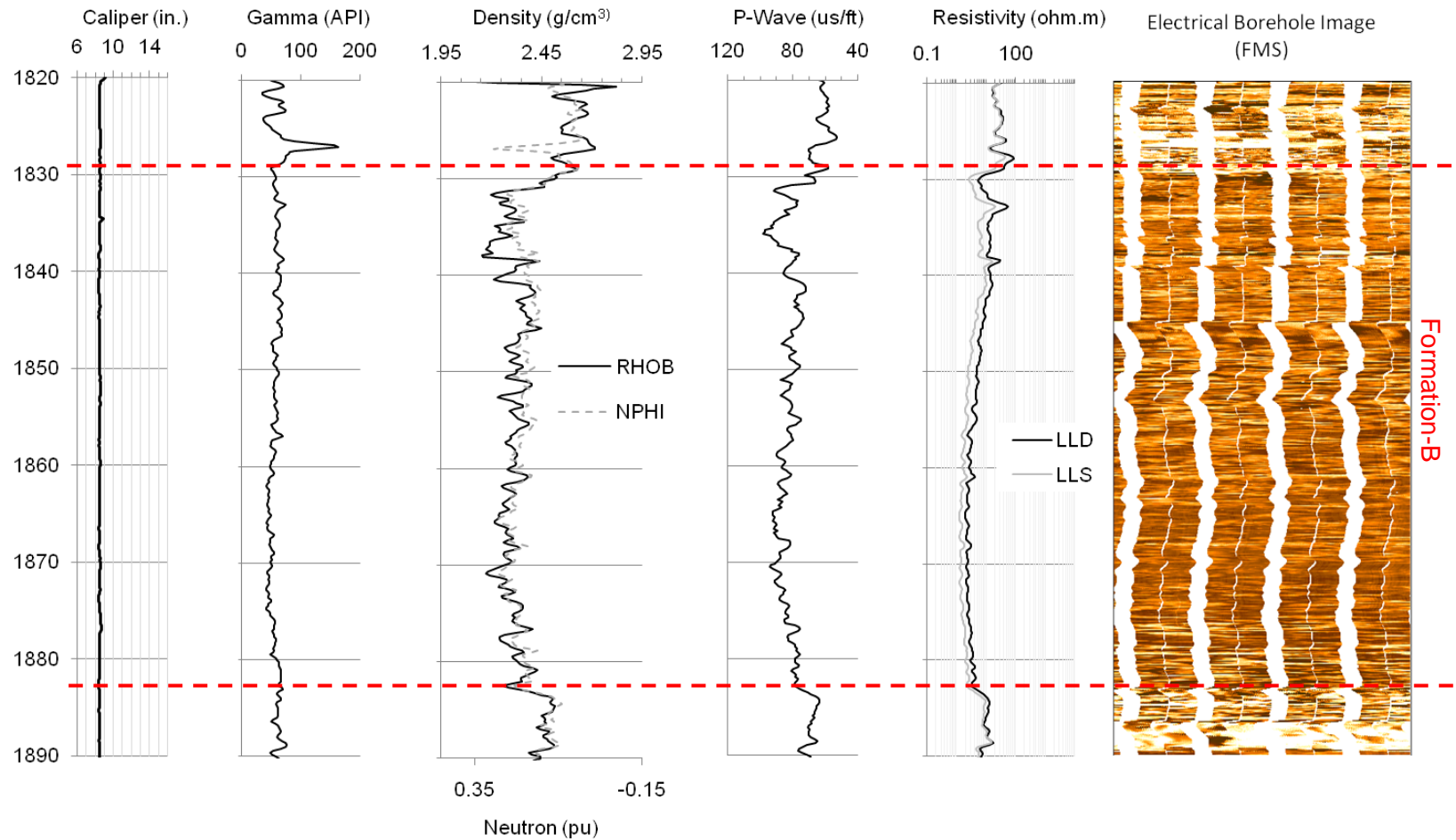


Figure 4.3. Wireline and FMS electrical image log plots for the well P Formation-B. Panels from left to right; (1) caliper, (2) gamma ray, (3) bulk density (RHOB) & neutron porosity (NPHI), (4) P-wave transit time, (5) deep and shallow resistivity (LLD and LLS respectively), and (6) FMS Electrical borehole image.

The statistical methods described below can be grouped as either (1) characterisation or (2) quantification of heterogeneity. Although used in characterising spatial variability, variograms will be dealt with separately due to the breadth of this topic

4.3.1 *Characterising Heterogeneity*

As previously discussed a simple glance at the log plots of Formation-A and -B (figures 4.2 and 4.3 respectively) suggests that Formation-A is more “heterogeneous” than Formation-B. The next step in completing a standard petrophysical analysis is to produce crossplots of the well log data; these also give visual clues as to the relative heterogeneities of the two zones (figure 4.4). Here we see Formation-A has a diverse distribution of values across the plots indicating its heterogeneous nature. Formation-B on the other hand is more clustered along a linear trend.

Basic statistics can be used to characterise the variation in distributions of values within data sets, Table 4.1 shows the values returned for bulk density, neutron porosity and P-wave transit time (sonic slowness) measurements for Formation-A and -B, histogram distributions are provided in figure 4.5 for comparison. No corrections have been applied to the “raw” well log data for fluid type (gas/oil/water) as this study is investigating the heterogeneity of the complete system.

Clearly the two formations have different levels of heterogeneity in their physical properties relating to the underlying reservoir geology; with Formation-A consisting of varied lithologies and porosity systems and Formation-B being predominantly carbonate packstone and grainstone facies (chapter 3). We can see that Formation-A generally has low responses which are highly skewed and have a lower kurtosis (explained in table 4.1 caption). Simply looking at the range in values and standard deviation indicates that Formation-B has a lower degree of heterogeneity; both statistics suggest that Formation-B is almost half as variable as Formation-A.

Figure 4.5 and table 4.1 demonstrate that basic statistics can be used to characterise variation within a dataset, producing a suite of numbers which describe data distributions. However we

need to complete and understand the full suite of statistical test to achieve what is still a fairly general numerical characterisation of heterogeneity.

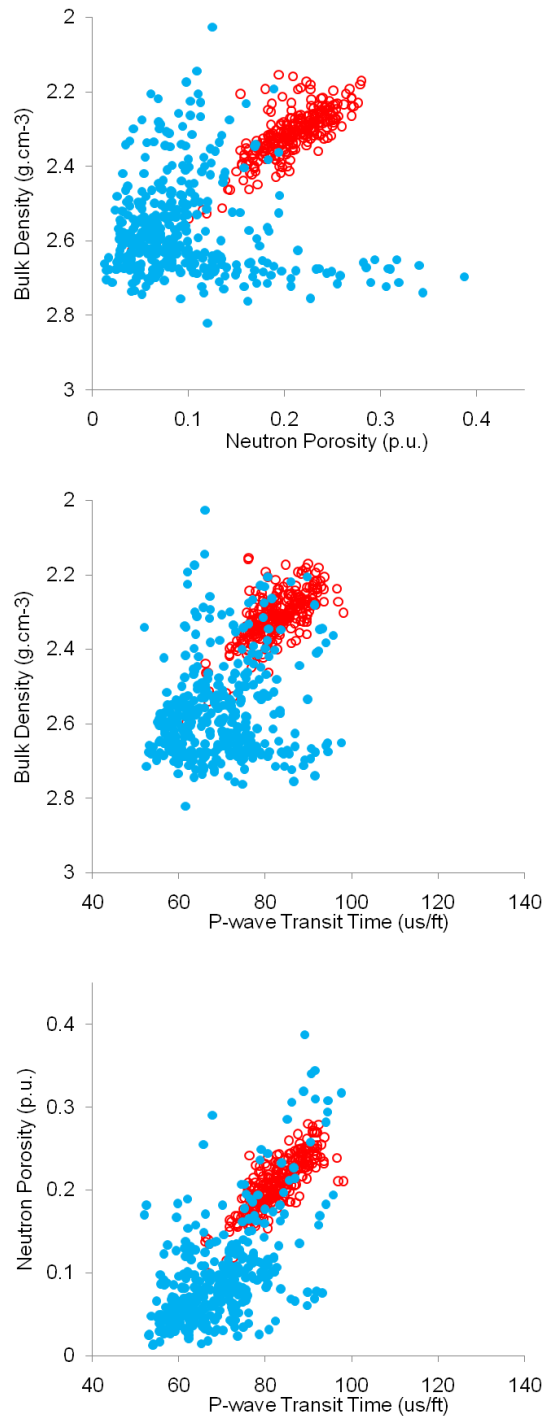


Figure 4.4. Crossplots of neutron porosity – bulk density (top), P-wave transit time – bulk density (middle) and P-wave transit time – neutron porosity (bottom); for Formation-A (blue circles) and -B (red, open circles).

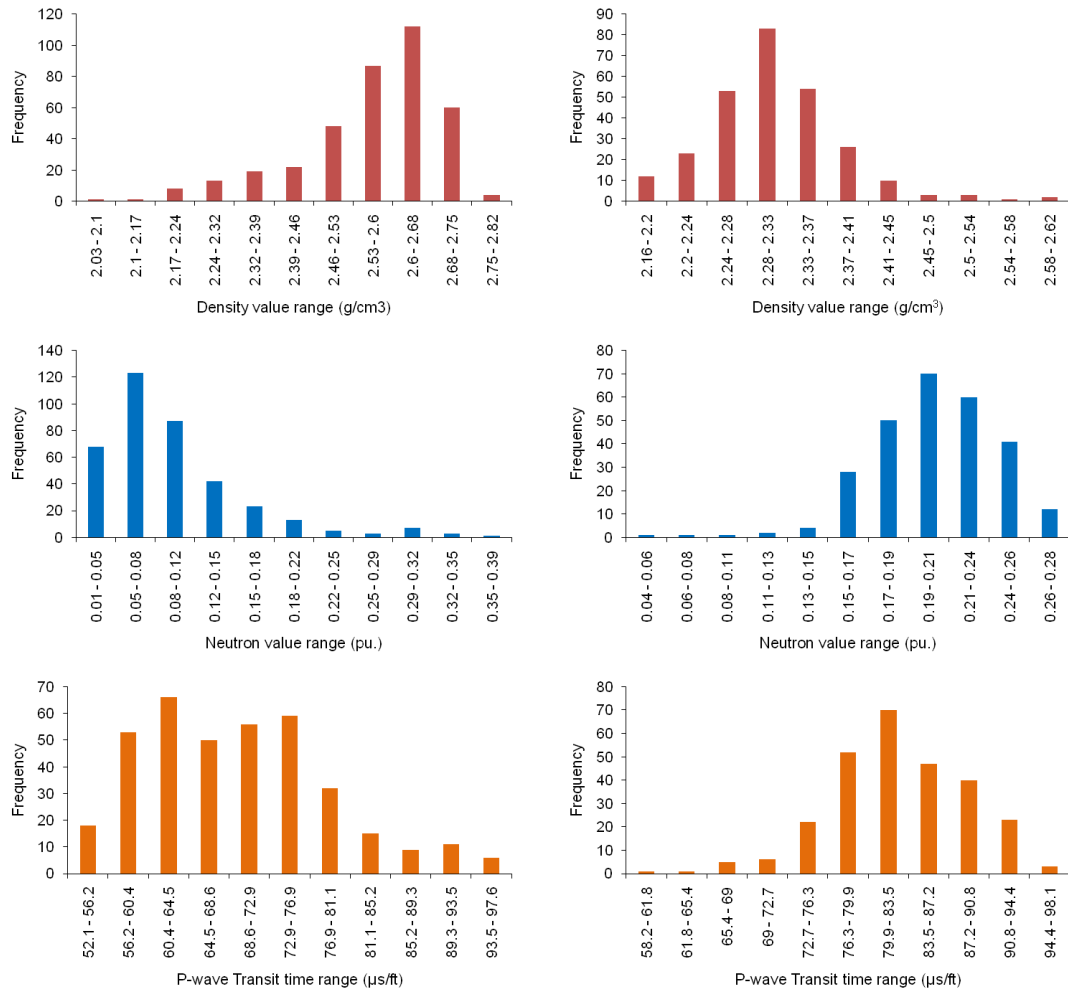


Figure 4.5. Histogram distributions for bulk density (top), neutron porosity (centre), and P-wave travel time (bottom); for Formation-A (left) and Formation-B (right).

	Bulk Density (g.cm ⁻³)		Neutron Porosity (p.u.)		P-wave travel time (µs/ft)	
	Formation	Formation	Formation	Formation	Formation	Formation
	-A	-B	-A	-B	-A	-B
Mean	2.57	2.31	0.09	0.21	69.4	82.5
Mode	2.60	2.32	0.08	0.21	59.4	89.4
Median	2.60	2.31	0.08	0.21	68.7	82.6
Standard Deviation	0.1281	0.0693	0.0622	0.0340	9.5063	6.1539
Maximum	2.82	2.63	0.39	0.28	97.6	98.1
Minimum	2.03	2.16	0.01	0.04	52.1	58.2
Skewness	-1.1708	0.8654	1.8063	-0.7911	0.6046	-0.4135
Kurtosis	1.2052	2.5258	3.9320	2.4152	-0.0605	0.7920

Table 4.1. Results of statistical analysis for the bulk density, neutron porosity and compressional sonic velocity values of Formation-A and Formation-B. Statistical analysis; (a) mean, mode and median averages, (b) standard deviation and variance, (c) maximum, minimum and range between minimum and maximum, (d) skewness (measure of the asymmetry of a distribution, positive indicates higher values are more common than lower values), and (e) kurtosis (measure of the spread of data around a mean, more positive indicates single peak around a mean with less tails, more negative indicates less of a mean peak and larger tails).

The main problem with this simple set of statistics is that scale is not taken into account; for example two datasets of interbedded lithologies may have different thicknesses (different numbers of data points) but will produce the same statistical responses. The application of semi-variogram analysis can give us a more specific method for characterising petrophysical heterogeneities.

4.3.1.(a) Semi-variogram Analysis

The semi-variogram is a common geostatistical technique, used for modelling in a wide variety of scientific disciplines (including mineral and hydrocarbon exploration). Figure 4.6 illustrates the methodology for generating a semi-variogram, and also shows the three values that aid characterisation of numerical heterogeneity; the sill – maximum semi-variance, range – lag distance taken to reach this sill, and the nugget effect – intrinsic/short term variability below scale of investigation.

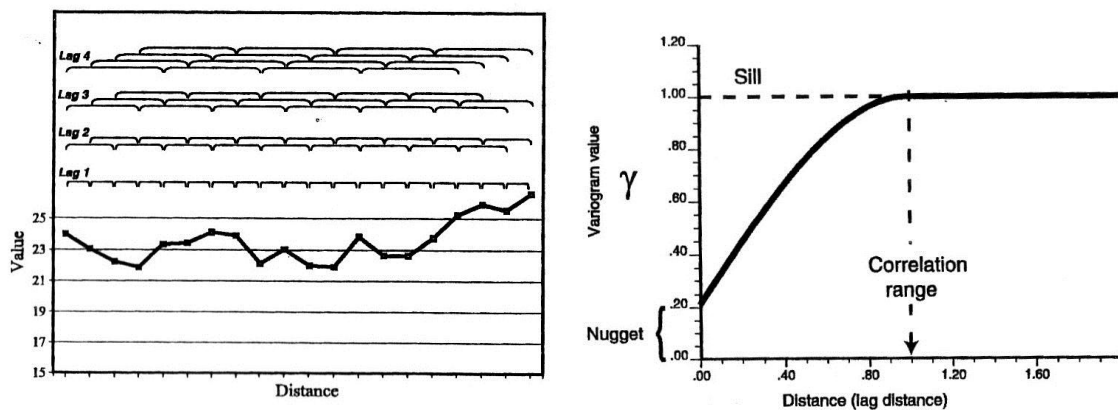


Figure 4.6. Illustration of (a) the methodology for generating a semi-variogram and (b) key value obtained from their analysis. [Semi-variogram methodology: 1) First the semi-variance between each point is calculated (lag1), lag 2 is the semi-variance between every other point, lag 3 is the semi-variance between every three points, and so on, 2) the semi-variance for each lag is then plotted against lag distance to produce the semi-variogram] (Frykman & Deutsch 2002).

Various other parameters and features may be documented from a semi-variogram analysis but are not detailed in this review (see references for further information). The semi-variance (sill) will increase as properties become more dissimilar. Frykman and Deutsch (2002) comment that the range is the distance at which little or no correlation occurs between points, and suggest that

lower range values represent higher system variability. Table 4.2 shows the values obtained from semi-variogram analysis on well logs from Formation-A and -B.

Curve	Fm.	Lag	Nugget	Sill	Range	Model	Fm.	Lag	Nugget	Sill	Range	Model
Density	A	1	0.01116	0.02302	25.22	Exp	B	1	0.00011	0.0044	1.21	Exp
Density	A	2	0.01135	0.0228	25.36	Exp	B	2	0.00013	0.00438	1.29	Exp
Density	A	5	0.01167	0.02504	34.66	Exp	B	5	0.00001	0.00439	4.34	Sph
Density	A	10	0.01172	0.02354	30.22	Exp	B	10	0.00001	0.00441	2.03	Exp
Neutron	A	1	0.00018	0.00352	0.76	Exp	B	1	0.00044	0.00146	14.46	Exp
Neutron	A	2	0.0002	0.00353	0.89	Exp	B	2	0.00045	0.00146	14.72	Exp
Neutron	A	5	0.00019	0.0035	1.32	Exp	B	5	0.00049	0.00171	22.17	Exp
Neutron	A	10	0.00011	0.00358	2.28	Exp	B	10	0.00053	0.00255	47.38	Exp
Sonic	A	1	43.7	195.2	79.85	Exp	B	1	4.6	39.13	3.21	Exp
Sonic	A	2	45.5	132	81	Sph	B	2	5.3	39.32	3.41	Exp
Sonic	A	5	44.2	197.5	81	Exp	B	5	6	39.84	3.95	Exp
Sonic	A	10	43.5	201.7	81	Exp	B	10	5.2	40.11	4.49	Exp

Table 4.2. Results from semi-variogram analysis on bulk density, neutron porosity, and P-wave transit time (Sonic) well logs for Formation-A (left) and Formation-B (right). Model: Exp – exponential, Sph – Spherical. Note that lag distance is in metres.

Table 4.2 suggests that the P-wave transit time measurements show greater variability than neutron porosity and bulk density in both zones because of the high sill values. However, it is suggested that the semi-variance sill values cannot be directly compared between the different measurements because they have different measurement scales (for example sonic varies from 40-140us/ft, while density varies from 1.95-2.95g.cm⁻³), instead we should compare range values. For example, Formation-A neutron porosity has the lowest range values which indicate that sill values are met at short distances between data point; i.e. maximum semi-variance is met very quickly for the neutron porosity dataset, suggesting it is more heterogeneous than the longer range sonic data. This suggests that porosity heterogeneity is of high importance here (which is an opposing view to the low amplitude and frequency variation of porosity downhole in figure 4.2). Interestingly, in Formation-B neutron porosity has the highest range values which indicate that porosity is less heterogeneous in this formation. On a side note table 4.2 shows semi-variogram analyses over four increasing lag distances, generally this indicates that increasing the lag (decreasing the resolution) will increase the semi-variance and the range –

supporting the interpretation that low frequency heterogeneities dominate this reservoir. The heterogeneities present within the different data types cannot be directly compared as semi-variance is still an artefact of the range of data present (table 4.1) rather than the internal variation within the dataset.

Calculating a suite of basic statistics and semi-variogram analysis for petrophysical well log data clearly allows the heterogeneities present within a reservoir unit to be characterised and understood, based on different physical properties measured by the different tools. However there is no single value to define the heterogeneity of dataset as being “x.x”, to enable direct comparison between different well logs, formations and reservoirs. To achieve a direct comparison *heterogeneity measures* are required.

4.3.2 Heterogeneity Measures

Heterogeneity measures are geostatistical techniques which provide a single value for heterogeneity in a dataset. Published heterogeneity measures, such as the Lorenz coefficient and the coefficient of variation, have been in common use throughout most scientific disciplines, and are frequently used in establishing porosity and permeability models in exploration. This and later chapters of this thesis show that development and application of heterogeneity measures to petrophysical well log data can aid understanding of variation in lithologies, rock fabrics (including porosity systems and pore connectivity), and fluid flow / hydraulic units (see chapters 5 – 6). Using physical property well log data, means the focus is on the application of static measures of heterogeneity without correlation (Lake & Jensen 1991). Measures with correlation are of more use for dynamic data, such as permeability. Methodologies for single property heterogeneity measures, commonly used in reservoir modelling, and also newly developed dual-property measures are presented below.

4.3.2(a) The Lorenz Coefficient

Where commonly used in hydrocarbon exploration modelling, the Lorenz Curve is a plot of cumulative flow capacity against cumulative thickness (Lake & Jensen 1991).

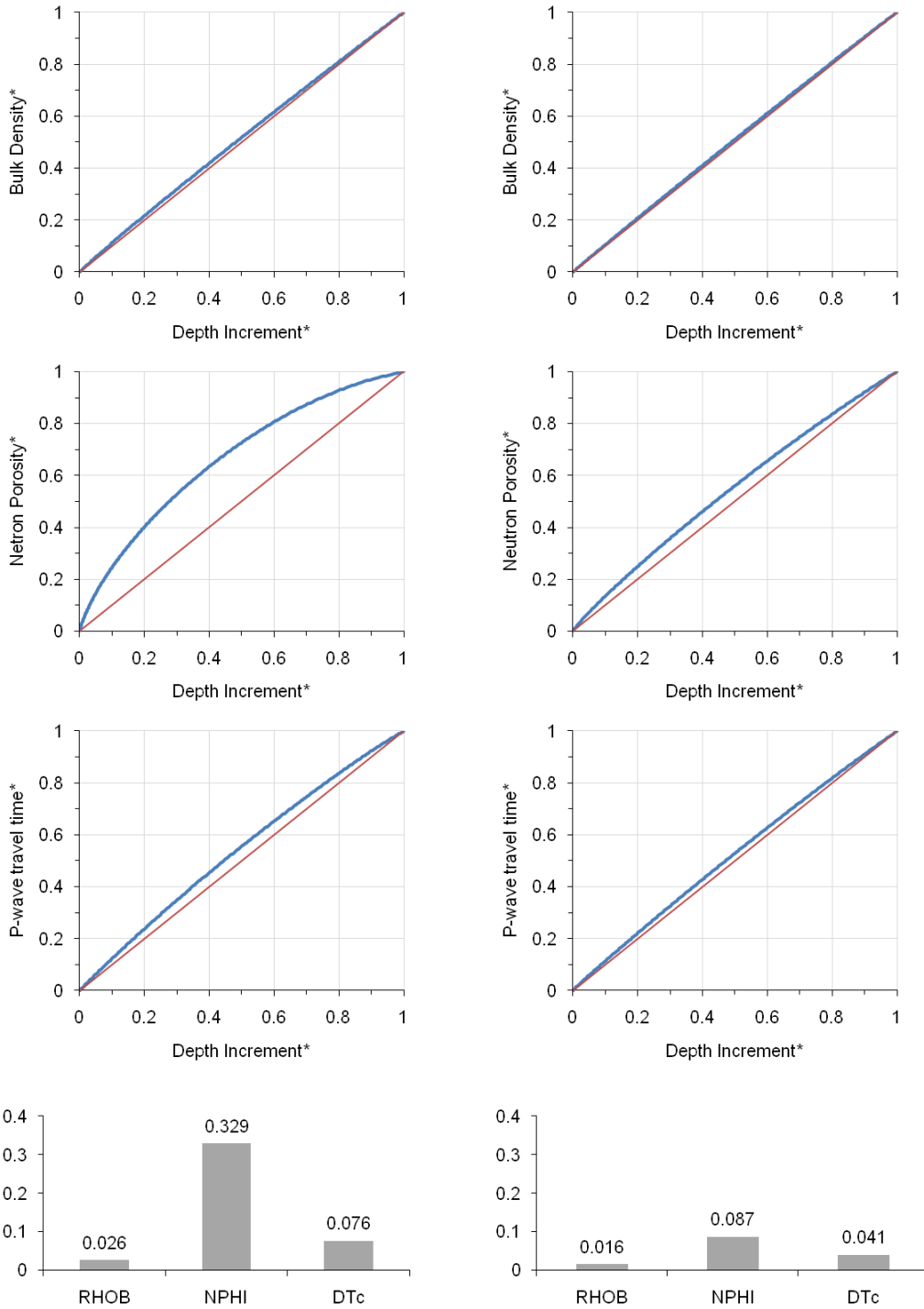


Figure 4.7. Lorenz Plots and bar charts illustrating Lorenz coefficients for bulk density, neutron porosity and P-wave transit time measurements of Formation-A and -B (left and right respectively). The pink diagonal line represents the line of perfect equality (pure homogeneity). [*cumulative values, normalised from 0 – 1].

Formation	Density	Neutron Porosity	Sonic
A	0.026	0.329	0.076
B	0.016	0.087	0.041

Table 4.3. Lorenz Coefficients for bulk density, neutron porosity, and P-wave transit time (Sonic) of Formations-A and -B (see figure 4.7).

In this application of the Lorenz coefficient the cumulative of the property (for example bulk density), sorted from low to high values, is plotted against cumulative measured depth increment (Figure 4.7). In a purely homogeneous formation, the cumulative property will increase by a constant value with depth, this is known as the “line of perfect equality” (Sadras & Bongiovanni 2004). An increase in the heterogeneity of the property will move the Lorenz Curve further away from the line of perfect equality. The Lorenz Coefficient (Lc) is calculated as twice the area between the Lorenz Curve and the line of perfect equality, a pure homogeneous system returns an Lc value of zero. Maximum heterogeneity would be shown by an Lc value of one. Lake and Jensen (1991) suggest that typical Lc values for reservoirs are between 0.3 and 0.6.

The Lorenz Curves and coefficients (figure 4.7 and table 4.3) clearly show that Formation-A is more heterogeneous than Formation-B, Formation-A being almost twice as heterogeneous according to this measure. It is noted that all values fall below the typical reservoir values given by Lake and Jensen (1991) above; their work focuses on detailed core measurements of porosity and permeability, chapter 5 will show that higher resolution datasets can produce high Lc values. The Lorenz Coefficients indicate that the neutron porosity values are more heterogeneous in both formations. Statistics and variogram analyses discussed in section 4.3.1 suggested that P-wave transit time measurements are more heterogeneous based upon the distribution of data. Here however, we are looking at the internal variation within a dataset and so the values more accurately reflect the heterogeneity found within a formation. P-wave transit time is also shown to be relatively heterogeneous; indicating that while porosity is the key heterogeneity, textural controls (facies and pore types) are also important.

4.3.2(b) Coefficient of Variation

The coefficient of variation (Cv) is a measure of variability relative to mean values. As previously stated, a homogeneous formation will have a Cv of zero (Elkateb *et al.* 2003). Therefore the Cv should provide a simple measure of heterogeneity. The most commonly used method for calculating the coefficient of variation is shown below (Equation 4.2), although

numerous variations on this approach can be found in published literature. Lake and Jensen (1991) comment that the estimate of Cv is negatively biased.

$$Cv = \frac{\sqrt{\sigma^2}}{\bar{x}} \tag{Equation 4.2}$$

[Where: Cv – coefficient of variation, $\sqrt{\sigma^2}$ - standard deviation, and \bar{x} - mean]

Formation	Density	Neutron	Sonic
A	0.050	0.656	0.137
B	0.030	0.164	0.075

Table 4.4. Coefficient of variation values for bulk density, neutron porosity and P-wave transit time (sonic) well logs from Formation-A and -B.

The coefficient of variation, again, confirms that Formation-A is more than twice as heterogeneous as Formation-B, and in Formation-A we see that the neutron porosity well log records the strongest heterogeneity signature at 0.656 (table 4.4 and figure 4.8). The coefficient of variation is perhaps the most simple of the heterogeneity measures discussed here, and yet comparable values are obtained relating to similar features detailed by the other more complex methods.

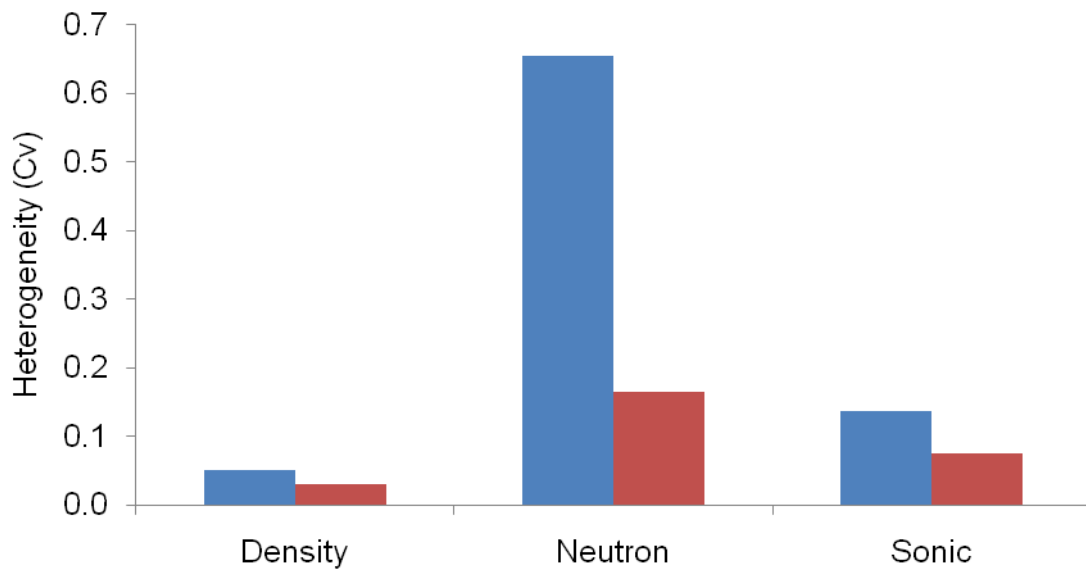


Figure 4.8. Coefficient of variation values for bulk density, neutron porosity and P-wave transit time (sonic) of Formation-A (blue) and Formation-B (red), see table 4.4.

4.3.2(c) Dykstra-Parsons Coefficient

Another commonly published heterogeneity measure, based on permeability variation, is the Dykstra-Parsons coefficient (V_{DP}). A method for calculating V_{DP} , provided by Jensen *et al.* (2000), begins by ranking data in order of decreasing magnitude. Probabilities are then assigned, based on percentage of values greater than the average (Maschio & Schiozer 2003), and plotted against the original values (permeability data is plotted on a log axis, but with static well log data this does not appear to be required except in the case of the resistivity data).

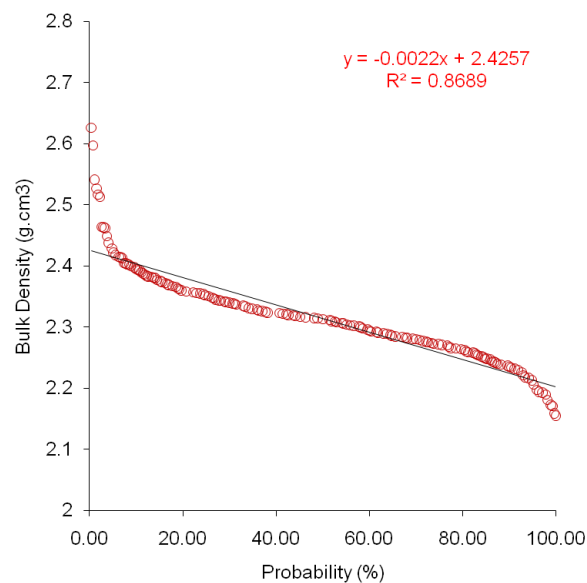


Figure 4.9. An example of a Dykstra-Parsons plot for bulk density of Formation-B.

The slope and intercept of a line of best fit, for all data, from this plot (figure 4.9) is then used to calculate the 50th and 84th percentile, which are used in equation 4.3 to derive V_{DP} .

$$V_{DP} = \frac{x_{50} - x_{84}}{x_{50}} \quad (\text{Equation 4.3})$$

[Where x_{50} – 50th property percentile, and x_{84} – 84th property percentile]

Lake and Jensen (1991) suggest that lower values of V_{DP} (0 – 0.5) represent small heterogeneities (zero being homogeneous), while larger values (0.7–1) indicate large to extremely large heterogeneities. Most reservoirs have V_{DP} values between 0.5 and 0.9. The values obtained for Formation-A and -B are shown in table 4.5 and figure 4.10.

Formation	Density	Neutron	Sonic
A	0.058	0.463	0.131
B	0.026	0.144	0.068

Table 4.5. Dykstra-Parsons coefficient values for bulk density, neutron porosity, and P-wave transit time (sonic) of Formation-A and -B.

The Dykstra-Parsons coefficient values indicate that Formation-A is more heterogeneous, in the cases of bulk density and P-wave transit time Formation-A appears around twice as heterogeneous (table 4.5).

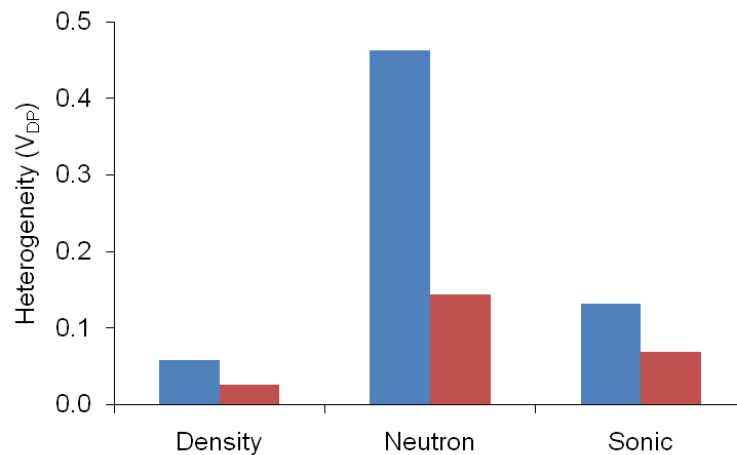


Figure 4.10. Dykstra-Parsons Coefficient for bulk density, neutron porosity and compressional sonic velocity of Formation-A (blue) and Formation-B (red).

As seen with previous measures the neutron porosity values record the highest heterogeneity supporting the view that variations in porosity content and pore types are key. Using the ranges provided by Lake and Jensen (1991) the heterogeneities present in Formation-A and -B, recorded by the Dykstra-Parsons coefficient, indicate relatively small-scale heterogeneities are present. Again this is expected to relate to the scale of investigation here.

4.3.2(d) Dual Lorenz Coefficient

A number of established relationships between petrophysical well logs exist which are used in the interpretation and characterisation of lithology, porosity and fluid content (such as density-neutron and density-sonic; figure 4.4). It was therefore decided to modify the standard Lorenz coefficient to detail heterogeneity with two variable properties. The technique simply replaces

cumulative depth increment with a second property, for example cumulative density against cumulative neutron porosity (figure 4.11 - top).

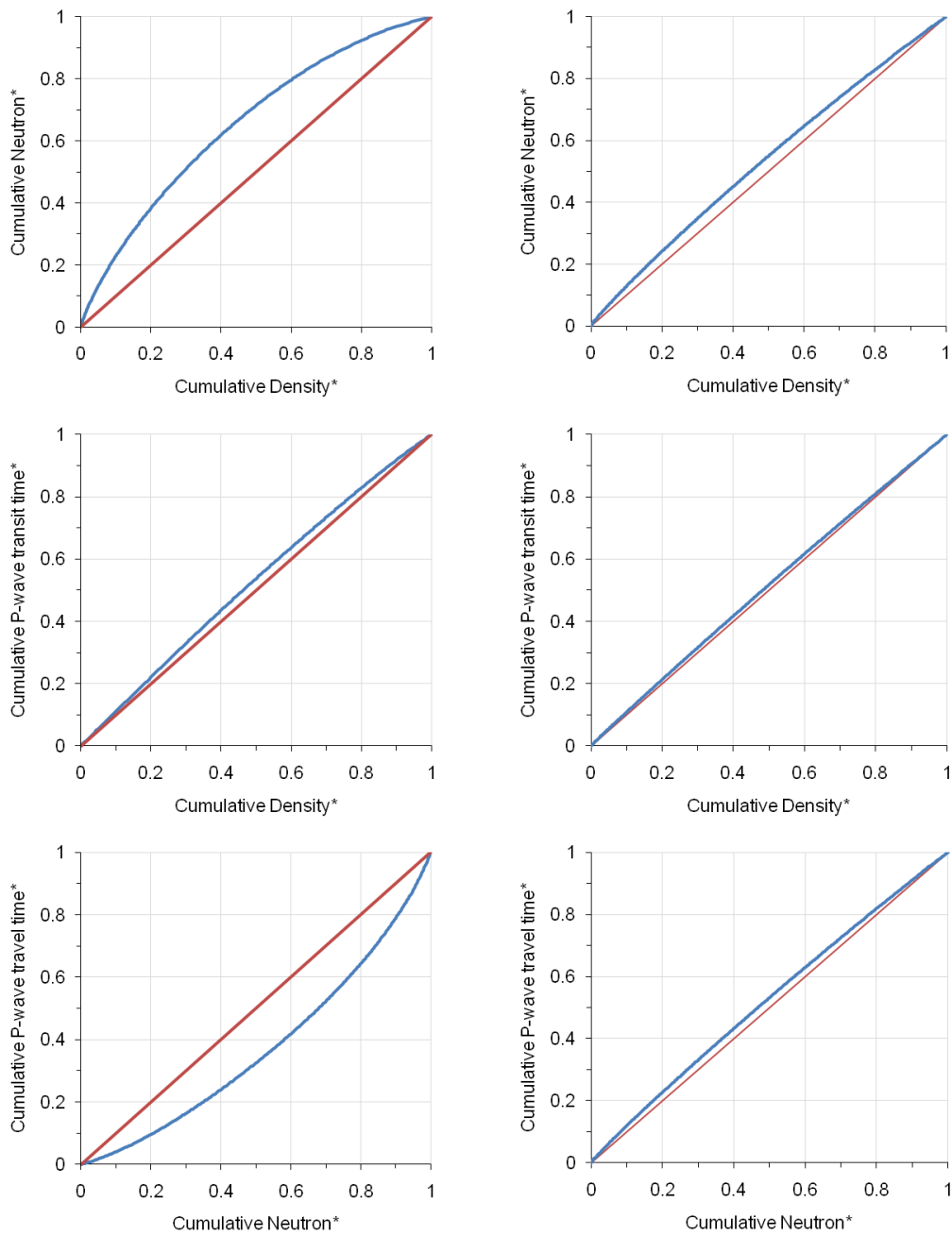


Figure 4.11. Dual Lorenz Plots and Coefficients for bulk density & neutron porosity (top), bulk density & P-wave transit time (middle), and neutron porosity & P-wave transit time (bottom), of Formation-A (left) and Formation-B (right).

Both properties are individually sorted in increasing magnitude and successive values are summed to produce a cumulative variable, which is finally normalised from zero to one. As

with the standard Lorenz coefficient, in a homogeneous system it would be expected that both properties increase by a constant increment, generating a perfect diagonal from 0,0 to 1,1 on the Lorenz Plot (the line of perfect equality). The Dual-Lorenz Coefficient is calculated as twice the area between the Lorenz Curve and the line of perfect equality, where zero is homogeneous. Here examples are presented based on density-neutron, density-sonic and neutron-sonic relationships (figure 4.11 & table 4.6). In figure 4.11 some examples show negative Lc (e.g. Formation-A P-wave transit time – neutron porosity); this is because in these data the property on the x axis is more variable, Absolute values of Lc are therefore used for comparison.

Formation	Density-Neutron	Density-Sonic	Neutron-Sonic
A	0.307	0.051	0.257
B	0.071	0.025	0.046

Table 4.6. Dual-Lorenz coefficient values for Bulk Density-Neutron Porosity, Bulk Density-Sonic, and Sonic-Neutron Porosity relationships of Formation-A and -B (P-wave transit time – Sonic).

It is obvious from the Lorenz plots that Formation-A is more heterogeneous than Formation-B. As would be expected, the Density-Neutron Dual-Lorenz Coefficient shows the highest heterogeneity for both formation (table 4.6), closely followed by the Neutron-Sonic results. Looking at the Lorenz Plots of figure 4.11 with the cross-plots of figure 4.4 we can see that the heterogeneities present in Formation-A are primarily concerned with lithological variation, indicated by the spread of data points across the lithology lines (figure 4.4 – blue circles); note that there is a limited gas effect in the system decreasing density and neutron porosity values. In the case of Formation-B points cluster around the limestone lithology lines (figure 4.4 – red open circles), giving generally low Dual Lorenz heterogeneity values, while spread along the lines indicates porosity variation is of most importance. Again it is the neutron porosity log response which is capturing maximum heterogeneities.

4.3.2(e) *t*-Tests

Following from the theory in Dual Lorenz Coefficients that a homogeneous system will have two properties with identical variation, the *t*-Test is one of the most commonly used statistical

techniques used to assess how similar two populations of data are in relation to their means and the spread of data around the mean (equation 4.3).

$$t = \frac{\bar{x}_a - \bar{x}_b}{\sqrt{\frac{S_a^2}{n_a} + \frac{S_b^2}{n_b}}} \quad (\text{Equation 4.3})$$

[Where \bar{x} – mean, S – standard deviation, and n – number of samples]

The null hypothesis assumes that both populations of data have the same mean and standard deviations is true and so a “ t ” of zero will be returned, and this in turn suggests homogeneity. The t-Test assumes that both populations are composed of random variables which have normal distributions. As discussed above, we are using the t-Test to investigate the heterogeneity in the relationships between two petrophysical well logs such as bulk density, neutron porosity, and compressional sonic transit time. As these have considerably different ranges of values (density commonly varies from 2 to 3 g.cm⁻³, neutron values from 0 to 100%, and sonic from 40 to 140 μ s/ft), data are normalised from 0 to 1 to allow direct comparison while still capturing their internal variability (table 4.7). A negative t-value will be returned if the mean of population “ a ” is smaller than that of population “ b ”, however absolute values are still comparable with deviation from zero in either a negative or positive direction representing increased difference between the two normalised datasets, or increased heterogeneity.

Formation	Density-Neutron	Density-Sonic	Neutron-Sonic
A	2.851	1.846	<i>0.974</i>
B	<i>2.422</i>	<i>1.851</i>	<i>0.544</i>

Table 4.7. t-Test values returned for Bulk Density-Neutron Porosity, Bulk Density-Sonic, and Sonic-Neutron Porosity relationships of Formation-A and -B (sonic – P-wave transit time). [Negative t-values are indicated by italics; absolute values are presented for ease of comparison as discussed above].

Formation-A is shown to be only slightly more heterogeneous than Formation-B when comparing values. The t -Test is comparing the similarities between two datasets from a single formation; therefore we cannot logically compare values between zones as in previous examples. Here, the t-Test is providing a measure of heterogeneity between different measures

of the same formation. As described above for the Dual-Lorenz Coefficient we see that the returned t -Test values for the bulk density-neutron porosity relationship show maximum heterogeneity values, closely followed by those for neutron porosity – P-wave transit time in both zones. Therefore the t -Test is a good measure to compare different datasets within an individual formation, but comparisons between different formations and reservoirs are less suitable because of the normalisation of measurement scales. Care should also be taken as it is possible for two properties of a system to track identical variation downhole, thus the system is still heterogeneous but the t -Test will return lower t values.

4.4 Use of Heterogeneity Measures

This chapter has provided examples of the application of five heterogeneity measures. The key points for each heterogeneity measure are as follows;

Lorenz Coefficient (Lc)

- Graphical plot allows for visual comparison with actual Lc value obtained
- Straight forward method to apply to any data
- Pure homogeneity is shown by $Lc = 0$, maximum heterogeneity is as $Lc = 1$
- Heterogeneity of different tools, formations and reservoirs can be directly compared
- Negative values may complicate automated sorting and normalisation steps, however negative data are uncommon in well log datasets (analyst must be aware if present)

Coefficient of Variation (Cv)

- Very simple calculation; requires only the mean and standard deviation
- No pre-processing (e.g. sorting or normalisation) of data is required
- Pure homogeneity is shown by a Cv of zero, but there is no maximum value for heterogeneity (∞)
- Heterogeneity of different tools, formations and reservoirs can be directly compared, however as there is no maximum heterogeneity value the different scales of well log data may influence heterogeneity results

Dykstra-Parsons Coefficient (V_{DP})

- Complicated pre-processing of data required; use of ranking and probability requires additional knowledge from analyst
- Actual values used in the V_{DP} calculation come from best fit trend line to the data, adding slight error
- Pure homogeneity is shown by $V_{DP} = 0$, maximum heterogeneity is as $V_{DP} = 1$
- Classification scheme established for naming V_{DP} values as small and large heterogeneity

Dual Lorenz Coefficient (DLc)

- Newly developed technique modified from the Lorenz Coefficient
- Based on established petrophysical well log relationships, allows quantification of the heterogeneity between two well log datasets
- Straight forward method to apply to any data
- Pure homogeneity is shown by $DLc = 0$, maximum heterogeneity is as $DLc = 1$
- Heterogeneity of different tools, formations and reservoirs can be directly compared
- Negative values may complicate automated sorting and normalisation steps, however negative data are uncommon in well log datasets (analyst must be aware if present)

The t-Test (tT)

- Tests the null hypothesis that both data populations have the same mean and standard deviation (i.e. if both populations have the same variation). If test is proved true then it is assumed to show homogeneity
- Assumed both populations are random variables on the same scale, and so data is normalised prior to analysis
- Returning a t -value of zero suggests homogeneity, increasing t shows increased heterogeneity. There is no maximum t -value for heterogeneity (∞)
- Shows strong correlation to other heterogeneity measures.
- Not strictly measuring heterogeneity; if downhole data is highly variable but the two data types follow similar patterns then a low t -value will be returned. The t -Test provides a measure of the heterogeneity between different data.
- Limited application in comparing different formations and reservoirs

Each of the measures provides a quantitative estimate as to which formation is more

heterogeneous numerically, and which petrophysical well log best captures heterogeneity (based

upon the tools measurement specifications). The results suggest there is no best practise choice from these heterogeneity measures, indeed it seems that the choice of which measure one should use is often based solely upon the analysts' preferences, abilities, and knowledge. The fact that all measures discussed here point toward similar numerical answers as to how heterogeneous Formation-A and -B is reassuring.

The complex pre-processing associated with the Dykstra-Parson coefficient, combined with the way that key values are chosen from a line of best fit, may allow for error to be added whilst also meaning that the technique cannot be easily run without a good understanding of the underlying statistical and mathematical computations. The *t*-Test provides a comparison of the variation between two datasets from a single formation, rather than quantifying the heterogeneity downhole through a formation; while this study has shown good correlation between this and other heterogeneity measures, it is suggested that this test should not be used alone. The coefficient of variation is the simplest technique presented here, yet results are robust in comparison to the other measures. However care should be taken when comparing values as there is not a fixed scale of heterogeneity. The Lorenz and Dual Lorenz coefficients are the only measures that quantify heterogeneity between finite values, zero and one (homogeneous and extreme heterogeneous respectively). As such these two techniques are the most useful for quantifying heterogeneity in well log data, within individual reservoir units and for comparison between different reservoir units and locations. When looking at reservoir heterogeneities with complex lithological and textural controls, or as part of an initial assessment, it seems logical to use the modified dual property measures presented here to gain an overview. However, when investigating the heterogeneity of an individual property, such as porosity or permeability, then use of a standard measure is sufficient.

As with any data interpretation, understanding the measuring tool used and what it is actually responding to within the formation is key, and this will aid in the understanding of what heterogeneities are being described and why. More detailed, reservoir-specific work can reveal one heterogeneity measure to be of particular use, depending upon observation scale,

measurement type and reservoir controls. This suite of techniques can be easily applied to any petrophysical dataset at a formation scale, providing a comprehensive understanding of heterogeneities and underlying controls which can be further investigated at a more detailed scale of investigation, incorporating other numerical data acquired from core, image log and sedimentological analysis. Indeed, Jensen *et al.* (2000) comment that heterogeneity measures are not a substitute for detailed geological study, measurements and analysis. They suggest that, at this scale, heterogeneity measures provide a simple way to begin assessing a reservoir, guiding investigations toward more detail analysis of spatial arrangement and internal reservoir structures which may not be shown directly.

4.5 Summary of Heterogeneity Measures from the Whole Reservoir Datasets

This section provides a summary of heterogeneity values obtained, using the Lorenz coefficient and Coefficient of Variation, for the well log data through the complete successions of all five reservoir units used in this study. To recap from chapter 3, reservoirs studied in this work are; Formation-A and -B of Panna and Mukta – two carbonate-dominated reservoirs, where Formation-A is a heterogeneous mix of carbonate facies and shale beds and Formation-B is packstone- and grainstone-dominated carbonate. Panna and Mukta are two neighbouring fields, where Panna is suggested to have undergone more substantial alteration during a multiphase diagenetic history; and the Abiod chalk – an autochthonous chalk succession.

The “homogeneous chalk” of the Abiod chalk shows significantly less numerical heterogeneity than the Panna and Mukta zones (table 4.8); higher heterogeneities in gamma ray and P-wave transit time are expected to relate to the high measurement values toward the top and bottom of the Abiod succession, relating to the larger volumes of investigation incorporating over- and underlying shale properties.

Well Log Measurement	Reservoir / Unit	Lorenz Coefficient (Lc)	Coefficient of Variation (Cv)
Gamma Ray	Panna – Formation A	0.220	0.431
	Panna – Formation B	0.077	0.135
	Mukta – Formation A	0.225	0.464
	Mukta – Formation B	0.105	0.193
	Miskar - Abiod	0.185	0.477
Bulk Density	Panna – Formation A	0.026	0.050
	Panna – Formation B	0.016	0.030
	Mukta – Formation A	0.014	0.029
	Mukta – Formation B	0.026	0.047
	Miskar - Abiod	0.019	0.037
Neutron Porosity	Panna – Formation A	0.329	0.656
	Panna – Formation B	0.087	0.164
	Mukta – Formation A	0.516	1.193
	Mukta – Formation B	0.361	0.668
	Miskar - Abiod	0.085	0.155
P-wave Transit time	Panna – Formation A	0.076	0.137
	Panna – Formation B	0.041	0.075
	Mukta – Formation A	0.055	0.115
	Mukta – Formation B	0.075	0.136
	Miskar - Abiod	0.053	0.098
Deep Resistivity	Panna – Formation A	0.428	0.915
	Panna – Formation B	0.445	1.048
	Mukta – Formation A	0.546	1.171
	Mukta – Formation B	0.810	2.320
	Miskar - Abiod	0.300	0.535

Table 4.8. The heterogeneity values obtained for the well log data through the whole sections of Formation-A and -B of wells P and M, and the Abiod chalk of well A. Heterogeneity measures: Lorenz coefficient (Lc) and the coefficient of variation (Cv).

Formation-A of both Panna and Mukta is shown to be more heterogeneous than Formation-B in terms of the well log data, with the exception of the bulk density and P-wave transit time measurements of the well M.

This supports the basic sedimentological observations provided in chapter 3. Chapter 3 also suggests that, according to the current geological model, the Panna field was affected more strongly by multi-phase diagenetic events than the neighbouring Mukta field. This has resulted in a more complex mixture of porosity types and connectivity in Panna (Wright 2007).

This increased heterogeneity in carbonate rock properties is however not observed in the well log-based heterogeneity measures, at this scale, where Mukta shows stronger numerical heterogeneities than Panna (table 4.8). The density and P-wave transit time data of Formation-A show slightly stronger heterogeneity. These findings suggest that the higher complexity of secondary pore types observed in the Panna field have had the affect of decreasing, or rather over-printing, the original heterogeneous signatures of bulk reservoir properties seen in the Mukta field. It is therefore expected that the use of multi-scale heterogeneity logs will allow investigation of relationships between numerical well log variation and the physical properties recorded for the different fields.

4.6 Conclusions

Heterogeneities within carbonate reservoirs are clearly complex, occurring at a variety of scales and with a number of geological origins. A geological heterogeneity may be defined as the complexity or variability of a specific system property, or measured/derived parameter in space and/or time. When investigating heterogeneity the type of heterogeneity should be defined in terms of grain/pore components and structural features, or lack thereof. Once defined, it is possible to quantify the heterogeneity within a specified volume of rock (or scale).

Heterogeneity measures provide information as to how heterogeneous properties are, which can be compared and related to underlying features. However it is through statistics and semi-variogram analyses that we can quantitatively characterise heterogeneity in terms of the amplitude and frequency of any variation present.

Although the Lorenz coefficient and Dykstra-Parsons techniques described in this work were originally developed for use with siliciclastic permeability data (and indeed outside of the geological sciences) there are no obvious reasons why these methods could not be applied to the quantification of heterogeneities in other petrophysical measurements and derived parameters, such as porosity and saturation.

All five heterogeneity measures have produced very similar responses or output in this study; for example neutron porosity is the most heterogeneous well log measurement in well P Formation-A. The Dykstra-Parsons coefficient is the most complex technique, requiring additional application and understandings of mathematical and statistical methodologies. The t-Test provides an alternative method for comparing data from individual formations, but its use for comparing heterogeneity between different formations and zones seems limited. The Coefficient of Variation is the easiest technique to apply, but there is no upper limit on the value returned for extreme heterogeneity. This research has a preference for the Lorenz and Dual Lorenz coefficient as a relatively simple and robust technique which provides simple graphical and numerical outputs for interpretation, where heterogeneity varies between zero (homogeneous) and one (maximum heterogeneity).

The Dual property heterogeneity measures may be of particular use in constraining the heterogeneities in initial work or reviewing a reservoir model. Applying the broad spectrum of measures to an initial dataset allows confirmation of interpretations, while more detailed work may well indicate one measure to be of more use than another. Choice between heterogeneity measures ultimately depends upon the analysts' experience and abilities.

When looking at heterogeneity in petrophysical well logs, for whole formations or zones, an understanding of the tool / measurement device is of importance, so that we can understand what underlying geological and reservoir features are controlling the numerical heterogeneities observed.

In terms of Formation-A and -B, used to illustrate the techniques presented throughout this chapter, Formation-B appears more homogeneous and is by chance the main producing reservoir unit of the two. However it is worth noting that a more detailed study of Formation-A is suggesting that the more heterogeneous flow units have better reservoir quality / potential (discussed further in chapter 6).

The application of heterogeneity measures to more detailed studies of both inclined and horizontal wells would be expected to shed more light on spatial continuity of physical properties, which would inform modelling and cross-well correlation practices. Where petrophysical properties are measured in three directions, such as core-based sonic velocity and well log electrical anisotropic investigations, there is potential to combine analyses with heterogeneity measures to further constrain spatial variations.

Chapter 5. How to make a Heterogeneity Log

5.1. Introduction

Chapter 4 illustrates how numerical well log data can be examined using simple statistics and semi-variogram analysis so that variation in the distribution of values can be characterised. To gain a single value of heterogeneity, where 0 is homogeneous and 1 (≥ 1) is heterogeneous, we can use the Heterogeneity Measures. Chapter 4 shows how these statistical techniques can be applied to a complete dataset through a reservoir or formation to quantify the heterogeneity in wireline well log data; this has basic implications for modelling and comparing reservoirs of different types. However, to further understand scalar numerical heterogeneity in well log data, which may be related to underlying geological and physical property variation, a novel application of the heterogeneity measures has been developed; the Heterogeneity Log (or H.Log).

This chapter will describe the technique developed for producing a Heterogeneity Log, before chapter 6 discusses its application to reservoir properties and use in addressing exploration requirements (i.e. fluid flow zonations, reservoir quality, and sampling). Limited interpretations will be presented in this chapter, with the main emphasis focussing on describing the Heterogeneity Log technique itself.

5.2. Heterogeneity Measures – a summary

A summary of the methodologies for the heterogeneity measures used is outlined below (see section 4.2.2 for full discussion of techniques and associated references).

5.2.1. *Lorenz Coefficient*

To calculate the Lorenz coefficient the cumulative of the property (for example neutron porosity), sorted from low to high values, is plotted against cumulative measured depth

increment (figure 5.1). In a purely homogeneous formation the cumulative property will increase by a constant value with depth, giving the “line of perfect equality”. An increase in the heterogeneity of the property will move the actual Lorenz Curve away from the line of perfect equality. The Lorenz coefficient (Lc) is calculated as twice the area between the Lorenz Curve and the line of perfect equality, a pure homogeneous system returns an Lc value of zero.

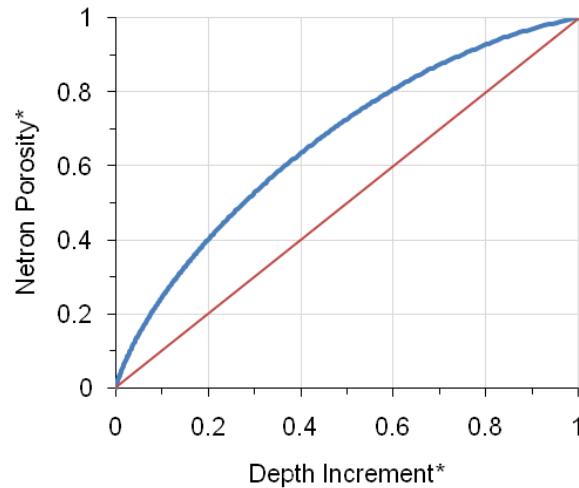


Figure 5.1. Lorenz Plot for neutron porosity as well P Formation-A data (*cumulative values, normalised from 0 – 1). The pink diagonal line represents the line of perfect equality (pure homogeneity).

5.2.2. Coefficient of Variation

The coefficient of variation (Cv) is a measure of variability relative to the mean. The most commonly used method for calculating the coefficient of variation is shown below (Equation 5.1), numerous variations on this approach can be found in published literature. A purely homogeneous formation will have a Cv of zero.

$$Cv = \frac{\sqrt{\sigma^2}}{\bar{x}} \quad (\text{Equation 5.1})$$

Where: Cv – coefficient of variation, $\sqrt{\sigma^2}$ - standard deviation, and \bar{x} – mean.

5.2.3. Dual Lorenz Coefficient

The Dual Lorenz Coefficient builds on the basic method of the standard Lorenz Coefficient, but takes established relationships between petrophysical well logs, such as density-neutron, into

account. The technique simply replaces cumulative depth increment with a second property. Both properties are individually sorted in increasing magnitude and successive values are summed to produce a cumulative variable, which is then normalised from zero to one. As with the standard Lorenz coefficient, in a homogeneous system both properties would be expected to increase by a constant increment (the line of perfect equality). The Dual Lorenz Coefficient is calculated as twice the area between the Lorenz Curve and the line of perfect equality, where zero is homogeneous.

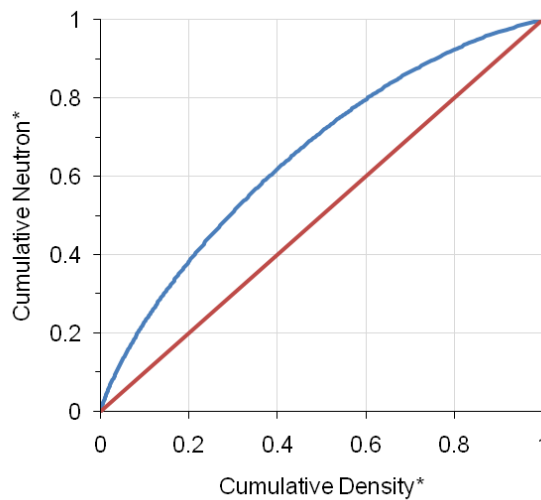


Figure 5.2. Dual Lorenz Plot for bulk density-neutron porosity from well P Formation-A data (*cumulative values, normalised from 0 – 1). The red diagonal line represents the line of perfect equality (pure homogeneity).

5.2.4. *t*-Tests

The *t*-Test is one of the most common statistical techniques used to assess how similar two populations of data are in relation to their means and the spread of data around the mean (equation 5.2). Here, we are assuming that a homogeneous system will have two properties with identical variation, although actual values and scale or measurement will differ according to measurement type.

$$t = \frac{\bar{x}_a - \bar{x}_b}{\sqrt{\frac{S_a^2}{n_a} + \frac{S_b^2}{n_b}}} \quad \text{(Equation 5.2)}$$

Where \bar{x} – mean, S – standard deviation, and n – number of samples, for population a and b ,

The null hypothesis that both populations of data have the same mean and standard deviation is assumed to be true, therefore if a t value of zero is returned it indicates homogeneity. The t -Test assumes that both populations are composed of random variables which have normal distributions; this is considered true with regard to the different wireline data being used.

However, as mentioned above both data sets should be of the same range in values, but well log data exist on different scales (density commonly varies from 1.65 to 2.5 g/cm³, and sonic from 40 to 140 μ s/ft). Data are therefore normalised from 0 to 1 to allow direct comparison while still capturing internal variability. A negative t -value will be returned if the mean of population a is smaller than that of population b , however absolute values are still comparable with deviation from zero in either a negative or positive direction representing increased difference between the two normalised datasets, or increased heterogeneity.

5.3. The Heterogeneity Log: the basic principles

The Heterogeneity Log (H.Log) applies a statistical technique for the quantification of numerical heterogeneity in wireline log data to a series of specified depth intervals downhole. As described in chapter 3, the environmental and wireline log calibrations were confirmed prior to analysis with Q/C and Q/A of the data.

Taking, for example, the neutron porosity wireline log from Formation-A of well P, the first step is to divide the well log data into 10m intervals downhole from the top of the section. The data within each of these 10m windows are then run through the various heterogeneity measures described above (e.g. the Lorenz coefficient). This gives a heterogeneity value for the data window. That heterogeneity value is assigned to each depth level represented in the data window, producing a H.Log on a comparable depth scale to the original data (figure 5.3).

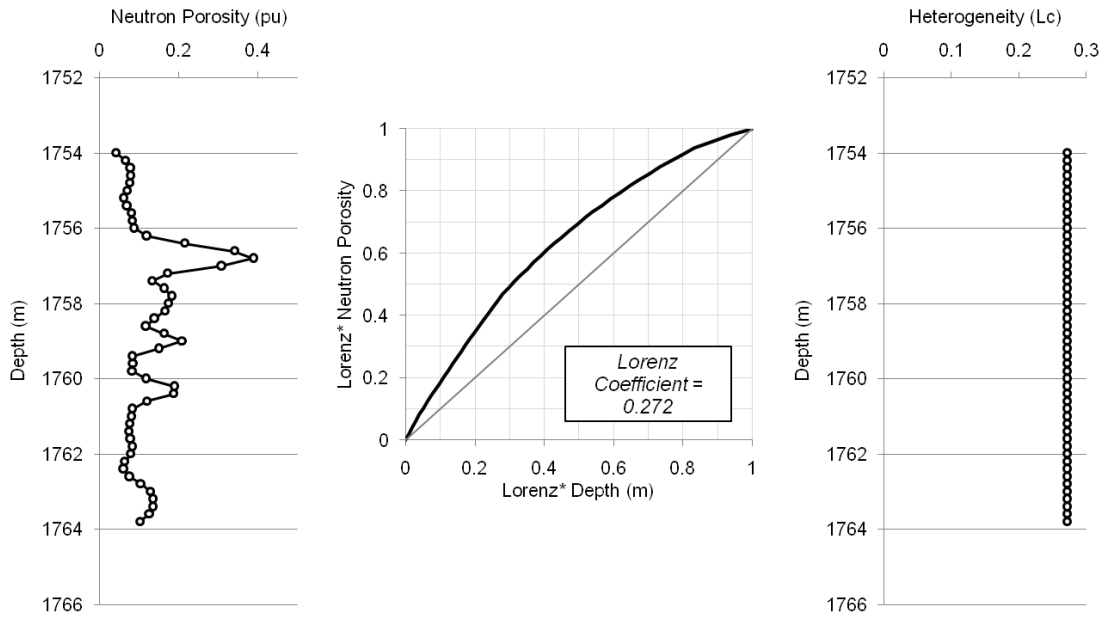


Figure 5.3. Generation of a 10m Lorenz coefficient Heterogeneity Log block from neutron porosity well log data (well P). Left to right; (1) Initial neutron porosity well log data, (2) Lorenz plot of the data, and (3) Lorenz coefficient (Lc) Heterogeneity Log block generated for this depth interval. Lorenz* - cumulative and normalised variable from 0-1.

This process is repeated for the consecutive 10m data windows downhole, generating a complete H.Log for the neutron porosity measurements of this section. The whole process is then repeated for the well log data using different sized data windows; 5m, 2m, and 1m (figure 5.4). Figure 5.4 illustrates some key features of the different scaled H.Logs. All of the H.Logs show the same broad features in terms of general lows and highs; in this example we see a low heterogeneity mid-section, with heterogeneity increasing towards the top and bottom of Formation-A. It is clear that the Lorenz coefficient responds to contrasts in high and low values within the data window, along with the more general frequency and amplitude of variation; compare for example the H.Logs at 1770m and 1790m. As the data window size decreases from 10m to 1m more detail is displayed. However, caution is taken with interpreting “higher resolution” features from the 1m H.Log as only 5 measurements are used in this analysis (one every 20cm). In this smaller data window we see that peaks and troughs produce significant heterogeneity contrasts, almost reproducing the original well log signature.

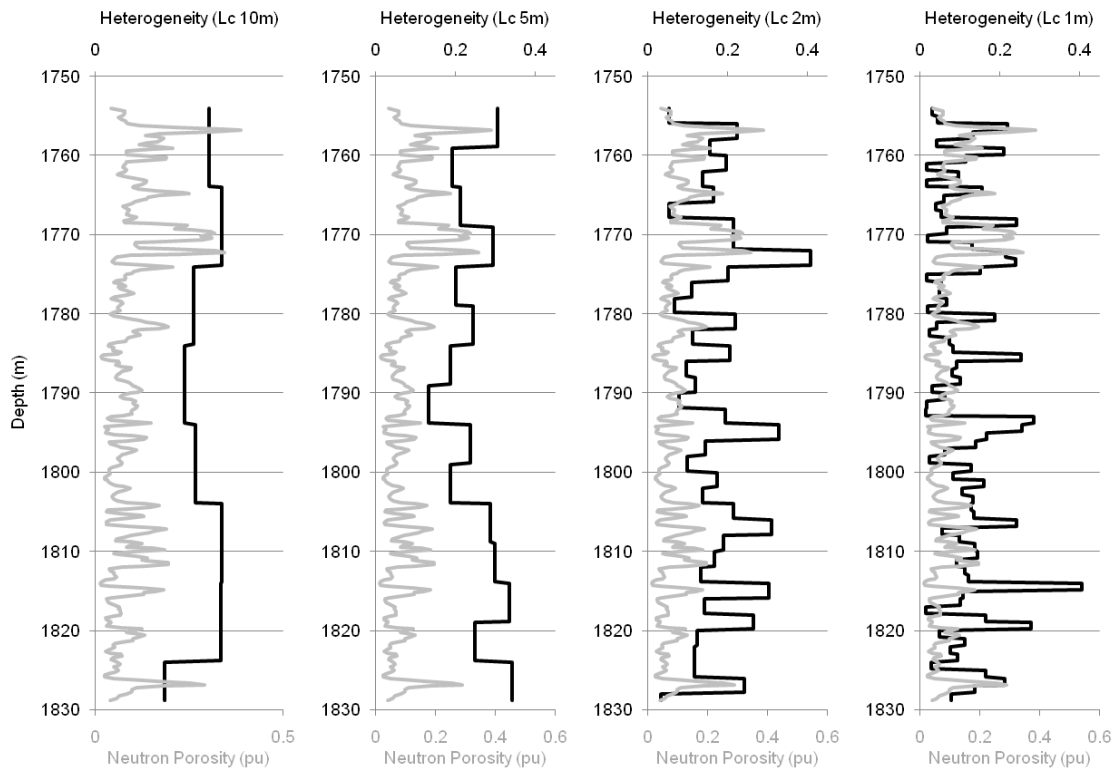


Figure 5.4. Left to right; 10m, 5m, 2m and 1m window Lorenz coefficient Heterogeneity Logs & original neutron porosity wireline well log data for Formation-A of well P. Note that a heterogeneity value of 0 = homogeneous.

Heterogeneity logs are produced for the other wireline log data using the same technique (figure 5.5). It can be seen in figure 5.5 that the same broad heterogeneity features are seen in all H.Logs; with higher heterogeneity at 1764-1774m, followed by a sudden decrease before gradually rising toward to bottom of the succession. There are obviously internal differences between the different wireline measurement type heterogeneity; this is discussed further in chapter 6 with regard to their application. To recap briefly; (1) the gamma ray measurement responds to radioactive elements, typically the presence of muds (shale) and uranium enrichment in carbonates, (2) bulk density respond to the bulk rock properties in terms of mineralogy and pore volume, (3) neutron porosity typically details hydrogen ion concentration, assumed to exist only in the pore space, (4) P-waves move through solid material and so travel times are influenced by pore volume and texture, affecting travel paths, and grain densities in terms of their

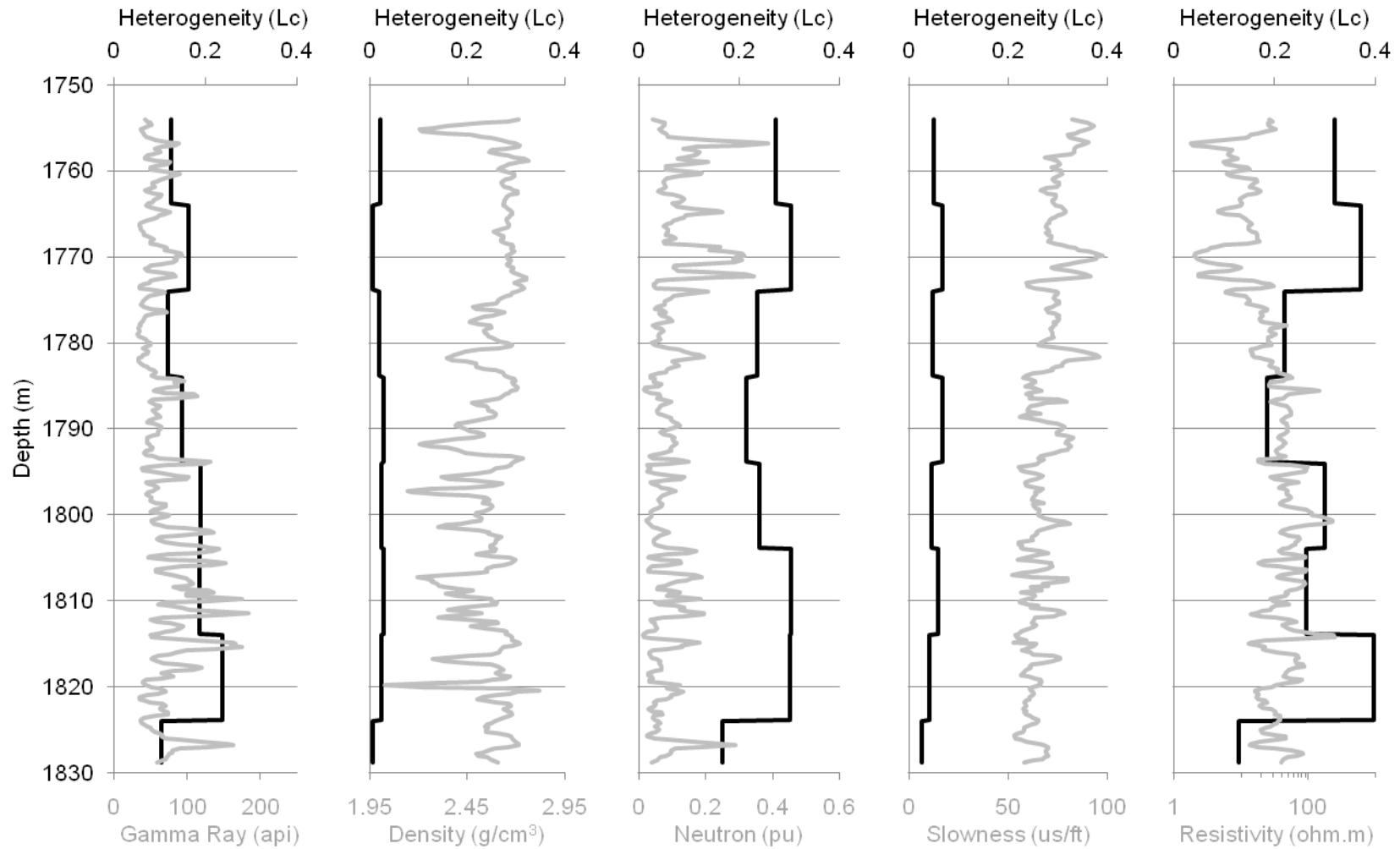


Figure 5.5. 10m window Lorenz coefficient Heterogeneity Logs & original wireline well log data for Formation-A of well P. Well log datasets from left to right; natural gamma ray, bulk density, neutron porosity, P-wave transit time (slowness), and deep resistivity. Note that a heterogeneity value of 0 = homogeneous.

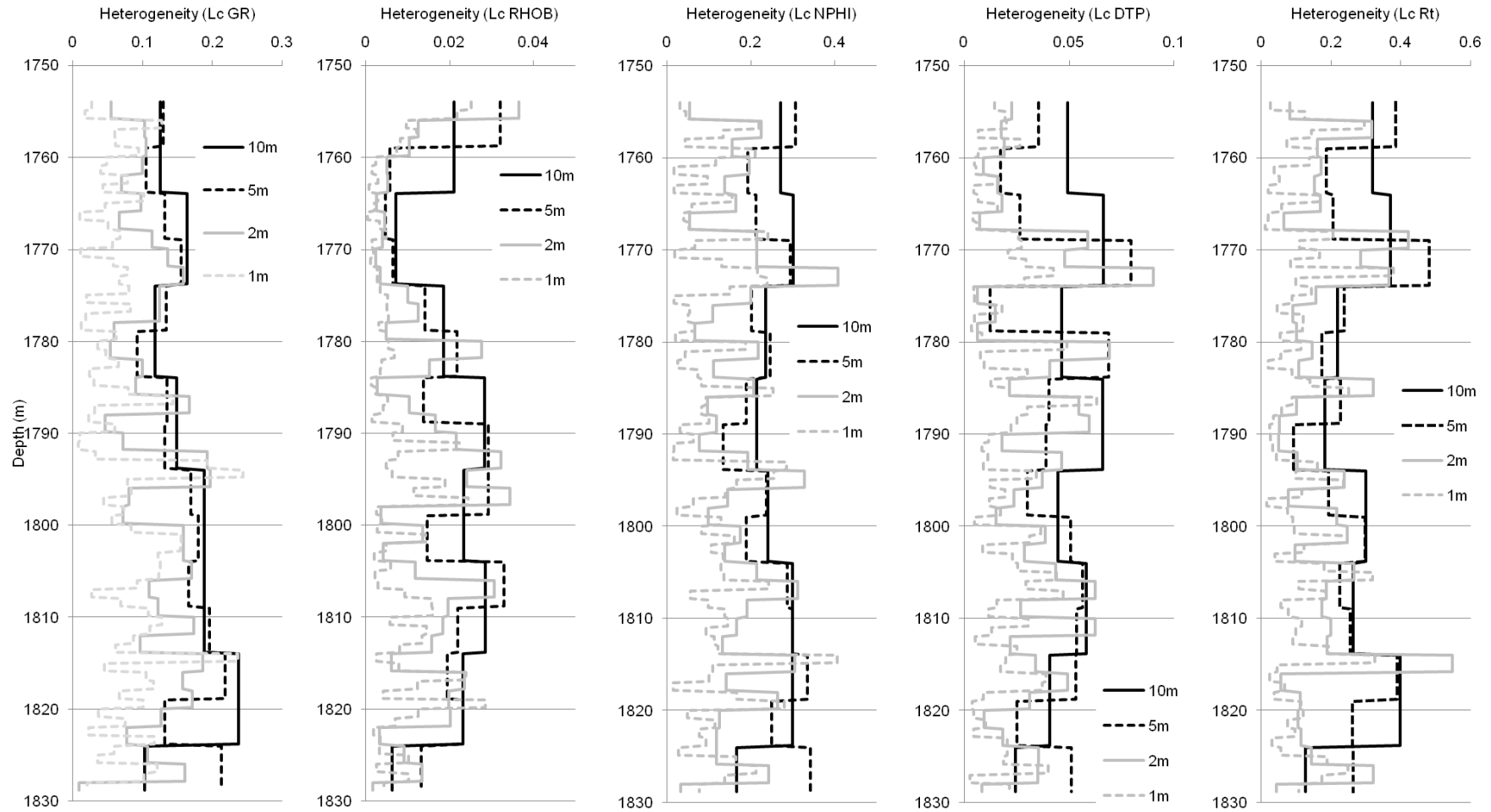


Figure 5.6. 10m, 5m, 2m and 1m window Lorenz coefficient Heterogeneity Logs for Formation-A of well P. Well log datasets from left to right; natural gamma ray (GR), bulk density (RHOB), neutron porosity (NPFI), P-wave transit time (DTP), and deep resistivity (Rt). Note that a heterogeneity value of 0 = homogeneous, and scales vary for display purposes.

speed, and (5) resistivity measurement are typically influenced by pore fluids (and thus porosity) and the presence of clay minerals. Interestingly the data peak seen in all data at ~1827m, corresponding to a thick mudstone bed, does not seem to influence the heterogeneity value in the 10m H.Log; in fact lowest heterogeneity is seen.

The main exception to the heterogeneity features described above is the H.Log for bulk density, where heterogeneity values are around an order of magnitude smaller and the typical high heterogeneity at 1764-1774m is reverse to the lowest heterogeneity value. This will be discussed further in section 5.5, with regard to the effect of normalising data prior to H.Log processing.

Figure 5.6 illustrates that similar trends in heterogeneity are seen on the 4 scales of all well log-derived H.Logs. Again, the 1m H.Log is almost replicating variation in the original dataset. There are obviously differences in the heterogeneity shown by H.Logs from the different well log data, however they also record similar major high and low features. Examples of these are high heterogeneity peaks around 1773m, 1794m, 1817m, and 1828m, along with lows around 1764m, 1780m, and 1812m. These features are suggested to be of particular interest, bearing in mind the fact that the 5 different measurements occur at different times, at different sections of the tool string, and that the measurements respond to the different properties of different volumes of rock.

The actual relationships of these features in numerical heterogeneity are not discussed in this technique based chapter; the following chapter of this thesis will examine these further. The 2m H.Logs show the maximum difference between high and low heterogeneity values in the case of the Formation-A of well-P. The complete suite of 2m H.Logs for Formation-A of well P are shown in Figure 5.7. Again, the four heterogeneity measure types identify the same key heterogeneity features in terms of peaks and troughs. The two major peaks at 1772-1774m and 1794-1796m, for example, can be clearly correlated across the suite.

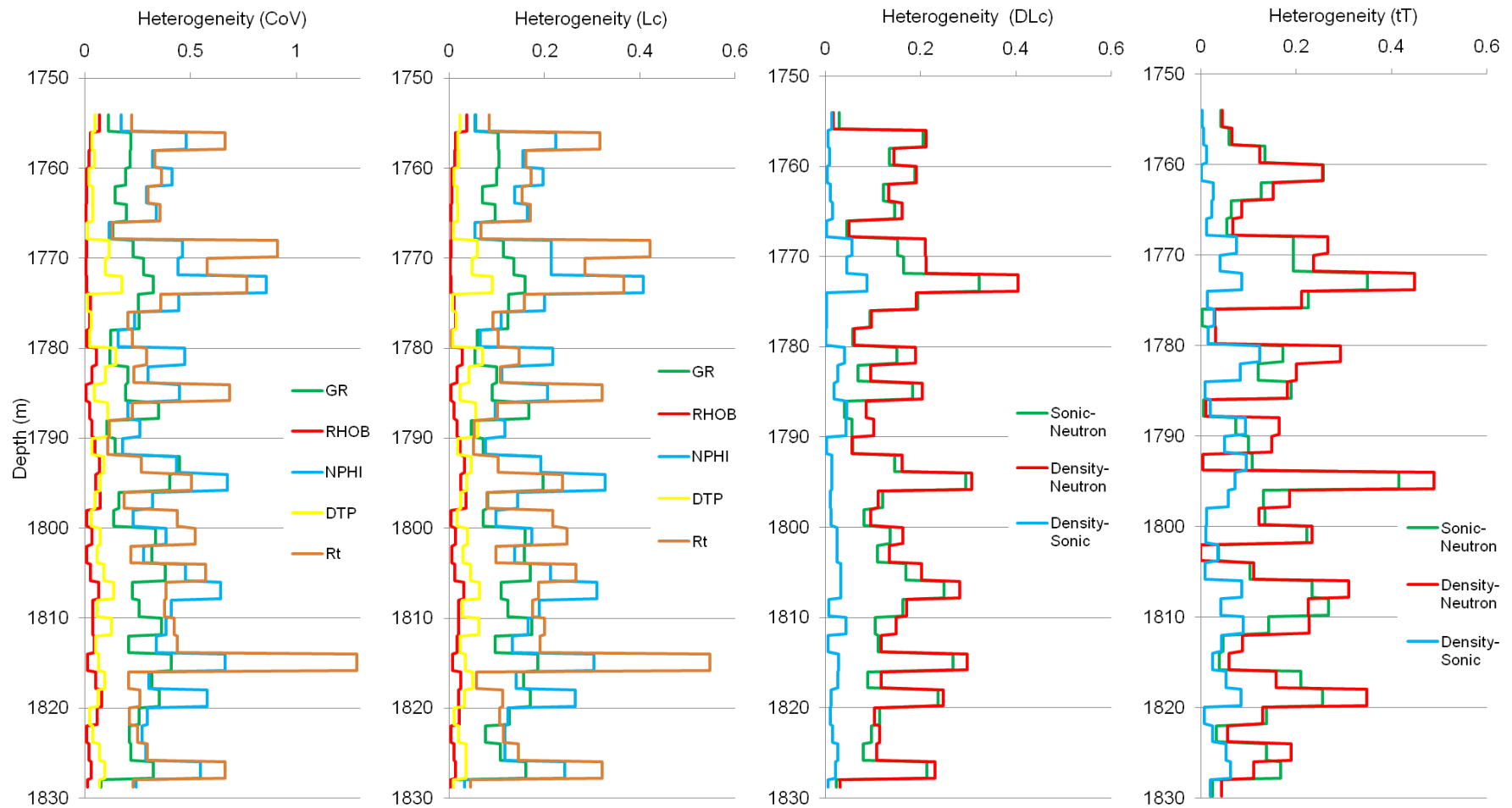


Figure 5.7. Heterogeneity Logs for Formation-A of well P, using 2m data window. Heterogeneity measures from left to right; Coefficient of variation (CoV), Lorenz coefficient (Lc), Dual Lorenz coefficient (DLc), and t-Test (tT). Well log datasets ; natural gamma ray (GR), bulk density (RHOB/density), neutron porosity (NPHI/neutron), P-wave transit time (DTP/sonic), and deep resistivity (Rt). Note that a heterogeneity value of 0 = homogeneous.

It is interesting to note that in the case of this dataset, the highest heterogeneity values are seen in the neutron porosity H.Logs. This same feature was documented in chapter 4, where a single heterogeneity value was generated for the complete succession. This will be discussed further in chapter 6, but is believed to relate to porosity and textural variability being most important in terms of the geology of this unit (chapter 3).

This dominance in neutron porosity heterogeneity is also apparent in the dual property measures (Dual Lorenz coefficient and *t*-Test); where the resultant H.Logs for neutron-sonic and density-neutron show stronger correlation to the neutron porosity H.Log than either P-wave transit time or bulk density respectively.

5.4. Offsetting the data windows

The basic H.Log methodology begins by analysing the numerical heterogeneity in the well log data from the top of the succession. It was decided to run a series of 2m H.Logs at successively larger offsets from the top of the succession, to investigate the effect of averaging and shoulder effects based on the downhole position of the data windows, on the resultant H.Logs; i.e. starting the data windows 20cm, 40cm, 60cm, and so on, from the top of the dataset.

Figure 5.8 illustrates the effect of offsetting the data window on the gamma ray Lorenz coefficient H.Logs. Visually it is apparent that the same general pattern in features of high and low heterogeneity is captured throughout, with different magnitudes being key differences. The following statistical tests have been completed in order to quantify this variability from the non-offset (original) data.

Variance (Equation 5.3; Lind *et al.*, 2010) is the average squared deviation from the mean, or simply it is a measure of the spread or dispersion of data about the mean (Davis 2002). If two datasets have the same variance then they show similar distributions of data around a mean, and therefore in the case of this study we would expect similar patterns in heterogeneity downhole.

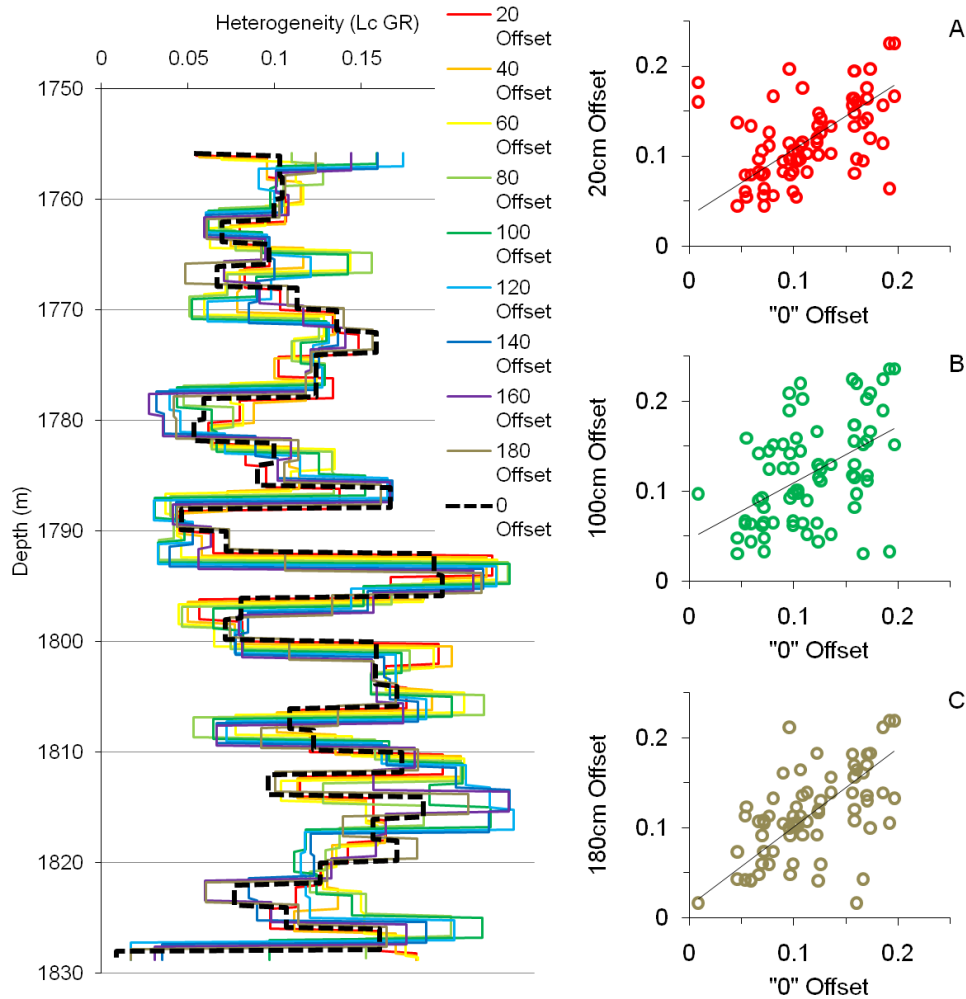


Figure 5.8. Illustrating the effect of offsetting the data window downhole at 20cm increments; Left presents all calculated data for the Lorenz coefficient 2m H.Logs from gamma ray wireline data, Right: crossplots of heterogeneity from the original H.Log (“0 Offset) against the 20cm offset (A), 100cm offset (B), and 180m offset (C); see table 5.1.

The covariance (Equation 5.4; Borradaile 2003) measures the strength of covariation between two variables, or rather the joint variation of two variables about a common mean (Davis 2002; Jensen *et al.* 2000). If the two datasets show the same features and magnitudes then one would expect covariance to equal the original variance. In the case of the gamma ray Lorenz H.Log (table 5.1) we see that covariance varies from 0.0019 (for the original H.Log varying with itself, which is the same as its variance) to a minimum of 0.0017 at the 80cm offset. To investigate the significance of this we calculate a correlation coefficient, based on the variance and covariance (Equation 5.5, Borradaile, 2003).

$$s = \frac{\sum(X-\bar{X})^2}{n-1} \quad (\text{Equation 5.3})$$

Where; s – variance of variable, X – value of each observation in the dataset, \bar{X} – sample mean, and n – number of samples

$$s_{xy} = \frac{\sum(X-\bar{X}) \times (Y-\bar{Y})}{n-1} \quad (\text{Equation 5.4})$$

Where; s_{xy} – covariance, X and Y – value of each observation in variables “ x ” and “ y ”, \bar{X} and \bar{Y} – sample mean for variables “ x ” and “ y ”, and n – number of samples (same for both variables)

$$R = \frac{s_{xy}}{\sqrt{s_x^2 \times s_y^2}} = \frac{\text{covariance}(x,y)}{\sqrt{\text{variance}(x) \times \text{variance}(y)}} \quad (\text{Equation 5.5})$$

Where; R – correlation coefficient s_{xy} – covariance of variable “ x ” and “ y ”, s_x^2 – variance of variable “ x ”, and s_y^2 – variance of variable “ y ”

The correlation coefficient (R), or coefficient of correlation, describes the strength of a relationship between two sets of variables (Lind *et al.* 2010). A correlation coefficient of zero shows no correlation between the two variables, while a value of +1 suggests perfect correlation where y increases with x (-1 also shows perfect correlation where y decreases with x). The correlation coefficient is not the same as the slope of a regression trend line fitted in a crossplot of the two variables (Borradaile 2003). Correlation coefficients are unit-less values, their use is generally more qualitative than quantitative. For example in table 5.1 we see a minimum correlation of 0.483 between the non-offset and 100cm offset H.Logs which is deemed “moderate”, while the average for all offset logs shows good correlation at 0.642. By squaring the correlation coefficient the coefficient of determination (R^2) is obtained. This is a proportion, or percentage, of total variation in variable y that is explained, or accounted for, by variation in variable x (Lind *et al.* 2010); if x is the original H.Log data, and y is the offset data. For example 57% and 66% of the variability in H.Logs with data windows offset by 20cm and 180cm, respectively, are accounted for in the original H.Log with 0cm offset.

Comparing (X/Y)	0cm Offset (X & Y ₁)	20cm Offset (Y ₂)	40cm Offset (Y ₃)	60cm Offset (Y ₄)	80cm Offset (Y ₅)	100cm Offset (Y ₆)	120cm Offset (Y ₇)	140cm Offset (Y ₈)	160cm Offset (Y ₉)	180cm Offset (Y ₁₀)	Averages
Variance, s^2 (Y ₁₋₁₀)	0.0019	0.0018	0.0021	0.0026	0.0030	0.0032	0.0035	0.0031	0.0026	0.0022	0.0026
Covariance, s_{xy} (X/Y ₁₋₁₀)	0.0019	0.0014	0.0013	0.0012	0.0012	0.0012	0.0013	0.0014	0.0015	0.0017	0.0014
Correlation, R (X/Y ₁₋₁₀)	0.997	0.756	0.630	0.523	0.485	0.483	0.520	0.566	0.647	0.816	0.642
Coefficient of determination, R^2 (X/Y ₁₋₁₀)	0.995	0.572	0.396	0.274	0.235	0.233	0.271	0.320	0.419	0.666	0.438
t -Test	258.2	22.12	15.50	11.75	10.61	10.56	11.66	13.12	16.25	27.04	39.69
Significance Level (p)	0.001	0.001	0.001	0.001	0.001	0.001	0.001	0.001	0.001	0.001	0.001

Table 5.1. Comparing the original gamma ray Lorenz H.Log data variability (X – 0cm offset), with subsequent offset data windows at 20cm increments (Y). See text for explanation and equations of statistical terms used. The general feature of correlation decreasing toward the 100cm offset data window is seen in all wireline log-derived H.Logs (density, neutron porosity, P-wave slowness, and resistivity – see Appendix C.1)

These values of R^2 , particularly the minimum of 23.3% for the 100cm offset H.Log, seem very low in comparison to the visual comparison of figure 5.8. To test the significance of these correlation coefficients, and therefore coefficients of determination, we can investigate the null hypothesis that correlation between the two variables is zero ($H_0: \rho = 0$) using the t -test shown in equation 5.6. If this hypothesis is proven true then the correlation is simply due to chance (Borradaile 2003; Davis 2002; Lind *et al.* 2010).

$$t = \frac{R \sqrt{n-2}}{\sqrt{1-R^2}} \quad (\text{Equation 5.6})$$

Where; t – test result (see text), R – correlation coefficient, R^2 – coefficient of determination, and n – number of samples (note that $n-2$ is the “degrees of freedom”)

The t value can then be compared to the table of significance for student’s t -distributions to obtain a value of significance, “ p ” (table 5.2). For example, the lowest t value of 10.56 is returned for the 100cm offset gamma ray H.Log, where $R = 0.48$. Therefore R^2 suggests that 23% of the variability in the 100cm offset H.Log is accounted for in the original H.Log with

0cm offset. We have 366 samples in the data set, giving 364 degrees of freedom. The resultant t value of 10.56 is greater than that given for both the 200 and infinity (∞) degrees of freedom value for a significance level of 0.001 (3.34 and 3.291 respectively). Therefore we can say that the “moderate-low” correlation of 0.50 is significant to a confidence level of 99.9%. This statement is in fact true of all the data shown (tables 5.1 & 5.3). A confidence level of 95% (p 0.05) is normally used in earth science to justify a correlation (Borradaile 2003).

Degrees of Freedom	Confidence Interval					
	80%	90%	95%	98%	99%	99.9%
	Levels of significance (p)					
	0.20	0.10	0.05	0.02	0.01	0.001
1	3.078	6.314	12.706	31.821	63.657	636.619
10	1.372	1.796	2.201	2.718	3.106	4.437
100	1.290	1.660	1.984	2.364	2.626	3.390
200	1.286	1.653	1.972	2.345	2.601	3.340
∞	1.282	1.645	1.960	2.326	2.576	3.291

Table 5.2. Table of significance for results of the student t distribution (Lind *et al.* 2010). Degrees of freedom = number of samples -2. For example if a sample with 10 degrees of freedom returns a t value of less than 2.201 then the null hypothesis that no correlation is present cannot be rejected at a 0.05 significance level (p), suggesting that no correlation is present and therefore that the R value occurs by chance. If the t value is greater than 2.201 then the null hypothesis is rejected, suggesting the R correlation is present with a significance of 0.05 (or a confidence level of 95%).

	Gamma Ray		Bulk Density		Neutron Porosity		Compressional Slowness		Deep Resistivity	
	Mean	Min/Max	Mean	Min/Max	Mean	Min/Max	Mean	Min/Max	Mean	Min/Max
Variance, s^2 (Y_{1-10})	0.0026	0.002/0.003	$7.7E^{-5}$	$6.5E^{-5}/9.2E^{-5}$	0.008	0.006/0.01	$3.0E^{-4}$	$1.9E^{-4}/4.3E^{-4}$	0.010	0.008/0.012
Covariance, s_{xy} (X/Y_{1-10})	0.0014	0.001/0.002	$5.4E^{-5}$	$3.5E^{-5}/8.4E^{-5}$	0.004	0.003/0.006	$2.5E^{-4}$	$1.4E^{-4}/4.1E^{-4}$	0.008	0.004/0.012
Correlation, R (X/Y_{1-10})	0.642	0.483/0.997	0.705	0.46/0.997	0.596	0.366/0.997	0.706	0.502/0.997	0.659	0.426/0.997
Coefficient of determination, R^2 (X/Y_{1-10})	0.438	0.233/0.995	0.528	0.212/0.995	0.396	0.134/0.995	0.525	0.252/0.995	0.471	0.182/0.995
t -Test	39.69	10.56/258.27	44.033	9.91/258.27	38.525	7.53/258.27	43.863	11.11/258.27	41.724	9.01/258.27
Significance Level (p)	0.001	0.001	0.001	0.001	0.001	0.001	0.001	0.001	0.001	0.001

Table 5.3. Average statistical characteristics showing the effects of offsetting the H.Log data window on the wireline data types (See Appendix C.1 for full results).

Table 5.3 summarises the effects of offsetting the start depth of the data window on the five H.Log types by presenting the average values obtained (with note of max-min range). The average R^2 for all the H.Log offsets shows that 50.9% (corresponding to R 0.713) of their variability is accounted for in the original 0cm offset values (with 99.9% confidence). Additionally the difference in covariance for the offset H.Logs is ~30%, and the average percentage difference in heterogeneity values at each depth is ~32%. These three statistics are therefore taken to suggest that an average error of $\pm 30\%$ can be assigned to the H.Logs, if required. On a side note it is shown that the neutron porosity H.Logs show the weakest correlations, this is expected to relate back to the fact that neutron porosity shows the strongest numerical heterogeneities in the well P data (both in terms of the whole formation, chapter 4, and the H.Logs of section 5.3 above).

This investigation into offsetting the data windows does not suggest any real statistical reason for not starting the H.Log calculation at the beginning of the dataset. We can see that general trends and magnitudes are captured to a 99.9% confidence limit. As with any numerical technique, this has highlighted the importance in awareness of the sampling window. Original data are of importance in establishing interpretations or in deriving relationships to other properties.

5.5. Normalisation

The effect of the difference in scale in the well log data set is mentioned previously in section 5.3; with, for example, density ranging from 1.95 to 2.95g.cm⁻³ while gamma ray radiation commonly varies from 0 to +250 API through a succession of varied lithologies. To investigate this all well log data has been normalised from 0-1 so that all measurements vary over the same scale. Heterogeneity logs were then generated for the normalised well log data (figure 5.9).

Visual inspection of figure 5.9 suggests that the H.Logs for density, neutron porosity, and deep resistivity show a similar pattern in heterogeneity features downhole. The key difference between normalised and original data being the magnitude of heterogeneity captured; this is

particularly true for the density H.Logs where a maximum difference of ~370% is seen. The P-wave transit time H.Logs show good similarity, with small differences at depths such as ~1794m and 1803m. The original and normalised-derived H.Logs for gamma ray show much weaker similarity, the heterogeneity analysis has been re-run to confirm these differences and the same heterogeneity log outputs were obtained. Figure 5.10 provides crossplots of the two H.Logs (normalised and original data) for each well log for reference. To calculate correlations numerically the statistical tests described in section 5.4 have been completed (table 5.4)

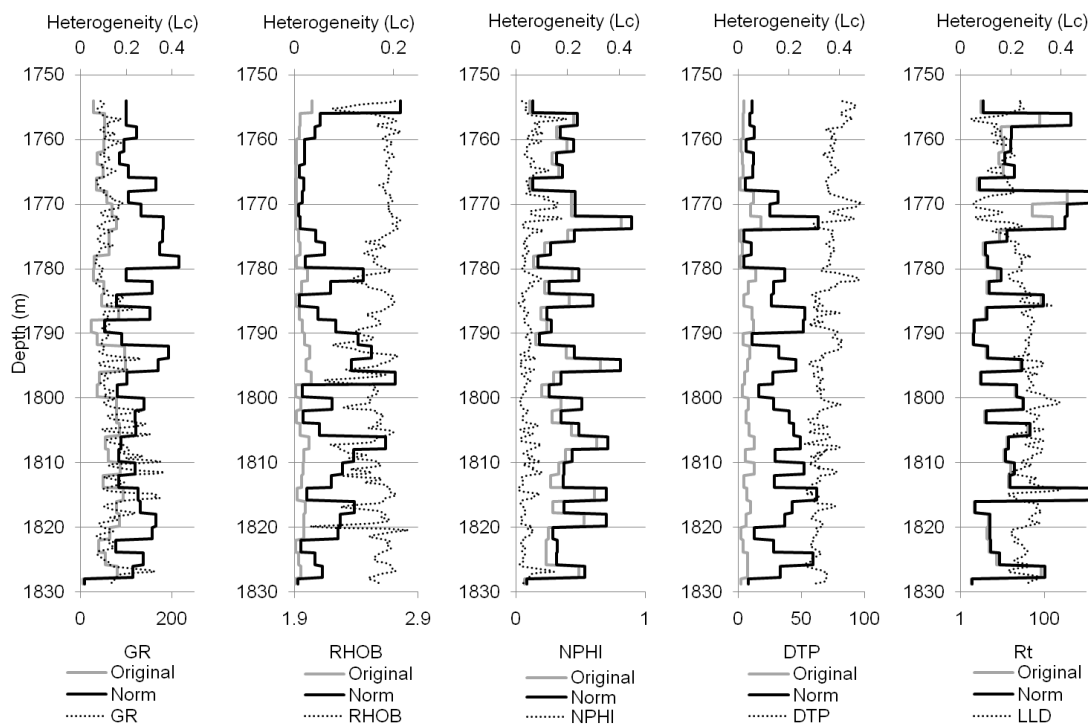


Figure 5.9. The original 2m H.Logs generated using the Lorenz coefficient for the well log data (left to right: gamma ray (GR), bulk density (RHOB), neutron porosity (NPHI), P-wave transit time (DTP), and deep resistivity (Rt)) presented with the 2m H.Logs derived following normalisation (Norm) of the well log data prior to heterogeneity quantification. The relevant well log data is presented on each plot, on the secondary axis (grey).

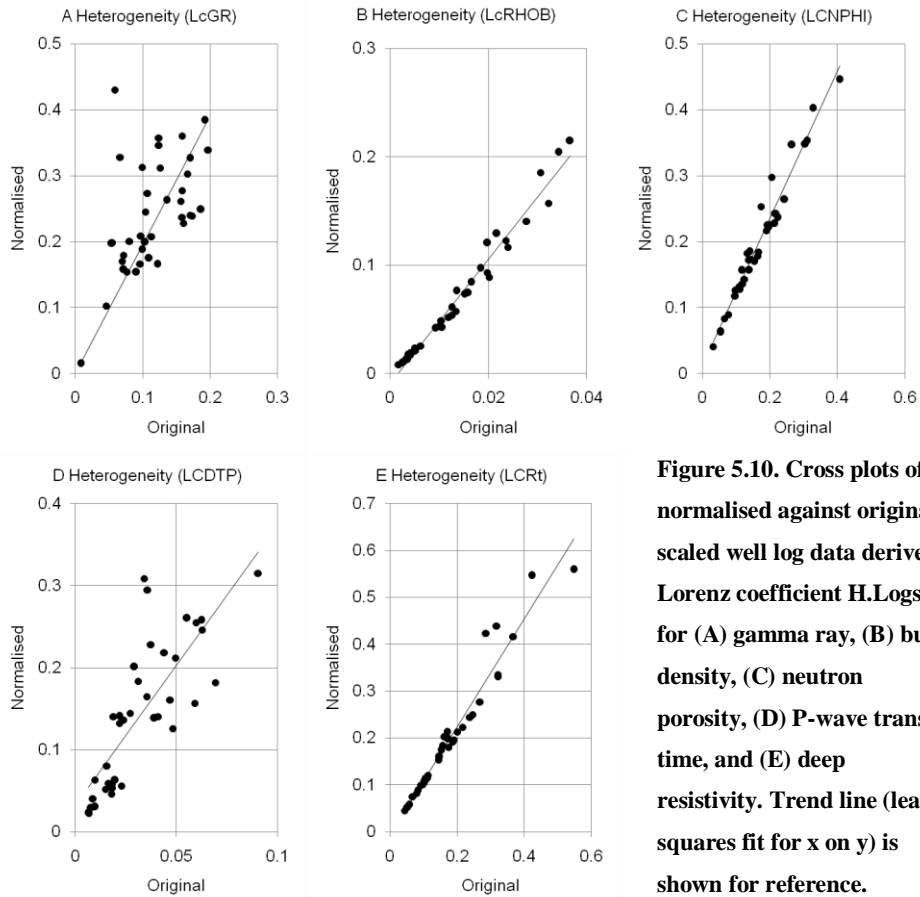


Figure 5.10. Cross plots of normalised against original scaled well log data derived Lorenz coefficient H.Logs for (A) gamma ray, (B) bulk density, (C) neutron porosity, (D) P-wave transit time, and (E) deep resistivity. Trend line (least squares fit for x on y) is shown for reference.

	Gamma Ray	Bulk Density	Neutron Porosity	P-wave Transit time	Deep Resistivity
Original data variance (X)	0.00198	0.00010	0.00635	0.00040	0.01237
Normalised data variance (Y)	0.00641	0.00321	0.00826	0.00748	0.01728
Covariance (X,Y)	0.00180	0.00054	0.00707	0.00137	0.01421
Correlation coefficient, $R(X,Y)$	0.506	0.984	0.976	0.792	0.972
Coefficient of determination (R^2)	0.256	0.969	0.953	0.628	0.945
t-Test	11.33975	108.1819	87.40045	25.11731	80.274
Significance Level (p)	0.001	0.001	0.001	0.001	0.001

Table 5.4. Statistical responses detailing correlations between the original and normalised well log data-derived Lorenz coefficient 2m H.Logs. See section 5.4 for relevant equations and discussion of techniques.

The statistics provided in table 5.4 support the suggestion that bulk density, neutron porosity and deep resistivity H.Logs show strong correlation between original and normalised measurement scales; R^2 indicate that ~97% of the variation present in the normalised H.Log is also captured in the original H.Log values downhole (with a significance of 0.001). This

correlation does however fall to 63% and 26% in the P-wave transit time and gamma ray logs respectively. A possible explanation is that this poorer correlation in heterogeneities, such as seen in the gamma ray data, originates from the process of normalisation forcing the minimum value to become zero, removing any background noise. This effectively keeps the local linear variation the same between neighbouring data points, but changes the scale over which the variation, or heterogeneity, is quantified; therefore potentially changing the derived heterogeneity value. However the question remains as to why this would not affect the normalisation of all the well log data in a similar way.

The normalised and original H.Logs for both the neutron porosity and resistivity measurements show strong correlation with low differences in the magnitudes of heterogeneity value (~10% on average). This suggests that normalisation prior to heterogeneity quantification has little effect on their outputs. Normalisation clearly has a significant effect on the gamma ray log, as discussed above, changing both magnitudes and fine-scale details of the resultant H.Log.

However, it is also observed that the broad heterogeneity features are similar downhole. The effect of normalising P-wave data prior to heterogeneity quantification is variable, with an R^2 67% correlation and for the most part similar patterns in heterogeneity are observed downhole. Two exceptions are noted at ~1794m and ~1803m where a significant increase in heterogeneity occurs, again this is expected to be an artefact of re-scaling creating larger relative variation in that data window.

Initial heterogeneity quantification from bulk density data formed the main reason for originally investigating the effect of normalisation on this technique; it was questioned as to whether the small-scale heterogeneity captured for the density well log was a result of low numerical variation (and therefore related physical properties) or it was simply an artefact of the small data-scale used for density (1.95-2.95g.cm⁻³). The R^2 value of 96.9% suggests excellent correlation between the original and normalised H.Logs; visually this is confirmed as the same features are present in both logs. It is the magnitude of variation that differs significantly here, although it is noted that the other normalised well log-derived H.Logs vary from 0 to 0.4 while

maximum normalised density heterogeneity is still significantly lower at 0.215. In figures 5.10 and 5.11 we can see that normalisation increases the heterogeneity values obtained for all the well log measurement types, and that this is more strongly pronounced in the density data (with a maximum difference between original and normalised H.Log value of ~400%).

In summary, similar patterns and heterogeneity features are identified by both original and normalised well log-derived H.Logs. Higher magnitudes of heterogeneity are identified in the normalised data. Gamma ray and P-wave transit time data provide different heterogeneity responses from the normalised data, however there is suggestion of a link to the scale of measurement being obscured and stretched. Interestingly this is not seen in the resistivity data where values vary across decade scales (0.0001-1000ohm.m). This suggests that added complexities are influencing this feature, which are not yet discovered in the study.

Normalising the well log data adds an additional step to the process of obtaining a Heterogeneity Log, which may be associated with the introduction of error either by the operator (calculation or rounding errors) or the scalar stretching observed here. Part of the interest in H.Logs is that they draw on the basic well log dataset to contrast physical properties. These contrasts will be influenced by the original data scale, reflecting the potential variability in well log measurement. For these reasons, including the observations above, this author believes that normalisation of the well log data prior to HM analysis does not provide a significant advantage and so is not required in this analysis.

5.6. Summary of H.Logs from the Studied Reservoir Units

Here a summary of the heterogeneity features and patterns identified for the five reservoir units of this study (figures 5.11 – 5.20); Formation-A and -B of wells P and M, and the Abiod chalk. The underlying geological and petrophysical properties were described in chapter 3, and relationships between the H.Logs and these rock properties will be discussed in chapter 6. Figure 5.7 illustrates that the outputs of the coefficient of variation and Lorenz coefficient H.Logs are comparable, as are the dual input H.Logs for Dual Lorenz coefficient and the *t*-Test.

For this reason, and to save repetition, full H.Log suites are presented only for the Lorenz and Dual Lorenz coefficient H.Logs here.

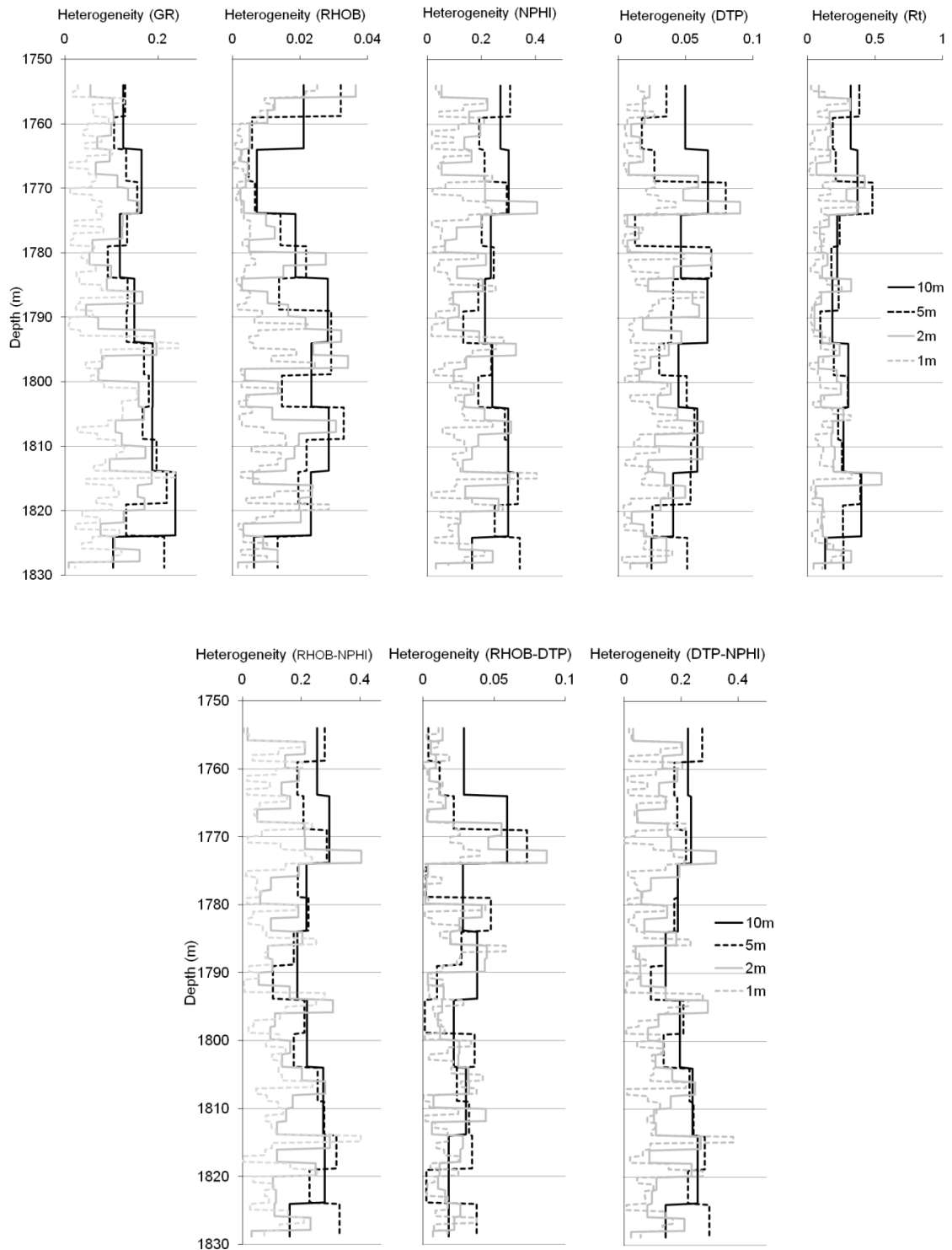


Figure 5.11. 10m, 5m, 2m and 1m window Lorenz (top) and Dual Lorenz (bottom) coefficient Heterogeneity Logs for Formation-A of well P. Well log datasets from top left to right; natural gamma ray (GR), bulk density (RHOB), neutron porosity (NPHI), P-wave transit time (DTP), and deep resistivity (Rt).

The heterogeneity features of Formation-A of well P have been described above; the key points are illustrated in figure 5.11, and are described as follows. High heterogeneity is seen at 1765-1775m before falling to the lowest values present in the section. Heterogeneity then increases gradually to ~1810-1820m before falling at the base of the zone. The smaller scale H.Logs reveal high frequency and amplitude changes downhole, localised high and low heterogeneity features can be correlated across the suite of H.Logs. Maximum heterogeneity values are recorded in the neutron porosity and deep resistivity measurements. Lowest heterogeneity values are seen in the bulk density-derived H.Logs, the high seen in other well log variability at 1765-1775m becomes a low heterogeneity feature in the density data. The dual property H.Logs show strong correlation to the highly heterogeneous neutron porosity H.Log. Clearly Formation-A's heterogeneous geological nature is recorded in the well log data.

Formation-B of well P shows significantly less heterogeneity than Formation-A, as would be expected from the descriptions in chapter 3. Lower amplitude signals are seen downhole, in comparison to Formation-A. In general higher heterogeneity is recorded at the top of the succession, decreasing sharply at 1840m, and continuing to decrease gradually to the bottom of the zone. The high heterogeneous feature at the top of the section is not seen in the gamma ray H.Log (figure 5.13). In Formation-B, the highest heterogeneity is seen in the deep resistivity log. Again lowest heterogeneity is seen in the density H.Log (<0.03).

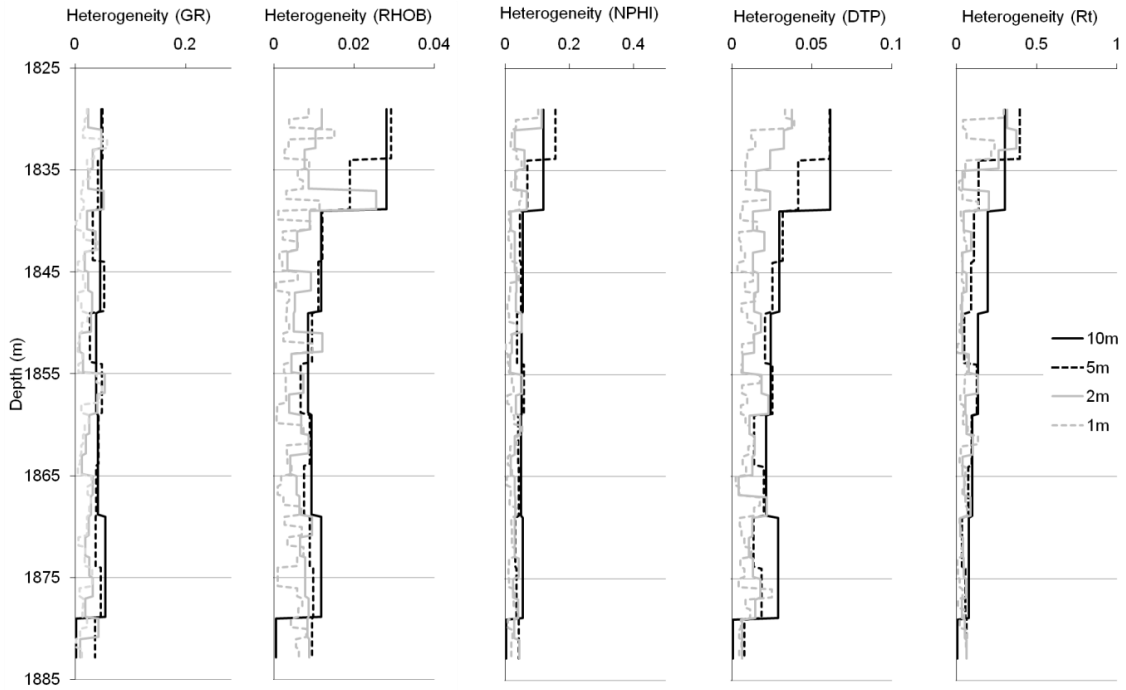


Figure 5.12. 10m, 5m, 2m and 1m window Lorenz coefficient Heterogeneity Logs for Formation-B of well P. Well log datasets from left to right; natural gamma ray (GR), bulk density (RHOB), neutron porosity (NPHI), P-wave transit time (DTP), and deep resistivity (Rt).

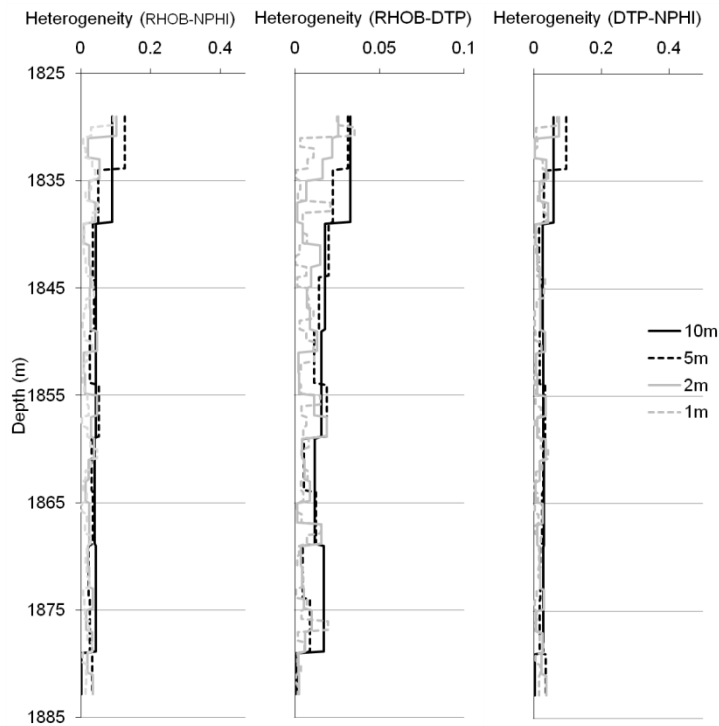


Figure 5.13. 10m, 5m, 2m and 1m window Dual Lorenz coefficient Heterogeneity Logs for Formation-B of well P. Well log datasets from left to right; bulk density-neutron porosity (RHOB-NPHI), bulk density-P-wave transit time (RHOB-DTP), and P-wave travel time-neutron porosity (DTP-NPHI).

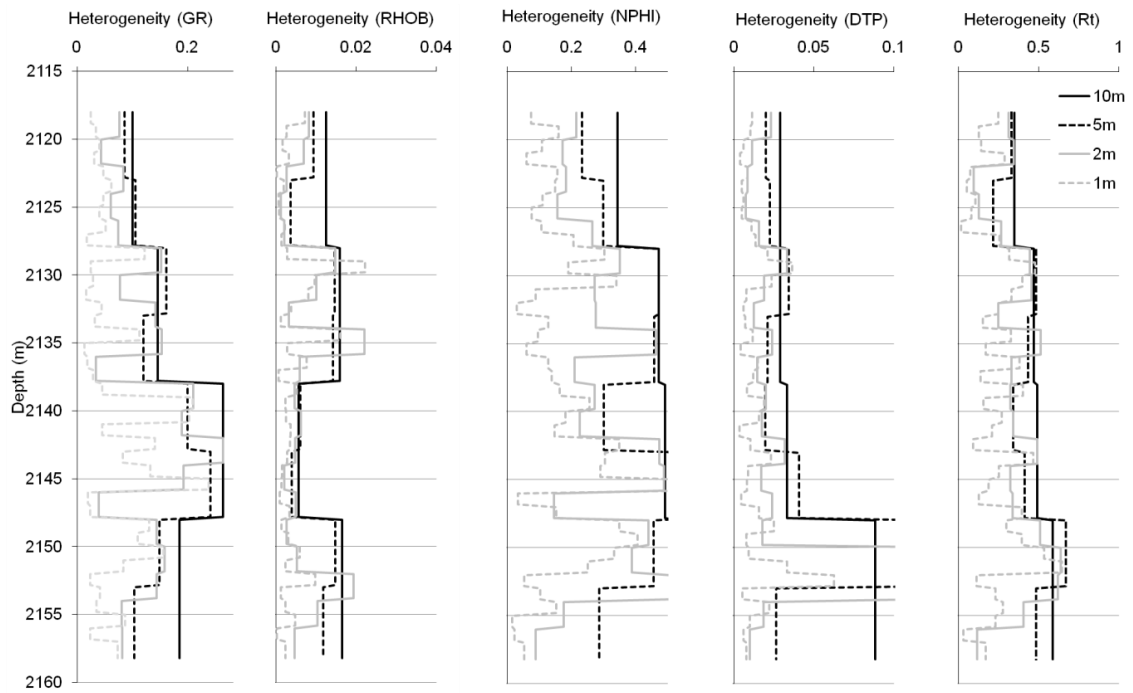


Figure 5.14. 10m, 5m, 2m and 1m window Lorenz coefficient Heterogeneity Logs for Formation-A of well M. Well log datasets from left to right; natural gamma ray (GR), bulk density (RHOB), neutron porosity (NPHI), P-wave transit time (DTP), and deep resistivity (Rt).

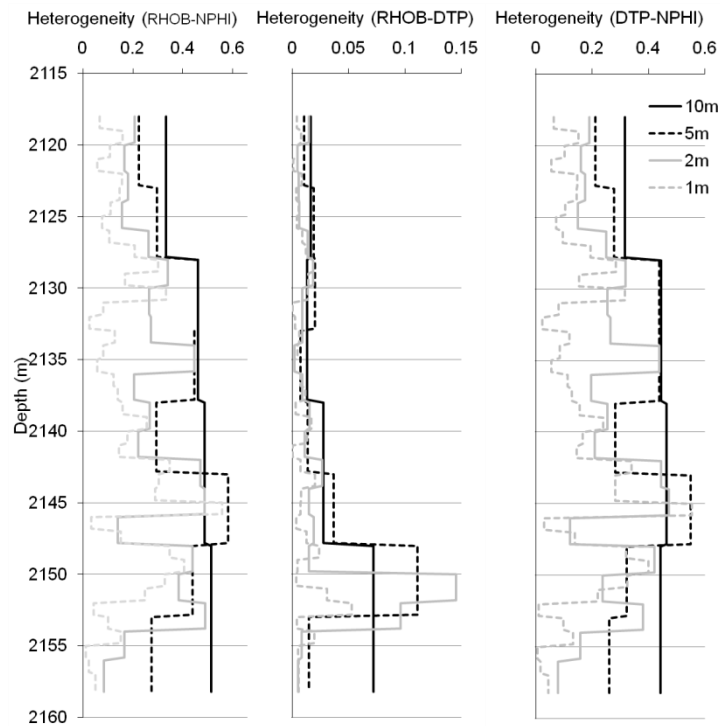


Figure 5.15. 10m, 5m, 2m and 1m window Dual Lorenz coefficient Heterogeneity Logs for Formation-A of well M. Well log datasets from left to right; bulk density-neutron porosity (RHOB-NPHI), bulk density-P-wave transit time (RHOB-DTP), and P-wave travel time-neutron porosity (DTP-NPHI).

Figures 5.14 and 5.15 show the H.Logs from Formation-A of well M. Overall large amplitude and frequency changes in heterogeneity are seen downhole. Highest heterogeneities are identified in the lower section of this zone (2145-2155m). Again the general high and low features can be correlated across the H.Log suite. Neutron porosity and deep resistivity H.Logs show highest heterogeneities, with density having lowest values again. There is a significant decrease in heterogeneity of the density data 2138-2146m which is not observed in the other H.Log types.

The well M Formation-B data shows similar amplitude changes in heterogeneity to its Formation-A, with lower frequency changes downhole (figure 5.16). The neutron porosity and P-wave transit time H.Logs show a gradual decrease in heterogeneity downhole; Neutron porosity and P-wave transit time show a sharp decrease in heterogeneity in the upper section of the formation (~2167m).

In general lower frequency changes in heterogeneity are observed in these data. The density H.Logs show the lowest heterogeneity. The gamma ray, density and resistivity H.Logs show lower amplitude heterogeneity changes downhole, with an overall increase in the middle of the zone which is punctuated by lowest heterogeneity values around 2185m.

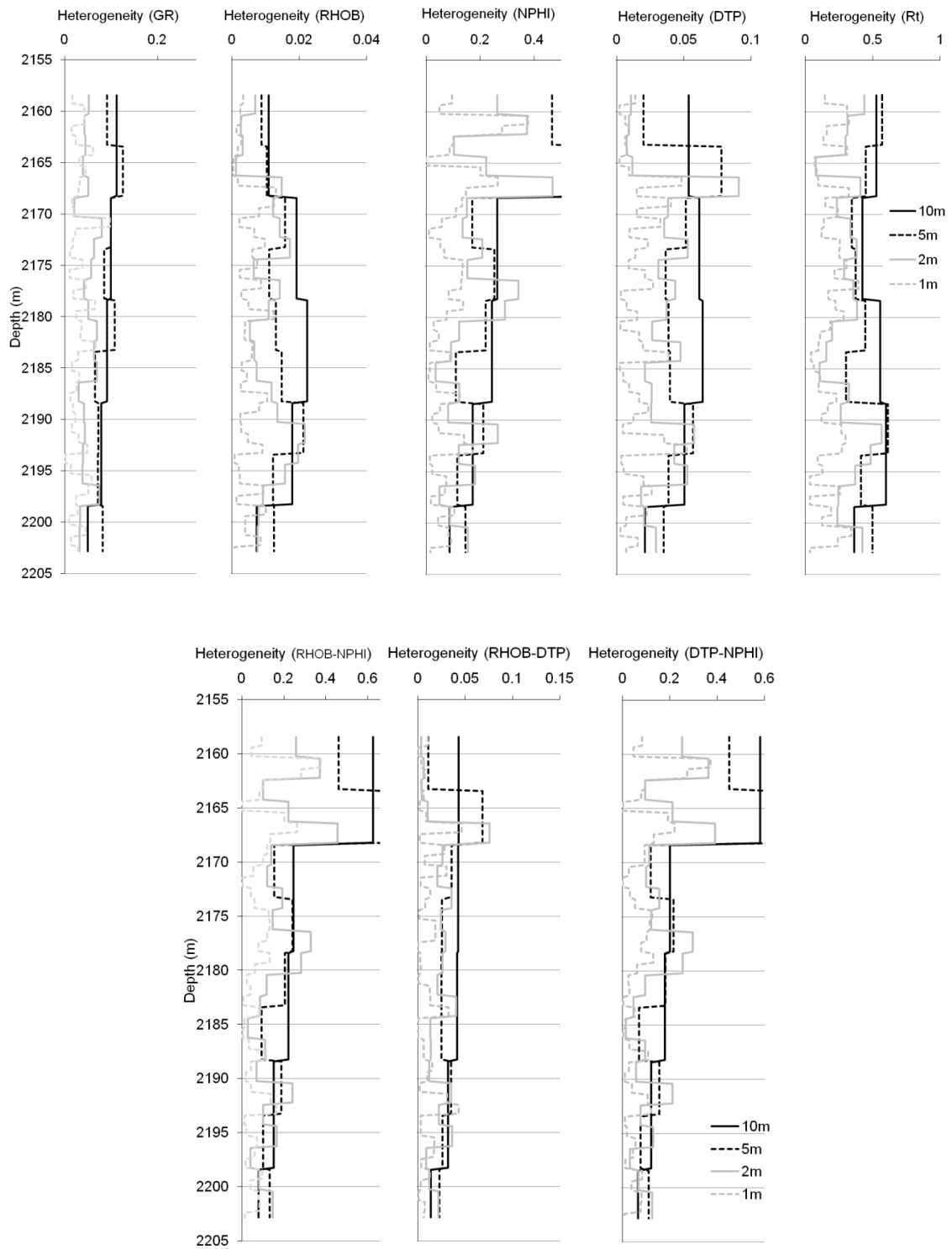


Figure 5.16. 10m, 5m, 2m and 1m window Lorenz (top) and Dual Lorenz (bottom) coefficient Heterogeneity Logs for Formation-B of well M. Well log datasets from top left to right; natural gamma ray (GR), bulk density (RHOB), neutron porosity (NPHI), P-wave transit time (DTP), and deep resistivity (Rt).

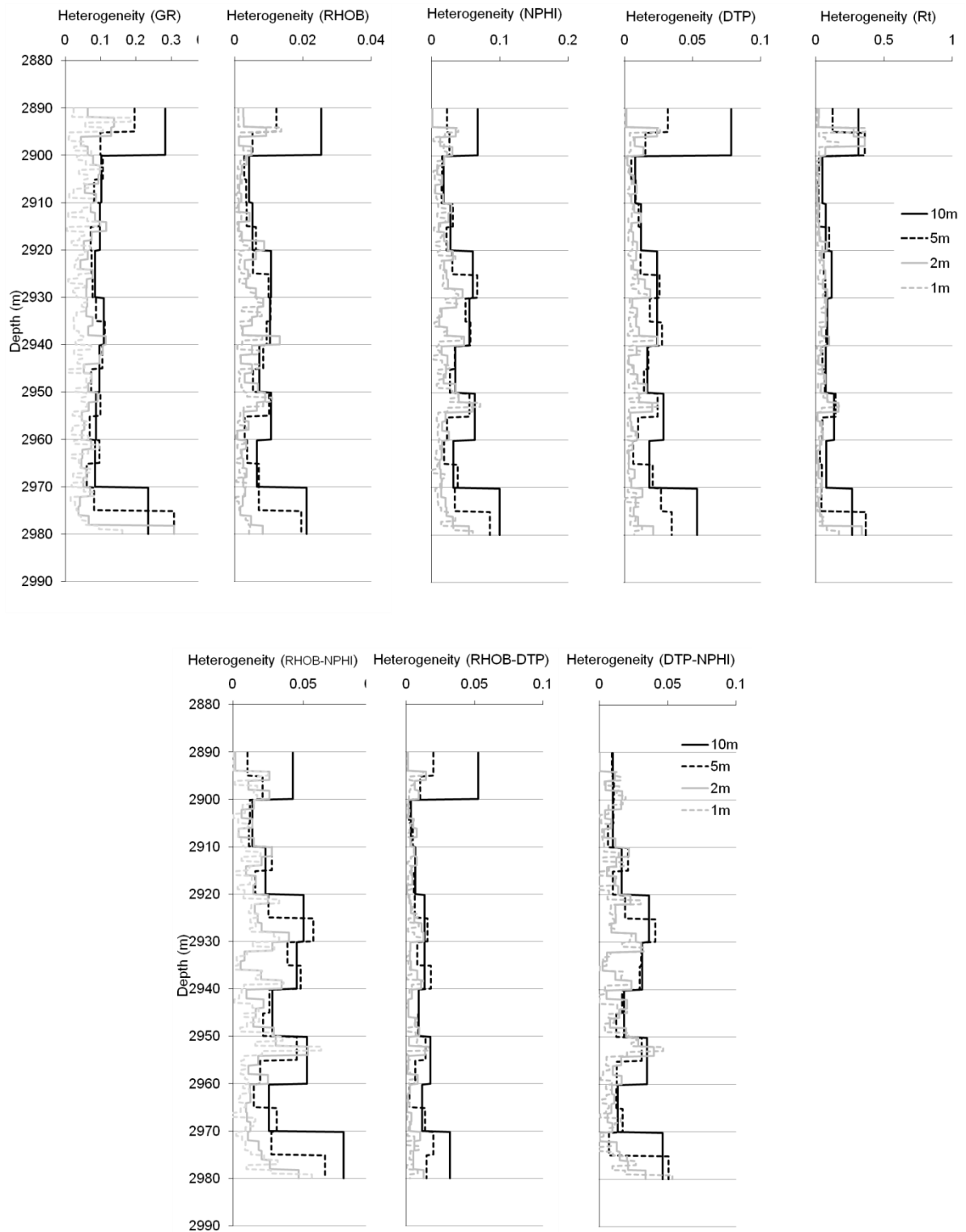


Figure 5.17. 10m, 5m, 2m and 1m window Lorenz (top) and Dual Lorenz (bottom) coefficient Heterogeneity Logs for the Abiod of well A. Well log datasets from top left to right; natural gamma ray (GR), bulk density (RHOB), neutron porosity (NPHI), P-wave transit time (DTP), and deep resistivity (Rt).

The single property-based H.Logs of figure 5.17 suggest the Abiod chalk of well A is of low heterogeneity throughout, with high heterogeneity upper and lower sections. From 2900 to

2970m very low frequency and amplitude heterogeneity changes occur downhole. The dual property H.Logs (figure 5.17) do not record the high upper and lower sections. The localised high and low features can be correlated across the H.Log suite.

Clearly Formation-A of wells P and M is the more heterogeneous reservoir unit, with high frequency and amplitude variability down hole in both wells. Formation-B is also shown to be less heterogeneous in both wells, however it is interesting to note this zone shows stronger heterogeneity features in well M (significance and cause of this will be discussed further in chapter 6). Visual comparison suggest that significant high/low heterogeneity features can be correlated between the zones of well P and M, for example the sharp decrease in heterogeneity at the top of Formation-B followed by a gradual decrease to the bottom of the formation. The Abiod chalk is shown to be the least heterogeneous of the reservoir units studied. It is expected that the internal numerical heterogeneity in all reservoir units studied may be used to characterise the underlying geological structures and properties.

Referring back to comments made in section 5.5, if the well log data for each reservoir unit has been normalised prior to heterogeneity analysis then comparison between zones/reservoir would have been more limited. Again, by using the original well log data scale then the heterogeneity scale is kept constant for all studies.

5.7. Conclusions

- The Heterogeneity Measures described in chapter 4 can be applied to petrophysical data to quantify numerical heterogeneity; where 0 is homogeneous and 1 is extreme heterogeneous.
- A Heterogeneity Log (H.Log) can be produced by applying a heterogeneity measure (Coefficient of variation, Lorenz coefficient, Dual Lorenz coefficient and/or the *t*-Test) to well log data windows of specified depth increments; 10m, 5m, 2m and 1m. Increased resolution is seen as the window size decreases. It is suggested that care be taken with the 1m H.Log as it comprises only five data points, this effectively replicates

the original wireline log data . The 2m H.Log is found to have the maximum difference between high and low values; suggesting optimal variation is captured here.

- Similar high and low heterogeneity features are seen in the H.Logs for all well log data; gamma ray, bulk density, neutron porosity, P-wave transit time and resistivity.
- The effect of offsetting the data window at 20cm intervals downhole is shown to have limited impact on the 2m H.Log. Similar relative high and low patterns in the heterogeneity are seen, on average a correlation coefficient (R) of 0.713 shows that ~50% (R^2) of the variation seen in the offset data is also recorded in the original H.Log data (with 99.9% confidence). The average difference in covariance and percentage difference in values for the offset H.Logs is ~30%, this is taken to suggest that an error of $\pm 30\%$ may be applied to the H.Logs.
- Normalising the well log data so that all measurement types have scales from 0 to 1, prior to heterogeneity quantification, is shown to have limited impacts of the outputs. The neutron porosity and resistivity H.Logs show minimal differences in values of <10%, and correlations of 97-98%, suggesting normalisation has minimal effect on heterogeneity quantification. Bulk density shows strong correlation of 97%, yet values increase by a maximum of 400%. While this increase in magnitude of heterogeneity values make easier interpretation, adding an additional step to the quantification of numerical heterogeneity is not necessary. This is particularly the case as part of the interest in the H.Log technique is that analysis and application of the different well log data allows comparison of the physical property measurement on their associated scales of investigation and measurement. It is these scales that will impact on the heterogeneity contrasts and relationships documented through the succession. As with all analysis, awareness and relationships to the original well log data should be examined within the study to ensure appropriateness of interpretations. This exercise has allowed confirmation that absolute values do not impact the result of numerical heterogeneity analysis.

- Formation-A of both wells P and M is shown to be most heterogeneous, with high amplitude and frequency changes through the succession. Formation-B is less heterogeneous, although it shows stronger heterogeneity features in well M. General trends in heterogeneity can be compared between the same zones in the two wells. The Abiod chalk is the least heterogeneous reservoir unit studied, although numerical wireline log data is not as homogeneous as one might expect for a chalk. Further discussion of the results is reserved for chapter 6.

Chapter 6. Reservoir Characterisation Using Numerical Heterogeneity

6.1. Introduction

The standard application of the heterogeneity measures to petrophysical well log data from complete reservoir units is presented in chapter 4, before the Heterogeneity Log (H.Log) is introduced in chapter 5. It is shown that heterogeneity measures quantify the numerical variation, or heterogeneity, in well log data producing a single output value that allows comparison between measurements, reservoirs and their sub-units. This work favours the Lorenz and Dual Lorenz coefficient techniques, as discussed in chapter 4.

This chapter investigates whether relationships between numerical heterogeneities identified in the various H.Logs can be used to characterise the physical properties of the carbonate reservoirs studied; primarily in terms of wireline-derived porosity and permeability. It will then discuss how heterogeneity zones can be identified, and the use of these zones in reservoir compartmentalisation and in constraining flow zones (or hydraulic units). The heterogeneity of the individual flow zones will be quantified so that relationships between reservoir / flow zone quality and heterogeneity can be investigated. In the final section the link between numerical heterogeneity, as shown in the H.Logs, and optimal sampling will be discussed

6.2. Carbonate Physical Properties relationships to the Heterogeneity Logs

To aid the identification of relationships between the various H.Logs and the well log-derived physical properties (shale volume, porosity and permeability; see chapter 3), cross plots are produced and discussed here. Many plots show poor correlation, with correlation coefficients lower than 0.15. Plots with good correlation of >0.5 (with coefficient of determination, R^2 , greater than 0.25; see chapter 5) and/or strong spreading trends are presented and discussed

here. Firstly key observations and trends are presented, before discussing the observed link between numerical heterogeneity, porosity and permeability.

6.2.1. Shale Volume & Heterogeneity

In this study shale volume is derived from the spectral gamma ray and density-neutron well logs (chapter 3). In terms of the reservoirs studied, shale (or mudrock) is a dominant feature in Formation-A of wells P and M. The Abiod chalk and Formation-B are referred to as “clean” carbonate, with minimal background shale volume; as such no relationship between heterogeneity and shale volume is observed in these reservoir units.

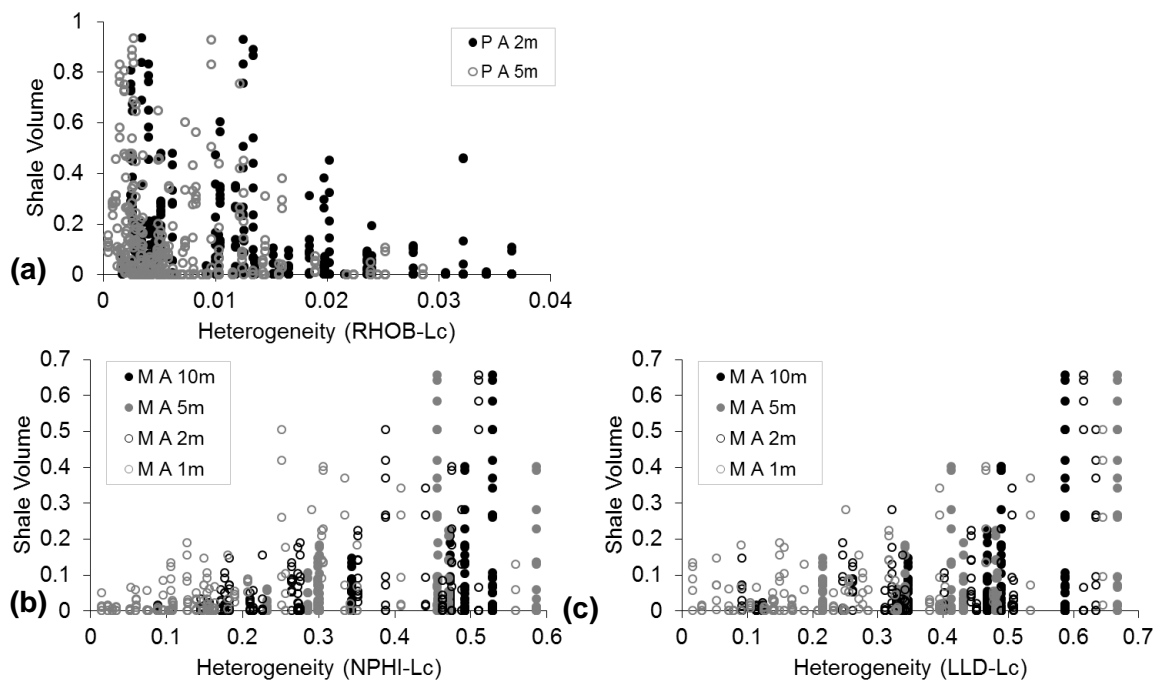


Figure 6.1. Crossplots of shale volume against Lorenz coefficient H.Log values; (a) 5 & 2m bulk density (RHOB) of Formation-A of well P, (b) 10, 5, 2, & 1m neutron porosity (NPHI) from Formation-A of well M, and (c) 10, 5, 2, 1m deep resistivity (LLD) from Formation-A of well M.

Trends between heterogeneity and shale volume can be seen in crossplots from Formation-A (figure 6.1). The 5m and 2m density H.Logs of well P Formation-A show a larger spread of low to high shale volumes at low heterogeneity, with low shale volumes becoming more dominant at higher heterogeneities. With this observed trend, correlation coefficients of -0.24 and -0.33, respectively, suggest that low correlation exists and accounts for ~10% of the variation (R^2 0.06 and 0.11).

In well M Formation-A neutron porosity and resistivity H.Logs show an opposing trend; with predominantly low shale volumes at low heterogeneity, with increasing data spread towards higher shale contents at higher heterogeneities. Here a moderate correlation coefficient of 0.4 occurs with the 5m and 2m H.Log values (R^2 0.16), while the 10m and 1m H.Logs show weaker correlation ~ 0.21 (R^2 0.04).

The presence of higher shale content is coincident with lower heterogeneity in the bulk density measurement (figure 6.1a). Mudrock (shale) is generally less dense than carbonate material (Rider 2002). The FMS electrical image of the well P Formation-A (chapter 3) suggests that mudrock is present as thick beds or within thick nodular limestone intervals. These metre thick facies units are characterised as low heterogeneity by the density H.Log. The neutron porosity log is sensitive to shales as they contain elements which have high thermal neutron properties, such as boron and other rare earth elements (REE). These elements have the effect of producing high neutron porosity values (Ellis & Singer 2007; Serra 1986). The neutron porosity log is seen to be less variable in carbonate-dominated sections (chapter 3). These two observations show a connection between shale and sudden changes in the neutron porosity log thus helping to explain why in Formation-A of well M higher shale content occurs with higher heterogeneity in the neutron porosity measurement (Figure 6.1b). Similarly the deep resistivity measurement shows strong value contrasts with higher shale content (Figure 6.1c). Shales generally show lower resistivity than carbonate material; for example shale: 0.5-1000 ohm.m, tight carbonate: 80-6000 ohm.m (Ellis & Singer 2007; Rider 2002), this can be seen through strong contrasts downhole in the deep resistivity log (chapter 3). The connection between higher numerical heterogeneity in deep resistivity and shale content may be explained in this way.

6.2.2. Porosity & Heterogeneity

An overarching observation from the H.Log – porosity plots is that lowest porosity values are often found in sections of higher numerical heterogeneity (figures 6.5 and 6.6).

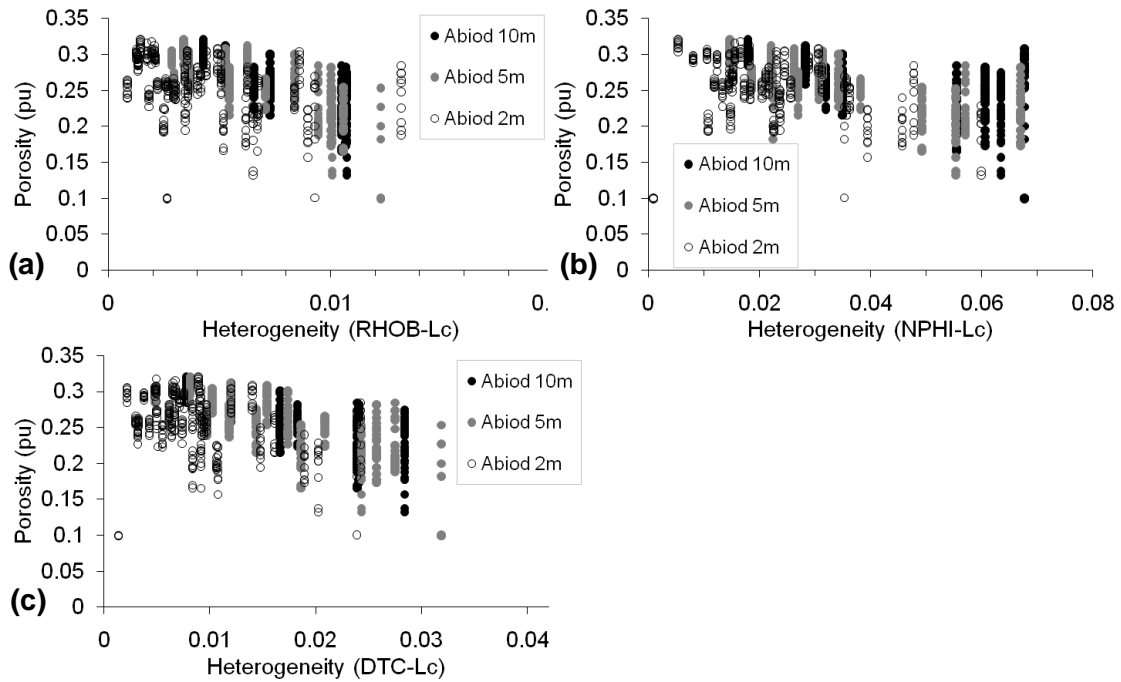


Figure 6.5. Crossplots of porosity against Lorenz coefficient H.Log values from the Abiod chalk of well A; (a) 10, 5 & 2m bulk density (RHOB), (b) 10, 5, 2m neutron porosity (NPHI), and (c) 10, 5, 2m P-wave transit time (DTC).

The Abiod chalk shows a good correlation between decreasing porosity and increasing numerical heterogeneity in bulk density, neutron porosity, and the P-wave transit time (figure 6.5). Average correlation coefficient of -0.6 suggests that ~36% of the variability in porosity is captured in the H.Log (correlation coefficient ranges from 0.3-0.8).

In the more heterogeneous reservoirs of Panna and Mukta relationships are seen between porosity and the bulk density, neutron porosity, and deep resistivity H.Logs. The neutron porosity and deep resistivity data show similar relationship to the Abiod data; with a general trend toward lower porosity with higher heterogeneity (figure 6.6). The less heterogeneous Formation-B shows strongest correlation between neutron porosity H.Log and porosity (correlation -0.5 – -0.7). The opposite is observed in the well P Formation-A's density H.Log, where higher porosity values are coincident with higher heterogeneity values (correlation coefficient ~0.43; figure 6.6a).

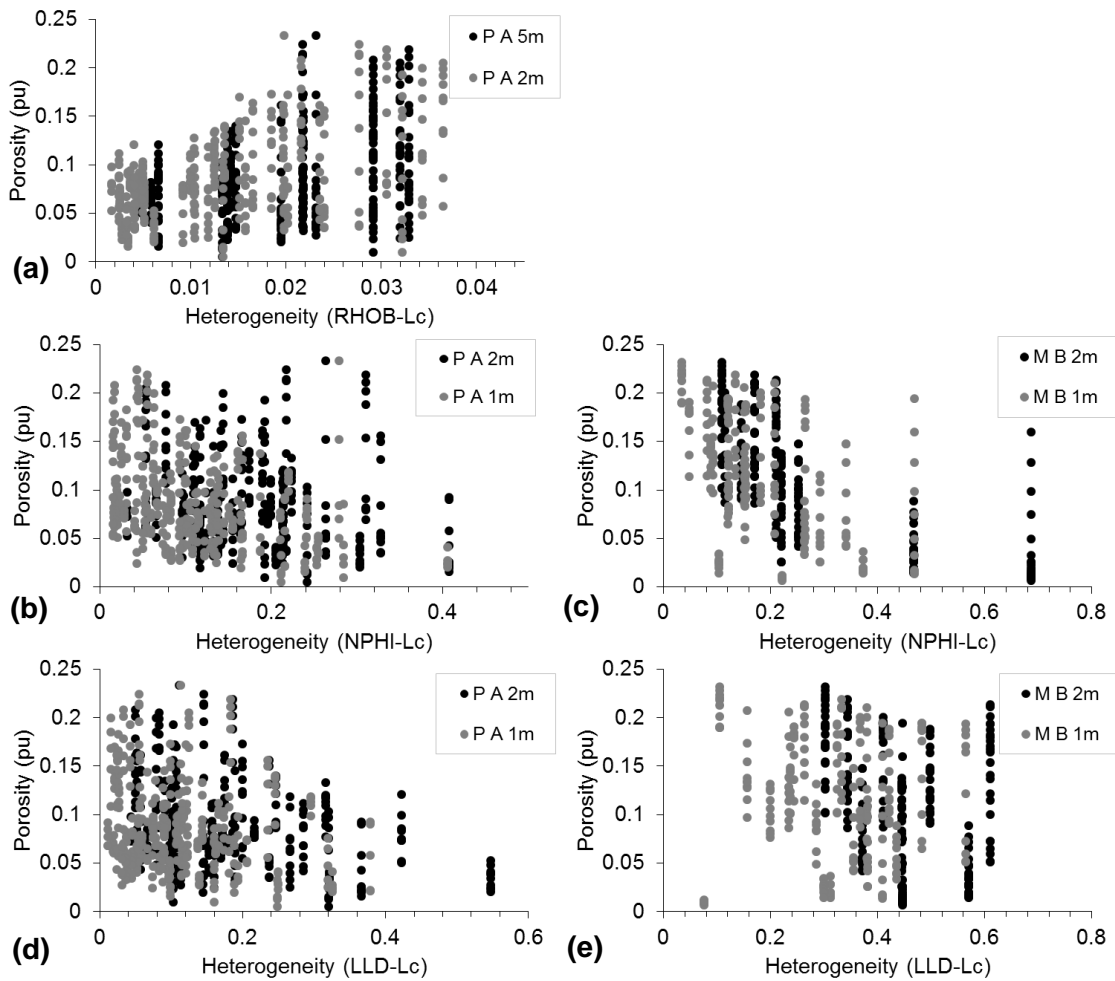


Figure 6.6. Crossplots of porosity against Lorenz coefficient H.Log values; (a) 5 & 2m bulk density (RHOB) from Formation-A of well P, (b) 2 & 1m neutron porosity (NPHI) from Formation-A of well P, (c) 2 & 1m neutron porosity (NPHI) from Formation-B of well M, (d) 2 & 1m deep resistivity (LLD) from Formation-A of well P, and (e) 2 & 1m deep resistivity (LLD) from Formation-B of well M.

Figure 6.6(b-d) shows a trend toward lower porosities with increased heterogeneity, suggesting that the more homogeneous the neutron porosity log response the better the porosity. This trend is strongest in Formation-B data, and is also seen in the more heterogeneous Formation-A where more outliers occur (correlations of -0.2 to -0.5 ; figure 6.6b). The deep resistivity measurements show a similar trend (6.6 d & e), with higher porosity values occurring at lower heterogeneities in both Formation-A and -B.

6.2.3. Permeability & Heterogeneity

Correlation between the permeability data and H.Log values is notably weaker than for porosity, however similar trends toward a decrease in data spread at high and low heterogeneities is observed.

The H.Log data for the Abiod chalk shows good correlation between numerical heterogeneity and permeability, a notable observation from figure 6.7 is that the lower permeabilities (<0.2mD) tend to occur with higher heterogeneity values. Correlations coefficients are found to be lower for Abiod permeability than porosity (averaging -0.35). This observation is in keeping with that of the porosity data above and it is believed that a link between homogeneity of grains shape/size and sorting is key – allowing a good porosity which is well connected, or permeable (discussed further in section 6.4.4).

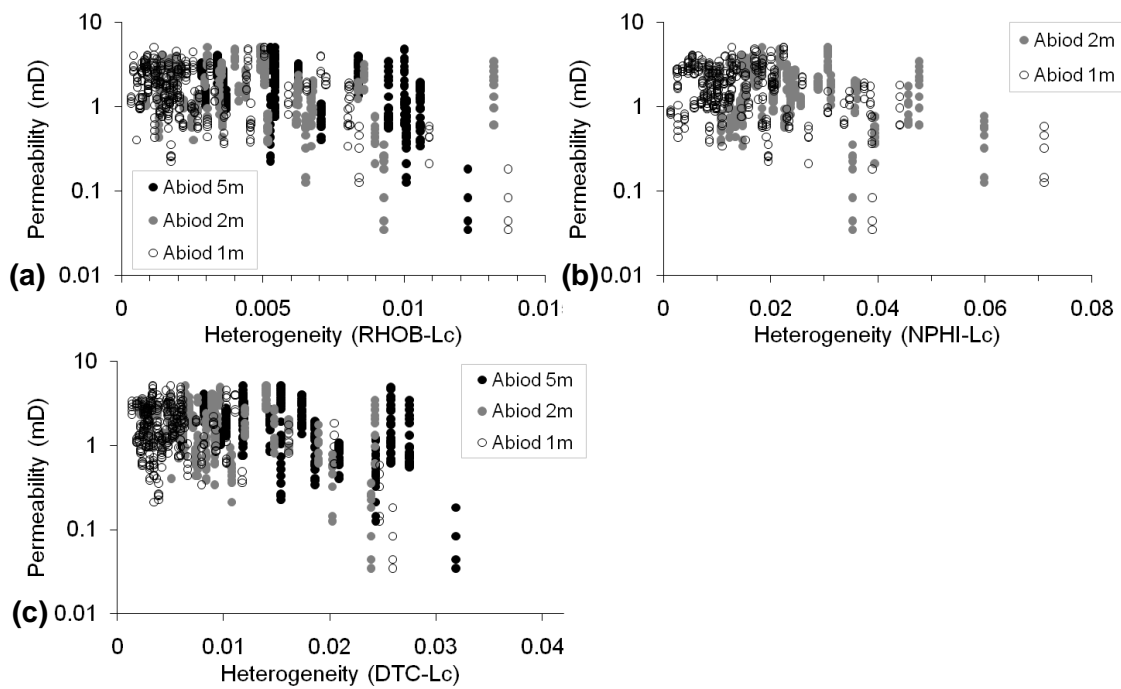


Figure 6.7. Crossplots of permeability against Lorenz coefficient H.Log values from the Abiod chalk of well A; (a) 5, 2 & 1m bulk density (RHOB), (b) 2 & 1m neutron porosity (NPHI), and (c) 5, 2, & 1m P-wave transit time (DTC).

As with the Abiod chalk, Formation-A of wells P and M show weaker relationships between H.Log heterogeneity value and permeability (when compared with the porosity data previously).

Correlation coefficients are less than -0.3 with a larger spread of outliers observed (figure 6.8), however similar general trends may be observed.

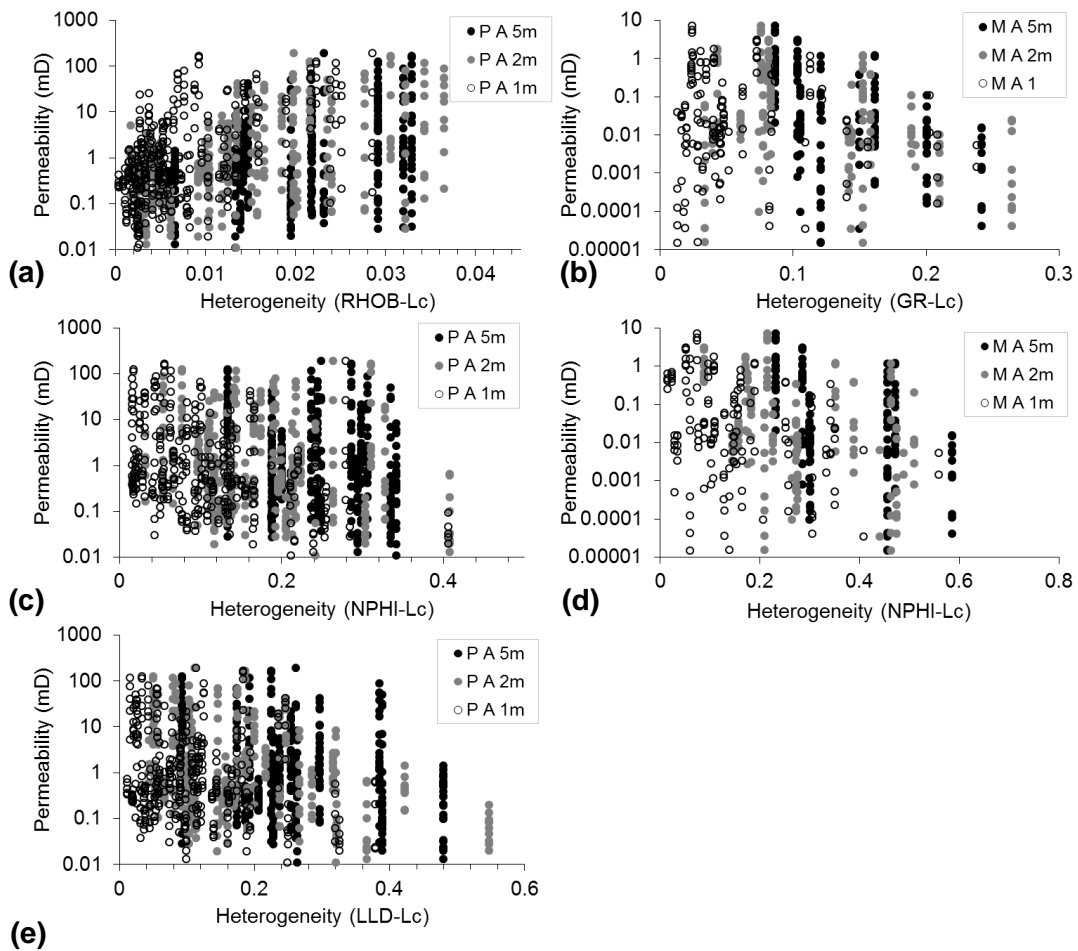


Figure 6.8. Crossplots of permeability against Lorenz coefficient H.Log values for Formation-A; (a) 5, 2 & 1m bulk density (RHOB) of well P, (b) 5, 2 & 1m gamma ray (GR) of well M, (c) 5, 2 & 1m neutron porosity (NPHI) of well P, (d) 5, 2 & 1m NPHI of well M, and (e) 5, 2 & 1m deep resistivity (LLD) of well P.

Again, lower permeability values are coincident with lower heterogeneity in the density values (correlation coefficients of 0.32, 0.42, and 0.42 for the 5m, 2m, and 1m H.Logs; figure 6.8a).

The H.Logs for gamma ray, neutron porosity and deep resistivity measurements show lower permeability values corresponding to higher permeability in Formation-A (figure 6.8 b-e).

Again this relationship is much weaker than that seen in the porosity data above, here the 5m H.Logs show strongest correlation at ~0.3. Formation-B of well M shows trends toward higher permeability at low heterogeneities (average correlation coefficient ~0.25; figure 6.9). Indeed, here the lowest permeabilities are predominantly found at higher heterogeneities, but care is

taken in this observation as permeability values are below the traditional 0.001mD cut-off often used by industry.

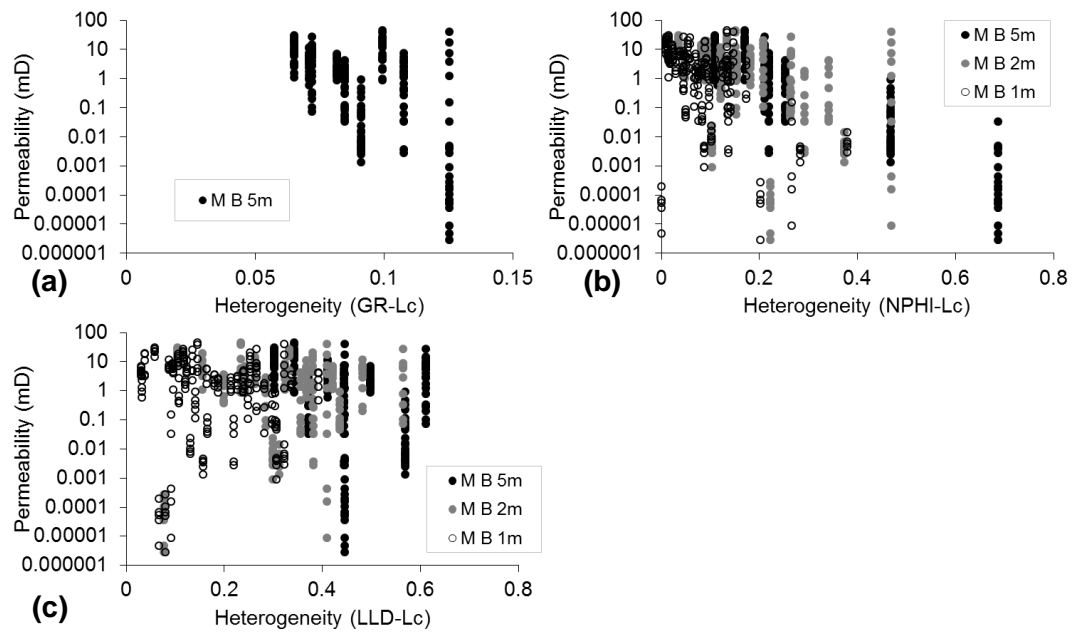


Figure 6.9. Crossplots of permeability against Lorenz coefficient H.Log values from Formation-B of well M; (a) 5m gamma ray (GR), (b) 5, 2 & 1m neutron porosity (NPHI), (c) 5, 2 & 1m deep resistivity (LLD).

6.2.4. Heterogeneity Logs and Physical Properties: discussion

The dominant finding here is that the heterogeneity logs cannot be used a direct indicator of porosity or permeability in the reservoir units studied. While rarely strong, the correlation coefficients can be used to suggest general trends in the relationships described above.

In the Abiod chalk all the H.Logs show both porosity and permeability decrease with increasing heterogeneity. This observation has comparisons to homogeneous clastic formations, such as aeolian sandstone, where increased sorting of grain size and shape allows for optimal packing of grains which in turn creates larger pore volumes (Beard & Weyl 1973; Rogers & Head 1961).

Formation-B provides a low heterogeneity example, exhibiting similar trends to the homogeneous end-member Abiod chalk. The trend is obscured in places by outliers, as expected, but in general lower porosity and permeability values are seen with higher heterogeneities. It is interesting to note that these trends are not observed in the H.Logs from the Formation-B of well P. It is possible that this reflects the geological interpretation that the

Panna field has undergone more complex diagenesis, increasing the intrinsic heterogeneity in features such as pore type and mineralogy (chapter 3).

There are two opposing trends observed in the “heterogeneous” Formation-A. The previous trend of lower porosity/permeability with increasing heterogeneity is seen in the neutron porosity, P-wave transit time, and deep resistivity H.Log data. However the bulk density H.Logs show increased porosity and permeability with heterogeneity, which is counter intuitive to previous findings.

Neutron porosity logs measures the volume of hydrogen ions in the rock, and can therefore be affected by pore volume, lithology (as described for shales above), and fluids (Rider 2002; Serra 1986). Formation-B is documented to have very low shale content, and fluids are suggested to be gas-dominated. As such porosity is expected to be the main control on the neutron log.

The density log responds to grain density (mineralogy/lithology) and volumes of pore space (Ellis & Singer 2007; Rider 2002; Serra 1986). A potential explanation for the link between increased heterogeneity in bulk density measurements and porosity/permeability is that the density log is responding to heterogeneities in the carbonate rock matrix, as well as porosity, which are not affecting the other petrophysical well logs.

Decreasing porosity/permeability with increasing heterogeneity trend may have two possible explanations; (1) the high porosity carbonate material is more homogeneous as with the Abiod chalk and clastic examples, or (2) the higher porosity units are thicker and so assert a stronger averaging effect on the H.Logs. Ideally a more complete core record could be used to tie the petrophysical and geological properties together. It may also be possible to relate the porosity and permeability features observed in Formation-A of well P, to the presence of thick shale beds which show log heterogeneity.

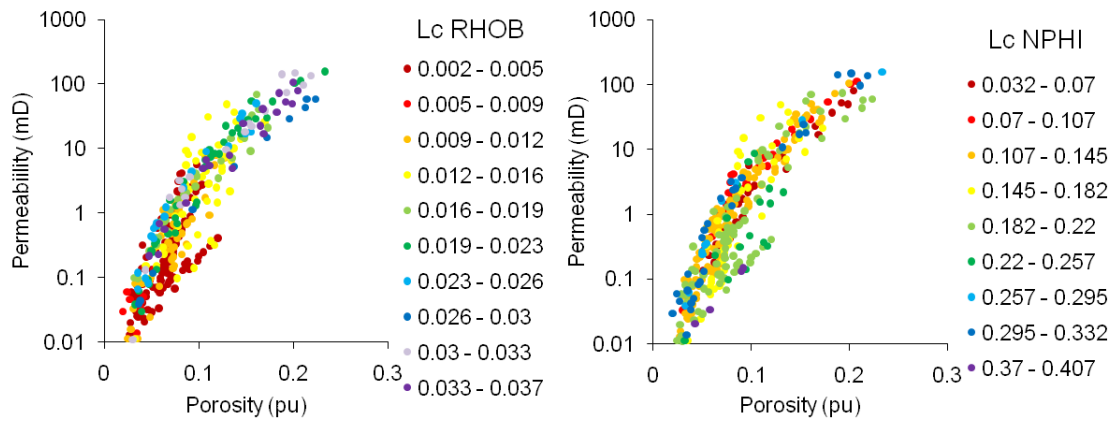


Figure 6.10. Porosity-permeability crossplots with Lorenz coefficient heterogeneity (Lc) on the z-axis, for Formation-A of well P. Wireline data: bulk density (RHOB) and neutron porosity (PHIE).

Finally, porosity-permeability cross plots do not suggest that numerical heterogeneity can add any further clarification to carbonate classifications schemes such as Lucia (1999) as the high and low classes are spread across the plot (Figure 6.10). As discussed above, however, it can be seen that with bulk density heterogeneity low heterogeneity values cluster toward lower porosity and permeability values.

6.3. Heterogeneity zones

The link between porosity, permeability and the H.Logs discussed above has lead this research to consider the identification and application of heterogeneity zones using the heterogeneity log values.

Chapter 3 illustrated how whole reservoir physical property data can be zoned using the Hydraulic Unit / Flow Zone Indicator (Amaefule *et al.* 1993) and Stratigraphic Modified Lorenz (Buckles 1965; Gunter *et al.* 1997) techniques. To zone the heterogeneity logs for each of the reservoir units of this study two techniques are investigated and modified accordingly; (1) The generalised distance, D^2 , and (2) Stratigraphic Modified Lorenz, *SML*, methods. All methods were initially tested on the H.Log data from Formation-A of well P to assess their application and benefits (sections 6.3.1&2); the *SML* method is found to be the most useful and robust technique for zoning the H.Log data, and has been further developed from published examples.

Comparisons to physical property data and flow zone indicator values is used to establish a more comprehensive method for defining fluid flow zones within a reservoir unit.

6.3.1. D^2 – Generalised Distance Boundary Method

A basic technique used to assign boundaries to numerical data, typically from transects or downhole, is the generalised distance method (Rossiter 2009; Webster 1973). This method is for data series comprising a single variable, the generalised distance is calculated for the difference between two halves of a moving data window (Davis 2002). The data window should comprise an even number of data points, Webster (1973) comments that this technique is particularly sensitive to data window size. Rossiter (2009) suggests this data window size should be constrained using autocorrelation.

Autocorrelation is a statistical technique used to compare parts of a data series so that similarities can be detected, data is assumed to exist over constant lag thickness (Borradaile 2003; Jensen *et al.* 2000). Borradaile (2003) elaborates that the data series is duplicated and offset by a successively larger lag distances with correlation coefficient calculated, allowing the data similarities to be computed along the data series. For this test the basic autocorrelation function of MatLab has been used. Figure 6.11 provides graphical outputs for autocorrelation analysis of H.Log data from well P Formation-A. The H.Log data is processed with individual heterogeneity value assigned to the mid-point of that data block, so for the 2m H.Log a value occurs every two metres. An autocorrelation of 1 shows correlation of the original series against itself, correlation decreases sharply with first lag shift. Typically the lag distance where autocorrelation first decreases to near zero is used to define how many data windows are required for that data (Rossiter 2009).

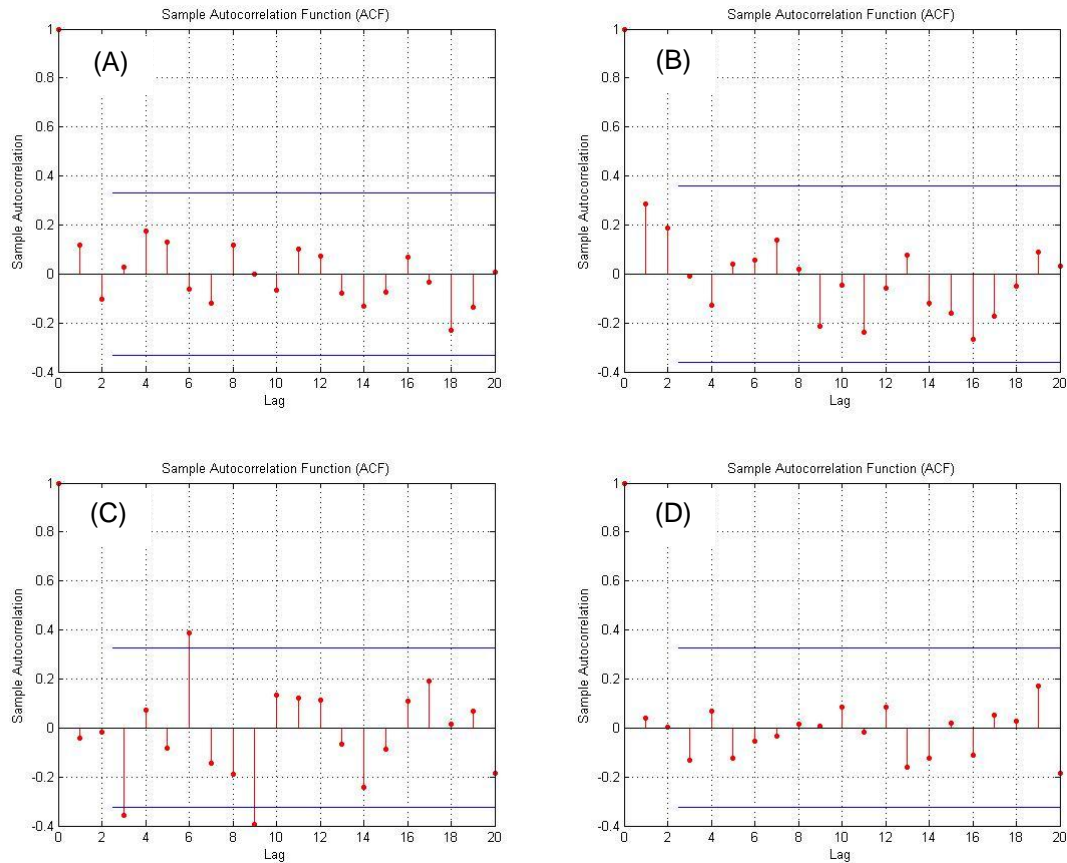


Figure 6.11. Autocorrelation function for the 2m Lorenz coefficient H.Logs of well P Formation-A; (A) gamma ray, (B) bulk density, (C) neutron porosity, and (D) P-wave transit time. 95% confidence limits are shown a blue horizontal lines. Lag distance is 2m and the series comprised 38 measurements.

H. Log	Autocorrelation Lag	Number of Boundaries	Number of windows	Data Window Size
Gamma Ray	3	13	15	5.2
Bulk Density	3	13	15	5.2
Neutron Porosity	2	19	21	3.6
P-wave Travel time	2	19	21	3.6
Deep Resistivity	2	19	21	3.6
<i>Average</i>	<i>2.4</i>	<i>16.5</i>	<i>18.5</i>	<i>4</i>

Table 6.1. Establishing an average window size the Generalised Distance (D^2) method for the well P Formation-A Lorenz coefficient H.Log data.

This lag can then be converted into an indication of how many data windows should be used for the Generalised Distance method (table 6.1); (1) the number of values in the series is divided by the autocorrelation lag distance to identify the number of window boundaries required, (2) the number of window boundaries plus two indicates the number of windows, and (3) the number of series values divided by the number of windows gives the suggest size of half data windows

required. As data windows are assumed even in number, the average size of 4 units is used in this analysis.

The generalised distance (D^2) is calculated using equation 6.1 (Davis 2002), effectively comparing the mean and variance of the two halves of the data window (comprising two values each). Figure 6.12 illustrates the boundaries suggested by D^2 for the neutron porosity H.Log, comparison is made to the actual 2m H.Log. The D^2 results for the 5m H.Log suggest one dominant zone boundary around 1803m, but few data points are provided in this analysis meaning limited interpretations can be made. 1m H.Log results are very noisy. Both appear to have little bearing on the heterogeneity log itself. Significant peaks in the 2m H.Log D^2 output suggest zone boundaries at 1768m, 1776m, 1791m, 1804m and 1820m. The 1m H.Log D^2 outputs show peaks at 1774m, 1782m, 1792m, 1810m, and 1824m, however their significance appears low because of the large noise level produced. No suitable method has been successfully applied to ascertain the significance of these peaks, it is simply their amplitude which can be used to justify boundary placement at this time (Davis 2002). Across the suite of H.Logs from the reservoir units studied the results suggest that the resolution of the 10m and 5m H.Logs are too low for meaningful interpretation of boundaries for heterogeneity zones using this technique.

$$D^2 = \frac{(\bar{X}_1 - \bar{X}_2)^2}{s_1^2 + s_2^2} \quad \text{(Equation 6.1)}$$

Where: D^2 – generalised distance, \bar{X} – mean of series 1 or 2, and s^2 – variance of series 1 or 2. [Series refers to half of the data window]

Figure 6.13 illustrates the D^2 peaks from the 2m Lorenz and Dual Lorenz coefficient H.Logs. No heterogeneity zone boundary can be correlated through all H.Logs, except at 1768m which is shown by neutron porosity, P-wave transit time, and deep resistivity. The density, neutron porosity and resistivity-based peaks show a good spread of strong boundary peaks throughout the section, while gamma boundaries are concentrate mid-section. It could be suggested that these three heterogeneity types may be of most use in reservoir characterisation.

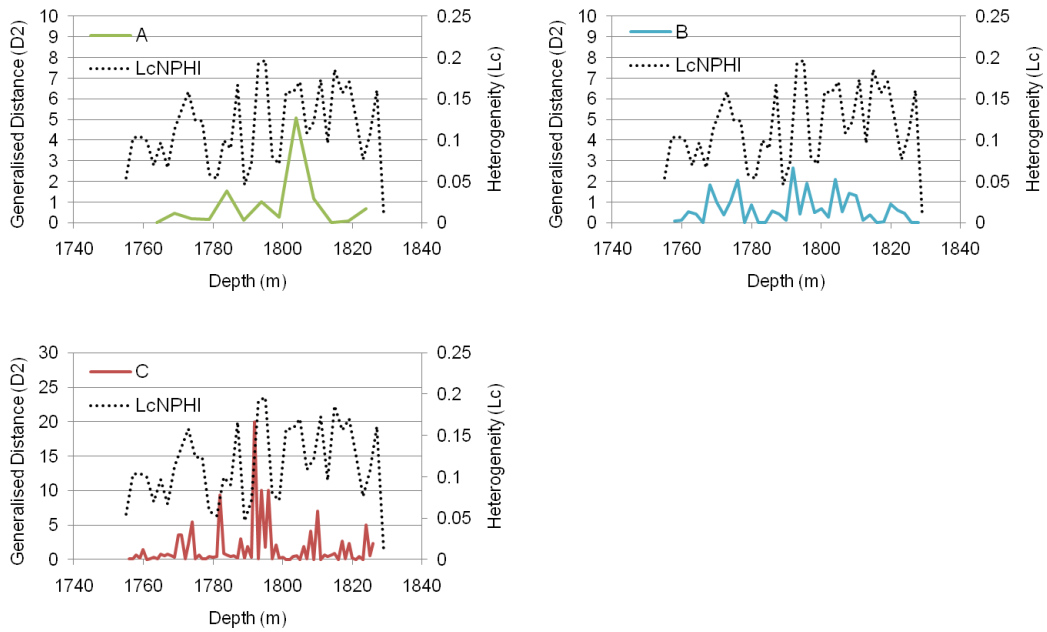


Figure 6.12. The Generalised Distance method suggested boundaries for the 2m Lorenz coefficient H.Log of neutron porosity (LcNPHI). A) 5m window, B) 2m window, and C) 1m window sizes.

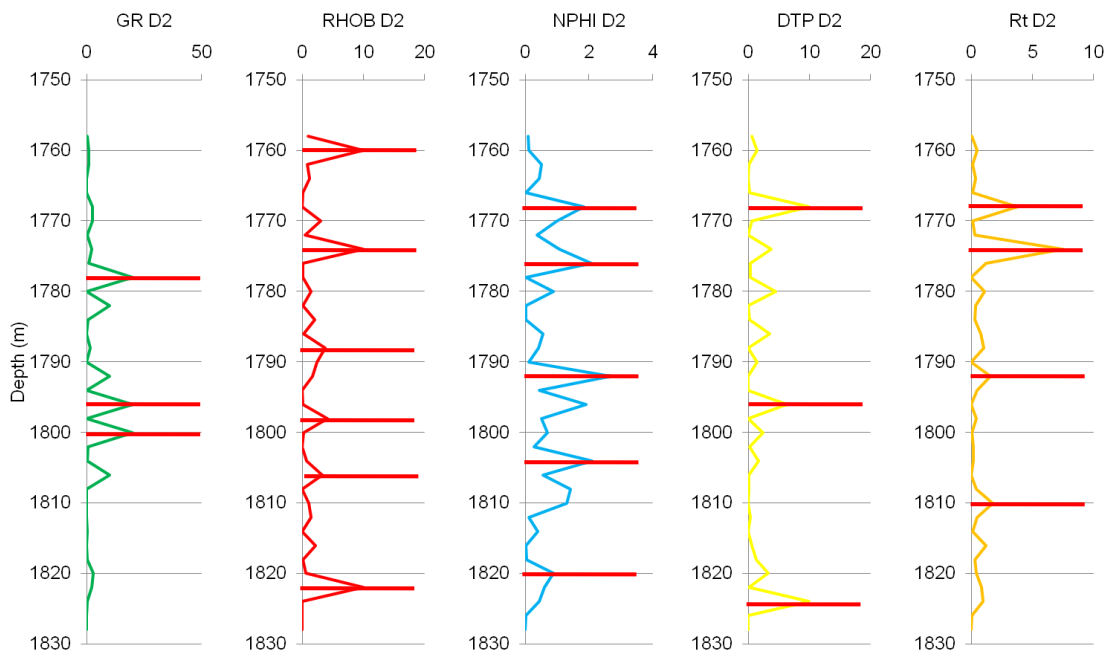


Figure 6.13. Generalised Distance D^2 peaks used to suggest locations of zone boundaries in the 2m H.Logs for the Lorenz coefficient. H.Logs: gamma ray (GR), bulk density (RHOB), neutron porosity (NPHI), P-wave travel time (DTC), and deep resistivity (Rt).

The D^2 method is traditionally used to define zones in soil transects of similar properties (Davis 2002), this is a limitation to this method for the heterogeneity zones. Looking at the original heterogeneity log (e.g. Figure 6.12); zones are not visually obvious based on similar values through the succession. Instead zoning may be better defined from relative contrasts in peaks and trough cycles.

Davis (2002) suggests that multi-variant cluster analysis can produce a more robust method for zoning data. Trials using the iterative non-hierarchical cluster analysis software (INCA) have not provided any significant findings to aid the identification of heterogeneity zones to-date.

6.3.2. Stratigraphic Modified Lorenz Plots (SML)

The Lorenz plot has been highly used in this research as the basis of a heterogeneity measure (the Lorenz coefficient). Chapter 3 (and Appendix B) details a modified use of this plot for identifying flow zones from porosity and permeability data, the stratigraphic modified Lorenz plot (Gunter *et al.* 1997). This method has application for zoning single variable data such as the H.Logs.

The traditional stratigraphic modified Lorenz plot displays cumulative porosity against cumulative permeability (normalised from 0-1 for display purposes); values are not sorted (as is done when calculating the Lorenz coefficient) so that original stratigraphic order is maintained (Doveton 1994). A change in slope around a 45° angle is then used to identify zones comprised of transmissive and storage unit (see appendix A for example).

This approach has been modified and advanced to investigate the identification of zones in numerical heterogeneity data. Firstly the Lorenz plot is produced by calculating the cumulative of the H.Log values downhole, this is normalised from zero to one (Figure 6.14). With the typical method, zone boundaries are then applied manually based on visual observation of changes in slope (Gunter *et al.* 1997).

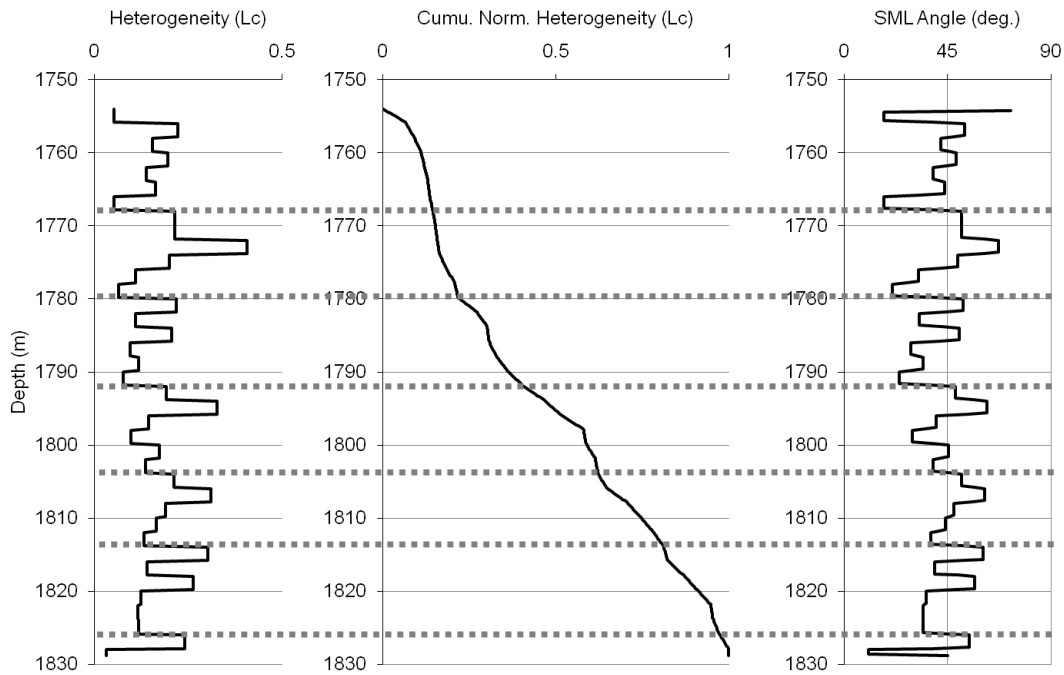


Figure 6.14. Graphical outputs of the Stratigraphic Modified Lorenz zoning method, for neutron porosity Lorenz coefficient (Lc) 2m H.Log of well P Formation-A. Left to right: original H.Log, cumulative heterogeneity values downhole normalised from zero to one, and the SML Angle.

This research has produced an angle of slope plot (the SML Angle) to aid identification of zone boundaries. The SML Angle is produced for three successive data points using the tangent trigonometric function as shown in Figure 6.15. Angle “a” is returned in radians and so converted to degrees by multiplying by the converter 57.2957705 (Weisstein 2010). The resultant SML Angle values are then plotted against depth (Figure 6.14). The SML Angle plot shows strong correlation to the original H.Log data, but has effectively been differentiated to produce a “rate of change” value. Angles greater than 45° occur where heterogeneity value increases relative to the average value, while decreased heterogeneity is shown smaller angles. In keeping with previous stratigraphic modified Lorenz work, a zone boundary is suggested to be shown by a distinct increase in the angle of slope above 45° .

Figure 6.14 illustrates how zone boundaries are identified using this technique. For the well P Formation-A neutron porosity H.Log, the SML method suggests zone boundaries at 1768m, 1780m, 1792m, 1803m, 1813m, and 1826m.

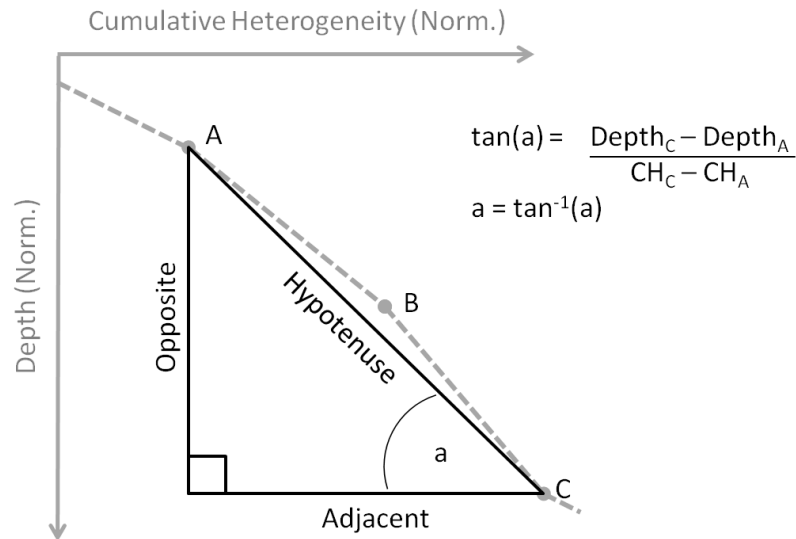


Figure 6.15. Calculating the SML Angle from the Lorenz plot, using the tangent trigonometric function. Cumulative heterogeneity and depth are normalised (Norm.). The angle (a) is calculated for points A & C, and then assigned to point B as a midpoint.

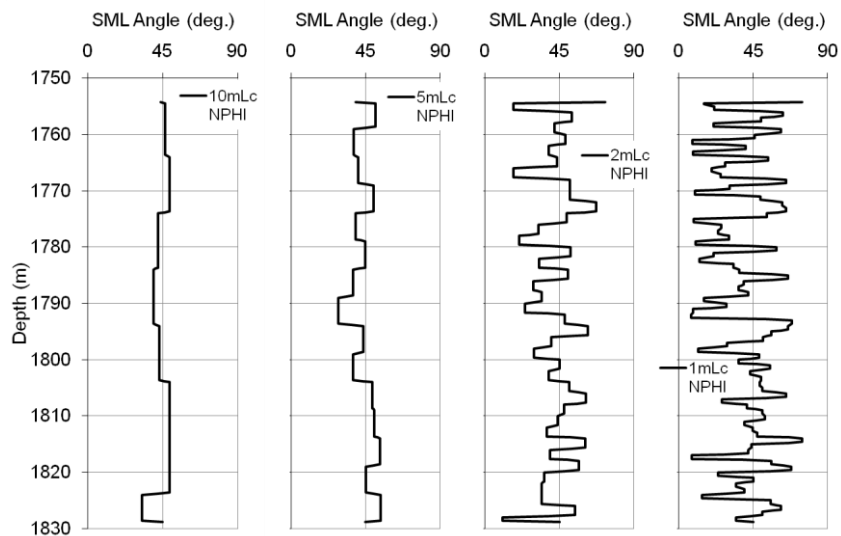


Figure 6.16. Stratigraphic Modified Lorenz (SML) angle values for the neutron porosity H.Logs (Lc NPHI) of well P Formation-A. Left to right: outputs for the 10m, 5m, 2m, and 1m H.Logs.

Unlike the generalised distance method (section 6.3.1), this method is easily applied to the original H.Log data without need for re-sampling so that a single value is processed for each heterogeneity block (data window).

Figure 6.16 shows that the SML method is easily applied to the 10m, 5m, 2m, and 1m H.Log data, and that zone boundaries can be identified at similar depth levels throughout. Again the

10m H.Log shows poor resolution for zoning the heterogeneity of the reservoir units studied, with low contrasts identifying only two zones. The 1m H.Log outputs are again suggested to be noisy; a suitable significance test has not yet been identified or applied for these data.

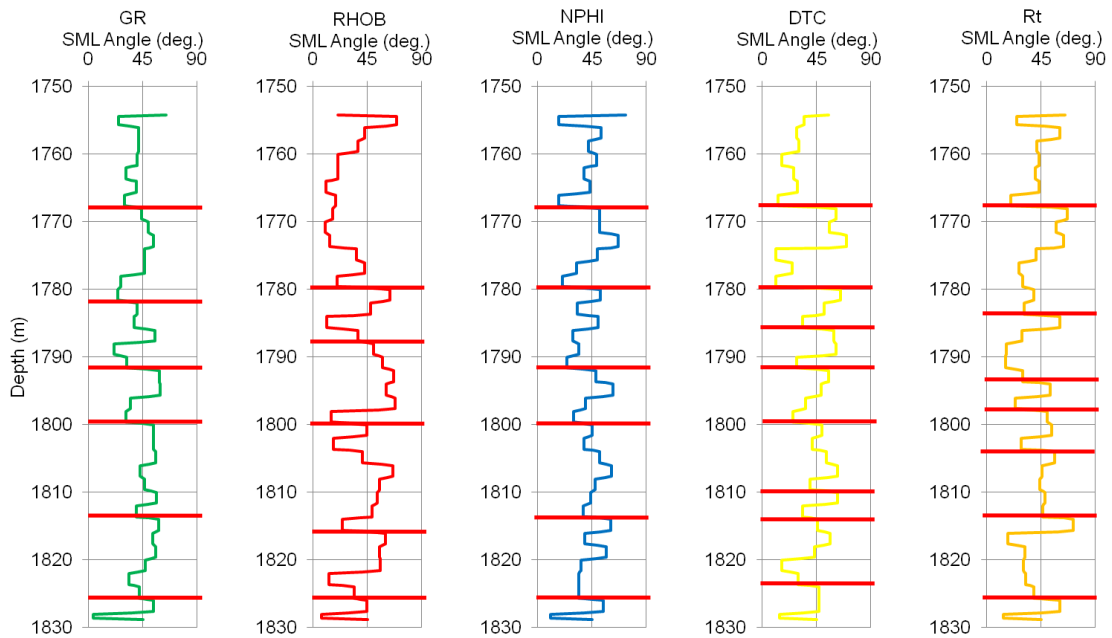


Figure 6.17. SML Angle plots and identified zone boundaries for the 2m Lorenz coefficient H.Logs: gamma ray (GR), bulk density (RHOB), neutron porosity (NPHI), P-wave travel time (DTC), and deep resistivity (Rt).

The SML Angle zone boundaries show fair correlation across the suite of H.Logs (Figure 6.17). For example consistent boundaries are found at 1768m, 1780-2m, 1791-2m, 1800m, ~1813m and at 1836m. In the mid-section the P-wave transit time and deep resistivity show a couple of additional boundaries which may be of less significance because of small value contrasts. This method clearly allows consistent sub-division of the H.Log data into zones based on the cyclical nature of heterogeneity observed, rather than comparing zones of similar values, as is the case with D^2 . This research does not discuss the identification and quantification of formal cyclicity and periodicities within the heterogeneity log data, although it is an avenue of potential further research.

6.3.3. Comparison of the D^2 and SML zoning methods

Both the generalised distance D^2 and stratigraphic modified Lorenz (SML) zoning methods have strengths and weaknesses for their application in identifying boundaries in heterogeneity log

data. Both provide a more robust method for zoning numerical data, rather than simply assigning boundaries by eye (with the consequence of introducing bias from the analyst).

D^2 provides a basic statistical technique for identifying boundaries in numerical data. These boundaries separate intervals with similar properties. The significance of peaks, and therefore boundaries, is visually assessed by comparing peak amplitudes across the series. In the case of these numerical heterogeneity data, intervals of similar properties are not of particular interest as the data show strong frequency and amplitude contrasts throughout.

The SML method provides a way of zoning the heterogeneity logs which can clearly be seen in the original data in terms of peak and trough contrasts. Rate of change methodologies such as this provide a simple and robust graphical method for assigning boundaries. Again, the negative point here is that significance of boundaries is not easily justified at this point.

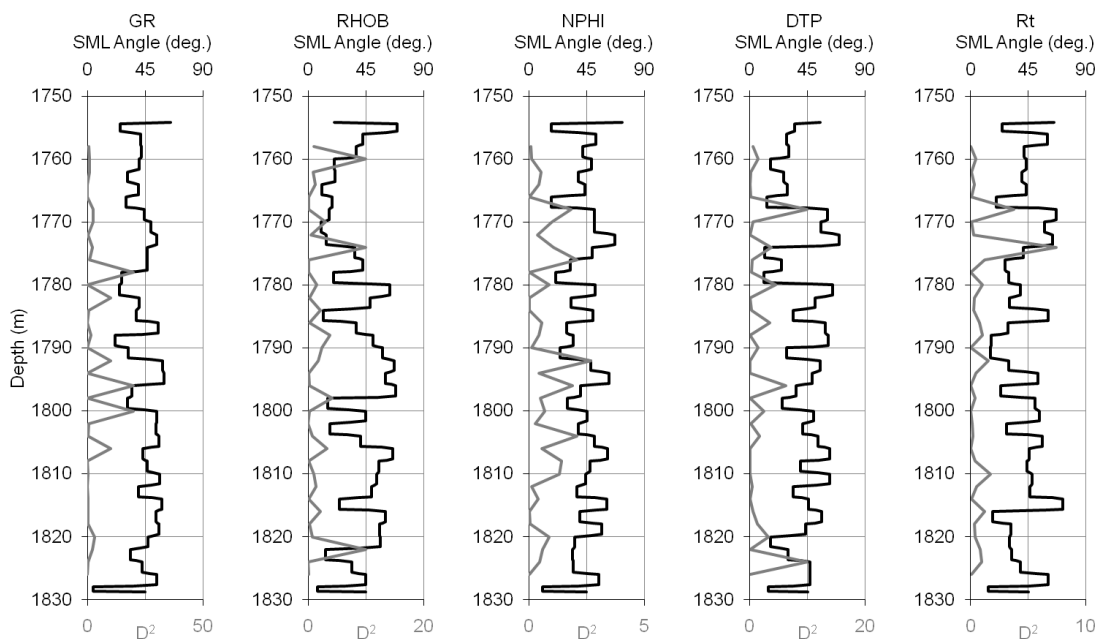


Figure 6.18. Comparison of the D^2 (grey) and SML angle (black) outputs used for assigning boundaries for heterogeneity zones in the H.Log data from well P Formation-A. H.Logs: gamma ray (GR), bulk density (RHOB), neutron porosity (NPHI), P-wave transit time (DTP), and deep resistivity.

Figure 6.18 compares the two zoning methods. Clearly it can be seen that peaks in D^2 separate intervals of similar heterogeneity, some of which do correspond to increases in the SML angle above 45° .

For the purposes of producing heterogeneity zones from the H.Logs, this research favours the SML Angle method because the heterogeneity zones established using the SML angle method can be more readily traced through the whole suite of measurements, based on high-low heterogeneity features, allowing the identification of more robust zones that are comparable to fluid flow zonations.

6.3.4. Heterogeneity Zones; aiding identification of Flow Barriers and Flow Zones

Techniques used to establish reservoir zones in hydrocarbon reservoirs are typically based on well log-derived (core calibrated) porosity and permeability relationships. A variety of complex statistical techniques have been applied to the identification of flow zones; for example discriminant analysis to predict reservoir rock-type groupings (Skalinski *et al.* 2005), electrofacies zonations using neural networks and K-nearest-neighbour clustering (Knecht *et al.* 2004), fuzzy logic inference (Qi & Carr 2006; Saggaf & Nebrija 2000), and the previously discussed Stratigraphic Modified Lorenz plot (Doveton 1994; Gunter *et al.* 1997; Hurley *et al.* 1999).

The industry standard for characterising reservoirs into flow zones appears to be Amaefule *et al.*'s (1993) Hydraulic Unit – Flow Zone Indicator methodology (Asgari & Sobhi 2006). As shown in Chapter 3, the basic premise of this technique is establishing a flow zone indicator (FZI, a function of porosity and permeability; equation B.19 - B.21, Appendix B). FZI values are plotted against normalised porosity to establish hydraulic units, which when plotted downhole can be used to subdivide reservoir units into fluid flow zones. It is common practise to assign zones boundaries to horizons with lowest FZI value (Amaefule *et al.* 1993; Cerepi *et al.* 2003), effectively producing reservoir compartments with flow potential in between low quality barriers.

The previous section has shown how numerical heterogeneity can be used to subdivide reservoirs into heterogeneity zones. Dominant zone boundaries can be seen in all five H.Logs

derived from wireline logs. The potential for heterogeneity zones, established using the 45° SML Angle method from the wireline-derived H.Logs, to be used in the identification of fluid flow zones is discussed below. This links back to section 6.2 where simple trends between physical properties were identified. In this section we focus on the Heterogeneity Logs and resultant zonations from 2m H.Logs; section 6.3.2 illustrated that the 10m and 5m H.Logs provided low resolution zoning capabilities (commonly identifying only 2 zones), and the 1m H.Log is suggested to be too noisy for adequately significant zonations to be obtained. In the accompanying figures (6.19-6.22) boundaries are shown in red, note that these are obtained from the fluid flow zonation methods with major boundaries being coincident with abrupt decreases in porosity, permeability and thus flow zone indicator. The following text compares the location of these flow zone boundaries to the heterogeneity-derived boundary indicator (SML Angle).

Figure 6.19 illustrates how low porosity and permeability values can be correlated to heterogeneity zone boundaries in the homogeneous end-member of this study, the Abiod chalk. The Abiod is typically divided into four zones by the operator, based on poro-perm properties; at 2928m, 2937m and 2952m. These levels can be seen to relate to significant decreases in porosity, permeability and FZI. SML Angle can be seen to increase significantly above 45° at these depths, this is often coincident with peak values. Neutron porosity and P-wave transit time H.Logs show highest SML angle values of ~60° with these boundary levels. Additional heterogeneity zone boundaries, identified by smaller increases in the SML Angle, do correlate to smaller localised decreases in the physical properties.

This is taken to suggest that the Abiod can be divided into four dominant heterogeneity zones which correspond to fluid flow zones, and that smaller-scale subzones can also be identified using a combination of the H.Logs and FZI values. The neutron porosity and P-wave transit time H.Logs show most potential for identifying fluid flow zone boundaries.

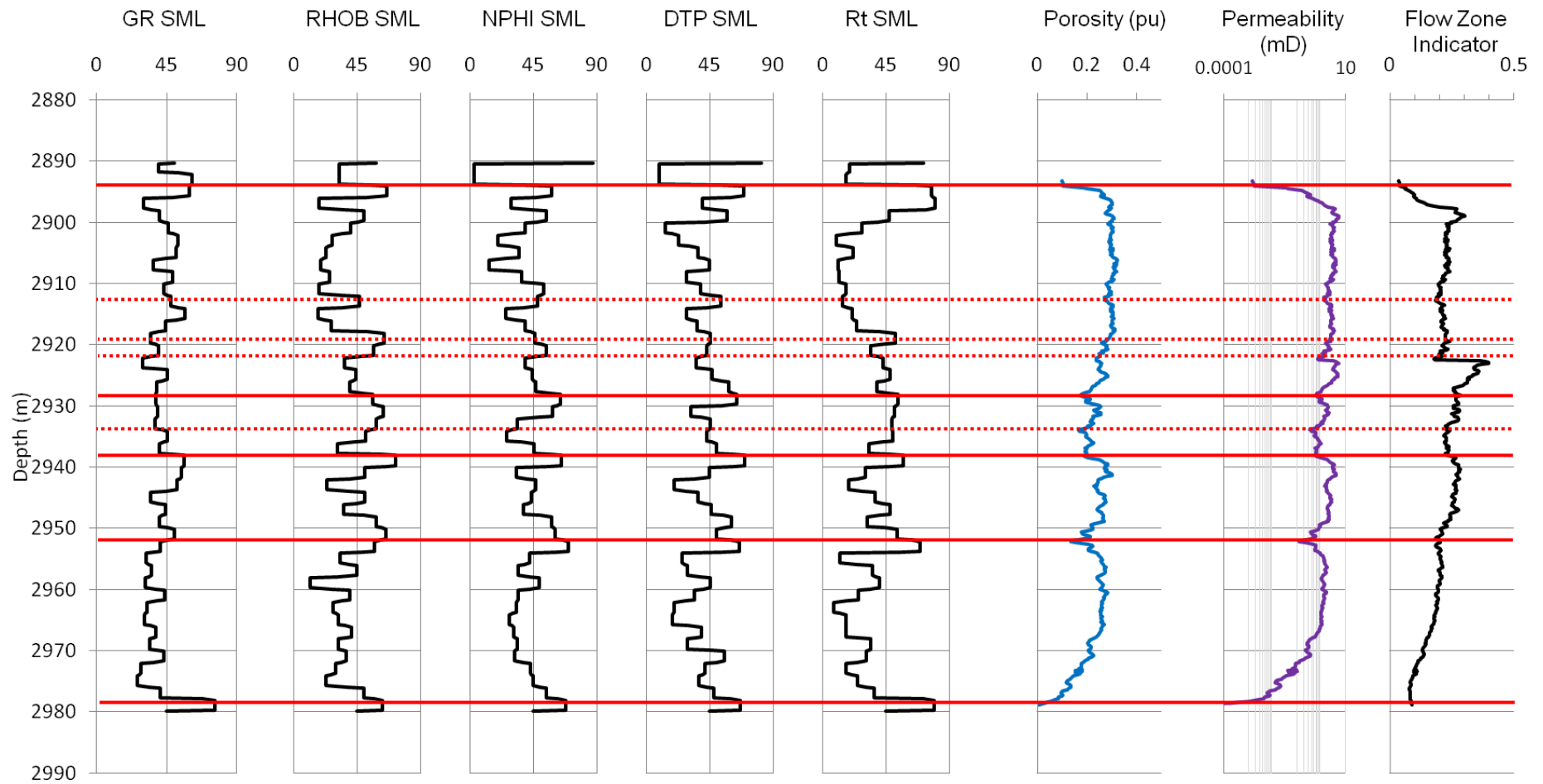


Figure 6.19. Comparing the SML Angle defined heterogeneity zones to porosity, permeability and flow zone indicator for the Abiod chalk of well A. Heterogeneity zones from the 2m Lorenz coefficient H.Logs: gamma ray (GR), bulk density (RHOB), neutron porosity (NPHI), P-wave transit time (DTP), and deep resistivity (Rt). Horizontal lines pick out reservoir zones based on lows in porosity and permeability corresponding to heterogeneity zone boundaries: solid red – major boundaries (operator), dotted red – minor boundaries.

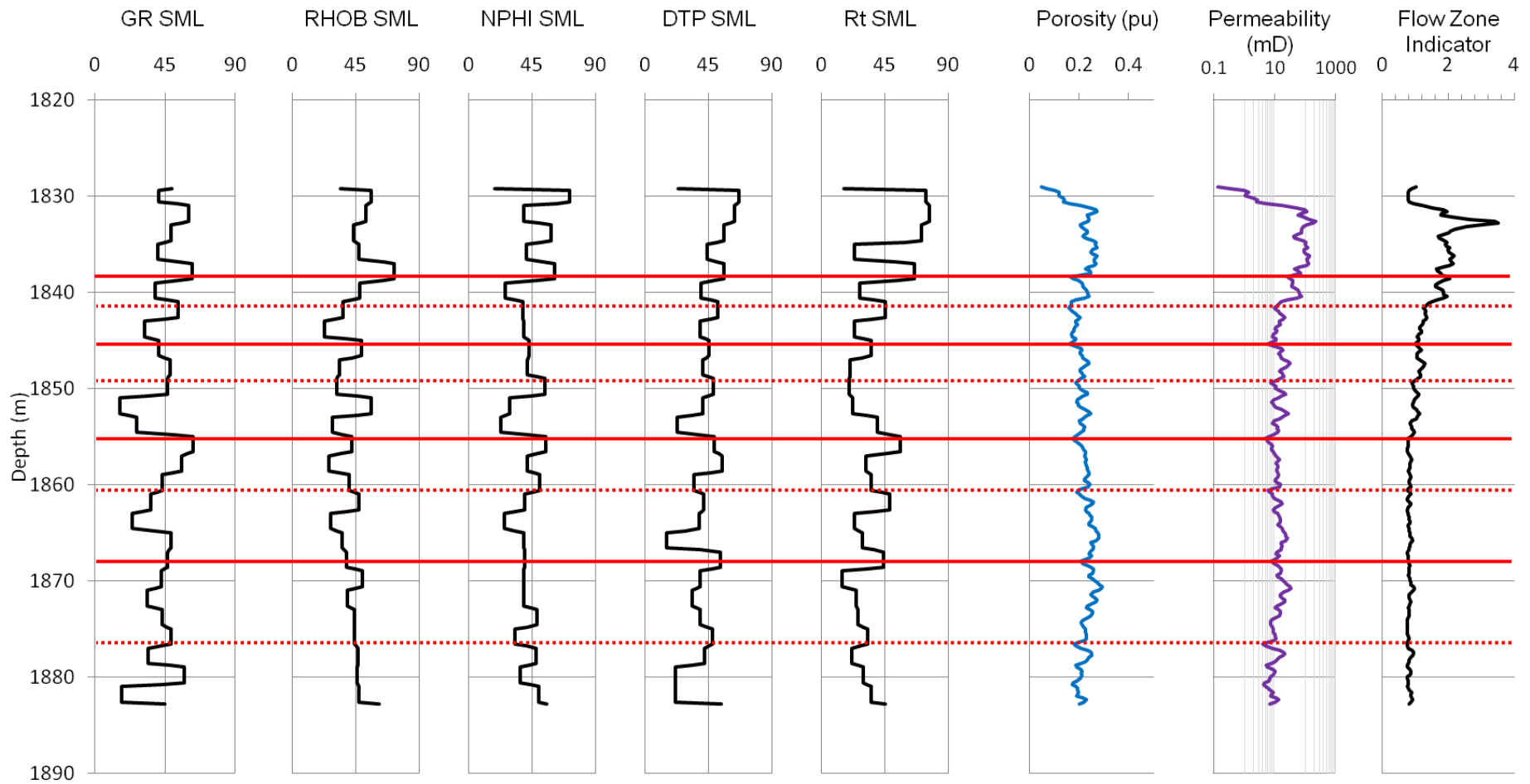


Figure 6.20. Comparing the SML Angle defined heterogeneity zones to porosity, permeability and flow zone indicator for Formation-B of well P. Heterogeneity zones from the 2m Lorenz coefficient HLogs: gamma ray (GR), bulk density (RHOB), neutron porosity (NPHI), P-wave transit time (DTP), and deep resistivity (Rt). Horizontal lines pick out reservoir zones based on lows in porosity and permeability corresponding to heterogeneity zone boundaries: solid red – major boundaries (operator), dotted red – minor boundaries.

To investigate the link between heterogeneity and fluid flow zones in a more heterogeneous example, the techniques are applied to Formation-B of wells P and M (figures 6.20 and 6.21). As with the Abiod, sudden decreases in porosity and permeability (troughs) show a correlation to increases in the SML Angle. However, these SML angles are in general around 40-50°, showing as high values relative to neighbouring data. Again the operator defined zones can be observed (at 1830m, 1838m, 1846m and 1867m for well P; and 2155m, 2166m, 2179m and 2196m for well M), with each formation comprising two subzones. The SML values suggest the well P 1846m and M 2179m boundaries are weak, being poorly shown in all the H.Log data. The heterogeneity zone boundaries suggest that these boundaries should be shifted down to 1855m and 2192m, respectively. If moved then these boundaries, between zones two and three, correspond to a stronger decrease in permeability and porosity. As mentioned above, SML peaks are lower in both Formation-Bs, and again P-wave transit time and neutron porosity H.Logs show best correlation, along with the deep resistivity H.Log. No single H.Log can be used to establish all zone boundaries corresponding to the flow zones; the suite of five logs together are required to justify heterogeneity zone boundaries. Formation-B plots (figures 6.20 and 6.21) suggest that simply using increases in the SML Angle above 45° to identify boundaries provides limited correlation, however it is noted that high points or peaks show a stronger potential here and indicate a modification to the basic technique.

The more heterogeneous reservoir in this study, Formation-A of Well P, also shows good correlation between heterogeneity zone boundaries and fluid flow zones. With the exception of bulk density data, flow zone boundaries can correspond to significant increases in the SML Angle above 45°, and/or highest value peaks through the succession. Figure 6.22 shows the major flow zone boundaries suggested by the operator; identified by large decreases in porosity and permeability at 1774m, 1786m, 1794m and 1805m, correspond to higher values of the SML angle (55-60°). This is particularly noticeable in the neutron porosity and deep resistivity H.Log data. Again, the heterogeneity data suggest additional subzones with weaker boundaries.

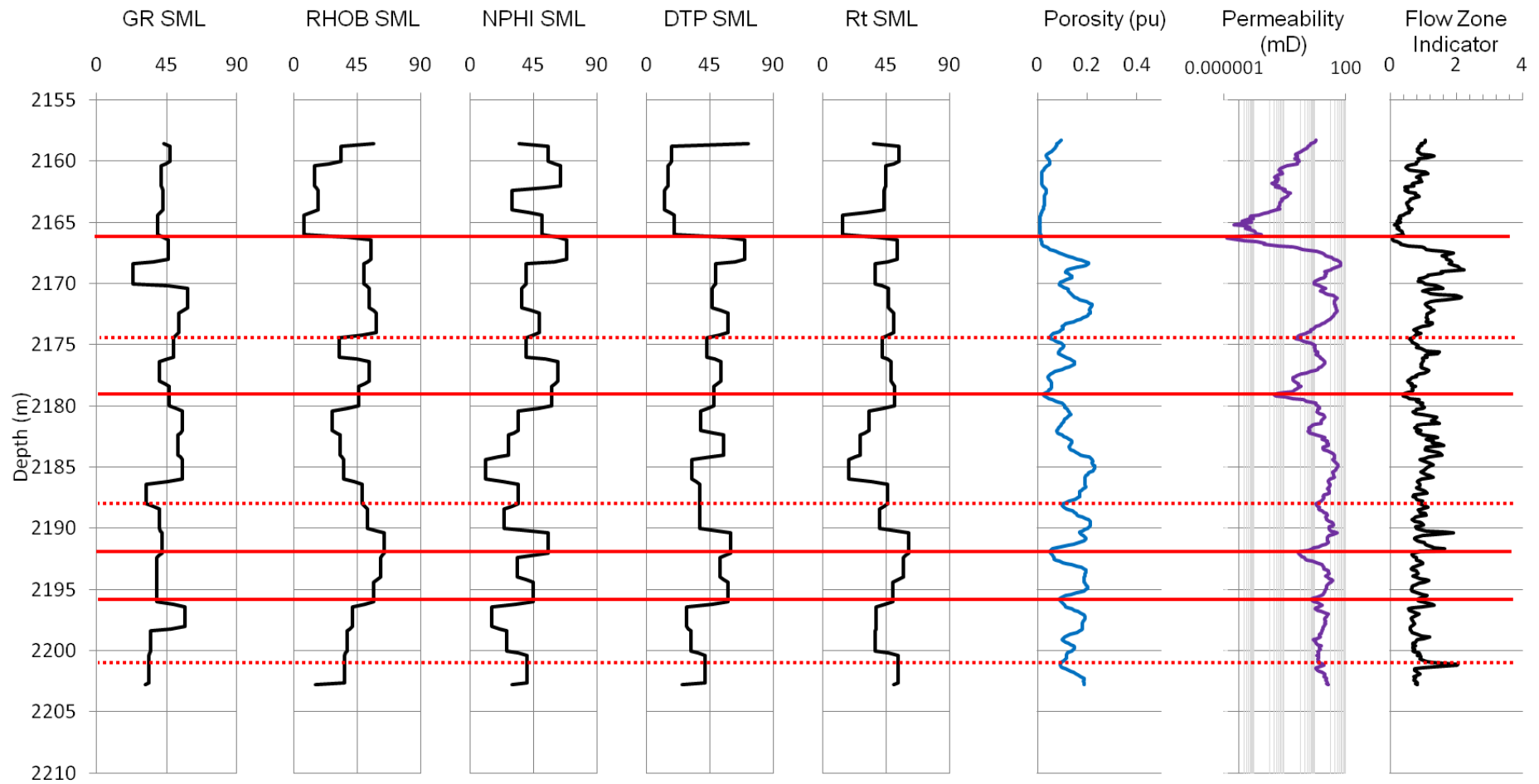


Figure 6.21. Comparing the SML Angle defined heterogeneity zones to porosity, permeability and flow zone indicator for Formation-B of well M. Heterogeneity zones from the 2m Lorenz coefficient H.Logs: gamma ray (GR), bulk density (RHOB), neutron porosity (NPHI), P-wave transit time (DTP), and deep resistivity (Rt). Horizontal lines pick out reservoir zones based on lows in porosity and permeability corresponding to heterogeneity zone boundaries: solid red – major boundaries (operator), dotted red – minor boundaries.

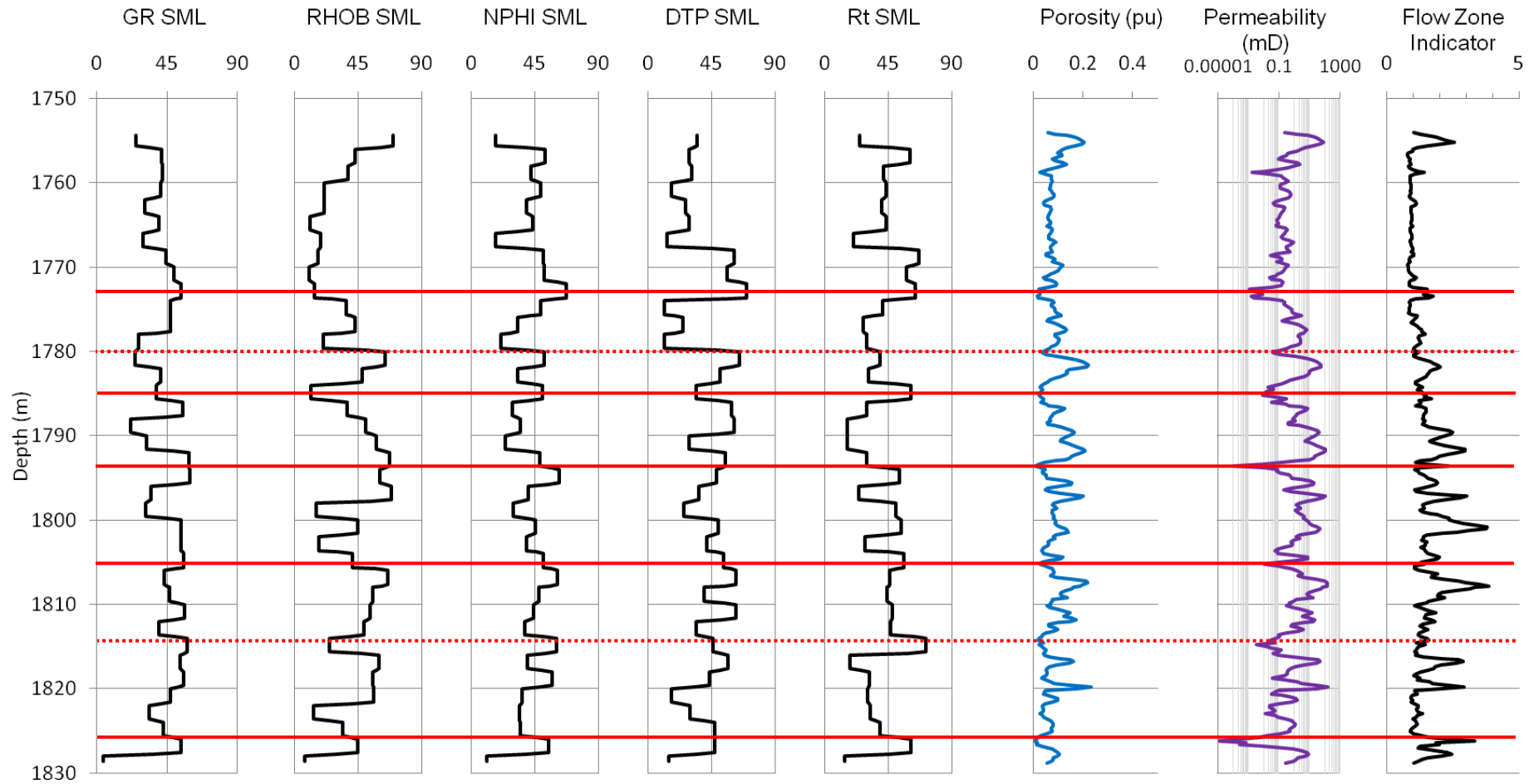


Figure 6.22. Comparing the SML Angle defined heterogeneity zones to porosity, permeability and flow zone indicator for Formation-A of well P. Heterogeneity zones from the 2m Lorenz coefficient H.Logs: gamma ray (GR), bulk density (RHOB), neutron porosity (NPHI), P-wave transit time (DTP), and deep resistivity (Rt). Horizontal lines pick out reservoir zones based on lows in porosity and permeability corresponding to heterogeneity zone boundaries: solid red – major boundaries (operator), dotted red – minor boundaries.

The previous discussion illustrates that the majority of poro-perm defined boundaries, and subsequent fluid flow zones, do coincide with heterogeneity boundaries. However supplementary work and application to additional reservoir datasets are needed to further constrain these relationships and the potential for using heterogeneity data to predict fluid flow zonations. Further work may also reveal suitable significance tests, and increase potential for statistical comparisons.

Significant mudstone beds and mud-rich carbonate occur throughout Formation-A (chapter 3). These mud-dominated horizons are generally considered to be of low porosity and permeability which can act as stratigraphic flow barriers, dividing reservoirs into compartments or flow zones / hydraulic units (Doveton 1994; Rider 2002; Serra & Serra 2003). Figure 6.23 illustrates that horizons of high log-derived shale volume can be related to the heterogeneity zone boundaries, when defined from peaks in the SML Angle (neutron porosity and deep resistivity H.Log zones show strongest correlation).

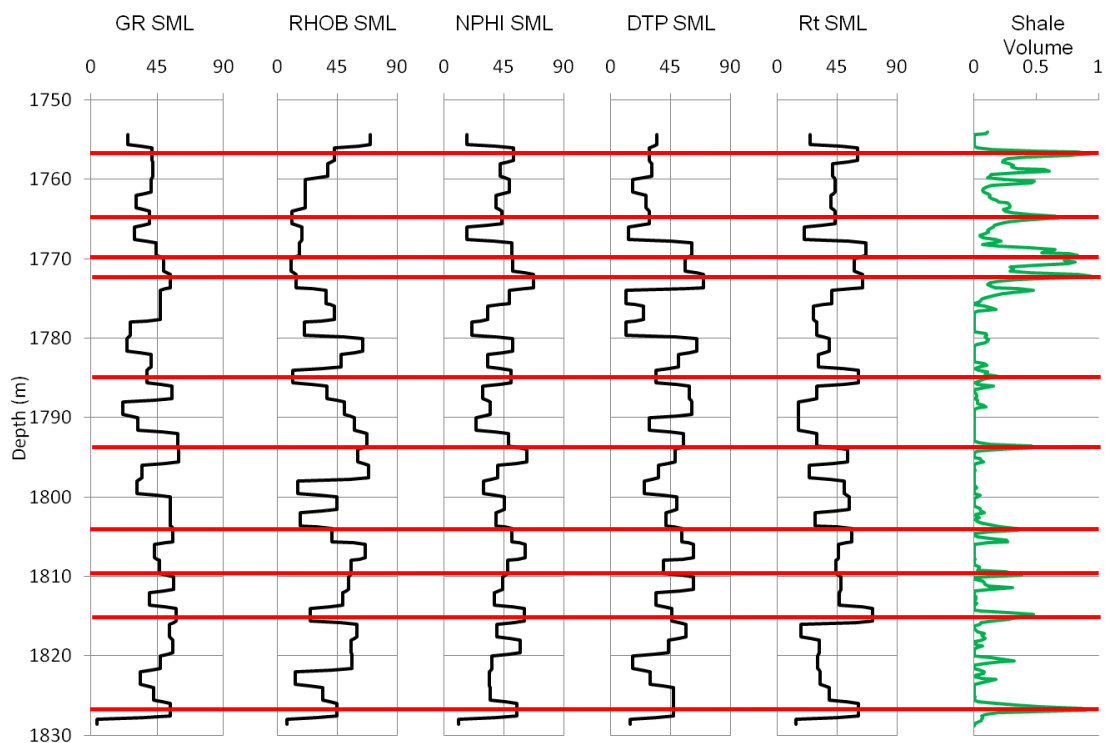


Figure 6.23. Comparing the SML Angle defined heterogeneity zones to shale volume for Formation-A of well P. Heterogeneity zones from the 2m Lorenz coefficient H.Logs: gamma ray (GR), bulk density (RHOB), neutron porosity (NPHI), P-wave transit time (DTP), and deep resistivity (Rt). Horizontal lines (red) pick out high shale values.

The flow zone boundaries (indicated by decreased FZI, porosity, and permeability; and confirmed against the operator’s current reservoir model) show general correlation with peak SML Angles (table 6.2). The depth values shown are for the first point of the data window used to produce the original H.Log. As such the peak applies to the subsequent 2m depth values. Table 6.2 shows a strong connection between the flow zone boundaries and the SML peaks, rather than the traditional increase in angle above 45°. An average of less the 2m difference is observed, which is deemed to be within error of the H.Log window size.

Reservoir	Flow Zone	GR SML Peak		RHOB SML Peak		NPHI SML Peak		DTP SML Peak		Rt SML Peak	
		Depth	Angle	Depth	Angle	Depth	Angle	Depth	Angle	Depth	Angle
Abiod	2890	2892	61	2894	65	2894	57	2894	69	2896	80
	2928	-	-	2930	63	2928	63	2928	64	2982	53
	2937	2938	56	2938	72	2938	64	2938	69	2988	57
	2952	2950	50	2950	65	2952	69	2952	65	2952	69
	2980	2978	76	2978	63	2978	77	2978	66	2978	79
Well P Formation -B	1829	1831	60	1829	55	1829	71	1829	66	1831	76
	1838	1837	62	1837	72	1837	60	1837	56	1837	65
	1846	1847	48	1845	48	1849	53	1849	48	1845	35
		1855	63	1855	42	1855	54	1857	54	1855	55
	1867	1865	48	1869	49	1867	39	1867	53	1867	53
1883	1879	57	1881	47	1881	49	-	-	1881	35	
Well M Formation -B	2158	2159	46	2159	33	2160	63	2158	17	2158	54
	2166	2166	45	2166	54	2166	68	2166	69	2166	52
	2179	2180	54	2176	53	2176	61	2176	52	2178	50
		2190	41	-	-	2190	55	2190	59	-	-
	2196	2196	56	2190	64	2194	44	2194	57	2190	60
Well P Formation -A	1754	1756	41	1754	69	1756	52	1754	34	1756	60
	1774	1772	53	1776	42	1772	67	1772	70	1772	63
	1786	1786	55	-	-	1784	50	1788	61	1784	60
	1794	1794	59	1796	68	1794	62	1792	54	1794	52
	1804	1804	55	1806	66	1806	61	1806	62	1804	55
	1826	1826	54	1826	44	1826	54	1826	47	1826	60
Well M Formation -A	2118	2118	32	2118	49	2118	36	2118	38	2120	43
	2129	2128	51	2128	64	2128	50	2128	48	2130	51
	2145	2142	65	2146	35	2144	59	2142	47	2142	53
	2158	2152	50	2152	70	2152	60	2150	78	2150	60

Table 6.2. Comparing the depth of peak H.Log SML Angles and their intensity (Angle units - degrees) to the flow zone boundaries identified from porosity-permeability lows. No value (-) indicates no comparable peak available. SML depth refers to the top of the data window, and includes the following 2m of depth values. H.Logs: gamma ray (GR), bulk density (RHOB), neutron porosity (NPHI), P-wave transit time (DTP) and deep resistivity (Rt).

The SML Angle is suggested to be an indicator of the strength of position of the heterogeneity boundary placement. For the most part values are in excess of 50° , justifying the placement of a heterogeneity boundary (table 6.2). Lower SML values (less than 45°) can be correlated to weaker porosity and permeability troughs (figures 6.18-6.21).

The P-wave transit time H.Log data shows the highest correlation of high angle boundaries ($>69^\circ$) to flow zone boundaries, closely followed by neutron porosity and deep resistivity H.Log boundaries (showing similar placement to fluid flow zones, with average angle intensities of 57°). The gamma ray heterogeneity boundaries show weakest comparison to fluid flow zones. Unlike the other properties the gamma ray measurement has little, if any, direct connection to pore volume or connectivity in a reservoir rock. These findings suggest that the SML Angle plots (and heterogeneity zone boundaries) can be used to identify flow zones through a reservoir unit. It would be suggested that calibration to porosity-permeability is required in initial well studies, but there is potential to use the H.Logs and SML Angle plots to identify these flow zones in subsequent wells.

It has been shown that heterogeneity zones can be identified from the H.Log data. These zone boundaries show correlation to decreased porosity and permeability (suggested in section 6.2 by trends toward lower poro-perm values at higher heterogeneities), and increased mud content. In the absence of continuous core and geological descriptions, the electrical borehole image (FMS) is used to link heterogeneity zonations to underlying geology in Formation-A of well P (Figure 6.24); zone boundaries are coincident with depths at which mudstone beds, low resistivity tight-carbonate and the nodular limestones are interpreted.

It is therefore suggested that these heterogeneity zonations can be used in reservoir characterisation as a means of identifying potential reservoir compartments or fluid flow zones. Strong correlation is shown between significant heterogeneity boundaries (with SML Angles greater than 50°) and major flow zone boundaries identified using the Amaefule's (1993) flow zone indicator curve.

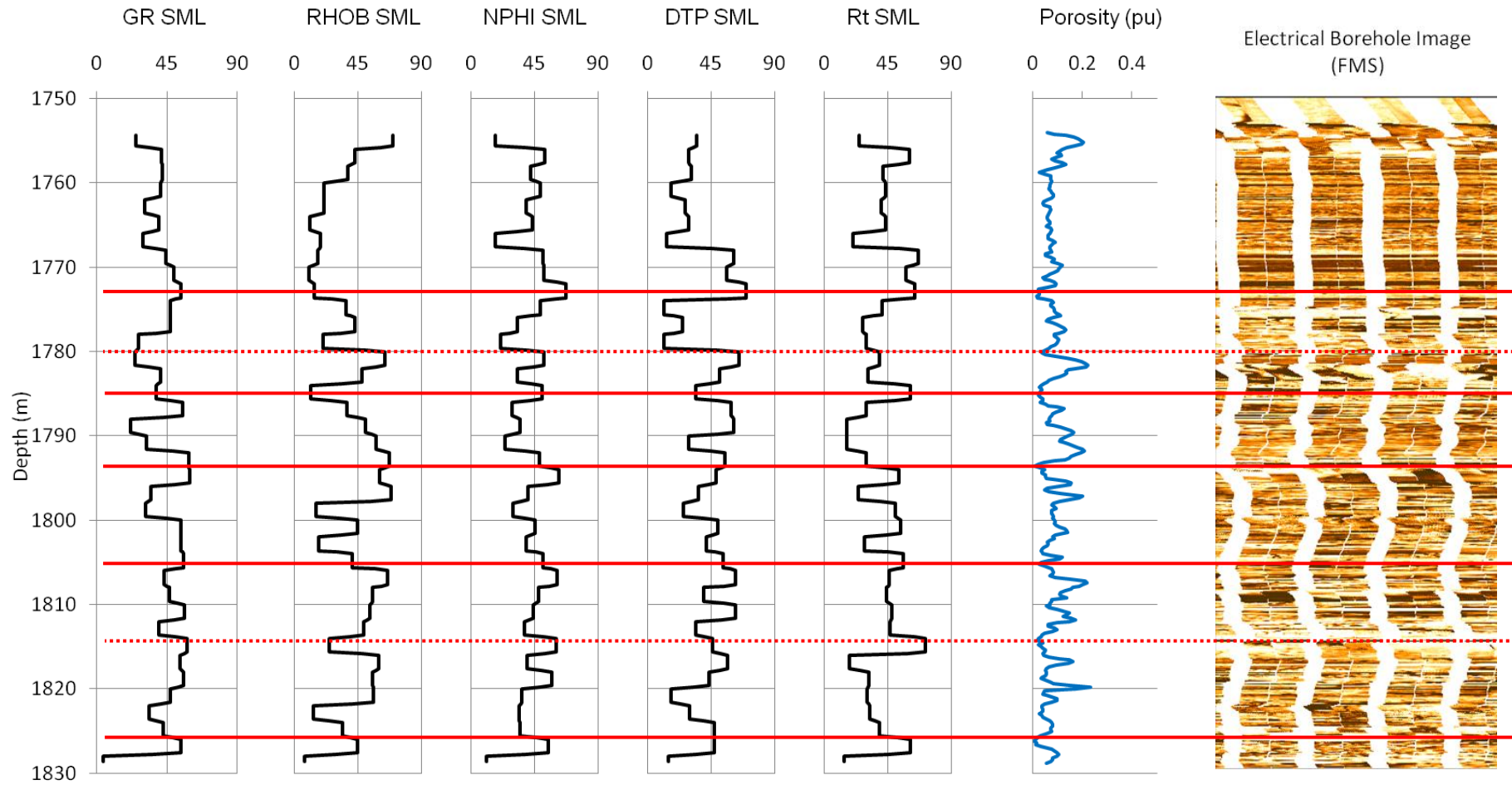


Figure 6.24. Comparing the SML Angle defined heterogeneity zones to the electrical borehole image (FMS) for Formation-A of well P. Heterogeneity zones from the 2m Lorenz coefficient H.Logs: gamma ray (GR), bulk density (RHOB), neutron porosity (NPHI), P-wave transit time (DTP), and deep resistivity (Rt). Horizontal lines pick out reservoir zones based in table 6.2: solid red – major boundaries (operator), dotted red – minor boundaries.

Even with the most complex of statistical techniques, the placement of boundaries within numerical data series often comes down to an analyst's interpretation of the data. This research suggests that H.Logs and their heterogeneity zonations may be used alongside pre-existing flow zone indicators to further justify boundary assignation producing a more robust model. Ideally the fluid flow zones suggested here would be confirmed using production and pressure test (MDT) data to confirm flow potentials downhole, however these data were not available for the wells within the time limits of this study.

6.4. Reservoir Quality and Heterogeneity

The previous sections of this chapter have shown a connection between the heterogeneity logs and porosity-permeability features of the carbonate reservoirs studied. In this section the heterogeneity measures are applied to the reservoir zones to investigate the connection between reservoir quality and heterogeneity. The Lorenz and Dual Lorenz coefficients are used (defined in chapter 4).

Reservoir quality refers to the potential of a reservoir rock to contain significant volume of hydrocarbon, which can be retrieved during production (Lucia 1999; Moore 2001a; Tiab and Donaldson 1996). As discussed in Chapter 2; the potential to store hydrocarbon is controlled by the porosity of the rock, while its accessibility is controlled by having interconnected pore space (permeability) – both of these properties being strongly related to sedimentological and diagenetic facies types, distributions, and geometries (Kupecz *et al.* 1997; Major and Holtz 1997; Moore 2001a). Kupecz *et al.* (1997) suggest that porosity and permeability are of particular importance for estimating reservoir quality during the exploration stage of reservoir management in particular, although it should be constantly re-addressed during the complete reservoir life cycle.

To gain an estimate of reservoir quality the Amaefule (1993) technique is applied to the log-derived porosity and permeability data to produce a normalised porosity (PHI_z), reservoir quality index (RQI), and flow zone indicator (equation B.18 - B.20, Appendix B). Plots of

normalised porosity against RQI, and the flow zone indicator (FZI), can be used to ascertain reservoir quality (Figure 6.25).

These plots (figure 6.25 and 6.26) provide a visual clue as to the relationship between reservoir quality and heterogeneity, the average flow zone indicator for each reservoir zone has been found to be of good comparison to quality, allowing tabulated comparison of ranked heterogeneity and quality (table 6.3).

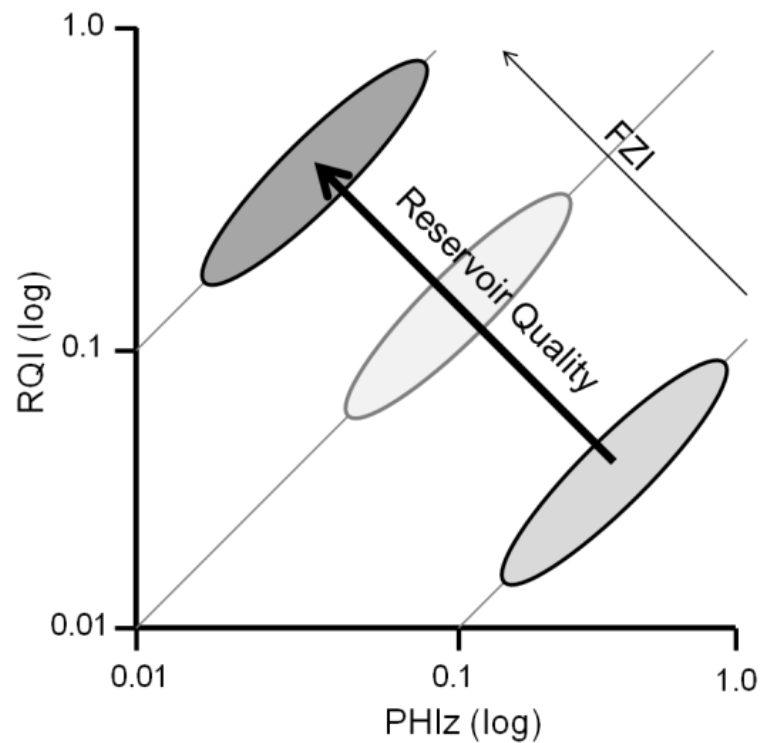


Figure 6.25. Reservoir quality (RQI) index plotted against normalised porosity (PHiz) on log-log plot. Reservoir quality increases with higher RQI at lower porosities, as does flow zone indicator (FZI) value.

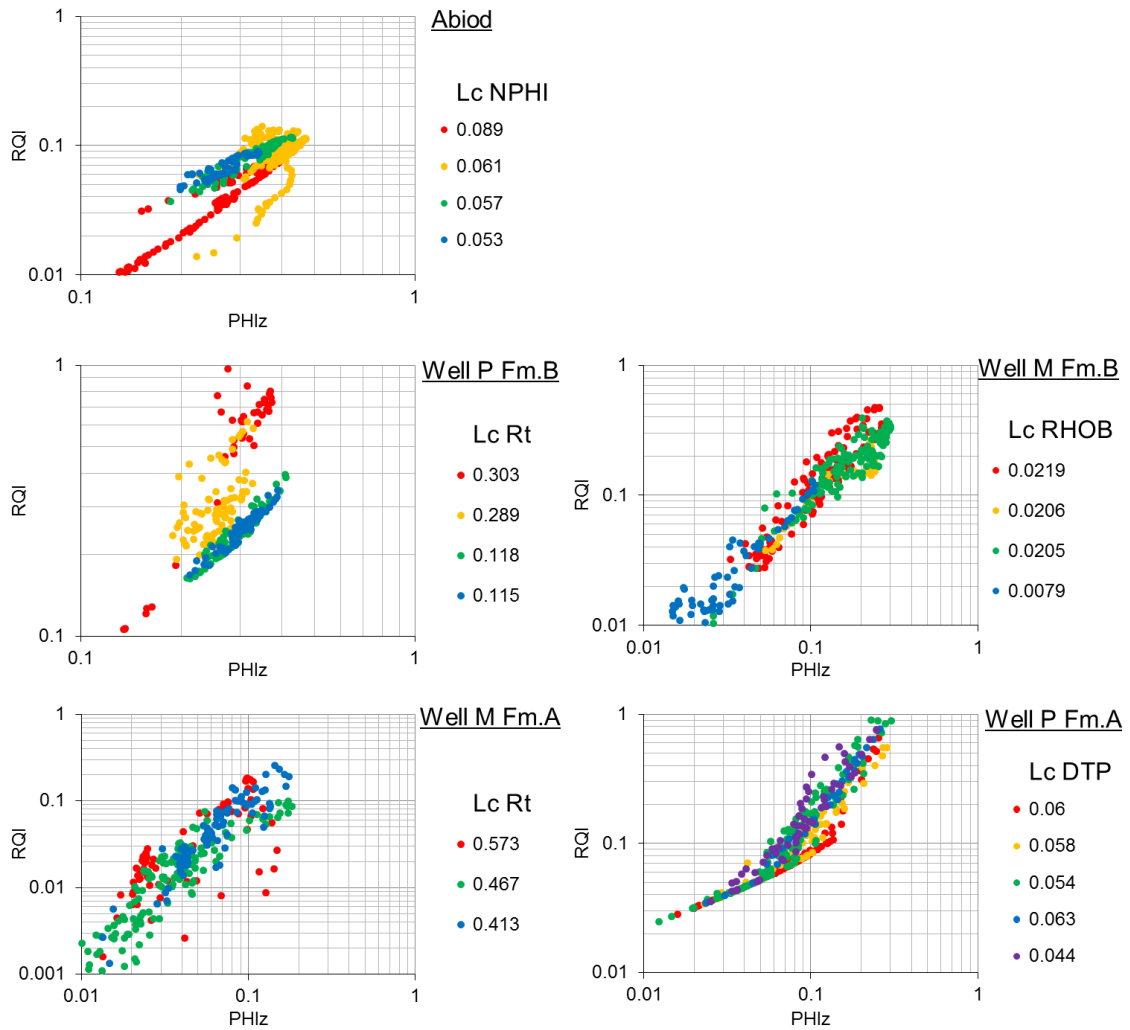


Figure 6.26. Normalised porosity (PHIz) – reservoir quality index (RQI) plots illustrating relationship between numerical heterogeneity (Lorenz coefficient; Lc) and reservoir quality (see Figure 6.24). Reservoirs: Abiod chalk, and Formation-A and –B of well P and well M. Heterogeneities: neutron porosity (NPHI), deep resistivity (Rt), bulk density (RHOB) and P-wave transit time (DTP). See Appendix C.2 for all plots.

The example for the Abiod chalk shown in Figure 6.26 is typical (table 6.3), where increased reservoir quality occurs with decreased numerical heterogeneity. Zone 4 is the exception to this rule, generally having a high heterogeneity and being spread across the plot. This zone is the thickest unit, which heterogeneity measures suggest to be composed of 3 additional zones (section 6.3.3).

Reservoir	Lorenz										Dual Lorenz						FZI	
	Lc GR	RK	Lc RHOB	RK	Lc NPHI	RK	Lc DTP	RK	Lc LLD	RK	DLc D-N	RK	DLc D-S	RK	DLc S-N	RK	Mean	RK
Abiod	0.219	4	0.016	3	0.061	3	0.03	3	0.155	3	0.0449	2	0.013	2	0.033	2	0.2210	2
Abiod	0.078	1	0.009	1	0.053	1	0.02	1	0.114	2	0.0446	1	0.011	1	0.034	3	0.2482	4
Abiod	0.15	2	0.011	2	0.057	2	0.027	2	0.084	1	0.0454	3	0.016	3	0.029	1	0.2477	3
Abiod	0.157	3	0.021	4	0.089	4	0.154	4	0.229	4	0.067	4	0.131	4	0.068	4	0.1546	1
Well P B	0.041	1	0.028	4	0.119	4	0.0632	4	0.303	4	0.0893	4	0.035	4	0.055	4	1.7918	4
Well P B	0.049	2	0.011	2	0.062	1	0.0269	1	0.289	3	0.051	1	0.016	1	0.035	2	1.2190	3
Well P B	0.066	3	0.01	1	0.065	2	0.0273	2	0.115	1	0.0548	3	0.017	2	0.038	3	0.8138	2
Well P B	0.077	4	0.012	3	0.067	3	0.0338	3	0.118	2	0.0546	2	0.022	3	0.033	1	0.8108	1
Well M B	0.087	3	0.0079	1	0.729	4	0.023	1	0.477	1	0.737	4	0.016	1	0.746	4	0.6738	1
Well M B	0.096	4	0.0219	4	0.335	3	0.072	4	0.643	4	0.313	3	0.05	4	0.262	3	1.0697	4
Well M B	0.082	2	0.0205	2	0.197	1	0.058	2	0.588	3	0.176	1	0.037	2	0.138	1	1.0096	3
Well M B	0.039	1	0.0206	3	0.201	2	0.06	3	0.5	2	0.179	2	0.039	3	0.141	2	0.8119	2
Well P A	0.148	2	0.015	1	0.303	4	0.06	4	0.355	5	0.291	4	0.045	5	0.248	4	1.0342	1
Well P A	0.164	3	0.019	2	0.269	2	0.058	3	0.318	3	0.252	2	0.04	4	0.212	2	1.2373	2
Well P A	0.142	1	0.026	4	0.158	1	0.063	5	0.108	1	0.132	1	0.037	3	0.095	1	1.7706	4
Well P A	0.203	4	0.022	3	0.272	3	0.044	1	0.296	2	0.252	2	0.022	1	0.228	3	1.7808	5
Well P A	0.229	5	0.028	5	0.33	5	0.054	2	0.339	4	0.307	5	0.027	2	0.278	5	1.5825	3
Well M A	0.149	1	0.012	1	0.384	1	0.029	2	0.413	1	0.373	1	0.017	2	0.357	1	0.9035	3
Well M A	0.234	3	0.013	2	0.805	3	0.028	1	0.467	2	0.819	3	0.015	1	0.818	3	0.4813	2
Well M A	0.189	2	0.014	3	0.597	2	0.082	3	0.573	3	0.585	2	0.068	3	0.517	2	0.3454	1

Table 6.3. The numerical heterogeneity values (Lorenz coefficient; Lc) returned for the reservoir sub-zones studied: Abiod of well A, and Formation-A and -B of wells P and M. The mean flow zone indicator (FZI) values for each sub-zone are shown as reservoir quality indicators. Data is ranked (RK) from low (1) to high (3-5) in each zone. Heterogeneity values coloured green if show the same rank sequence to FZI, and red if sequence is reversed (for trends observed in crossplots). Heterogeneities: gamma ray (GR), bulk density (RHOB), neutron porosity (NPHI), P-wave transit time (DTP), and deep resistivity (Rt). See Appendix C.2 for accompanying plots.

The finding of increased quality with decreased heterogeneity is comparable to that described in homogeneous clastic reservoirs, such as the Rotliegendes sandstones, where increased sorting and structureless sands are found to have extremely high reservoir quality and production levels (Glennie *et al.* 1978; Rogers & Head 1961).

The homogeneous nature of the Abiod chalk seen in thin section and core studies is clearly also reflected in the behaviour of its petrophysical properties. This relationship is best seen in the density, neutron porosity, and P-wave transit time heterogeneity data, and poorest in the gamma ray and deep resistivity. Highest heterogeneities are coincident with lowest average flow zone indicator values, these heterogeneities of 0.02 – 0.2 are lower than typical reservoir heterogeneity values (Lake & Jensen 1991).

Mixed relationships are observed in Formation-B. In all cases, except the gamma ray and neutron porosity heterogeneity, maximum heterogeneity is seen with highest reservoir quality estimate (table 6.3). These high heterogeneity values, in zone 4, are found to be an order of magnitude larger than in the other zones. Neutron porosity and P-wave transit time heterogeneity increase with decreasing reservoir quality for zones 1-3; giving similar relationships to the Abiod chalk, especially in the case of gamma ray heterogeneity. These relationships are not as clearly observed as in the Abiod, suggesting that increased geological heterogeneity in Formation-B rock and physical properties is having an effect. In fact, Formation-B deep resistivity and density heterogeneity shows increased quality with increase heterogeneity. The Dual Lorenz coefficient heterogeneities do not support either relationship, except that highest heterogeneity is coincident with highest reservoir quality. The Mukta Formation-B data is less well separated into zones, making observations of heterogeneity and quality relationships weaker (Figure 6.26), again highest reservoir quality estimates are coincident with higher heterogeneities but other features are more obscured. Bulk density, P-wave transit time, and deep resistivity suggest that lowest heterogeneity values occur with low reservoir quality indicator and normalised porosity (more notably seen in cross-plots). This feature is reversed for gamma ray and neutron porosity heterogeneity data.

Formation-A has been repeatedly shown to be the more heterogeneous reservoir unit studied, with mixed carbonate lithologies, mud-rich horizons and related highly variable physical properties. Reflecting this nature, heterogeneity and reservoir quality relationships are highly varied. Reservoir quality is seen to increase with heterogeneity for the bulk density and P-wave transit time data in well P. The increasing heterogeneity with decreasing quality trend can be observed in the neutron porosity, P-wave transit time, and Dual Lorenz coefficient data. In general trends are weak which is expected to relate to the heterogeneous nature of this reservoir unit, with high and low values being of most use.

In this carbonate reservoir porosity and permeability are suggested to be controlled by a complex, multi-phase diagenetic history (Khanna *et al.* 2007; Wright 2007). Geological features (or heterogeneities), which are expected to strongly influence reservoir quality, have been identified in the limited core studies of Panna and Mukta wells (Khanna *et al.* 2007; Wright 2007); including mud-rich horizons, complex pore type intermingling, fractures and stylolites. Porosity is suggested to have been enhanced by diagenesis, with related secondary mineralisation of dolomite, pyrite and dickite. Clearly in these reservoirs we would expect increased heterogeneities to be related to increased reservoir quality. The bulk density, P-wave transit time, and deep resistivity measurements do show trends toward higher reservoir quality and numerical heterogeneity overall (Figure 6.26 and table 6.3). This feature is particularly well demonstrated in Formation-B, with strong coincidence between highest and lowest values. All three of these measures would be expected to respond to the porosity, mud content and secondary mineralisation features, as is seen here.

In the Panna and Mukta reservoir formations bulk density shows the strongest trend between increased heterogeneity and rock quality, expected to relate to increased porosity-permeability with changes in the bulk rock mineralogy (including the introduction of pyrite minerals). This is closely followed by the P-wave transit time, reflecting textural and facies-based rock characteristics.

An observation across all reservoirs studied is that increased heterogeneity in neutron porosity measurements is coincident with decreasing reservoir quality. As discussed previously, assuming that the neutron porosity measurement responds primarily to volumes of hydrogen ions (H^+), and that these ions are predominantly only found in fluids in the pore space, then this relationship suggests that increased complexity and pore volume is linked to poorer reservoir quality. This finding is logical when looking at siliciclastic systems, and homogeneous chalks, (as discussed above for well-sorted sandstone examples); however this trend opposes the trends expected for the Panna and Mukta reservoirs (seen in the other well log measurements). Perhaps this trend in neutron porosity is suggesting that the bulk pore space needs to behave homogeneously to gain the best reservoir quality; i.e. the neutron porosity measurement is not responding to the localised or intrinsic geological heterogeneities, but is in fact looking at the porosity features as a whole. While bulk density heterogeneity is responding to these diagenetically enhanced pore types, volumes and associated minerals. Gamma ray measurements also show increased heterogeneity with quality in Formation-A. In the case of Panna and Mukta the gamma ray is thought to be resulting more from diagenetic enrichment of uranium than to mud content, or shale volume (Khanna *et al.* 2007). This may be considered to support this interpretation of bulk density heterogeneity. Applying the heterogeneity measures to spectral gamma ray measurements may help confirm the relationship between uranium content and quality. It is noted that these relationships between numerically quantified heterogeneity and reservoir have not been documented in other published works reviewed during this study.

6.4.1. Summary

There are really two dominant end-members with regard to the relationship between heterogeneity and reservoir quality; a homogeneous well-sorted sample, and a heterogeneous mix of grain and pore types, and sizes. If we take the example of a fruit bowl as an example (Figure 6.27); if only oranges (spheres) fill the bowl then it might be expected that perfect packing occurs, creating a maximum volume of pore space which is all interconnected. Fluid

could therefore be easily moved through the space, giving rise to high quality. Here increased homogeneity gives the highest reservoir quality, and, from this study, is considered to be the case in the Abiod chalk.

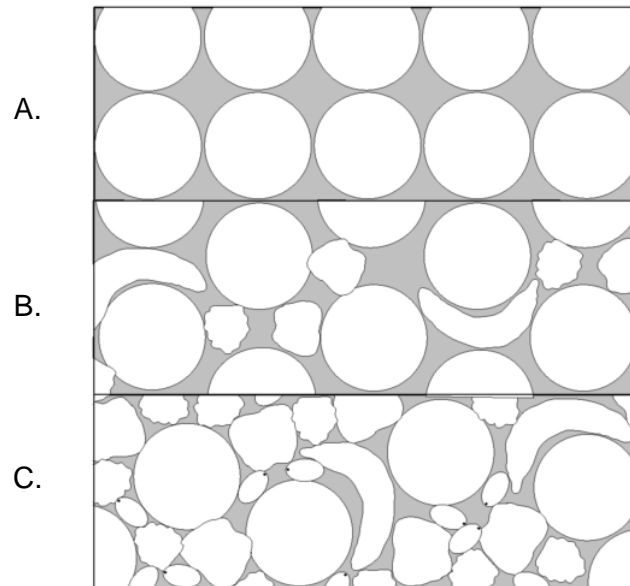


Figure 6.27. Schematic illustration of samples illustrating heterogeneity end-members, and an intermediate example to demonstrate how heterogeneity can influence reservoir quality. (A) homogeneous, (B) mixed, (C) heterogeneous.

If different fruits are added to the bowl, and the contents mixed together, then a heterogeneous mix is created (Figure 6.27c). On first appearance the volume of pore space would decrease due to differential packing of the different sized and shaped grains, and this would also decrease the connectivity. Here increased heterogeneity results in decreased reservoir quality. However, if we selectively remove all of the bananas from the bowl (without disturbing anything else) then the pore space and connectivity will be enhanced. Next the apples are selectively removed, again increasing the volume of space and its connectivity. Here, the original heterogeneity in fruit (or grains) has given rise to increased heterogeneity and volume of space (porosity). Hence fluids could be more readily moved through the sample. The Panna and Mukta reservoirs are considered examples where multi-phase diagenesis has selectively dissolved grains and corroded stylolites/fractures to enhance porosity (Wright 2007).

In the case of the wireline heterogeneity data two trends are seen for Panna and Mukta. Firstly the neutron porosity shows increased heterogeneity with decreased reservoir quality. This suggests that better quality results when the bulk porosity acts as a more homogeneous volume, ignoring individual pore sizes and shapes. Bulk density and P-wave transit time indicate increased heterogeneity with quality. Remembering that the density measurement responds to mineralogy (including secondary mineralisation of pyrite and dolomite) then it seems logical that increased porosity-permeability is associated with more heterogeneous bulk rock signatures. P-waves travel through the grains and so would be susceptible to heterogeneities in terms of the facies/texture of the diagenetically evolved carbonate material; although bulk porosity will affect travel times, the travel paths will be more complex.

6.5. Can Optimal Sampling strategies be identified using the Heterogeneity Logs?

The heterogeneity logs clearly provide an indicator of more heterogeneous horizons within a reservoir. It has also been shown that the heterogeneity of wireline data can be related to porosity and permeability. It therefore seems logical to investigate whether this numerical heterogeneity data can be used to give an indication of sampling requirements to optimally capture variations in reservoir properties, to aid reservoir characterisation and modelling.

Core samples are taken for calibration of wireline-derived physical property data, geological descriptions and additional analyses, such as investigating rock mechanics and reservoir fluids (Rider 2002; Tiab & Donaldson 1996). Typically a core plug sample is taken every 30cm (Corbett & Jensen 1992a), but often sampling is at a lower resolution than this because of financial and time constraints. A number of studies have investigated the potential for statistically justified sampling to obtain optimal sample coverage throughout siliciclastic reservoir units; primarily to further constrain the harmonic average used in modelling permeability (Corbett & Jensen 1992a, b; Jensen *et al.* 1997; Zheng *et al.* 2000). Corbett and Jensen's (1992a) study in particular shows that equation 6.2 (Hurst & Rosvoll 1991) can be used to

identify optimal sampling of permeability in siliciclastic reservoirs to allow estimation of the harmonic mean within 95% confidence limits.

$$N_o = 100 \times Cv^2 \quad (\text{Equation 6.2})$$

Where: N_o – number of samples, Cv – coefficient of variation (heterogeneity measure)

Zone	Porosity samples (N_o)	Permeability samples (N_o)	Zone thickness (m)	Porosity sample interval	Permeability sample interval
5	22	1472	19.8	0.91m	0.01m
4	29	496	11.8	0.41m	0.02m
3	23	244	7.8	0.34m	0.03m
2	20	363	10.8	0.53m	0.03m
1	37	763	23.8	0.65m	0.03m

Table 6.4. Optimal number of samples and sample spacing for the porosity and permeability variations derived from wireline data for Formation-A of well P, using equation 6.2. Sample spacing is calculated by dividing the thickness of the zone by the number of samples (N_o).

Table 6.4 shows the results of applying this technique to the wireline-derived permeability and porosity data from Formation-A of well P. As expected from the scale difference in the measurements, permeability data requires significantly more samples to capture the intrinsic variability than porosity. This number of samples (100-1000's) is comparable to that required for siliciclastic units classed as highly heterogeneous fluvial sediments by Corbett and Jensen (1992). Taking core plug samples at this frequency would not be effective; and the use of probe-permeability measuring devices would be more appropriate at the centimetre scales required. Interestingly, the number of porosity samples and sampling frequency (averaging a sample per 50cm) is more in keeping with traditional methods.

Applying the same technique (equation 6.2) to the wireline-derived heterogeneity data, for individual zones, shows poor correlation between porosity/permeability sample numbers and that indicated by the H.Logs (table 6.5). The coefficient of variation shows no similarities in identifying the number of samples. The same is true when the Lorenz coefficient (L_c) is substituted into the equation, except for gamma ray, although similar patterns in the relative number of samples are observed across the zones. Gamma ray L_c heterogeneity shows

correlation to the number of porosity samples in zones 5-3, but overestimates in zones 2 and 1. Zones 1 and 2 contain spikes in the gamma ray measurement against a low background measurement reflecting higher heterogeneity contrasts. This suggests that, with the exception of the gamma ray data, the optimal number of samples technique cannot be applied to raw wireline heterogeneity data to provide an early indication of sampling requirements. Scale of heterogeneity captured by the measurement scale of the original wireline (chapter 5) is expected to be the main problem in establishing a correlation between the number of samples suggested by the different data types. Similar results are found for Formation-B.

Zone	Porosity samples (N_o)	Permeability samples (N_o).	Coefficient of Variation				
			Gamma Ray (N_o)	Bulk Density (N_o)	Neutron Porosity (N_o)	P-wave transit time (N_o)	Deep Resistivity (N_o)
5	22	1472	15	2	47	3	213
4	29	496	36	1	132	6	123
3	23	244	102	3	91	13	47
2	20	363	103	2	162	4	153
1	37	763	37	3	78	2	72
Zone	Porosity samples (N_o)	Permeability samples (N_o)	Lorenz Coefficient				
			Gamma Ray (N_o)	Bulk Density (N_o)	Neutron Porosity (N_o)	P-wave transit time (N_o)	Deep Resistivity (N_o)
5	22	1472	22	0.2	92	4	126
4	29	496	27	0.4	72	3	101
3	23	244	20	0.7	25	4	12
2	20	363	41	0.5	74	2	87
1	37	763	52	0.8	109	3	115

Table 6.5. Optimal number of samples (N_o) for the wireline-derived porosity and permeability data, and for the raw wireline data of Formation-A of well P using equation 6.2. The Lorenz coefficient is substituted for the coefficient of variation in equation 6.2.

To investigate further and at different scales, it was decided to try applying the optimal sample number technique to the heterogeneity log (H.Log) data; looking to determine if a conversion factor could be identified in a more detailed comparison of wireline Lc heterogeneity values and the porosity/permeability sample numbers suggested. The use of crossplot relationships and best fit regressions were investigated across the suite of heterogeneity logs with no significant outcomes. Correlations are found to be less than 0.5 with significant scatter/noise; average

coefficient of determination being ~0.1 (10%). Extrapolating the best fit line back to zero heterogeneity (homogeneous) suggested that the number of samples required for a purely homogeneous system ranges from 1 to 37 (averaging 4 samples). This is quite a departure from what might be expected for a homogeneous system requiring perhaps a minimum of one sample to classify its physical properties.

This test study shows that the optimal number of samples technique can be applied directly to carbonate permeability and porosity data. However, this technique cannot be applied to wireline heterogeneity measures to produce a logical sample requirement reflecting the porosity or permeability data. The heterogeneity logs themselves can still be used as a visual clue to increased sampling requirements in heterogeneous intervals. It would be expected that if the heterogeneity techniques were applied to a larger database of different carbonate reservoirs, geological settings, and heterogeneity levels, then a relationship and/or conversion factor will be identified and could have significant application to exploration needs.

6.6. Summary & Conclusions

6.6.1 *Heterogeneity Logs and Physical Properties.*

- In the Abiod chalk lower porosity and permeability trend toward higher heterogeneity values, which is comparable to siliciclastic aeolian examples.
- Similar trends are seen in Formation-B, with increased scatter and outliers (especially in the Panna reservoir).
- Formation-A shows decreased porosity and permeability with increased heterogeneity in neutron porosity, P-wave transit time, and deep resistivity; and increased heterogeneity with porosity/permeability for gamma ray and bulk density data.
- Decreased porosity/permeability with increased numerical heterogeneity has two potential explanations. (1) high porosity carbonate is more homogeneous, as seen in

clastics, (2) higher porosity units are thicker and so exert stronger averaging effects on the heterogeneity zones.

- Numerical heterogeneity does not add any additional clarity to pre-existing porosity-permeability cross plot-based classifications schemes, such as that proposed by Lucia (1999).

6.6.2. *Heterogeneity Zones*

- Heterogeneity log data can be zoned using the (1) D^2 Generalised Distance and (2) Stratigraphic Modified Lorenz techniques. While the D^2 technique zones areas of similar data variability, the Stratigraphic Modified Lorenz technique defines zones based on high-low heterogeneity patterns. The Stratigraphic Modified Lorenz zone boundaries are more readily correlated across the suite of heterogeneity logs. This provides a robust output of heterogeneity zones, and is the preferred technique of this study. Comparison to poro-perm defined flow zone boundaries suggests corresponding heterogeneity boundaries be placed at high SML Angles, rather than the traditional increase in value over 45° .
- The 10m and 5m heterogeneity logs are of too low resolution to produce a comparable number of zones, while the noisy nature of the 1m heterogeneity log identifies an excessive number of zone boundaries. The 2m heterogeneity logs provide the most significant boundaries.
- Heterogeneity zone boundaries can show strong correlation to flow zone boundaries, if boundaries are placed at significant increases in SML Angle above 45° or at peak values; flow zone boundaries are defined using prominent lows in porosity, permeability and the representative Flow Zone Indicator. These correlations occur within error of the data window size of the heterogeneity log.
- This study suggests that heterogeneity zones be used alongside pre-existing flow zone identification techniques (such as Amaefule's Flow Zone Indicator) to identify more

robust flow zones within a reservoir unit – based on flow potential and internal heterogeneity.

6.6.3. *Heterogeneity and Reservoir Quality*

- Carbonate reservoir quality can be estimated using Amaefule *et al.*'s (1993) rock quality index, normalised porosity and flow zone indicators, derived from porosity and permeability well log data .
- The Abiod chalk shows increased reservoir quality with decreased numerical heterogeneity derived from the raw wireline measurements.
- Formation-B show increased quality with decreased heterogeneity for gamma ray and neutron porosity measurements. Bulk density, P-wave transit time, Deep resistivity and the Dual Lorenz coefficients indicate that highest heterogeneity values are coincident with highest reservoir quality; limited trend of increased heterogeneity and quality are observed here.
- Formation-A shows increased reservoir quality with decrease heterogeneity for neutron porosity and gamma ray measurements. Bulk density and P-wave transit time data show highest heterogeneities are coincident with highest reservoir quality; a limited trend of increased heterogeneity and quality are observed here.
- Abiod chalk acts in similar way to homogeneous clastic reservoirs, with best reservoir quality associated with well sorted and structureless sandstones.
- Formation-A and -B show weaker relationships, and these likely relate to their more heterogeneous geological nature. The relationship between increased heterogeneity and reservoir quality is of interest and is counter-intuitive to clastic examples. This relates to complex multi-phased diagenetic controls, which enhances pore volumes and connectivity in different ways with each consecutive phase (chapter 3). The Mukta data shows the weakest relationships, which is considered to relate to less diagenetic activity during burial of the Mukta formations.

6.6.4. Optimal Sampling and Heterogeneity

- A technique developed to indicate the optimal number of samples (N_o) required, capturing intrinsic permeability variation in clastic reservoirs, can be applied to carbonate permeability data. Application to carbonate porosity data indicate much lower sample numbers are required – this is suggested as being a minimum sampling level. In the case of Formation-A, the required number and spacing of samples is more suited to probe-permeability measurement than core plugs.
- This technique cannot be directly applied to the heterogeneity data from the raw wireline measurements to produce similar sampling requirements numerically. Use of the multi-scaled heterogeneity log data has yet to allow identification of a correction factor because of large data scatter. This suggests that added complexities, perhaps including carbonate pore and/or facies typing, need to be identified and considered for successful application.
- Heterogeneity logs can be used as a visual clue to increased or decreased sampling requirements with regard to the underlying heterogeneity of individual horizons.

6.6.5. Concluding Remarks

The over-arching findings of this chapter are that heterogeneity logs can be related to porosity-permeability in carbonate reservoirs, and as such show great potential for use in reservoir characterisation. While heterogeneity logs cannot be used directly to estimate porosity and permeability in the units studied here, general trends and high/low value correlations have been identified.

The development of heterogeneity zones, in the raw wireline data, with strong correlation to physical property-derived flow zone units is of particular interest. This study suggests using numerical heterogeneity alongside a pre-existing flow zone indicator technique, but as the heterogeneity techniques are applied to a more varied assortment of carbonate reservoir types

more robust correlations will be identified and so its use in reservoir characterisation will be better constrained.

The links between reservoir quality and numerical heterogeneity, and particularly the relationship between increased heterogeneity and quality observed in the Panna and Mukta fields; and suggested connection to underlying geological complexities, are of significance for industry. The increasing heterogeneity with decreasing quality trend, documented in the Abiod chalk and Formation-B, highlights that more homogeneous carbonates can, in principle, act in similar ways to traditional siliciclastic examples. Ideally these techniques will be applied to a future well dataset from the studied fields with high resolution core samples and pressure/production data to confirm the existence of flow zones and their actual production rates. It is noted that the presence of flow potential enhancing fractures has not been considered in this analysis.

Although wireline heterogeneity cannot be used to ascertain an optimal number of samples to characterise intrinsic heterogeneities, the H.Logs do provide a visual indication as to where sampling should be focussed. The heterogeneity zone boundaries combined with H.Log analysis may provide a foundation for assigning block unit dimension for subsequent reservoir modelling.

Chapter 7. Conclusions

In this research numerical heterogeneity in wireline log data has been investigated for carbonate reservoirs, using standard and modified heterogeneity measures. A novel technique – the Heterogeneity Log (H.Log) has been developed in this thesis, and results of numerical heterogeneity analyses have been applied to physical property data to investigate (1) poro-perm relationships, (2) the identification of fluid flow zones, (3) the link between reservoir quality and heterogeneity, and (4) the application of H.Log data to sampling strategies.

7.1. Discussion of the Hypotheses

This concluding chapter brings together the conclusions from the previous five chapters to consider the hypotheses first posed in Chapter 1;

H1 Scale-dependent geological and physical property heterogeneities within carbonate reservoirs can be clearly defined through the integration of wireline, core and electrical borehole image data;

The literature review of Chapter 2 clearly demonstrates that a key thread throughout carbonate petrophysical analysis, and indeed carbonate exploration in general, is variability or “heterogeneity” in physical grain components, chemical/mineralogical nature, porosity, and other geological features across all scales of observation and frequencies.

The research described in Chapter 3 demonstrates that detailed petrophysical analysis can be successfully calibrated to core data in carbonates. This enables the estimation and interpretation of physical properties such as shale volume, porosity, and permeability. This research also proves that log-derived properties can be correlated to geological features identified in core and the electrical borehole image, where available.

In the case of the reservoir units studies here, Chapter 3 shows that analysis of the three scales of petrophysical data (wireline log – electrical borehole image – core) can be used to identify

key heterogeneities in porosity and permeability data, which can in turn be related to geological heterogeneities described in core and borehole images; either from the studied well or by drawing cross-well correlations using the established geological model.

For example traditional cross-plots of wireline bulk density against neutron porosity clearly demonstrate that Formation-A of Panna and Mukta is the most heterogeneous unit, and that in the Miskar case study the Abiod chalk is most homogeneous. High amplitude and frequency variability is documented in the Formation-A shale volume, porosity and permeability estimates and relates to the diverse range of carbonate facies, pore-types and mud-rich horizons present. The Abiod chalk is the most homogeneous of the case studies but still shows low amplitude and frequency variation downhole, which are used here to establish reservoir zones. In all case studies, heterogeneities were found in this study to relate more to porosity and permeability than to mineralogical and facies-based variation in these carbonates.

H2 Numerical techniques from a range of disciplines (e.g. geology, soil mechanics, environmental science and ecology) can be used to investigate and quantify numerical heterogeneities in carbonate reservoirs;

Chapter 4 shows that basic statistics and semi-variogram analyses can be used to quantitatively characterise numerical heterogeneity in wireline log data, in terms of amplitude and frequency of variations present. Heterogeneity measures provide a single value quantifying heterogeneity, where zero is homogeneous and ≥ 1 is extremely heterogeneous. These measures allow the comparison of different data types within individual reservoir units, and cross-reservoir comparisons.

The Lorenz and Dykstra-Parsons coefficients were originally developed for use in modelling permeability in siliciclastic reservoirs, and were readily applied to wireline data from carbonate systems in this research. All five measures investigated and developed for this study (Lorenz, Dykstra-Parsons, Dual Lorenz, coefficient of variation, and *t*-Tests) produce similar outputs, and can clearly be used to ascertain the different heterogeneity levels of the different reservoir

units investigated. The Lorenz and Dual Lorenz coefficients are relatively simple yet robust measures which provide graphical and numerical outputs for interpretation, where heterogeneity varies between zero (homogeneous) and one (maximum heterogeneity). The specific ability to have a measure that can compare between different reservoirs increases the applicability of the measure.

Alongside applying the heterogeneity measures to complete reservoir unit datasets, Chapter 5 describes the development of the Heterogeneity Log (H.Log). The H.Logs allow the multi-scale aspect of heterogeneity to be investigated downhole. Similar high and low features are seen across the suite of H.Logs derived from different wireline measurements and at different resolutions (10m, 5m, 2m, and 1m). More detailed analysis of the H.Logs can be related to physical properties and underlying geological heterogeneity (discussed in Chapter 6, and in the following text).

In terms of the reservoirs used in this study the Abiod chalk (Miskar) always returns lowest heterogeneity values, followed by Formation-B (Panna and Mukta). The heterogeneous nature of Formation-A (Panna and Mukta), indicated by petrophysical analysis in Chapter 3, is confirmed. The Panna field returns stronger heterogeneity values than neighbouring Mukta field; this is attributed to a great diagenetic overprint affecting the Panna Field. The neutron porosity measurements show highest heterogeneity across the three fields, followed by P-wave transit time. Pore volume and types, rather than mineralogy and lithology, are therefore the more variable property in carbonate reservoirs at this scale of investigation.

H3 Carbonate reservoir heterogeneity can be used to constrain poro-perm relationships, and to identify key fluid flow zones;

The H.Logs, described in Chapter 5, produce a detailed dataset of numerical heterogeneity through a succession, across four scales of resolution.

Chapter 6 shows that in general lower porosity and permeability trend toward higher heterogeneity values, which is best illustrated in the Abiod chalk; relationships show more

scatter as reservoir heterogeneity increases. Similar relationships are identified in well-sorted and more structureless siliciclastic reservoirs (e.g. aeolian sandstones), where homogeneity allows optimal packing of grains to increase pore space and connectivity. An opposing trend is seen in the heterogeneous Formation-A of wells P and M, where porosity and permeability increase with heterogeneity in gamma ray and bulk density measurements. Numerical heterogeneity is not found to add to pre-existing poro-perm classification schemes.

The Heterogeneity Log data can be zoned using the Stratigraphic Modified Lorenz method, developed in Chapter 6, based on high-low heterogeneity features through the carbonate succession. Heterogeneity zone boundaries can be correlated across the suite of measurements, and show strong correlation to flow zone boundaries (defined using significant low porosity and permeability values). These heterogeneity zonations can be used alongside pre-existing flow zone indicator methods to produce more robust outputs. As the technique is applied to more reservoir units it is expected that stronger heterogeneity zone correlations will be made. Even the low heterogeneity contrasts identified in the Abiod chalk can be used to zone the reservoir into meaningful units.

H4 Numerical heterogeneity can be linked to reservoir quality in carbonates;

Comparing numerical heterogeneity to reservoir quality, derived from Amaefule *et al.*'s (1993) cross-plot and Flow Zone Indicators, indicates two end-member relationships in Chapter 6.

Increasing reservoir quality with decreasing heterogeneity is the more common relationship, with limited scatter; this is especially well presented in examples from the Abiod chalk. A weaker trend is identified from neutron porosity and gamma ray measurements of Formation-A and -B of wells P and M. This characteristic is again similar to siliciclastic reservoirs, where homogeneous sandstone examples typically show the best reservoir quality and production capabilities. The weaker relationships observed in the Panna and Mukta wells are suggested to reflect the more heterogeneous bulk characteristics of these reservoirs.

The bulk density and P-wave transit time data of Formation-A of wells P and M show highest reservoir quality coincident with highest heterogeneity, accompanied by scattered relationships of increased heterogeneity and quality. This is observed to a lesser extent in Formation-B. This observation most likely relates to complex multi-phase diagenetic processes; enhancing pore volume and connectivity through different phases of corrosion and dissolution. Again the fact that relationships are poorer in the Mukta field suggest a weaker diagenetic influence, a conclusion that is supported by the geological interpretations.

Neutron porosity heterogeneity reflects bulk porosity, in that to obtain high reservoir quality a more homogeneous porosity and permeability is required. While the bulk density and P-wave transit time measurements are perhaps more influenced by smaller-scale grain and textural features within the carbonate matrix.

H5 An improved understanding of numerical heterogeneity can be used to inform optimal sampling strategies through a reservoir succession.

A statistical technique developed to ascertain the optimal number of samples to characterise permeability in siliciclastic reservoirs, can be applied to carbonate permeability and porosity data. Porosity is suggested to require tens of samples, and hundreds for permeability which is better represented with probe-permeability style sampling.

This technique cannot be directly applied to the wireline focussed heterogeneity data to produce similar sampling indications. Further analysis of the H.Log data, on a wider selection of carbonate reservoirs, should provide a conversion factor.

For now, the Heterogeneity Logs provide a visual guide as to where sampling should be focussed at horizons of increased heterogeneity and vice versa. On a related note, the combined use of H.Logs and heterogeneity zones will aid how block units are established in reservoir modelling to enhance the capture of intrinsic heterogeneities within the model.

The positive research findings of hypotheses *H3* and *H4*, increase confidence in the placement of flow zone boundaries through a succession; enabling the production of a more holistic and robust reservoir model, that is based not only on the physical properties but includes an indication of underlying geological heterogeneities and their associated relationships to flow zone characteristics. Equally, the suggested application of heterogeneity zone boundaries to defining block thicknesses in such models would aid their construction. The links between reservoir quality and heterogeneity have been noted in previous geological studies, but no similar work providing numerical quantification of heterogeneity in carbonate reservoirs was identified through the literature review conducted as part of this research.

7.2. Suggested Further Work

A number of avenues for further work are suggested. As with any body of research additional questions and requirements have been raised to further constrain interpretations and analyses.

Ideally this heterogeneity study would be applied to a well drilled with continuous core, formation pressure testing and production data. A full core record would allow for the underlying geological features to be fully constrained and related to the wireline derived heterogeneity measures. Continuous core would also allow for more detailed sampling to ascertain physical property data and fully calibrate the wireline-derived estimates, while also allowing more research into petrophysical parameters in carbonates (such as Archie's m exponent). Potentially numerical heterogeneity might be used as an indicator of Archie exponent values or optimal sample coverage to ascertain them with more confidence. Pressure test and production data are required to fully ground-truth the presence of fluid flow zones and their correlation to heterogeneity zones.

This work has focussed on near vertical wells, allowing heterogeneity through the succession to be investigated. It would be of interest to also apply these techniques to horizontal wells so that lateral heterogeneity can be analysed and compared. Additionally, applying the heterogeneity measures to multiple wells from a reservoir would be expected to provide insight into lateral

heterogeneities, supporting cross-well correlations and modelling. In the Panna and Mukta fields are any of the lateral heterogeneity in physical properties related to large faults and fractures; suggested to be the main conduits of fluids during diagenesis? Combining vertical, horizontal and multi-well analysis would allow a heterogeneity model to be established, alongside the existing physical property model.

Inclusion of petrophysical tools with significantly different measurement resolutions (for example electrical borehole image, logging while drilling, and nuclear magnetic resonance logging tools), with seismic and core data, would provide an interesting dataset to further investigate the additional numerical heterogeneities at larger- and finer-scales. Additionally, detailed measurements on carbonate outcrops would provide a fascinating opportunity to truly constrain spatial relationships between geological and petrophysical properties, with numerical heterogeneities.

This work has focused on carbonate reservoirs but these numerical techniques could be applied to siliciclastic reservoirs; enabling inter-reservoir comparison, whilst also cross-checking the suitability and application of the heterogeneity measures to reservoir data for which they were originally developed. The application to siliciclastic complexities such as thin-bedded heterolithic reservoirs could prove equally rewarding.

Appendix A. Glossary

Report Specific;

H.Log – Heterogeneity Log

SML – Stratigraphic Modified Lorenz technique

D^2 – Generalised Distance Boundary technique

Heterogeneity Measures;

Cv – Coefficient of Variation

Lc – Lorenz Coefficient

V_{dp} – Dykstra-Parsons Coefficient

DLC – Dual Lorenz Coefficient

t – t-Test value

Wireline Log Data Acronyms;

Cali – Caliper

DRHO - Density Correction

DTP/C – P-wave Transit time (slowness)

FMS – Fullbore Microscanner (electrical borehole image)

GR – Gamma Ray

NPHI – Neutron Porosity

PTRA – Potassium-Thorium Ratio (SGR)

RHOB – Bulk Density

Rt / LLD – Deep Resistivity

Rxo / LLS – Shallow Resistivity

SGR – Spectral Gamma Ray

Petrophysical Acronyms & Symbols;

RCA – Routine Core Analysis

SCAL – Special Core Analysis

Vsh – Shale Volume

GRI – Gamma Ray Index

GR_{log} – Gamma Ray Log Measurement

GR_{min} – Minimum GR Value

GR_{mac} – Maximum GR Value

\emptyset_e – Effective Porosity (PHIE)

\emptyset_T – Total Porosity (PHIT)

$\emptyset_{N_{log}}$ – Neutron Porosity Log Measurement

\emptyset_{N_m} – Rock Matrix Neutron Porosity Value

\emptyset_{N_f} – Fluid Neutron Porosity Value

$\emptyset_{N_{sh}}$ – Shale Neutron Porosity Value

ρ_{log} – Bulk Density Log Measurement

ρ_m – Rock Matrix or Grain Density

ρ_f – Fluid Density

ρ_{sh} – Shale Density

$\Delta T_{c_{log}}$ – P-wave Transit Time Log
Measurement

ΔT_{c_m} – Matrix P-wave Transit Time

ΔT_{c_f} – Fluid P-wave Transit Time

$\Delta T_{c_{sh}}$ – Shale P-wave Transit Time

S_w – Water Saturation

S_{w_a} – Archie Water Saturation

S_{w_s} – Simandoux Water Saturation

$S_{w_{in}}$ – Indonesian Water Saturation

S_{hc} – Hydrocarbon Saturation

$S_{w_{irr}}$ – Irreducible Water Saturation

R_w – Water Resistivity value

R_{sh} – Shale Resistivity value

m – Archie Porosity (or cementation)
exponent

n – Archie Saturation exponent

a – Archie Structural Parameter (constant)

c – Irreducible Bulk Volume Water

k – Permeability

RQI – Reservoir Quality Index

$\emptyset_z / PHIZ$ – Pore Volume to Grain Volume
Ratio (normalised porosity)

FZI – Flow Zone Indicator

HCIIP – Hydrocarbons Initially in Place

GRV – Gross Rock Volume

N/G – Net to Gross

FVF – Formation Volume Factor

p.u. – Porosity Units

mD – milli-Darcy (Permeability Units)

Statistical Symbols and

Acronyms;

H_o – Hypothesis for t-Test

n – Number of Samples

N_o – Optimal Number of Samples

ρ – Significant Level

R – Correlation Coefficient / Coefficient of
Correlation

R^2 – Coefficient of Determination

s – Variance

s_{xy} - Covariance

$S^2 / \sqrt{\sigma^2}$ – Standard Deviation

\bar{x} – Mean Value

∞ - Infinity

Appendix B: Petrophysical Analysis Methodology.

This appendix summarises the techniques used for detailed petrophysical analysis in this study. A variety of standard techniques are used as appropriate for different datasets and properties. Here all of the techniques are detailed using the Panna well P dataset (discussion of results is not included here, please see chapter 3).

B.1. Shale Volume (Vsh)

Petrophysicists assign the term shale to the presence of clay minerals and grain-sized particles; either as an individual dominant lithology (mudstone), heterolithic thin beds at or below tool resolution, or as a percentage of the total lithology (i.e. shaly-sands and shaly-carbonates). A petrophysical “shale” is seen to have three key attributes; clay mineralogy constituting the framework of the rock, nanometre sized pores and nano-Darcy permeability, and grains of large surface area which allow for water to be absorbed on surfaces and bound inside the platelets (Katahara 2008).

There are a number of methods used to derived shale volume from wireline logs, ranging in complexity. The most standard equation is based solely on the gamma ray log, GR (the Gamma Ray Index; equation B.1). This assumes a linear relationship between shale volume and GR, non-linear versions are available (Larionov 1969) but do not add to analysis in the case of reservoirs studied here. In this case it is assumed that gamma radiation of a mudrock originates from the potassium and thorium content of minerals such as mica, while uranium is absorbed onto the surface of clay minerals (Ellis & Singer 2007; Hurst 1990; Serra 1986).

$$Vsh = \frac{GR_{log} - GR_{min}}{GR_{max} - GR_{min}} = GRI \quad (\text{Equation B.1})$$

Where: Vsh = Shale volume (fraction), GR_{log} - gamma ray log measurement, GR_{min} - minimum gamma ray value recorded in the section, and GR_{max} is the maximum record value, GRI – Gamma Ray Index.

In some lithologies uranium enrichment can cause misleading GR highs. If spectral gamma ray data is available then it is possible to establish a potassium-thorium ratio curve (PTRA) which removes this uranium effect from the gamma ray signature. Equation B.2 (Serra 1986) illustrates how Vsh is derived from the PTRA curve.

$$Vsh = \frac{PTRA_{log} - PTRA_{mx}}{PTRA_{sh} - PTRA_{mx}} \quad (\text{Equation B.2})$$

Where: V_{sh} = Shale volume (fraction), $PTRA_{log}$ -potassium-thorium ration measurement, $PTRA_{mx}$ – minimum potassium-thorium ratio value recorded in the section, and $PTRA_{sh}$ is the maximum record value.

To confirm the max and min values a flagged crossplot is used to remove the non-matrix trend, leaving a clear “cloud” of shale points (figure B.1, table B.1).

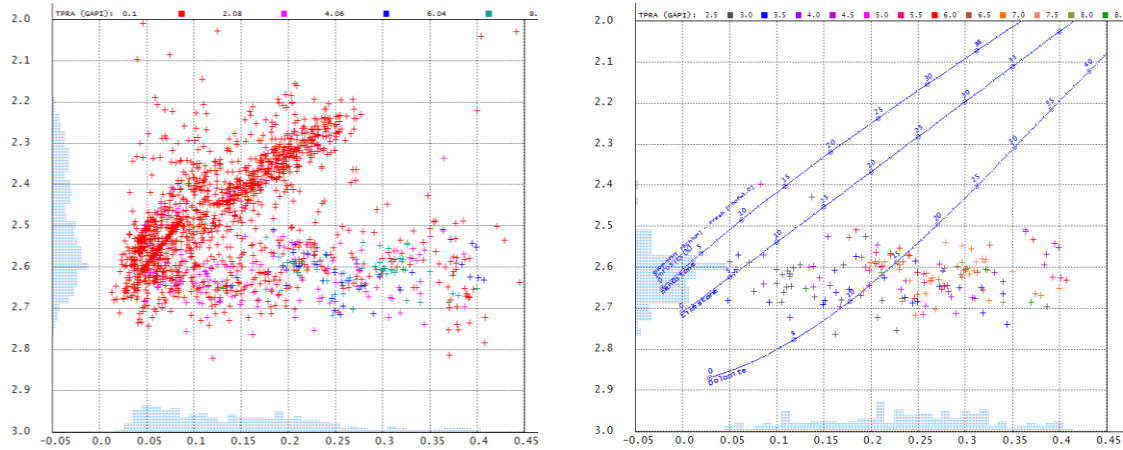


Figure B.1. Bulk density-neutron porosity cross plots, PTRAs on z-axis. Left – all values, right – shale values only.

Bulk density and neutron porosity measurements can also be used to estimate V_{sh} , effectively based on the principle of neutron-density separation (equation B.3), based on either average rock values or core measured properties (Serra 1986). Note that when the matrix value is requested this refers to the grain component, for example a sand or limestone grain.

$$V_{sh} = \frac{(\varnothing N_{log} - \varnothing N_m) / (\varnothing N_f - \varnothing N_m) - (\rho_{log} - \rho_m) / (\rho_f - \rho_m)}{(\varnothing N_{sh} - \varnothing N_m) / (\varnothing N_f - \varnothing N_m) - (\rho_{sh} - \rho_m) / (\rho_f - \rho_m)} \quad \text{(Equation B.3)}$$

Where: V_{sh} = Shale volume (fraction), $\varnothing N_{log}$ – neutron porosity log measurement, $\varnothing N_m$ – matrix neutron response, $\varnothing N_f$ – fluid neutron response, $\varnothing N_{sh}$ – shale neutron response, ρ_{log} –bulk density log measurement, ρ_m – matrix density, ρ_f – fluid density, ρ_{sh} – shale density.

The constants used in equations B.1 – B.3 were originally taken from standard tables, with better estimates acquired from re-iterative log analysis and crossplots (figure B.1, table B.1).

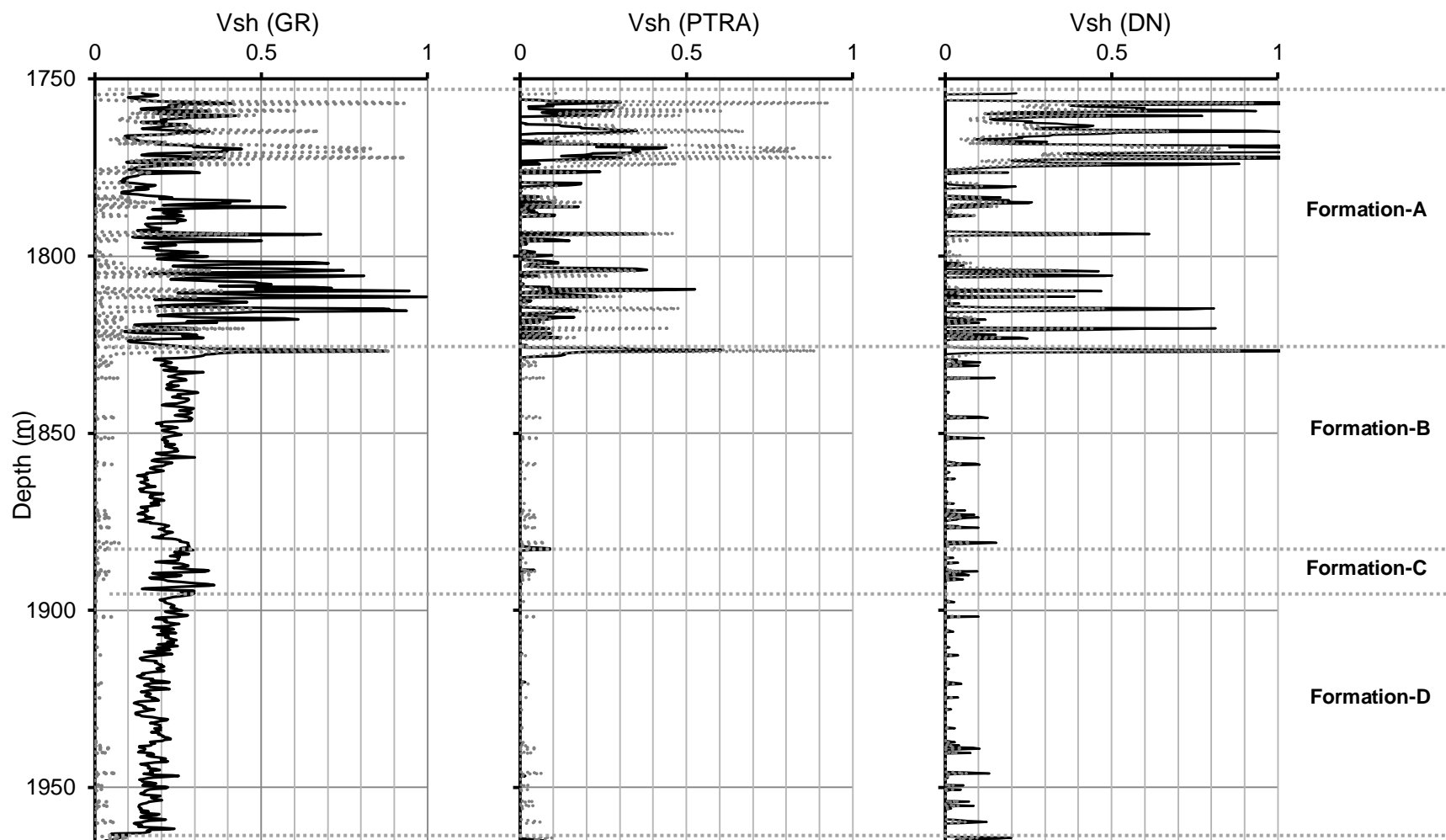


Figure B.2. Shale Volume (Vsh) estimations from wireline logs. from left to right; (a) Total gamma ray, (b) potassium-thorium ratio, and (c) density-neutron. Note the grey dotted line on each plot is the used Vsh curve – an average of curves *b* and *c*.

An average of the PTRA and density-neutron Vsh estimates is used for further analysis (figure B.2)

	Gamma Ray (API)	Potassium- Thorium Ratio		Bulk Density	Neutron Porosity
Max value	184.328	8.035	Matrix value	2.70	0.00
Min value	20.154	1	Shale value	2.59	0.30
			Fluid value	0.6	0.7

Table B.1. Constant values use in well P Vsh estimations using equations B.1 – B.3.

Figure B.2 shows comparison of the three Vsh techniques used here. Clearly the total gamma ray estimate is too high for the Panna successions; predicting shale content of 20% in “clean” Formation-B and -D. Previous investigations have shown this is due to uranium enrichment by diagenesis (Khanna *et al.* 2007). The PTRA and density-neutron Vsh estimates are very similar, and correspond well to the mud log and limited core plug description downhole.

B.2. Porosity (\emptyset)

Porosity is not directly measured downhole, but is estimated from petrophysical and chemical measurements. The neutron porosity log predominately measures the concentration of hydrogen ions (H^+) which are assumed to be in the pore space. However this should be used with care as the lithology lines on a traditional neutron-density crossplot show a small matrix effect on the neutron log, where at 0% porosity there is a slight negative neutron measure for sandstone and limestone (figure B.3.a). More commonly published relationships between density, neutron and sonic measurements are used to estimate porosity. Analyses generally incorporate the Vsh estimation and fluid parameters into corrections within these calculations, thus calculating an effective rather than a total porosity.

Equations B.4 to B.6 (Serra 1986) show how the effective porosity (connected minus the bound water) can be derived from single well log measurements. Again a number of constant values are required. Initially standard rock type values were used and these were refined using density-neutron and density-sonic cross plots (figure B.3, table B.2). To obtain an estimate of total porosity we can use equation B.7 to correct for shale content. It can be seen that dual property calculations are more robust and effective at estimating porosity (figure B.4). Here we can simply use the averages, as is done within the hydrocarbon industry (equation B.8, (Serra 1986)).

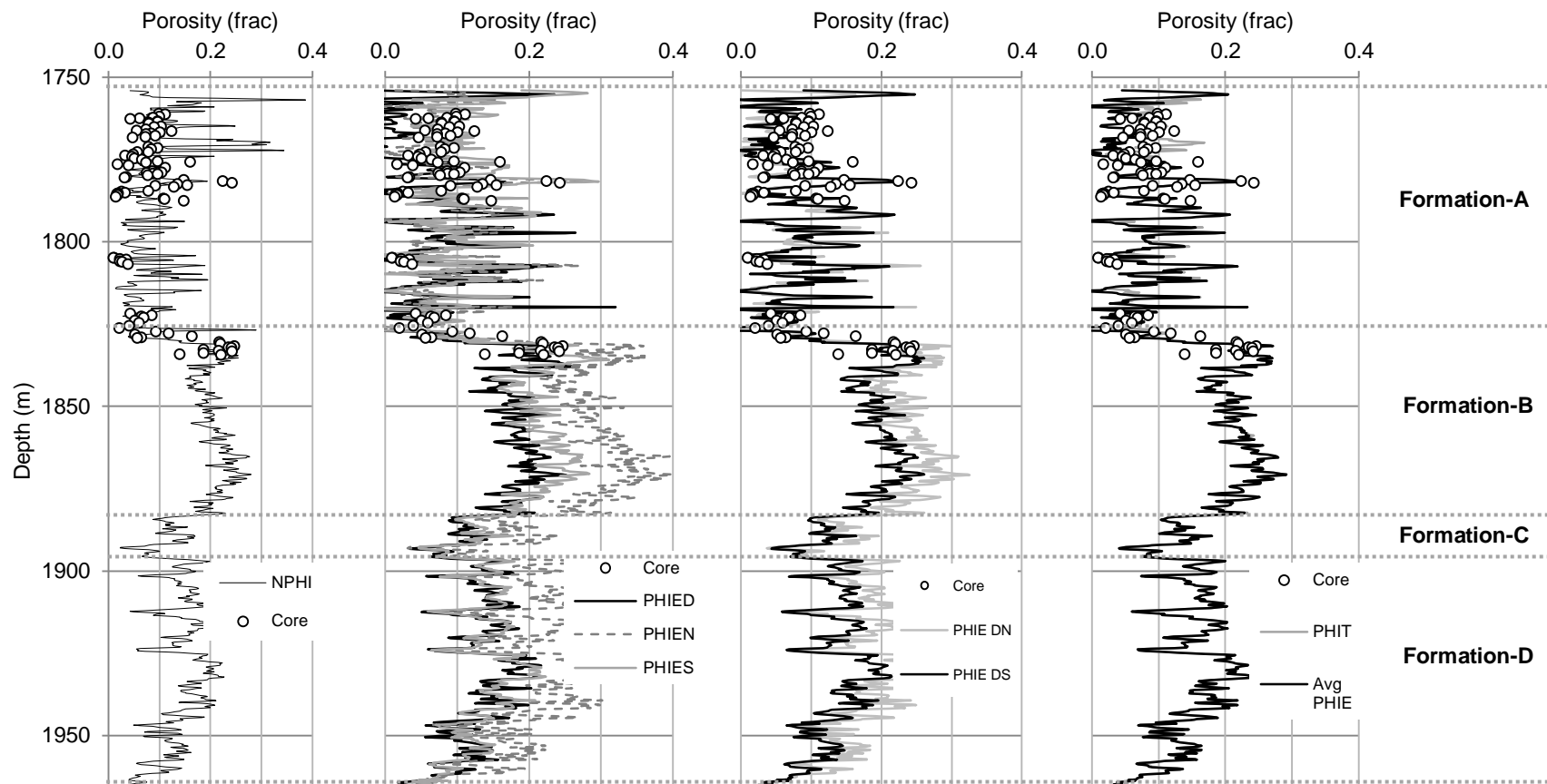


Figure B.4. Log-derived porosity plots for well P. From left to right; (1) original neutron porosity log, (2) log-derived effective porosity (PHIE) for density (black), neutron porosity (grey dashed), and compressional sonic velocity (grey), (3) PHIE for density-neutron relationship (grey) and density-sonic (black), and (4) average PHIE curve used for analysis.

$$\phi_e = \frac{(\phi N_m - \phi N_{log} - (\phi N_m - \phi N_{sh}) \times Vsh)}{(\phi N_m - \phi N_f)} \quad \text{(Equation B.4)}$$

Where: ϕ_e – Effective Porosity (fraction), Vsh – Shale Volume, ϕN_{log} – neutron porosity log measurement, ϕN_m – matrix neutron porosity value, ϕN_f – fluid neutron porosity value, ϕN_{sh} – shale neutron porosity value.

$$\phi_e = \frac{(\rho_m - \rho_{log} - (\rho_m - \rho_{sh}) \times Vsh)}{(\rho_m - \rho_f)} \quad \text{(Equation B.5)}$$

Where: ϕ_e – Effective Porosity (fraction), Vsh – Shale Volume, ρ_{log} – bulk density log measurement, ρ_m – matrix density, ρ_f – fluid density, ρ_{sh} – shale density.

$$\phi_e = \frac{(\Delta Tc_m - \Delta Tc_{log} - (\Delta Tc_m - \Delta Tc_{sh}) \times Vsh)}{(\Delta Tc_m - \Delta Tc_f)} \quad \text{(Equation B.6)}$$

Where: ϕ_e – Effective Porosity (fraction), Vsh – Shale Volume, ΔTc_{log} – compressional sonic velocity log measurement, ΔTc_m – matrix P-wave Transit time log value, ΔTc_f – fluid P-wave Transit time value, ΔTc_{sh} – shale P-wave Transit time value.

$$\phi_T = \phi_e / (1 - Vsh) \quad \text{or} \quad (\rho_m - \rho_{log}) / (\rho_m - \rho_f) \quad \text{(Equation B.7)}$$

Where: ϕ_T – Total porosity, ϕ_e – effective porosity, Vsh – shale volume, ρ_{log} – bulk density log measurement, ρ_m – matrix density, ρ_f – fluid density.

	Bulk Density	Neutron Porosity	Compressional Sonic Velocity
Units	g.cm ⁻³	pu	μs/ft
Matrix value	2.70	0.00	47.5
Shale value	2.59	0.30	85.7
Fluid value	0.60	0.70	210.0

Table B.2. Constant values use in porosity estimations using equations B.4 – B.6.

$$\phi_e = (D\phi_e + N\phi_e) / 2 \quad \text{or} \quad (D\phi_e + S\phi_e) / 2 \quad \text{(Equation B.8)}$$

Where: ϕ_e – effective porosity, $D\phi_e$ – density derived effective porosity, $N\phi_e$ – neutron derived effective porosity, $S\phi_e$ – compressional sonic derived porosity.

To investigate the best fit log-derived porosity estimate figure B.4 shows log-porosity plotted with the limited core measurement. It can be seen that while all curves capture similar frequency and magnitude variations to that seen in core, the original neutron porosity does not capture the low value record, and density-derived porosity shows strongest fit. More robust estimations are gained from combining sonic velocity or neutron porosity values with the density estimates. While both density-sonic and density-neutron porosity estimates are similar for the upper section, in the lower half it can be seen that density-sonic estimates are 2-4 p.u. higher. In this case an average of the two derived curves is used for the remainder of this study,

showing a strong correlation with the core data (figure B.5). It is noted that at 1760-1770m effective porosity significantly underestimated core porosity, unlike total porosity. This is a mudstone-rich horizon and so the porosity difference may be accounted for.

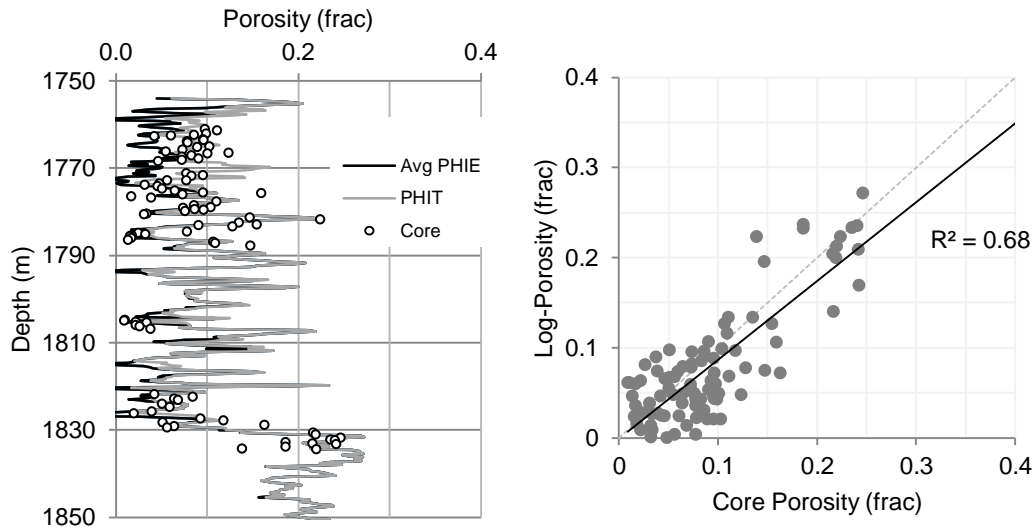


Figure B.5. left; average porosity estimation plotted against core porosity measurements for 1750-1850m section, right; cross plot of log-derived and core measured porosities. Effective porosity (PHIE) shows 0.68 correlation with core, total porosity (PHIT) shows correlation of 0.72.

Formation-A is seen to consist of highly variable porosity at a high frequency, captured in both core and log-derived measurements. It can be seen that low effective porosity correlates with increase shale content, noting that total porosity increases with shale content. The top of Formation-B shows a sharp rise in porosity to 20-25%, with low variability down hole. Formation-C shows a sharp decrease in porosity to ~10%, before rising again into Formation-D. Porosity reaches a maximum of ~20% in Formation-D and shows low frequency variation to the bottom of the formation.

B.3. Saturation

Water saturation (S_w) refers to the volume of water occupying the porosity in a reservoir. The term $(1-S_w)$ will therefore give the hydrocarbon saturation (S_h). A variety of empirical relationships have been documented for the estimation of saturation from the deep resistivity measurement (R_t), porosity (\emptyset), and shale volume (V_{sh}), the most standard technique being Archie (equation B.9 (Archie 1942)). The Archie equation is known for being great in siliciclastic successions but weaker in carbonate rocks where pore geometry and surface conductivity may lead to added complications, particularly in obtaining simple m and n exponent values from special core analysis (see chapter 2). Alternative approaches by Simandoux (Equation B.10, (Simandoux 1963)) and the Indonesian equation (Equation B.11,

(Poupon & Leveaux 1971)) are used here for comparison. These are both typically used as shaly-sand models for saturation, the carbonate successions dealt with here have varying shale content and so the use of these shaly-sand models is investigated. When shale volume is zero then the Simandoux and Indonesian models should reduce to Archie. Constant parameters used in these equations are found in reference tables and from core analysis reports (table B.3). Shale resistivity is derived from a cross plot of shale volume and deep resistivity measurement, showing a range of 3-7ohm.m (figure B.6). It is noted that ideally the shale resistivity measurement would be taken from a large, underlying, shale bed; which was not available for this dataset.

$$S_{W_a} = \sqrt[n]{a/\phi_e^m \times \left(\frac{R_w}{R_t}\right)} \quad \text{(Equation B.9)}$$

$$S_{W_S} = \left(\frac{\sqrt[2]{(Vsh/R_{sh})+(4 \times \phi_e^m)} - Vsh}{(a \times R_w \times (1-Vsh) \times R_t)} - \frac{Vsh}{R_{sh}} \right) / \left(\frac{2 \times \phi_e^m}{a \times R_w \times (1-Vsh)} \right) \quad \text{(Equation B.10)}$$

$$S_{W_{in}} = \frac{\sqrt[2]{1/R_t}}{Vsh^{1-(0.5 \times Vsh)} / \sqrt[2]{R_{sh}} + \sqrt[2]{\phi_e^m / (a \times R_w)}} \quad \text{(Equation B.11)}$$

Where: S_{W_a} – Archie Saturation, S_{W_S} – Simandoux Saturation, $S_{W_{in}}$ – Indonesian Saturation, ϕ_e – effective porosity, Vsh – shale volume, R_w – resistivity of the fluid (water), R_t – deep resistivity measurement, R_{sh} – shale resistivity, a – structural parameter (constant), m – cementation exponent, n – saturation exponent.

	a	m	n	R_w (ohm.m)	R_{sh} (ohm.m)
Value	1	2	2	0.12	5

Table B.3. Constant values used in well log-based saturation estimation for well P, obtained from special core analysis (SCAL).

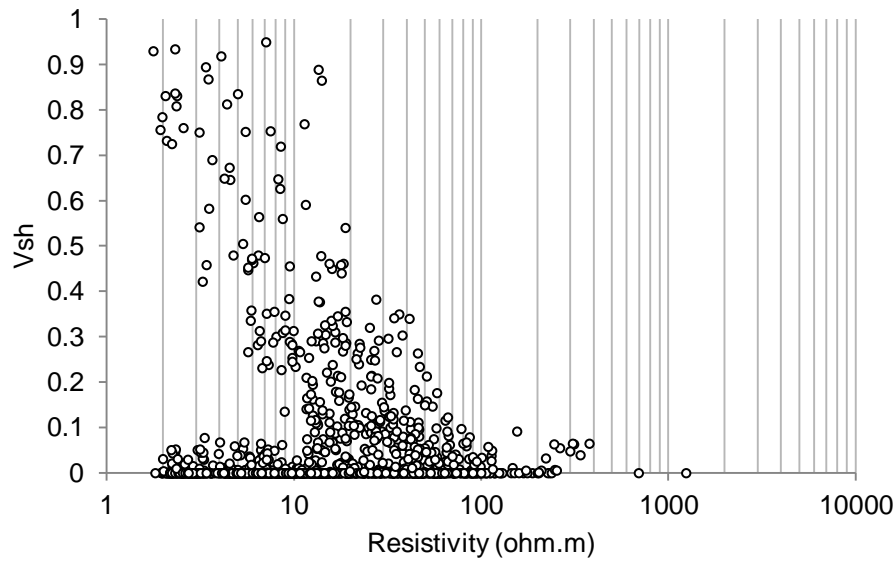


Figure B.6. Shale volume plotted against resistivity. Highest shale volumes found to have resistivities of 3-7ohm.m, the average of 5ohm.m is used in calculations.

Figure B.7 shows the results of the different log-derived saturation estimations for well P, as expected Simandoux and Indonesian saturation estimates only deviate from Archie at horizons where shale content is greater than zero. In general we see that increased shale content corresponds to increase in the total water saturation, as would be expected. Formation-A shows high frequency and amplitude variability. The upper section is known to be low porosity and shale-rich, here we see complete water saturation. Downhole through Formation-A water saturation is seen to rise and fall with shale content, low shale content corresponding to low total water saturation. The hydrocarbon is expected to be natural gas, indicated by the bulk density-neutron porosity overlay. A sharp decrease in water saturation is seen at the top of Formation-B, followed by a gradual rise to ~95% at 1855m, from here saturation shows limited variation around 90%. Formation-B is therefore suggested to contain water which transitions in to hydrocarbon upwards through the zone, again bulk density-neutron porosity overlay suggests that this hydrocarbon is natural gas. Formation-C shows a sharp decrease in water saturation. Formation-D shows water saturation increasing downhole, with high frequency variation. Again this illustrates the presence of hydrocarbon above water in this geological zone.

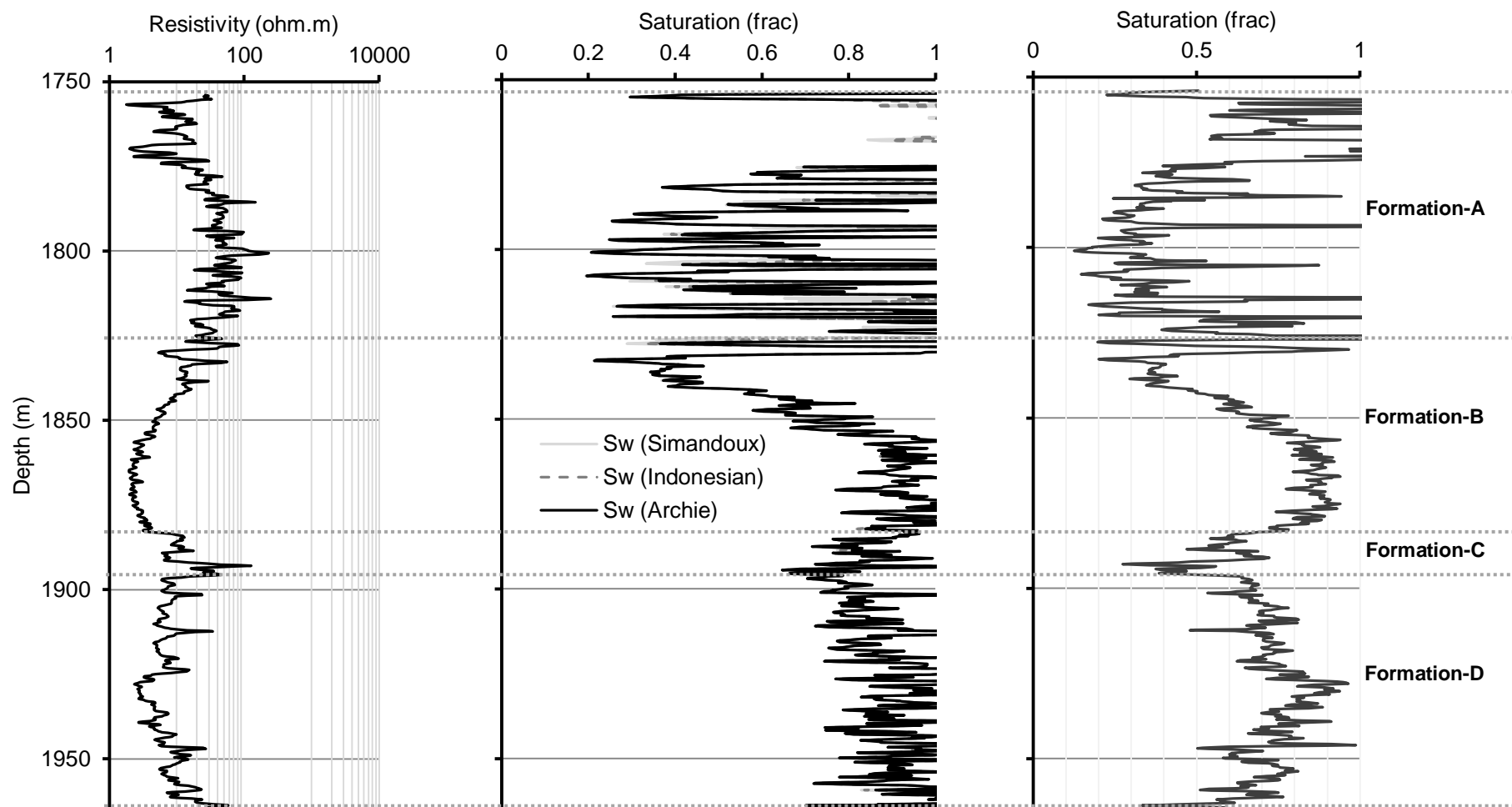


Figure B.7. Saturation estimations from well P. Left to right; (1) Deep resistivity measurements (R_t), (2) Saturation estimation based on Archie, Simandoux and Indonesian equations, and (3) Average saturation estimation used for future analysis [note $1-S_w$ = hydrocarbon saturation].

Although not necessarily part of routine petrophysical analysis, an estimation of irreducible water saturation ($S_{w_{irr}}$) is also calculated. This is used later in log-derived permeability estimation. Irreducible water saturation is the volume of water that cannot be removed from a rock without applying undue pressure or temperature (Ellis & Singer 2007). This water is thought to be trapped in small pore throats with high capillary forces and adhering around grain boundaries. It also includes water bound within the mineral structure of mudstone, or shaly, components of the rock. $S_{w_{irr}}$ should always be less than the total water saturation, it is noted that this is observed here even although water saturation estimates are not factored directly into the equations.

Two methods are used for estimating $S_{w_{irr}}$ from well log data. Equation B.12 (Buckles 1965) derives irreducible water saturation from effective porosity and a constant referred to as the Buckles number (c). The Buckles number is referred to as the irreducible bulk volume water (equation B.12). The basis of the model is that a volume of the total saturation is held in small pores with high capillary forces that effectively trap the fluid. The smaller the pore volume then the stronger the forces (Doveton 1994). Well P shows c values ranging from 0.007 – 0.204, which fall within the typical vuggy and intergranular limestone ranges; 0.005-0.02 and 0.01-0.06 respectively (Holmes *et al.* 2009). Doveton (1994) provides a linear version based on effective porosity and the Buckles number (equation B.13). Both methods should give the same $S_{w_{irr}}$ value and so are useful for cross checking.

$$S_{w_{irr}} = c \times \phi_e \quad \text{(Equation B.11)}$$

$$\text{Log}(c) = \frac{\text{Log}(a \times R_w) - (n-m) \times \text{Log}(\phi_e) - \text{Log}(R_t)}{n} \quad \text{(Equation B.12)}$$

$$\text{Log}(S_{w_{irr}}) = \text{Log}(c) - \text{Log}(\phi_e) \quad \text{(Equation B.13)}$$

Where: $S_{w_{irr}}$ – Irreducible water saturation, ϕ_e – effective porosity, R_w – resistivity of the fluid (water), R_t – deep resistivity measurement, a – structural parameter (constant), m – cementation exponent, n – saturation exponent, c – irreducible bulk volume water.

As expected both techniques give similar $S_{w_{irr}}$ values through the succession, with values never being higher than total water saturation. The shale-rich horizons show higher $S_{w_{irr}}$ values (figure B.9, left). Formation-C shows a decrease in the $S_{w_{irr}}$ which corresponds to the water saturation; in general we see a decrease in $S_{w_{irr}}$ with increasing effective porosity (figure B.9, right). It would be expected that low effective porosity would be associated with smaller-scale pore sizes, therefore with increase capillary forces maintaining a higher $S_{w_{irr}}$.

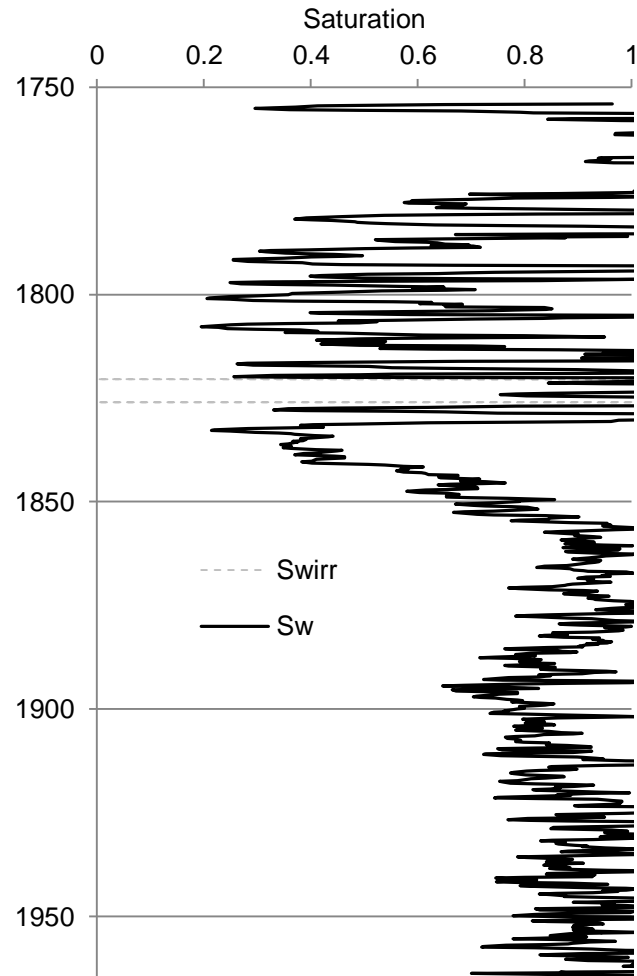


Figure B.8. Well log-derived irreducible water saturation ($S_{w_{irr}}$) and water saturation (S_w) curves for well P. $S_{w_{irr}}$ derived from equations B.11 and B.13 provide the same value.

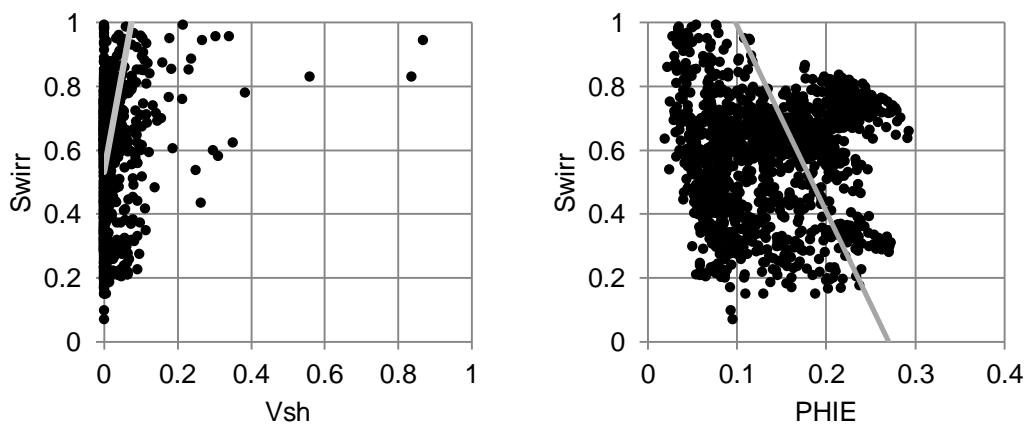


Figure B.9. Cross plots of irreducible water saturation against shale volume (left) and effective porosity (right). Trendline added to plots for illustrative purposes, see text.

B.4. Permeability (k)

Permeability is the ability for fluid(s) to flow through the interconnected pore space, and fractures, of a rock (Tiab & Donaldson 1996). Permeability is measured as part of routine and special core analysis. It is possible to estimate permeability from wireline logs based on relationships established for porosity and saturation. Chapter 2 discusses how poro-perm relationships are less easily constrained in carbonates due to their highly variable nature. Petrophysical analysis of the carbonate reservoirs used in this study has shown that the different log-derived permeability models (equations B.15-B.18), described below, have varying successes when applied. This can be confirmed through comparison with core data. Constants have been modified within limits defined by authors to produce best fit for the core data, for example the Morris and Biggs (1967) “ C ” value varies between 80 and 250 depending on oil-gas content.

$$k = \left(\frac{80 \times \phi_e^2}{S_{w_{irr}}} \right)^2 \quad \text{(Equation B.15; Morris & Biggs, 1967)}$$

$$k = 100 \times \left(\frac{\phi_e^2}{S_{w_{irr}}^2} \right) \quad \text{(Equation B.16; modified Tixier, 1949)}$$

$$k = 300 \times \left(\frac{\phi_e^2 \times (1 - S_{w_{irr}})}{S_{w_{irr}}} \right) \quad \text{(Equation B.17; modified Coates, 1981)}$$

$$k = \left(\frac{300}{m^2} \right) \times \left(\frac{\phi_e^2}{S_{w_{irr}}^2} \right) \quad \text{(Equation B.18; Coates & Dumanoir, 1974)}$$

Where: k – permeability, $S_{w_{irr}}$ – Irreducible water saturation, ϕ_e – effective porosity, m – cementation exponent.

Figure B.10 shows a comparison of the different permeability estimates in well P. Throughout Formation-A the four permeability curves show similar features and record variable magnitude changes downhole which correlate well to core data. In Formation-B to -D equations B.15-16 show a decade higher permeability than equations B.17-18, except for Formation-C where all models follow the same pattern. Limited core data for Formation-B to -D have hindered ground truthing of this variation, plotting all available core data from other Panna well has increased this dataset and allowed more robust correlation to be performed (figure B.11). Although in cross plot the Coates (1981) equation reproduces the spread of data points captured in core, when plotted against depth we can see much larger-scale variation than expected. In this work the Morris & Briggs (1967) model of permeability is used and provides a best fit for the available data.

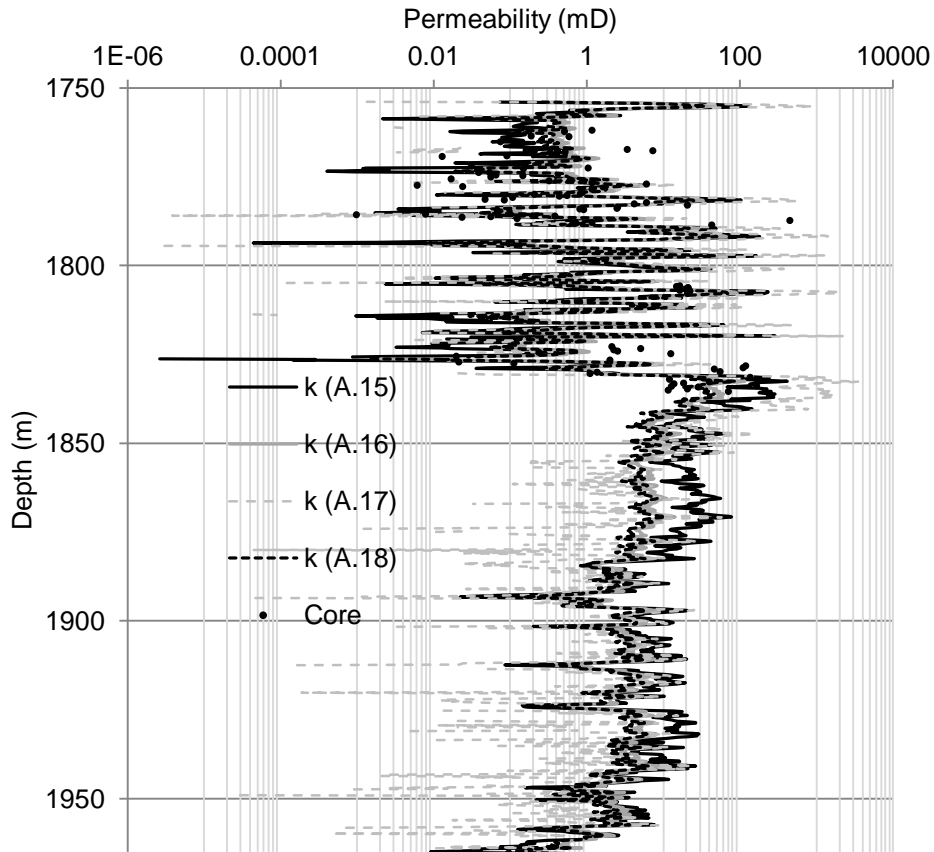


Figure B.10. Depth plot of the four log-derived permeability models for well P. Equations are given in the text above.

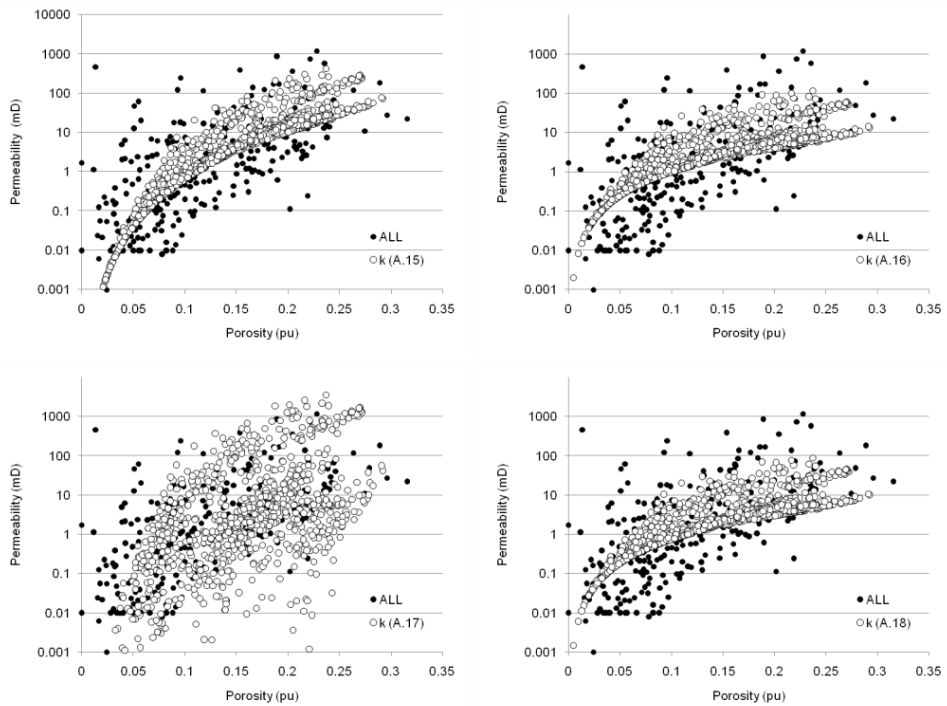


Figure B.11. Porosity-Permeability cross plots. Closed circles – available routine core analysis data from Panna field, open circles – log-derived porosity and permeability data. Permeability equations given in text above.

B.5. Fluid Flow Zones

A flow unit or zone is a formation zone with similar hydraulic characteristics, that can be identified and characterised from its petrophysical properties (Tiab & Donaldson 1996). Characterisation can be completed on both core and well log-derived data, particularly porosity and permeability. For the case of the analysis of the overall Panna data, with limited core data in Formation-A and -B, flow unit analysis is completed on the log-derived data. Two main techniques are identified in the literature for flow zone analysis; Hydraulic Units (Amaefule *et al.* 1993) and stratigraphic modified Lorenz plots (Gunter *et al.* 1997).

“A hydraulic unit is the representative elementary volume of total reservoir rock within which geological and petrophysical properties that affect fluid flow are internally consistent and predictably different from properties of other rock volume” (Amaefule *et al.* 1993). This technique is based on the Kozeny-Carmen permeability equation, and was primarily developed to aid permeability prediction from well log and core data. Three key derived values are required; reservoir quality index (*RQI*), pore volume-to-grain volume ratio (ϕ_z), and the flow zone indicator (*FZI*), these are detailed in equations B.19-21. Note that in equation B.19 constant 0.0314 is used to convert permeability from millidarcies to μm^2 as per Kozeny-Carmen (Amaefule *et al.* 1993).

$$RQI = 0.0314 \times \sqrt{\frac{k}{\phi_e}} \quad (\text{Equation B.19})$$

$$\phi_z = \left(\frac{\phi_e}{1-\phi_e} \right) \quad (\text{Equation B.20})$$

$$FZI = \frac{RQI}{\phi_z} \quad (\text{Equation B.21})$$

Where: *k* – permeability, ϕ_e – effective porosity, *RQI* – reservoir quality index, ϕ_z – pore volume-to-grain volume ratio, *FZI* – flow zone indicator.

Histograms or cumulative frequency plots of log (*FZI*) values, sorted from low to high, are then used to determine the number of hydraulic units (figure B.12). Here, log (*FZI*) is used to aid the capture of a normal distribution. Hydraulic unit values are presented in table B.5, dividing the complete Panna succession into ten hydraulic types (figure B.13).

	HU1	HU2	HU3	HU4	HU5	HU6	HU7	HU8	HU9	HU10
FZI	0.03	0.06	0.10	0.16	0.20	0.79	1.78	5.01	11.22	15.85

Table B.5. Hydraulic unit threshold values from well log-derived *FZI* plots.

Plotting hydraulic units against depth reveals several flow units with transmissive upper and storage-type lower sections (figure B.13). These are displayed in figure B.16, and discussed with the results of the stratigraphic modified Lorenz plot.

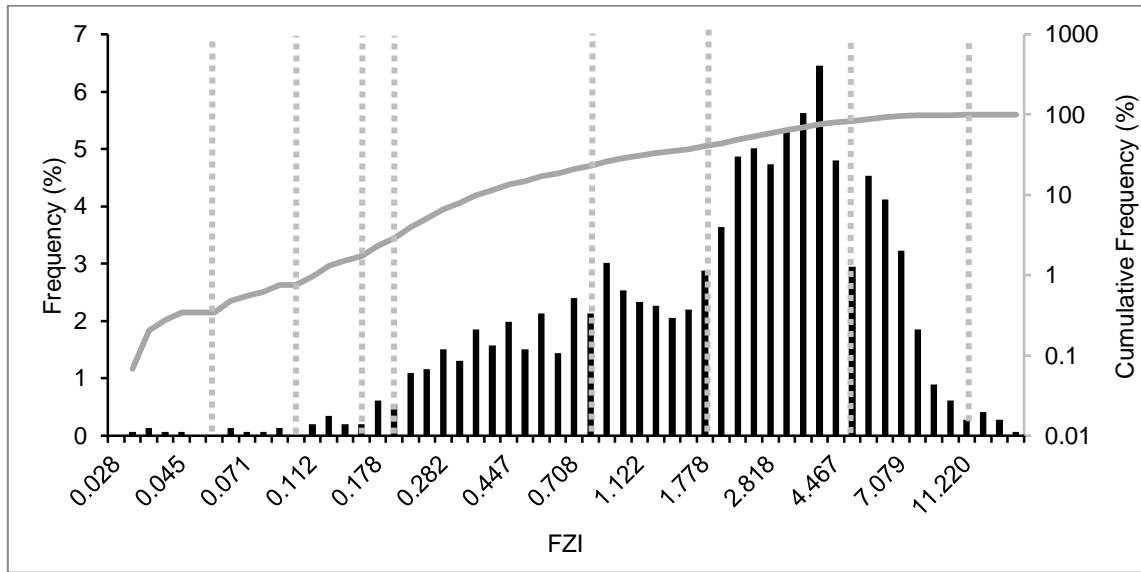


Figure B.12. Frequency histogram and cumulative frequency plot for log-derived *FZI* values of well P. Picked hydraulic unit values are indicated by the vertical gray dotted lines (table B.5).

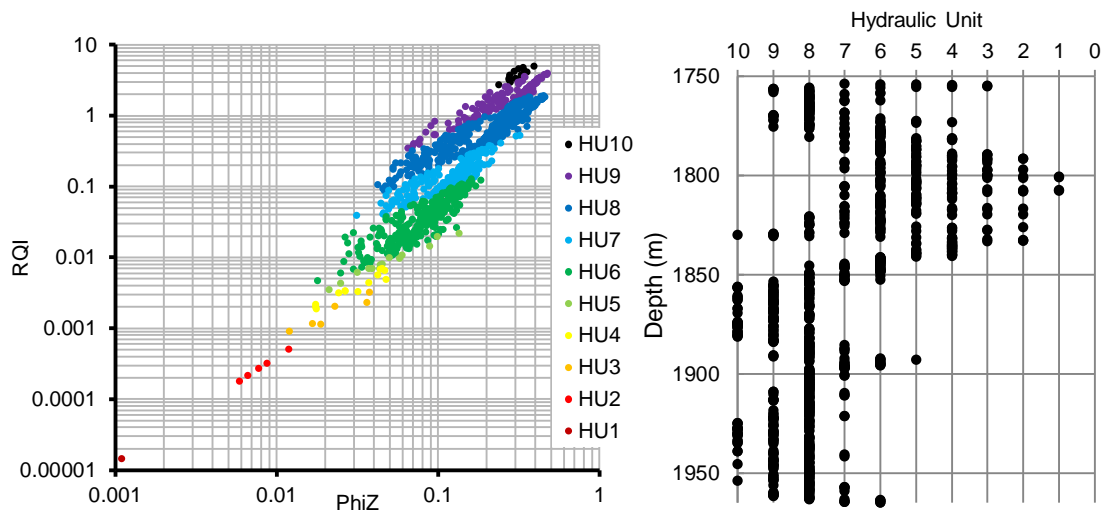


Figure B.13. Left – log-log $RQI-\Phi_z(\Phi_iZ)$ plot showing reservoir quality increases from hydraulic unit 1 to 10. Right – hydraulic unit-depth plot. Note HU 10 is highest quality, and HU 1 is lowest quality.

The basic Lorenz plot is used to detail heterogeneity in poro-perm data prior to modelling. Here porosity and permeability data are sorted from small to large values before cumulative values are cross plotted. This is discussed further in chapter 4. The stratigraphic modified Lorenz (SML) plot displays cumulative storage capacity (porosity x measurement interval) and flow capacity (permeability x measurement interval) through a succession, without sorting, so that original stratigraphic order is maintained (figure B.14). In this plot a steep gradient (slope $>45^\circ$)

shows permeability increases more than porosity and so indicates a transmissive unit, the reverse is true for shallow gradients (slope <math><45^\circ</math>) which indicate storage units, or *barriers*. A flow zone is therefore comprised of a transmissive and barrier unit (Gunter *et al.* 1997). A clear relationship can be seen between barrier units and low flow capacity; low reservoir quality lithologies such as siltstone and shales (Pranter *et al.* 2004). Figure B.14 (right) has been annotated to illustrate this zonation.

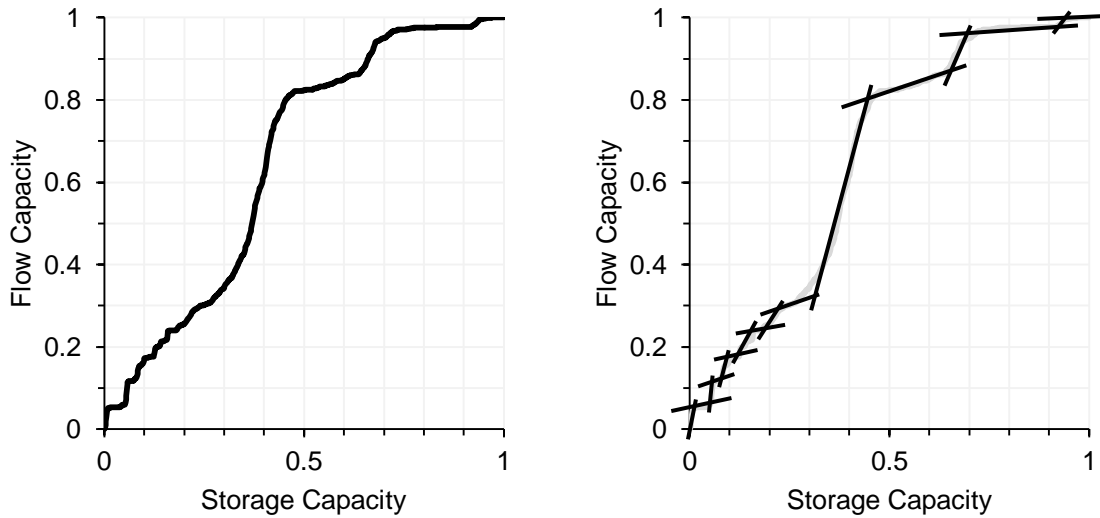


Figure B.14. Stratigraphic modified Lorenz plot for well P log-derived porosity and permeability data. Left – original plot, right – annotated plot to illustrate transmissive and barrier units.

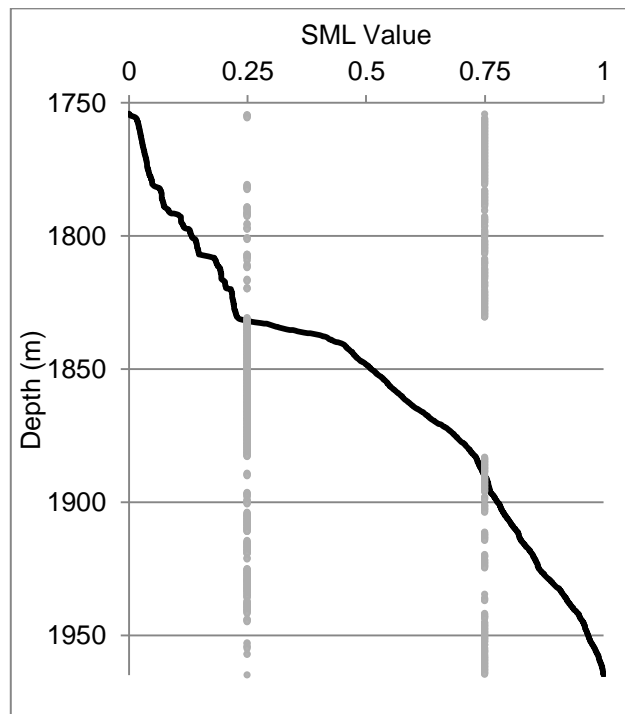


Figure B.15. SML depth plot for well log-derived porosity and permeability data of well P.

As these plots display cumulative normalised data, the top of the well is at (0,0) and the bottom of the succession is at (1,1). To aid interpretation it was decided to plot the SML variability against depth (figure B.15), by averaging the flow and storage capacity values for each depth. The two plots show the same features. In figure B.15 an increase in the SML value (a shallow gradient) shows transmissive units, while decreasing and steep trend indicates the presence of a barrier. To further constrain unit depths, slope is converted to an angle (based on Pythagoras theorem). On figure B.15 points with a slope less than 45° are shown by grey dots at 0.25 SML value, while other angles are plotted at 0.75 SML value.

Figure B.16 shows FZI, Hydraulic units and the SML depth plots. The three flow unit indicators have been used to pick an optimal number of fluid flow zones based on sharp contrasts in properties; i.e. significant breaks in slope of the SML plot.

Flow Zone Number	Top Depth (m)	Bottom Depth (m)
FZ1	1754.0	1778.6
FZ2	1778.6	1786.0
FZ3	1786.0	1804.6
FZ4	1804.6	1827.6
FZ5	1827.6	1853.4
FZ6	1853.4	1882.0
FZ7	1882.0	1894.4
FZ8	1894.4	1923.0
FZ9	1923.0	1953.0
FZ10	1953.0	1964.8

Table B.6. Depth of the 10 flow zones of well P (see figure B.16).

At this scale, looking at the complete succession, some of the finer-scale flow units in Formation-A have been can grouped together (such as those of flow zone 3 & 4). Comparing the three techniques it is clear that detail is lost in the SML plot technique. This is of particular importance in flow zone 5-6 where the general trend of transmissive-barrier is obvious, however the sharp contrast in FZI and hydraulic units led to the decision to break this unit into two.

Amaefule *et al.* (1993) state that hydraulic units may be defined by geological attributes as well as petrophysical properties. We now discuss how fluid flow and geological zones are related. Fluid flow zones show broad correlation with the geological zonations

Formation-A corresponds to FZ1-4, although it is noted that the highly heterogeneous character of Formation-A is reflected in FZ3 and 4 where numerous small-scale flow zones are grouped together (expanded in chapter 6). The bottom of FZ4 overlaps into Formation-B, where the basal unconformity /palaeokarst is clearly represented in the log data.

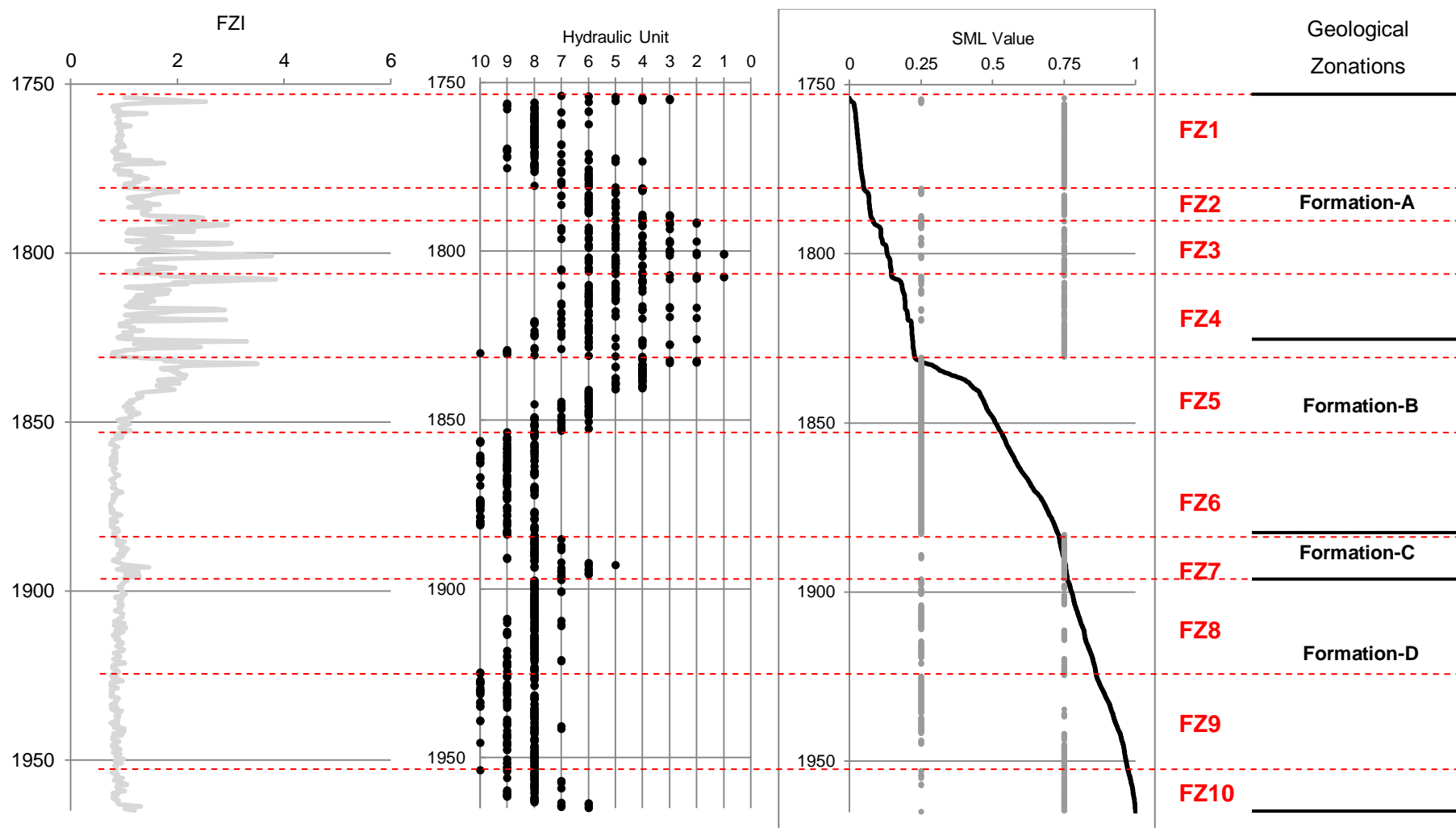


Figure B.16. Left – flow zone indicator depth plot, centre – hydraulic units depth plot, right – stratigraphic modified Lorenz depth plot for well log-derived porosity and permeability data of well P.

This suggests that the formal Formation-A/-B transition may not be as clearly represented in the physical property data. Formation-B corresponds to FZ5-6. As discussed above, SML suggests these are two parts of the same fluid flow zone, however sharp changes in the FZI and hydraulic units suggest a high contrast between a transmissive top (FZ5) and storage-based bottom (FZ6). Formation-C corresponds to FZ7. It is noted that this flow zone is suggested to have a high flow quality from the log analysis. However core data from elsewhere in the Panna field show the tight nature of this zone from mercury injection pore size distribution data (Khanna *et al.* 2007). Formation-D corresponds to flow units FZ8-10, indicating a higher flow quality top and bottom unit.

In summary the best flow zone potentials are identified in Formation-A and -B, because of thick high quality hydraulic units with high flow zone indicators.

Appendix C. Supplementary Data

C.1. Chapter 5: Offset Data Tables (see Table 5.1)

Comparing (XY)	0cm Offset (X & Y ₁)	20cm Offset (Y ₂)	40cm Offset (Y ₃)	60cm Offset (Y ₄)	80cm Offset (Y ₅)	100cm Offset (Y ₆)	120cm Offset (Y ₇)	140cm Offset (Y ₈)	160cm Offset (Y ₉)	180cm Offset (Y ₁₀)	Averages
Variance, s^2 (Y ₁₋₁₀)	0.0019	0.0018	0.0021	0.0026	0.0030	0.0032	0.0035	0.0031	0.0026	0.0022	0.0026
Covariance, s_{xy} (X/Y ₁₋₁₀)	0.0019	0.0014	0.0013	0.0012	0.0012	0.0012	0.0013	0.0014	0.0015	0.0017	0.0014
Correlation, R (X/Y ₁₋₁₀)	0.997	0.756	0.630	0.523	0.485	0.483	0.520	0.566	0.647	0.816	0.642
Coefficient of determination, R^2 (X/Y ₁₋₁₀)	0.995	0.572	0.396	0.274	0.235	0.233	0.271	0.320	0.419	0.666	0.438
t-Test	258.2	22.12	15.50	11.75	10.61	10.56	11.66	13.12	16.25	27.04	39.69
Significance Level (p)	0.001	0.001	0.001	0.001	0.001	0.001	0.001	0.001	0.001	0.001	0.001

Table C.1. Comparing the original gamma ray Lorenz H.Log data variability (X – 0cm offset), with subsequent offset data windows at 20cm increments (Y). For Formation-A, well P.

Comparing (XY)	0cm Offset (X & Y ₁)	20cm Offset (Y ₂)	40cm Offset (Y ₃)	60cm Offset (Y ₄)	80cm Offset (Y ₅)	100cm Offset (Y ₆)	120cm Offset (Y ₇)	140cm Offset (Y ₈)	160cm Offset (Y ₉)	180cm Offset (Y ₁₀)	Averages
Variance, s^2 (Y ₁₋₁₀)	8.4E-05	8.5E-05	7.4E-05	6.8E-05	6.5E-05	7.0E-05	7.4E-05	7.0E-05	9.2E-05	9.0E-05	7.7E-05
Covariance, s_{xy} (X/Y ₁₋₁₀)	8.4E-05	7.6E-05	6.4E-05	5.1E-05	4.0E-05	3.5E-05	3.8E-05	4.7E-05	6.4E-05	7.5E-05	5.7E-05
Correlation, R (X/Y ₁₋₁₀)	0.997	0.897	0.809	0.677	0.544	0.460	0.483	0.610	0.722	0.856	0.705
Coefficient of determination, R^2 (X/Y ₁₋₁₀)	0.995	0.805	0.655	0.458	0.295	0.212	0.233	0.372	0.521	0.733	0.528
t-Test	258.27	38.87	26.38	17.60	12.39	9.91	10.54	14.71	19.94	31.72	44.03
Significance Level (p)	0.001	0.001	0.001	0.001	0.001	0.001	0.001	0.001	0.001	0.001	0.001

Table C.2. Comparing the original bulk density Lorenz H.Log data variability (X – 0cm offset), with subsequent offset data windows at 20cm increments (Y). For Formation-A, well P.

Comparing (X/Y)	0cm Offset (X & Y ₁)	20cm Offset (Y ₂)	40cm Offset (Y ₃)	60cm Offset (Y ₄)	80cm Offset (Y ₅)	100cm Offset (Y ₆)	120cm Offset (Y ₇)	140cm Offset (Y ₈)	160cm Offset (Y ₉)	180cm Offset (Y ₁₀)	Averages
Variance, s^2 (Y ₁₋₁₀)	0.0062	0.0056	0.0055	0.0067	0.0086	0.0095	0.0101	0.0089	0.0080	0.0071	0.0076
Covariance, s_{xy} (X/Y ₁₋₁₀)	0.0061	0.0045	0.0034	0.0029	0.0029	0.0028	0.0033	0.0038	0.0046	0.0055	0.0040
Correlation, R (X/Y ₁₋₁₀)	0.997	0.771	0.585	0.446	0.396	0.366	0.417	0.508	0.650	0.828	0.596
Coefficient of determination, R^2 (X/Y ₁₋₁₀)	0.995	0.595	0.343	0.199	0.156	0.134	0.174	0.258	0.422	0.686	0.396
t-Test	258.27	23.20	13.81	9.53	8.24	7.53	8.77	11.28	16.35	28.28	38.53
Significance Level (p)	0.001	0.001	0.001	0.001	0.001	0.001	0.001	0.001	0.001	0.001	0.001

Table C.3. Comparing the original neutron porosity Lorenz H.Log data variability (X – 0cm offset), with subsequent offset data windows at 20cm increments (Y). For Formation-A, well P.

Comparing (X/Y)	0cm Offset (X & Y ₁)	20cm Offset (Y ₂)	40cm Offset (Y ₃)	60cm Offset (Y ₄)	80cm Offset (Y ₅)	100cm Offset (Y ₆)	120cm Offset (Y ₇)	140cm Offset (Y ₈)	160cm Offset (Y ₉)	180cm Offset (Y ₁₀)	Averages
Variance, s^2 (Y ₁₋₁₀)	4.1E-04	3.3E-04	2.7E-04	2.4E-04	2.2E-04	1.9E-04	2.5E-04	3.0E-04	3.9E-04	4.3E-04	3.0E-04
Covariance, s_{xy} (X/Y ₁₋₁₀)	4.1E-04	3.2E-04	2.4E-04	1.8E-04	1.6E-04	1.4E-04	1.7E-04	2.2E-04	3.1E-04	3.7E-04	2.5E-04
Correlation, R (X/Y ₁₋₁₀)	0.997	0.880	0.725	0.587	0.537	0.502	0.538	0.638	0.767	0.887	0.706
Coefficient of determination, R^2 (X/Y ₁₋₁₀)	0.995	0.775	0.525	0.345	0.289	0.252	0.289	0.406	0.588	0.786	0.525
t-Test	258.27	35.46	20.11	13.88	12.18	11.11	12.21	15.83	22.85	36.72	43.86
Significance Level (p)	0.001	0.001	0.001	0.001	0.001	0.001	0.001	0.001	0.001	0.001	0.001

Table C.4. Comparing the original P-wave transit time Lorenz H.Log data variability (X – 0cm offset), with subsequent offset data windows at 20cm increments (Y). For Formation-A, well P.

Comparing (X/Y)	0cm Offset (X & Y ₁)	20cm Offset (Y ₂)	40cm Offset (Y ₃)	60cm Offset (Y ₄)	80cm Offset (Y ₅)	100cm Offset (Y ₆)	120cm Offset (Y ₇)	140cm Offset (Y ₈)	160cm Offset (Y ₉)	180cm Offset (Y ₁₀)	Averages
Variance, s^2 (Y ₁₋₁₀)	0.0124	0.0122	0.0094	0.0086	0.0086	0.0082	0.0095	0.0103	0.0105	0.0114	0.0101
Covariance, s_{xy} (X/Y ₁₋₁₀)	0.0124	0.0106	0.0075	0.0053	0.0044	0.0043	0.0054	0.0066	0.0082	0.0104	0.0075
Correlation, R (X/Y ₁₋₁₀)	0.997	0.862	0.697	0.515	0.428	0.426	0.495	0.585	0.719	0.870	0.659
Coefficient of determination, R^2 (X/Y ₁₋₁₀)	0.995	0.743	0.485	0.265	0.184	0.182	0.245	0.342	0.517	0.758	0.471
t-Test	258.27	32.52	18.58	11.50	9.07	9.01	10.91	13.79	19.77	33.82	41.72
Significance Level (p)	0.001	0.001	0.001	0.001	0.001	0.001	0.001	0.001	0.001	0.001	0.001

Table C.5. Comparing the original deep resistivity Lorenz H.Log data variability (X – 0cm offset), with subsequent offset data windows at 20cm increments (Y). For Formation-A, well P.

C.2. Chapter 6: Reservoir Quality – Heterogeneity Plots
(see Figure 6.26)

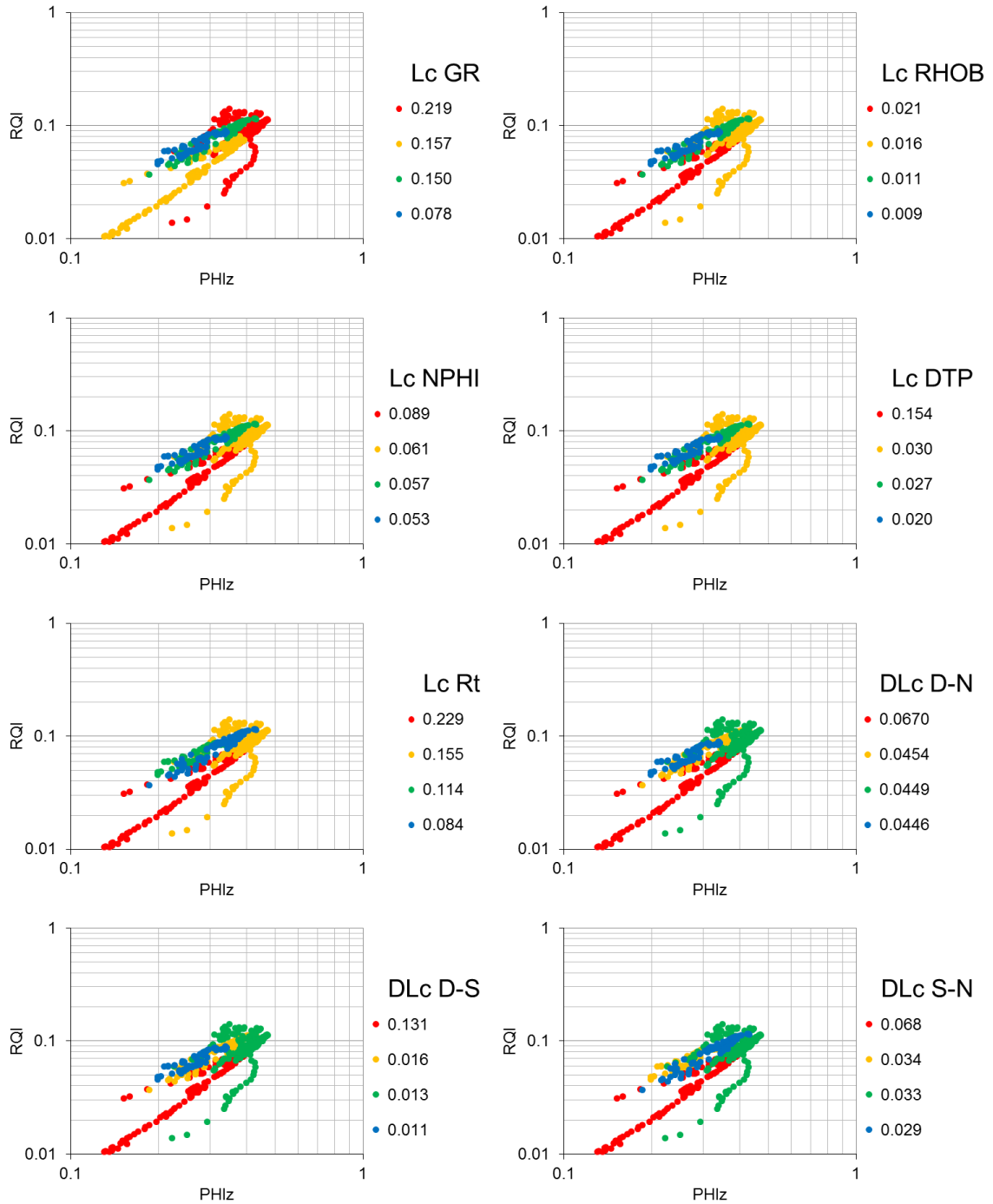


Figure C.1. Normalised porosity (PHIz) – reservoir quality index (RQI) plots illustrating relationship between numerical heterogeneity (Lorenz coefficient: Lc, and Dual Lorenz coefficient: DLc) and reservoir quality. For the Abiod chalk of well A. Heterogeneities: gamma ray (GR), bulk density (RHOB/D), neutron porosity (NPHI/N), P-wave transit time (DTP/S), and deep resistivity (Rt).

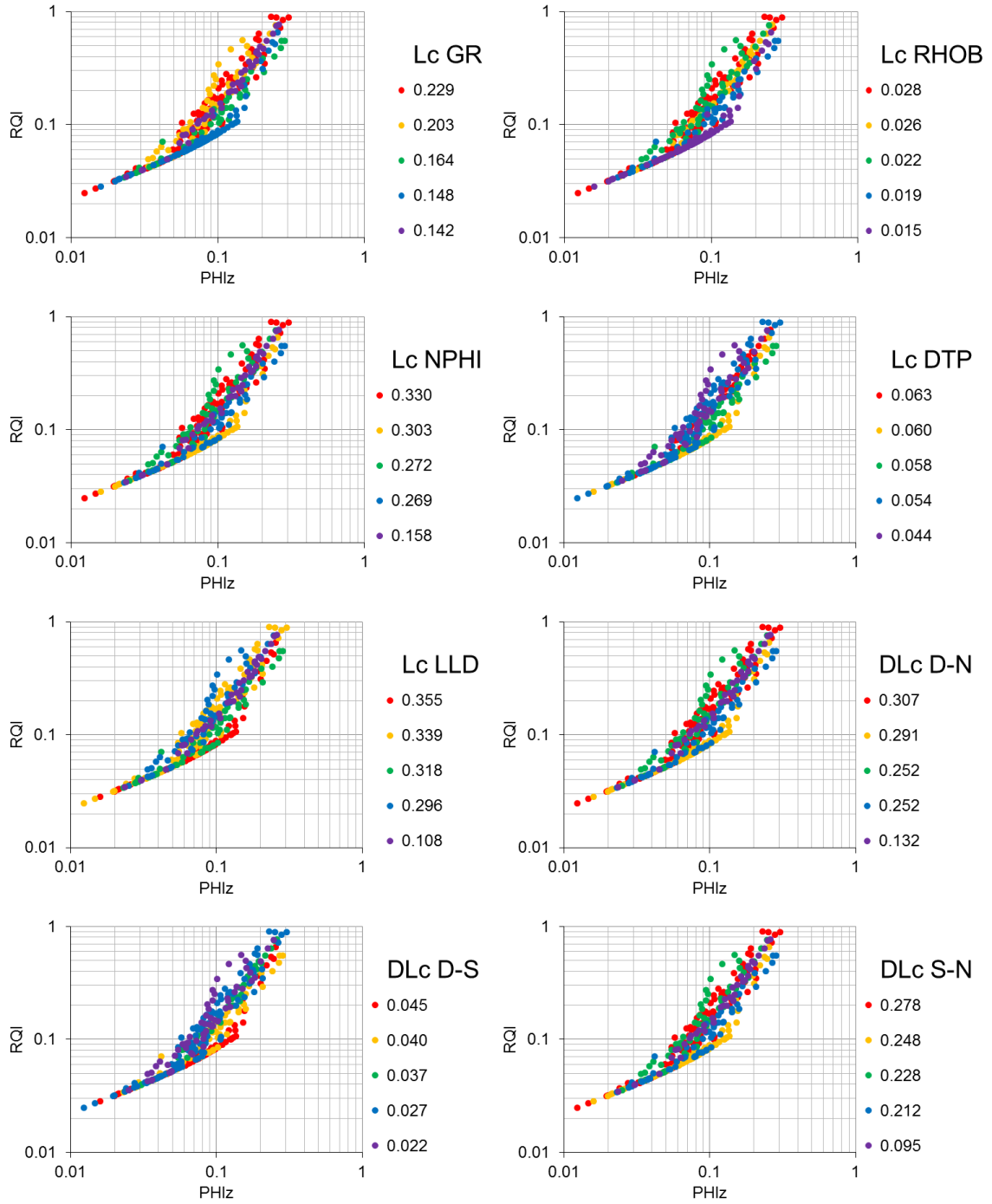


Figure C.2. Normalised porosity (PHIz) – reservoir quality index (RQI) plots illustrating relationship between numerical heterogeneity (Lorenz coefficient: Lc, and Dual Lorenz coefficient: DLc) and reservoir quality. For Formation-A of well P. Heterogeneities: gamma ray (GR), bulk density (RHOB/D), neutron porosity (NPHI/N), P-wave transit time (DTP/S), and deep resistivity (Rt).

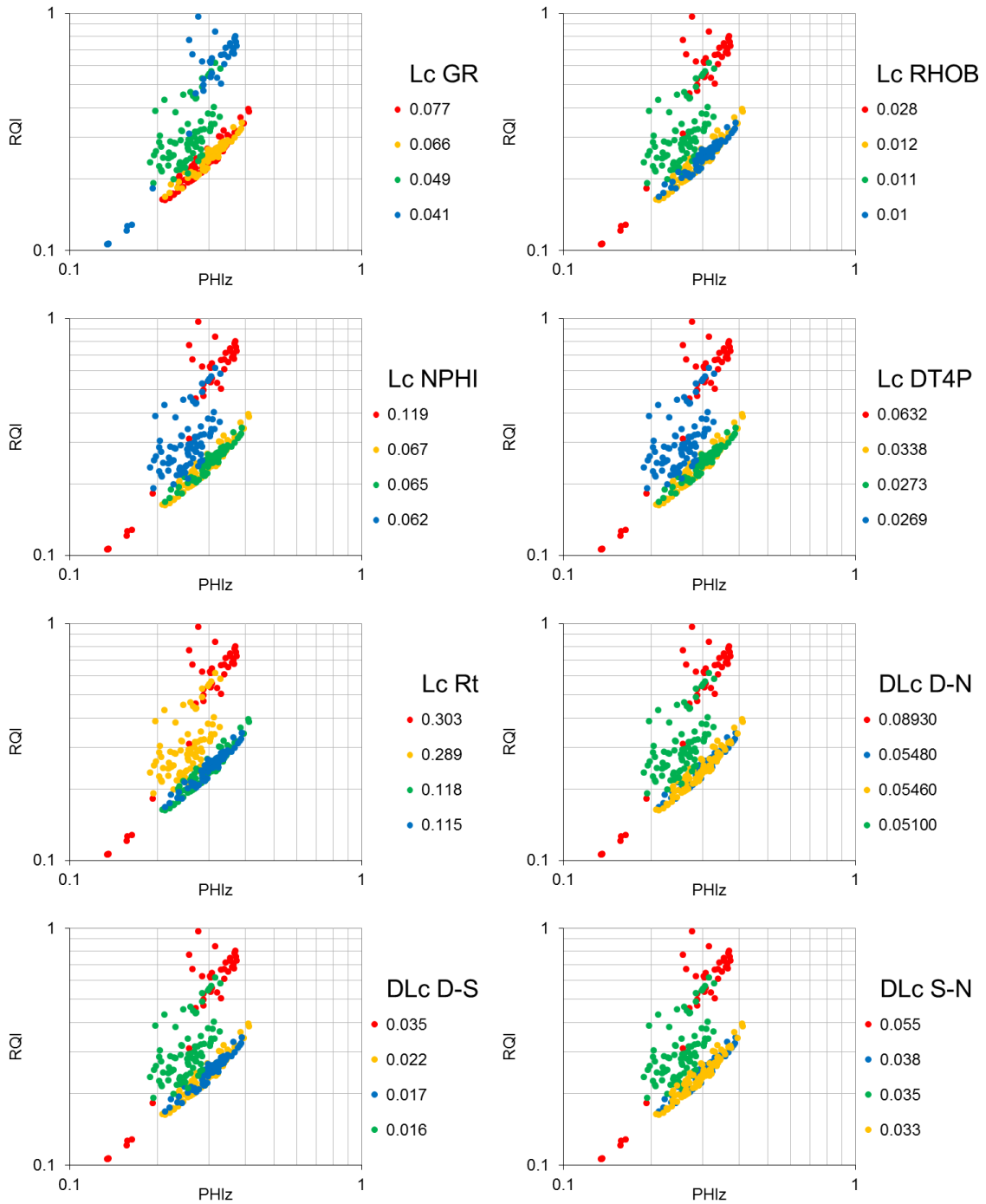


Figure C.3. Normalised porosity (PHIz) – reservoir quality index (RQI) plots illustrating relationship between numerical heterogeneity (Lorenz coefficient: Lc, and Dual Lorenz coefficient: DLc) and reservoir quality. For Formation-B of well P. Heterogeneities: gamma ray (GR), bulk density (RHOB/D), neutron porosity (NPHI/N), P-wave transit time (DTP/S), and deep resistivity (Rt).

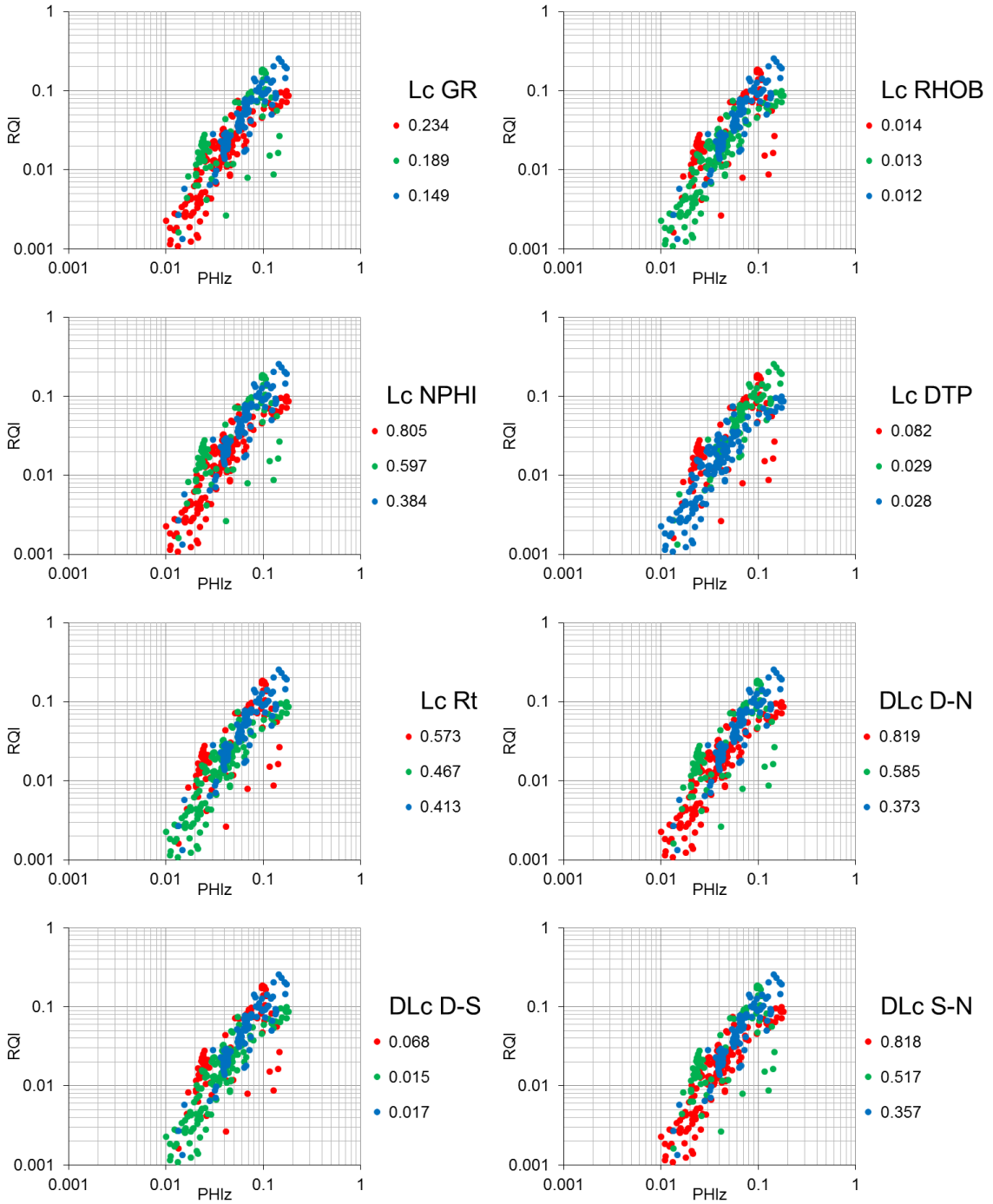


Figure C.4. Normalised porosity (PHIz) – reservoir quality index (RQI) plots illustrating relationship between numerical heterogeneity (Lorenz coefficient: Lc, and Dual Lorenz coefficient: DLc) and reservoir quality. For Formation-A of well M. Heterogeneities: gamma ray (GR), bulk density (RHOB/D), neutron porosity (NPHI/N), P-wave transit time (DTP/S), and deep resistivity (Rt).

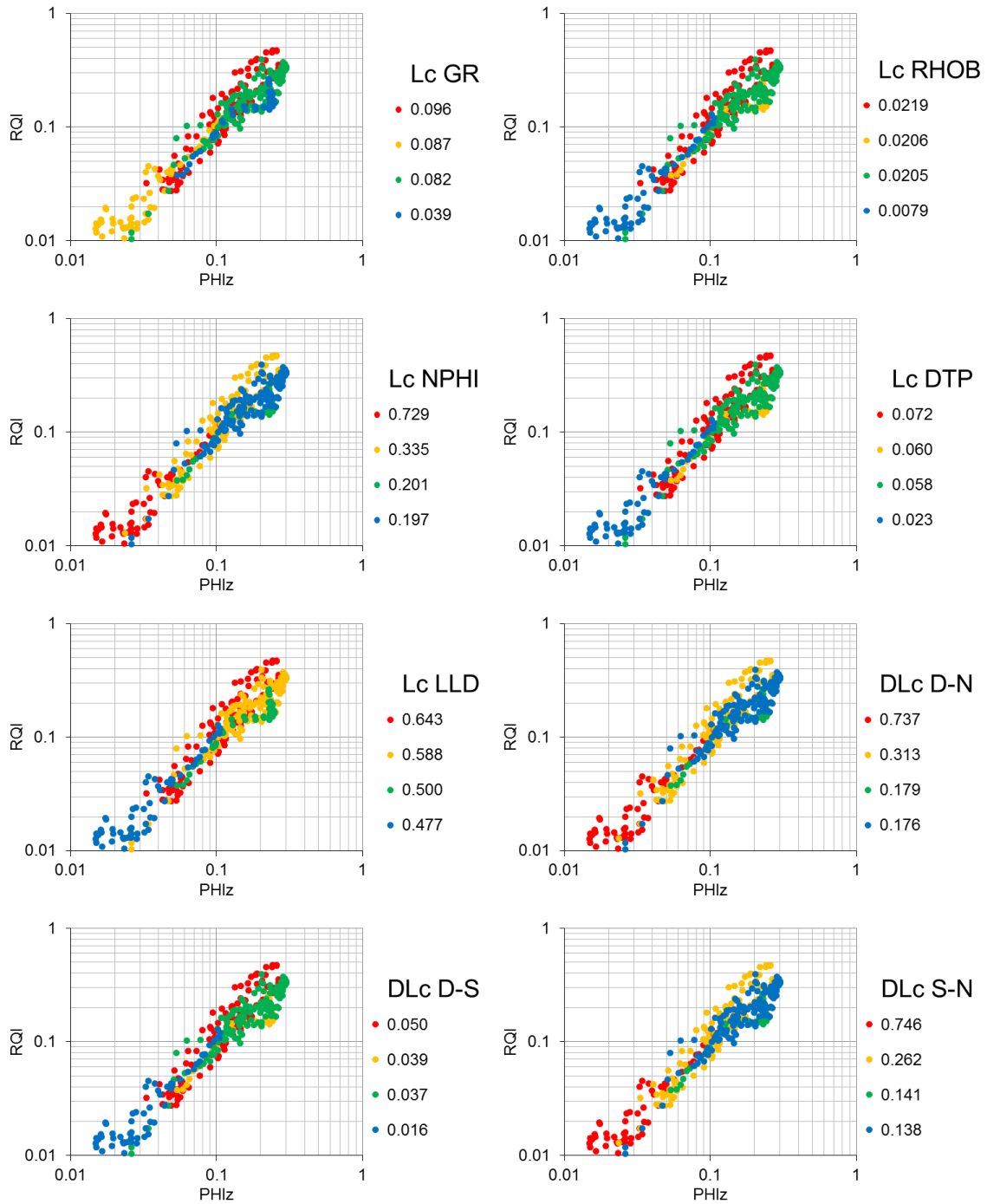


Figure C.5. Normalised porosity (PHIz) – reservoir quality index (RQI) plots illustrating relationship between numerical heterogeneity (Lorenz coefficient: Lc, and Dual Lorenz coefficient: DLc) and reservoir quality. For Formation-B of well M. Heterogeneities: gamma ray (GR), bulk density (RHOB/D), neutron porosity (NPHI/N), P-wave transit time (DTP/S), and deep resistivity (Rt).

Bibliography

- Aguilera, R. 2004. Integration of geology, petrophysics, and reservoir engineering for characterization of carbonate reservoirs through Pickett plots. *AAPG BULLETIN*, **88**, 433-446.
- Aguilera, R. 2006. Sandstone vs. Carbonate Petroleum Reservoirs: a global perspective on porosity-depth and porosity-permeability relationships: Discussion. *AAPG BULLETIN*, **90**, 807-810.
- Aguilera, R. & Aguilera, M. S. 2003. Improved Models for Petrophysical Analysis of Dual Porosity Reservoirs. *Petrophysics*, **44**, 1-15.
- Ahr, W. M., Allen, D., Boyd, A., Bachman, H. N., Smithson, T., Clerke, E. A., Gzara, K. B. M., Hassall, J. K., Murty, C. R. K., Zubari, H. & Ramamoorthy, R. 2005. Confronting the carbonate conundrum. *Oilfield Review*, **17**, 18-29.
- Akbar, M., Petricola, M., Watfa, M., Badri, M. A., Charara, M., Boyd, A., Cassell, B., Nurmi, R., Delhomme, J.-P., Grace, M., Kenyon, B. & Roestenburg, J. W. 1995. Classic interpretation problems; evaluating carbonates. *Oilfield Review*, **7**, 38-57.
- Akbar, M., Vissarpragada, B., Alghamdi, A. H., Allen, D., Herron, M., Carnegie, A., Dutta, D., Olesen, J.-R., Chourasiya, R. D., Logan, D., Steif, D., Netherwood, R., Russell, S. D. & Saxena, K. 2001. A snapshot of carbonate reservoir evaluation. *Oilfield Review*, **12**, 20-41.
- Alam, H., Paterson, D. W., Syarifuddin, N., Busono, I. & Corbin, S. G. 1999. Reservoir potential of carbonate rocks in the Kutai Basin region, east Kalimantan, Indonesia. *Journal of Asian Earth Sciences*, **17**, 203-214.
- Amaefule, J., Altunbay, M., Kersey, D. G. & D.K, K. 1993. Enhanced Reservoir Description: Using Core and Log Data to Identify Hydraulic (flow) Units and Predict Permeability in Uncored Intervals/Wells. *68th Annual Technical Conference and Exhibition of the Society of Petroleum Engineers*. Houston, Texas: SPE 26436.
- Anselmetti, F. S. & Eberli, G. 1999. The Velocity-Deviation Log: A tool to predict pore type and permeability trends in carbonate drill holes from sonic and porosity or density logs. *AAPG BULLETIN*, **83**, 450-466.
- Archie, G. E. 1942. The Electrical Resistivity Log as an Aid in Determining Some Reservoir Characteristics. *Petroleum Technology*, **5**, 54-62.
- Archie, G. E. 1952. Classification of carbonate reservoir rocks and petrophysical considerations. *Bulletin of the American Association of Petroleum Geologists*, **36**, 278-298.
- Asgari, A. A. & Sobhi, G. A. 2006. A fully integrated approach for the development of rock type characterization, in a middle east giant carbonate reservoir. *Journal of Geophysics and Engineering*, **3**, 260-270.
- Asquith, G. 1985. *Handbook of Log Evaluation Techniques for Carbonate Reservoirs*. ed.).The American Association of Petroleum Geologists, Tulsa, USA,
- Babadagli, T. & Al-Salmi, S. 2004. A review of permeability-prediction methods for carbonate reservoirs using well-log data. *Spe Reservoir Evaluation & Engineering*, **7**, 75 - 88.

- Beard, D. C. & Weyl, P. K. 1973. Influence of Texture on Porosity and Permeability of Unconsolidated Sand. *AAPG BULLETIN*, **57**, 349-369.
- Bhattacharya, S., Doveton, J. H., Carr, T. R., Guy, W. R. & Gerlach, P. M. 2005. Integrated core-log petrofacies analysis in the construction of a reservoir geomodel: A case study of a mature Mississippian carbonate reservoir using limited data. *AAPG BULLETIN*, **89**, 1257-1274.
- Borradaile, G. 2003. *Statistics of Earth Science Data: their distribution in Time, Space and Orientation*. ed.).Springer, Germany,
- Boya-Ferrero, M., Stephenson, B., Manoharan, J. & Dombrowski, A. 2004. The Al Kharrata East Field: integration solving the puzzle of a highly heterogeneous tight fractured carbonate reservoir. *SPWLA 45th Annual Logging Symposium*.
- Buckles, R. S. 1965. Correlationg and Averaging Connate Water Saturation Data. *The Journal of Canadian Petroleum*, **9**, 42-52.
- Burrows, N. & Thethi, J. 2010. *Press release: BG Group confirms high productivity from well tests on Tupi North-East in the Santos Basin, Brazil*. (<http://www.bg-group.com/MediaCentre/Press/Pages/24Mar2010.aspx>). [online]. World Wide Web.
- Cerepi, A., Barde, J. & Labat, N. 2003. High-resolution characterisation and integrated study of a reservoir formation: the danian carbonate platform in the Aquitaine Basin (France). *Marine and Petroleum Geology*, **20**, 1161-1183.
- Choquette, P. & Pray, I. 1970. Geologic nomenclature and classification of porosity in sedimentary carbonates. *AAPG BULLETIN*, **54**, 207-250.
- Coe, A. (ed.) 2003. *The Sedimentary Record of Sea-Level change*. ed.). Cambridge University Press, Cambridge,
- Corbett, P. W. M. & Jensen, J. L. 1992a. Estimating the mean permeability: how many measurements do you need? *First Break*, **10**.
- Corbett, P. W. M. & Jensen, J. L. 1992b. Variation of reservoir statistics according to sample spacing and measurement type for some intervals in the Lower Brent Group. *The Log Analyst*, **33**, p. 22-41.
- Davis, J. C. 2002. *Statistics and Data Analysis in Geology*. (3rd ed.).John Wiley & Sons, New York,
- Doveton, J. H. 1994. *Geologic Log Analysis Using Computer Methods*. ed.).AAPG, Tulsa,
- Duey, R. 2008. Logging and Formation Evaluation: Advice for carbonates. *E&P*, **8**.
- Dutilleul, P. 1993. Spatial heterogeneity and the design of ecological field experiments. *Ecology*, **74**, 1646-1658.
- Egermann, P. & Lenormand, R. 2005. A new methodology to evaluate the impact of localized heterogeneity on petrophysical parameter (relative permeability, capillary pressures) applied to carbonate rocks. *Petrophysics*, **45**, 335-345.
- Ehrenberg, S. N. 2004. Factors controlling porosity in Upper Carboniferous - Lower Permian carbonate strata of the Barents Sea. *AAPG BULLETIN*, **88**, 1653-1676.

- Ehrenberg, S. N. & Nadeau, P. H. 2005. Sandstone vs. carbonate petroleum reservoirs; a global perspective on porosity-depth and porosity-permeability relationships. *AAPG BULLETIN*, **89**, 435-445.
- Elkateb, T., Chalaturnyk, R. & Robertson, P. 2003. An overview of soil heterogeneity: quantification and implications on geotechnical field problems. *Canadian Geotechnical Journal*, **40**, 1-15.
- Ellis, D. V. & Singer, J. M. 2007. *Well Logging for Earth Scientists*. (2nd ed.).Springer, Netherlands,
- Estebaan, M. 1998. Porosity types and patterns in the Eocene-Oligocene Limestones of the Panna-Mukta areas, Bombay offshore, India. *Carbonates International*, 111p.
- Esteban, M. & Taberner, C. 2003. Secondary porosity development during late burial in carbonate reservoirs as a result of mixing and/or cooling of brines. *Journal of Geochemical Exploration*, **78-79**, 355-359.
- Frazer, G., Wulder, M. & Niemann, K. 2005. Simulation and quantification of the fine-scale spatial pattern and heterogeneity of forest canopy structure: A lacunarity-based method designed for analysis of continuous canopy heights. *Forest and Ecology Management*, **214**, 65-90.
- Frykman, P. 2001. Spatial variability in petrophysical properties in the Upper Maastrichtian chalk outcrops at Stevns Klint, Denmark. *Marine and Petroleum Geology*, **18**, 1041-1062.
- Frykman, P. & Deutsch, C. 2002. Practical application of geostatistical scaling laws for data integration. *Petrophysics*, **43**, 153-171.
- Ghafoori, M. R., Roostaerian, M. & Sajjadian, V. A. 2008. Secondary Porosity; a key parameter controlling the hydrocarbon production in heterogeneous carbonate reservoirs (case study). *SPWLA 49th Annual Logging Symposium, May 25-28, 2008*. Edinburgh, Scotland: SPWLA.
- Glennie, K. W., Mudd, G. C. & Nagtegaal, P. J. C. 1978. Depositional environment and diagenesis of Permian Rotliegendes sandstones in Leman Bank and Sole Pit areas of the UK southern North Sea. *Journal of the Geological Society*, **135**, p 25-34.
- Gomaa, N., Al-Alyak, A., Ouzzane, D., Saif, O., Okuyiga, M., Allen, D., Rose, D., Ramamoorthy, R. & Bize, E. 2006. Case Study of Permeability, Vug Quantification, and Rock Typing in a Complex Carbonate. *SPE Annual Technical Conference and Exhibition*. San Antonio, Texas: SPE 102888.
- Goswami, B. G., Singh, H., Bhatnagar, A. K., Sinha, A. K. & Singh, R. R. 2007. Petroleum Systems of the Mumbai Offshore Basin, India. *AAPG Annual Convention (April 1-4, 2007)*. Long Beach, California.
- Gribble, C. & Hall, A. 1999. *Optical Mineralogy: Principles and Practices*. ed.).UCL Press Limited, London,
- Gunter, G. W., Finneran, J. M., Hartmann, D. J. & Miller, J. D. 1997. Early determination of reservoir flow units using an integrated petrophysical method. *Proceedings of the Society of Petroleum Engineers Annual Technical Conference and Exhibition*, **SPE Paper 38679**, 373-380.

- Holmes, M., Holmes, D. & Holmes, A. 2009. Relationship between Porosity and Water Saturation: Methodology to Distinguish Mobile from Capillary Bound Water. *AAPG Annual Convention, June 7-10 2009*. Denver, Colorado: AAPG.
- Hook, J. R. 2003. An Introduction to Porosity. *Petrophysics*, **44**, 205-212.
- Hurley, N. F., Pantoja, D. & Zimmermann, R. A. 1999. Flow Unit Determination in a Vuggy Dolomite Reservoir, Dagger Draw Field, New Mexico. *SPWLA 40th Annual Logging Symposium*.
- Hurst, A. 1990. Natural gamma-ray spectrometry in hydrocarbon-bearing sandstones from the Norwegian Continental Shelf. In: Hurst, A., et al. (eds.) *Geological Applications of Wireline Logs, Geological Society Special Publications No. 48*. Geological Society of London, London, 211-222.
- Hurst, A. & Rosvoll, L. 1991. Permeability variations in sandstones and their relationship to sedimentary structures. In: Lake, L. W., et al. (eds.) *Reservoir Characterisation II*. Academic Press, San Diego, California, p 166-196.
- Jackson, P., Jarrard, R., CJ, P. & Pearce, J. 1995. Resistivity/Porosity/Velocity Relationships from Downhole Logs: an aid for evaluating pore morphology. *Proceedings of the Ocean Drilling Program, Scientific Results*, **133**, 661-681.
- Jennings, J. W. & Lucia, F. J. 2003. Predicting permeability from well logs in carbonates with a link to geology for interwell permeability mapping. *Spe Reservoir Evaluation & Engineering*, **6**, 215-225.
- Jensen, J. L., Lake, L. W., Corbett, P. W. M. & Goggin, D. J. 2000. *Statistics for Petroleum Engineers and Geoscientists*. (2nd ed.).Elsevier, London,
- Jensen, J. L., Thomas, S. D. & Corbett, P. W. M. 1997. On the bias and sampling variation of the harmonic average. *Mathematical Geology*, **29**, 267-276.
- Katahara, K. 2008. What is shale to a petrophysicist? *The Leading Edge*, **6**, 738-741.
- Kazatchenko, E., Markov, M., Mousatov, A. & Pervago, E. 2005. Simulation of the electrical resistivity of dual-porosity carbonate formations saturated with fluid mixtures. *46th Annual SPWLA Logging Symposium*. New Orleans, LA: Society of Petrophysicists & Well Log Analysts-Spwla.
- Kearey, P. 2001. *Dictionary of Geology*. (2nd ed.).Penguin Reference, London,
- Kennedy, M. C. 2002. Solutions to some problems in the analysis of well logs in carbonate rocks. In: Lovell, M. & Parkinson, N. (eds.) *Geological applications of wireline logs*. American Association of Petroleum Geologists, London United Kingdom, **13**, 61-73.
- Khanna, M., Rajput, E., Santaram, T. V. & Kakani, A. K. 2007. *G&G Modelling Status Report: Panna Field, India. February 2007. Proprietary Report*.
- Klett, T. R. 2001. *Total Petroleum Systems of the Pelagian Province, Tunisia, Libya, Italy, and Malta—The Bou Dabbous—Tertiary and Jurassic-Cretaceous Composite*. U.S. Geological Survey Bulletin 2202-D

- Knecht, L., Mathis, B., Leduc, J., Vandenabeele, T. & Di Cuia, R. 2004. Electrofacies and Permeability Modeling in Carbonate Reservoirs using Image Texture Analysis and Clustering Tools. *Petrophysics*, **45**, 27-37.
- Lake, L. & Jensen, J. 1991. A review of heterogeneity measures used in reservoir characterization. *In Situ*, **15**, 409-439.
- Larionov, V. V. 1969. *Borehole Radiometry*. ed.).Nedra, Moscow,
- Li, H. & Reynolds, J. 1995. On definition and quantification of heterogeneity. *Oikos*, **73**, 280-284.
- Lind, D. A., Marchal, W. G. & Wathen, S. A. 2010. *Statistical Techniques in Business and Economics*. (14th ed.).McGraw-Hill/Irwin, New York,
- Lonoy, A. 2006. Making sense of carbonate pore systems. *AAPG BULLETIN*, **90**, 1381-1405.
- Lovell, M. & Kennedy, M. C. 2005. *Rocks and Fluids: Practical Petrophysics*. ed.).Nautilus Ltd, Berkshire, UK,
- Lucia, F. J. 1983. Petrophysical parameters estimated from visual description of carbonate rocks: a field classification of carbonate pore space. *JOURNAL OF PETROLEUM GEOLOGY*, **35**, 626-637.
- Lucia, F. J. 1995. Rock-Fabric/Petrophysical Classification of Carbonate Pore Space for Reservoir Characterisation. *AAPG BULLETIN*, **79**, 1275-1300.
- Lucia, F. J. 1999a. *Carbonate Reservoir Characterization*. ed.).Springer, Germany,
- Lucia, F. J. 1999b. Characterization of petrophysical flow units in carbonate reservoirs: Discussion. *AAPG Bulletin-American Association of Petroleum Geologists*, **83**, 1161-1163.
- Lucia, F. J. 2000a. Dolomitisation: A Porosity-Destructive Process. *2000-2001 AAPG distinguished lecturers; abstracts AAPG Bulletin*, **84**, 1879.
- Lucia, F. J. 2000b. Origin and petrophysics of carbonate rock fabrics. *2000-2001 AAPG distinguished lecturers; abstracts AAPG Bulletin*, **84**, 1879.
- Lucia, F. J., R., B. C. J., Rizzi, G. & Darke, G. 2004. Origin and petrophysics of dolostone pore space. *The geometry and petrogenesis of dolomite hydrocarbon reservoirs Geological Society Special Publications*, **235**, 141-155.
- Mabrouk, A., Belayouni, H., Jarvis, I. & Moody, R. T. J. 2006. Strontium, $\delta^{18}\text{O}$ and $\delta^{13}\text{C}$ as palaeo-indicators of unconformities: Case of the Aleg and Abiod formations (Upper Cretaceous) in the Miskar Field, southeastern Tunisia. *Geochemical Journal*, **40**, 405-424.
- Maschio, C. & Schiozer, D. 2003. A new upscaling technique based on Dykstra-Parsons coefficient: evaluation with streamline reservoir simulation. *JOURNAL OF PETROLEUM SCIENCE AND ENGINEERING*, **40**, 27-39.
- Montaron, B. 2008a. Carbonate Evolution. *Oil & Gas Middle East*, 27-32.
- Montaron, B. 2008b. Confronting Carbonates. *Oil Review Middle East (ADIPEC 2008 Issue)*, **5**, 132-135.

- Moore, C. H. 2001a. Carbonate diagenesis and porosity; state of the art and its future. *American Association of Petroleum Geologists 2001 annual meeting Annual Meeting Expanded Abstracts - American Association of Petroleum Geologists*, **2001**, 137.
- Moore, C. H. 2001b. *Carbonate Reservoirs: Porosity evolution and diagenesis in a sequence stratigraphic framework*. ed.).Elsevier, Amsterdam,
- Moore, C. H. & Becker, J. W. 1977. Diagenetic Constraints on use of Predictive Sedimentary Models in Exploration-Exploitation of Carbonate Reservoirs. *AAPG BULLETIN*, **61**, 815-816.
- Moore, C. H., Caline, B. & Belonin, M. 1999. Carbonate Reservoirs: Strategies for the Future. *AAPG BULLETIN*, **83**, x.
- Morris, R. L. & Biggs, W. P. 1967. Using log-derived values of water saturation and porosity. *Transactions of SPWLA, 8th Logging Symposium. June 12-14 1967. Paper X. p. 1-26.*
- Naik, G. C., Gandhi, D., Singh, A. K., Banerjee, A. N., Joshi, P. & Mayor, S. 2006. Paleocene-to-early Eocene tectono-stratigraphic evolution and paleogeographic reconstruction of Heera-Panna-Bassein, Bombay Offshore Basin *The Leading Edge*, **25**, 1071-1077.
- Nichols, G. 2001. *Sedimentology and Stratigraphy*. ed.).Blackwell Science Ltd, Oxford,
- Nurmi, R., Charara, M., Waterhouse, M. & Park, R. 1990. Heterogeneities in carbonate reservoirs: detection and analysis using borehole electrical imagery. *In: Hurst, A., et al. (eds.) Geological applications of wireline logs. Geological Society Special Publications, London*, **48**, 95-111.
- Ozkaya, S. I., Lewandoswki, H. J. & Coskun, S. B. 2007. Fracture study of a horizontal well in a tight reservoir - Kuwait. *JOURNAL OF PETROLEUM SCIENCE AND ENGINEERING*, **55**, 6-17.
- Pomar, L. & Ward, W. 1999. Reservoir-scale Heterogeneity in depositional packages and diagenetic patterns on a reef-rimmed platform, Upper Miocene, Mallorca, Spain. *AAPG BULLETIN*, **83**, 1759-1773.
- Poppelreiter, M. C., Balzarini, M. A., Hansen, B. & Nelson, R. 2008. Realizing complex carbonate facies, diagenetic and fracture properties with standard reservoir modelling software. *In: Robinson, A., et al. (eds.) The Future of Geological Modelling in Hydrocarbon Development. The Geological Society of London, Special Publications, 309, London*, 39-49.
- Poupon, A. & Leveaux, J. 1971. Evaluation of Water Saturation in Shaly Formations. *SPWLA 12th Annual Logging Symposium*.
- Pranter, M., Hirstius, C. & Budd, D. 2005. Scales of lateral petrophysical heterogeneity in dolomite lithofacies as determined from outcrop analogues: Implications for 3D reservoir modeling. *AAPG BULLETIN*, **89**, 645-662.
- Pranter, M. J., Hurley, N. F. & Davis, T. L. 2004. Sequence-Stratigraphic, Petrophysical, and Multicomponent Seismic Analysis of a Shelf-Margin Reservoir: San Andres Formation (Permian), Vacuum Field, New Mexico, United States. *In: Eberli, G. P., et al. (eds.) Seismic Imaging of Carbonate Reservoirs and Systems: AAPG Memoir 81. American Association of Petroleum Geologists, Tulsa, Oklahoma*, 55-89.
- Pritchard, T. 2002. *Petrophysical Evaluation: Miskar Gas Field, Tunisia, Proprietary Report*.

- Qi, L. & Carr, T. R. 2006. Neural network prediction of carbonate lithofacies from well logs, Big Bow and Sand Arroyo Creek fields, Southwest Kansas. *Computers & Geosciences*, **32**, p. 947-964.
- Questiaux, J., Couples, G. D. & Ruby, N. 2010. Fractured Reservoirs with fracture corridors. *Geophysical Prospecting*, **58**, 279-295.
- Raddadi, M. C., Vanneau, A. A., Poupeau, G., Carrio-Schaffhauser, E., Arnaud, H. & Rivera, A. 2005. Interpretation of gamma-ray logs: The distribution of uranium in carbonate platform. *Comptes Rendus Geoscience*, **337**, 1457-1461.
- Ragland, D. 2002. Trends in cementation exponents (m) for carbonate pore systems. *Petrophysics*, **43**, 434-446.
- Ramamoorthy, R., Boyd, A., Neville, T. J., Seleznev, N., Sun, H., Flaum, C. & Ma, J. 2008. A New Workflow for Petrophysical and Textural Evaluation of Carbonate Reservoirs. *SPWLA 49th Annual Logging Symposium, May 25-28, 2008*. Edinburgh, Scotland: SPWLA.
- Reading, H. 1996. *Sedimentary Environments: Processes, Facies and Stratigraphy*. ed.).Blackwell Science Ltd, Oxford,
- Reddy, G. V., Kumar, P., Naik, S. B. R., Murthy, G. N., Vandana, Kaul, S. K. & Bhowmick, P. K. 2004. Reservoir Characterization Using Multi Seismic Attributes in B-172 Area of Heera-Panna-Bassein Block of Bombay Offshore Basin, India. *5th Conference & Exposition on Petroleum Geophysics*. India: Hyderabad-2004.
- Rider, M. 2002. *The Geological Interpretation of Well Logs*. (2 ed.).Rider-French Consulting Ltd., Sunderland,
- Rogers, J. J. W. & Head, W. B. 1961. Relationships between porosity, median size and sorting coefficients of synthetic sands. *Journal of Sedimentary Petrology*, **31**, 467-470.
- Rose, D., Hansen, P., Damgaard, A. & Raven, M. 2003. A novel approach to the real time detection of facies changes in horizontal carbonate wells using LWD NMR. *SPWLA 44th Annual Logging Symposium*.
- Rossiter, D. G. 2009. *Technical Note: Optimal partitioning of Soil Transects with R*. [online]. World Wide Web Address: http://www.itc.nl/~rossiter/teach/R/R_OptPart.pdf.
- Sadras, V. & Bongiovanni, R. 2004. Use of Lorenz curves and Gini coefficients to assess yield inequality within paddocks. *Field Crops Research*, **90**, 303-310.
- Saggaf, M. M. & Nebrija, E. L. 2000. Estimation of lithologies and depositional facies from wireline logs. *AAPG BULLETIN*, **84**, p. 1633-1646.
- Selly, R. C. 1998. *Elements of Petroleum Geology*. (2nd ed.).Academic Press Limited, London, U.K.,
- Serra, O. 1986. *Fundamentals of Well-Log Interpretation; 2. the interpretation of logging data*. ed.).Elsevier, Pau,
- Serra, O. & Serra, L. 2003. *Well Logging and Geology*. ed.).Serralog, France,

- Simandoux, P. 1963. Mesures Dielectriques en Milieu Poreux, Application a Mesure des Saturation en Eau, Etude du Comportement des Massifs Argileux. *Revue de l'Institut Francais du Petrole*, **Supplementary Issue**.
- Skalinski, M., Gottlib-Zeh, S. & Moss, B. 2005. Defining and predicting rock types in carbonates - Preliminary results from an integrated approach using core and log data from the Tengiz Field. *46th Annual SPWLA Logging Symposium*. New Orleans, LA: Society Petrophysicists & Well Log Analysts-Spwla.
- Sundberg, K. 1932. Effects of impregnating waters on electrical conductivity of soils or rocks. *Trans. AIME*, **97**, 367-391.
- Tabanou, J., Chabernaud, T., Goswami, J., Li, J., Horkowitz, J. P., Jacobsen, S., Neville, T. & Seydoux, J. 2004. How certain are we about reservoir parameter uncertainties? *SPWLA 45th Annual Symposium*.
- Taylor, K. 2003. *BG Tunisia: Miskar, Proprietary Report*.
- Thakre, A. N., Badarinadh, V. & Rajeev, K. 1997. Reservoir Heterogeneities of Bassein B-Limestone of Panna Field and the Need for Optimized Well Completions for Efficient Oil Recovery. *Proceedings Second Int. Pet. Conf.* New Delhi: PETROTECH-97.
- Tiab, D. & Donaldson, E. 1996. *Petrophysics: theory and practice of measuring reservoir rock and fluid properties*. ed.).Gulf Publishing Company, Houston,
- Timur, A. 1968. An investigation of permeability, porosity, and residual water saturation relationships for sandstone reservoirs. *The Log Analyst*, **9**, 8-17.
- Tixier, M. P. 1949. Evaluation of permeability from electric-log resistivity gradients. *Oil & Gas Journal*, p. 113.
- Tucker, M. & Wright, V. 1990. *Carbonate Sedimentology*. ed.).Blackwell Science Ltd, Oxford,
- Ulu, M. & Karahanoglu, N. 1998. Characterisation of the Karababa-C reservoir in the South Karakus oilfield, southeast Turkey. *Marine and Petroleum Geology*, **15**, 803-820.
- Wandrey, C. J. 2004. Bombay Geologic Province Eocene to Miocene Composite Total Petroleum System, India. In: Wandrey, C. J. (ed.) *Petroleum Systems and Related Geologic Studies in Region 8, South Asia*. U.S Geological Survey.
- Watfa, M., Standen, E., Petricola, M., Dennis, B. & Boyd, A. 1997. The Carbonate Challenge. *Middle East Well Evaluation Review*, **20**, 35-55.
- Webster, R. 1973. Automatic soil-boundary location from transect data. *Mathematical Geology*, **29**, p388-402.
- Weisstein, E. W. 2010. "Radian." *From MathWorld--A Wolfram Web Resource*. <http://mathworld.wolfram.com/Radian.html>. [online]. World Wide Web.
- Westphal, H., Eberli, G., Smith, L., Grammer, G. & Kislak, J. 2004. Reservoir characterisation of the Mississippian Madison Formation, Wind River basin, Wyoming. *AAPG BULLETIN*, **88**, 405-432.

- Wilson, M. E. J. & Evans, M. J. 2002. Sedimentology and diagenesis of Tertiary carbonates on the Mangkalihat Peninsula, Borneo: implications for subsurface reservoir quality. *Marine and Petroleum Geology*, **19**, 873-900.
- Winsauer, W. O., Shearing, H. M., Masson, P. H. & Williams, M. 1952. Resistivity of brine saturated sands in relation to pore geometry. *AAPG BULLETIN*, **36**, 253-277.
- Worthington, P. F. & Cosentino, L. 2005. The Role of Cutoffs in Integrated Reservoir Studies (SPE 84387). *2003 SPE Annual Technical Conference and Exhibition*. Denver.
- Wright, V. 2007. *Report on Sedimentological Studies of Mukta and Panna Cores, Proprietary Report*.
- Zampetti, V., Sattler, U. & Braaksma, H. 2005. Well log and seismic character of Liuhua 11-1 Field, South China Sea; relationship between diagenesis and seismic reflections. *Sedimentary Geology*, **175**, 217-236.
- Zheng, S. Y., Corbett, P. W. M. & Emery, A. 2003. Geological interpretation of well test analysis: A case study from a fluvial reservoir in the Gulf of Thailand. *JOURNAL OF PETROLEUM GEOLOGY*, **26**, 49-64.
- Zhengquan, W., Qingheng, W. & Yandong, Z. 1997. Quantification of spatial heterogeneity in Old Growth Forests of Korean Pine. *Journal of Forestry Research*, **8**, 65-69.